July 2016

Ocean Gateways and Glaciation: Planktic Foraminiferal Records from the Southern Ocean, Equatorial Pacific, and Caribbean

Andrew J. Fraass
UMass

OCEAN GATEWAYS AND GLACIATION: PLANKTIC FORAMINIFERAL RECORDS FROM THE SOUTHERN OCEAN, EQUATORIAL PACIFIC, AND CARIBBEAN

A Dissertation Presented

by

ANDREW JEFFREY FRAASS

Submitted to the Graduate School of the
University of Massachusetts, Amherst in partial fulfillment
of the requirements for the degree of

DOCTOR OF PHILOSOPHY

May 2016

Geosciences

OCEAN GATEWAYS AND GLACIATION: PLANKTIC FORAMINIFERAL RECORDS FROM THE SOUTHERN OCEAN, EQUATORIAL PACIFIC, AND CARIBBEAN

A Dissertation Presented

By

ANDREW JEFFREY FRAASS

Approved as to style and content by:

_____
R. Mark Leckie, Chair

_____
Robert DeConto, Member

_____
Isla S. Castañeda, Member

_____
Steven Burns, Member

_____
Elizabeth Dumont, Outside Member

_____
Steven Petsch, Graduate Program Director
Department of Geosciences

ACKNOWLEDGEMENTS

Becoming a paleontologist was a dream of mine since I was two years old. This dissertation is emblematic of reaching that goal I set for myself while in elementary school, and so while these acknowledgements are nominally about thanking people who aided this dissertation specifically, I cannot help but think about the entire road that led here.

My parents, Dick and Wendy Fraass, have always been my biggest supporters. While neither of them *really* understood my fascination with paleontology, they dutifully took me to every natural history museum possible. I have tried to live up to the examples they set as individuals, and as a scientist in the case of my father.

I cannot imagine doing what I do without my brother's humor, or his acting as a 'reality check'. His ability to say things that make me see actions in a different light, or at least search for better evidence for my current thinking, was an excellent set-up for trying to do a Ph.D..

I have had many, many friends, teachers, and others over the years who have either directly or indirectly helped me to get here. To name only a few, thank you Thomas Kehrer, Augie Salick, Mike Moffat, the Friedlanders, Doug Marsch, Katie Fillingham, Molly Patterson, Bob Geier, Allie Tessin and Tim Gallagher, Jane Bridges, Cat Lardas, Mike Martinez-Colon, Rob Hatfield, Debbie Wall-Palmer, and many more.

Scientific research, particularly one with long hours behind a microscope, can devolve into drudgery. I have these people to thank for helping that not be the case: Marc Maron, Doug Benson, Chris Carter, Joss Whedon, Jon Stewart, Gene Roddenberry,

Steven Moffat, Matt Gourley, Russell T. Davies, Paul F. Thompkins, Scott Aukerman, and many others.

I would be remiss if I did not thank D. Clay Kelly (University of Wisconsin). I was lucky he took me on as a student despite my academic record; I would probably not be getting a Ph.D. without that opportunity.

There are several people who helped in various aspects of this research, and I this document would have suffered greatly from their absesnse: Yi Ge Zhang, Mike Jercinovic, Dave Finkelstein, Bridget Wade, Paul Pearson, Dick Olsson, the rest of the Oligocene Planktic Foraminifera Working Group, Anne Le Friant, and Osamu Ishizuka. I would also like to thank my committee. Particularily, Steve Burns and Rob DeConto. Dr. Burns patiently explained how to work the mass spectrometer many times. Dr. DeConto, who not only was the PI for the grant that supported much of my time at UMass and the Mi-1 research, but who also set a wonderful example of teaching and provided critical insight into a number of the problems in this dissertation.

The Leckie Lab at UMass has been a wonderful place to spend about six years. It was not just a place to discuss science, but a supportive group of friends. I want to thank Emily Browning, Kendra Clark, Khalifa Elderbak, Serena Dameron, Chris Lowery, Renata de Mello, Amanda Parker, Ali Alibraham, Linnae Rondeau, Adriane Lam-Uzel, and Raquel Bryant for fruitful discussions and fun distractions. I also would like to thank the undergraduates who helped, particularily those who worked on sections of this dissertation: Megan Leckie (Site U1396), Laura Healy (Site 803), and Chelsea McQuaid (Site 744).

I can think of no one I would rather do a Ph.D. with than Mark Leckie. His ability to recall that one key piece of decades-old research, down to the figure constantly astounds me. Working through a problem with him is enjoyable, even when we would head down the same path multiple times. He has an ability to find that one solution, only simple in retrospect, which address all concerns. He also has fostered the environment that produced such a supportive lab.

There are two last people I need to thank. The first is my daughter Jane. Jane, you have been an enormous joy in my life for the past two and a half years. Your good nature, ability to make me laugh, and importantly your well-earned ability to sleep soundly, has done more to keep me balanced than nearly anything else.

Finally, I need to thank my wife, Susanna. This isn't my Ph.D., it's ours. You've been my sounding board for ideas, you've edited everything I've written (even this), and you've picked up all the slack in our life that I didn't have the wherewithal to handle. I cannot thank you enough for being my partner. Having you in my life has made me a better person, and a better scientist.

ABSTRACT

OCEAN GATEWAYS AND GLACIATION: PLANKTIC FORAMINIFERAL RECORDS FROM THE SOUTHERN OCEAN, EQUATORIAL PACIFIC, AND CARIBBEAN

MAY 2016

ANDREW J. FRAASS, B.S., UNIVERSITY OF WISCONSIN - MADISON

M.S., UNIVERSITY OF WISCONSIN - MADISON

Ph.D., UNIVERSITY OF MASSACHUSETTS, AMHERST

Directed by: Prof. R. Mark Leckie

Ocean gateway changes, once the best mechanism for driving abrupt climatic change, have fallen from favor. They have been largely replaced within the literature by changes in CO_2 concentration and orbital forcing. This dissertation looks at three intervals of relative stability (Oligocene), prolonged change (Plio-Pleistocene), or transient events (Oligocene/Miocene boundary) in order to better understand the oceanographic circumstances which govern 'events' in the paleoceanographic record.

Chapter 1 discusses the chronostratigraphy of Integrated Ocean Drilling Program (IODP) Site U1396 (Expedition 340) in the Caribbean Sea. A combination of paleomagnetostratigraphy, biostratigraphy, astrochronology, and correlation to Marine Isotope Stages (MIS) allows a high-resolution age model to be constructed. Sedimentation rates are calculated for the paleomagnetic and MIS age models, and with

and without volcanic sediments. The findings agree with shipboard determination of slowing sedimentation toward the present, and suggest either increased winnowing due to bottom-water flow or changes in productivity altering the biotic flux at the site.

Chapter 2 reexamines the Oligocene at Ocean Drilling Project (ODP) Sites 803 and 628 with revised taxonomic concepts. There are disagreements between the global compilations of macroevolutionary rates and the rates calculated at Site 803, though several hypotheses are discussed to explain the findings. A series of illustrations are presented to aid in taxonomic identification through this difficult interval.

Chapter 3 focuses on the Mi-1 event, discussing several new records: Deep Sea Drilling Program Site 78, ODP Site 803 (both equatorial Pacific Ocean), and ODP Site 744 (southern Kerguelen Plateau). After reviewing the leading hypotheses for Mi-1, the three new sites are used to test the paleoproductivity hypothesis, and use those records to investigate the importance of different orbital parameters. Lastly, the foram fragmentation index is employed to examine changes in the lysocline at the sites, demonstrating that there are dramatic global changes in the lysocline throughout the leadup to Mi-1. While carbonate sequestering carbon through the lysocline changes (or infact deepening Calcite Compensation Depth) cannot explain abrupt cooling events on their own (e.g., Coxall et al., 2005), a narrative discussion of the leadup to Mi-1 puts the lysocline changes in context with findings at other sites.

CONTENTS

Page

ACKNOWLEDGEMENTS iv

ABSTRACT vii

LIST OF TABLES xii

LIST OF FIGURES xiii

INTRODUCTION 1

CHAPTER 1: SEDIMENT ACCUMULATION AND PALEOCEANOGRAPHY OF THE NORTHEASTERN CARIBBEAN: IODP SITE U1396 OFF MONTSERRAT, LESSER ANTILLES 11

1.1 Abstract 11
1.2 Introduction 12
1.3 Methods 16

1.3.1 Geologic Setting and Shipboard Results 16
1.3.2 Astrochronology 21
1.3.3 Micropaleontology 24
1.3.4 Stable Isotopes 25

1.4 Results 28

1.4.1 Astrochronology 28
1.4.2 Benthic Isotope Values 28
1.4.3 Biostratigraphy 31
1.4.4 Hiatuses 35

1.5. Discussion 36

1.5.1 Biostratigraphy 41
1.5.2 Sedimentation 44

1.5.2.1 Age Scheme Mismatch 44
1.5.2.2 Sedimentation Rates 48
1.5.2.3 Local Volcanism/Regional Effects 51
1.5.2.4 Gateway Changes 52

1.6 Conclusions 58

2: OLIGOCENE PLANKTIC FORAMINIFERAL TAXONOMY AND EVOLUTION: AN ILLUSTRATED REVISION OF OCEAN DRILLING PROGRAM SITE 803 61

2.1 Abstract 61
2.2 Introduction 62
2.3 Methods 67

2.3.1 Site Description 67
2.3.2 Sample Preparation 68
2.3.3 Biostratigraphy 68

2.4 Discussion 68

2.4.1 Biostratigraphy 68
2.4.2 Evolutionary Metrics 75
2.4.3 Homeomorphy 78

2.5 Systematics 87

3: THE MI-1 EVENT: ORBITAL AND SECULAR CHANGES FROM LOW AND HIGH LATITUDES 130

3.1 Abstract 130
3.2 Introduction 131

3.2.1 Chronostratigraphy 132
3.2.2 Possible Causes of Mi-1 137

3.3 Methods 141

3.3.1 Geological Setting 141
3.3.2 Analytical Methods 145

3.3.2.1 Micropaleontological Methods 145
3.3.2.2 Stable Isotope Methods 154

3.4 Results 156

3.4.1 Chronostratigraphy 156

3.4.1.1 ODP Site 744 158
3.4.1.2 ODP Site 803 167
3.4.1.3 DSDP Site 78 168

3.4.2 Paleoceanography 168

3.4.2.1 ODP Site 744 168

3.4.2.1.1 Frequency Analysis 172

3.4.2.2 ODP Site 803 177
3.4.2.3 DSDP Site 78 178
3.4.2.4 Linear Correlations 179

3.5 Discussion 181

3.5.1 ODP Site 744 181
3.5.2 Sites 803 and 78 186
3.5.3 Carbonate Preservation 187

3.5.4 Timeline to Mi-1 190

3.6 Conclusions 194

CONCLUSION 196

APPENDICES

A DEPTH-SPLICER AND DESC-SPLICER: CODE FROM THE R-PROGRAMMING ENVIRONMENT 200
B COREDESC BREAKDOWN AND VISUAL INSPECTION: CODE FROM THE R-PROGRAMMING ENVIRONMENT 204
C NVOLC DEPTHS: CODE FROM THE R-PROGRAMMING ENVIRONMENT 208
D ASTROCHRONOLOGY WITH FLEXIBLE PALEOMAGNETIC CONTROL POINTS: CODE FROM THE R-PROGRAMMING ENVIRONMENT 210
E STABLE ISOTOPE DATA FROM SITE U1396 217
F TAXON TABLE: CODE FROM THE R-PROGRAMMING ENVIRONMENT 235
G AGE MODELS FOR MI-1: SITES 78, 744, AND 803 238
H STABLE ISOTOPE DATA FOR MI-1: SITES 78, 744, 803 244

WORKS CITED 258

LIST OF TABLES

Table Page

1.1 Table of planktic foraminifera biostratigraphic datums 32

LIST OF FIGURES

Figure Page

I.1 Position of gateways discussed in the introduction 2

I.2 Macroevolution in the planktic foraminifera 5

I.3 Oligocene stable isotope and orbital configuration 10

1.1 Site Map 17

1.2 Statigraphic data transformation process 19

1.3 Results of 0-1 Ma Evolutive Harmonic Analysis (EHA) 23

1.4 Summary of transformations from depth (CCSF-D) to Marine Isotope Ages for $\delta^{18}O$ record 27

1.5 Histogram of $\delta^{18}O$ offsets between benthic species 30

1.6 Summary of differences between Wade et al. (2011) age datums and findings at Site U1396 with important Scanning Electron Micrographs (SEM) 34

1.7 Summary of the two contrasting interpretations for the Brunhes chron chronostratigraphy 38

1.8 Summary of the age vs. depth relationship of the Site U1396 sediments 46

1.9 Summary of differences in different methods of age calculation 47

1.10 Summary of sedimentation rates, paleoceanographic events, and sediment character 49

2.1 Evolutionary context for Chapter 2 64

2.2 Graphic representation of species occurrences at Hole 803D 70

2.3 Age, Depth, and Sedimentation Rate changes 73

2.4 Differences in datum ages from the Berggren et al. (1985) and Berggren and Miller (1988) time scales to the Wade et al. (2011) calibration 74

2.5 Evolutionary metrics with time 76

2.6 Key taxonomic differences between homeomorphs *Subbotina projecta* and *Dentoglobigerina globularis* 79

2.7 Key taxonomic differences between homeomorphs *Dentoglobigerina prasaepis* v *Globoturborotalita euapertura* 80

2.8 Key taxonomic differences between *Chiloguembelina cubensis*, *C. adriatica*, and *C. ototara* 81

2.9 Key taxonomic differences between *Dentoglobigerina pseudovenezuelana*, *D. eotripartita*, *D. sellii*, and *D. tapuriensis* 82

2.10 Key taxonomic differences between *Paragloborotalia nana*, *P. opima*, and *P. mayeri* 83

2.11 Key taxonomic differences between *Globoturborotalita* 84

2.12 Variability within the genera *Dentoglobigerina* and *Subbotina* 85

2.13 Oligocene taxa 86

3.1 Summary of chronostratigraphic data 134

3.2 Stable isotope stratigraphy 136

3.3 Site Map 143

3.4 Depth vs. Age, Sites 78 and 803 144

3.5 Summary of data for ODP Site 803 148

3.6 Summary of data for DSDP Site 78 149

3.7 Summary of data for ODP Site 744 151

3.8 Carbon cycle and biota 153

3.9 Site 744 age diagnostic criteria 160

3.10 Site 744 stable isotope data 163

3.11 Site 744 key evolutive harmonic analyses 173

3.12 Mi-1 key evolutive harmonic analyses 176

3.13 Linear correlations 180

INTRODUCTION

Ocean gateway changes, once considered to be the best mechanism for driving abrupt climatic change, have fallen from favor. For example, the opening of the Drake Passage was the trigger for the glaciation across the Eocene/Oligocene boundary (33.9 Ma; Pälike et al., 2006b). The opening led to thermal isolation around Antarctica by allowing the Antarctic Circumpolar Current ("deep Circum-Antarctic Current" circa 1980) to freely circle the continent. Isolation allowed Antarctica to cool sufficiently driving the glaciation at the E/O boundary (Kennett and Shackleton, 1976; Kennett, 1977). Thermal isolation of the polar continent was effectively dogma in the paleoceanographic community as an attractive way to explain a series of observations: sedimentological (e.g., Keller and Barron, 1983) and stable isotopes (e.g., Shackleton and Kennett, 1975; Kennett, 1977; Miller et al., 1987, 1991, among others). In the early 2000's, attention shifted to the importance of atmospheric CO_2 levels, spurred by both finding that the Drake Passage opened for surface water flow at 41 Ma (Scher and Martin, 2006; though see Livermore et al., 2007 for a dissenting opinion) and that atmospheric CO_2 plays a larger role in controlling glaciation in modeling studies (DeConto and Pollard, 2003). Patterns of circulation, and especially the circulation around Antarctica has continued to be an area of active study, and Scher et al. (2015) recently demonstrated that deep circulation around Antarctica initiated directly *after* the glaciation at the E/O boundary (Oi-1) due to opening in the Tasmanian Gateway, rather than the Drake Passage (Figure I.1).

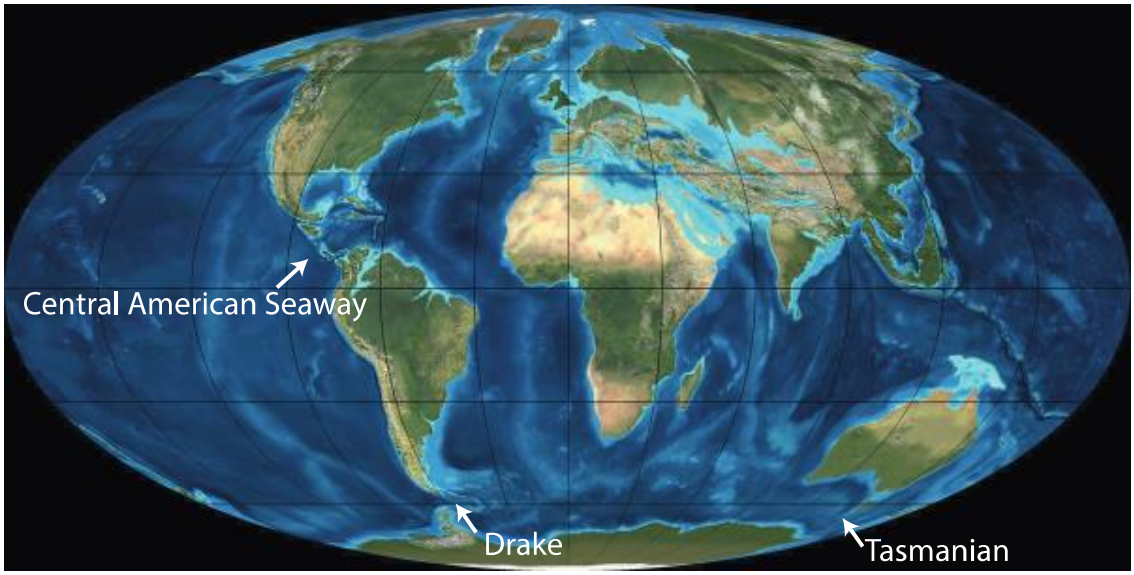

Figure I.1 Position of gateways discussed in Introduction. The base map is a reconstruction of Oligocene continental positions (Blakey, GPGeosystems).

Another, but still important, issue is that gateway opening is not a single one-and-done process. Tectonic processes are slow; the Tasmanian Gateway first began to open ~83 Ma (Hill and Exon, 2004), while the first evidence for ocean circulation was not until ~49 Ma (Bijl et al., 2013), with deep water circulation following ~20 myr after that (Scher et al., 2015). Superimposed on this geologically slow process is eustatic sea-level, which can operate on myr-scale to kyr-scale. For example, the 'closure' of the Central American Seaway (CAS) occurred several times, due to the growth of glacial ice on Antarctica lowering sea-level enough that the Panamanian Isthmus was closed, then opening as ice melted (Groenveld et al., 2014). The hypothesis that gateway changes can singularly drive events like Oi-1 at the Eocene/Oligocene boundary, becomes harder to support as the timing becomes more complex and opening events are repeated. If the last initial sea-level drop did not lead to more substantial glaciation, why would the next?

A portion of the answer is found in Earth's orbit, which has various periods on which it varies (Milankovitch, 1930; Hays et al., 1976). Zachos et al. (2001) depicts these in relation to Cenozoic climate, using carbon and oxygen isotopes as indicators of the carbon cycle and temperature/ice-volume respectively. Eccentricity is frequently associated with monsoon intensity (e.g., Gupta et al., 2001) or sea-level (e.g., Pälike et al., 2006b). Obliquity frequently is associated with ice growth, with cool southern hemisphere summers limiting ice melt (Zachos et al., 2001). Orbital parameters have been calculated back to the early Cenozoic (e.g., Laskar et al., 2010), and evidence for likely orbital driven changes have been found in time-periods far before that (e.g., the Permian; Wu et al., 2013). The development of ice on Antarctica may be driven by a combination of all three of these mechanisms; gateway changes, atmospheric CO_2 levels, and orbital drivers.

Foraminiferal evolution is intrinsically linked to oceanographic circumstances. Their evolution is controlled by a combination of factors, particularly an interaction between morphology, ecology, and climate (Ezard et al., 2011). Their species-level record is as complete or better than the best macrofossil genus-level records (Aze et al., 2011). They have been used for decades as biostratigraphic indicators, have a relatively robust fossil taxonomy and phylogeny (Aze et al., 2011), detailed records of first and last occurrences, and large distributions due to pelagic habitats (Norris, 2000). Their past evolutionary events have been connected to paleoceanographic changes (e.g., Cifelli, 1969; Lipps, 1970; Wei and Kennett, 1986; Norris, 1992; Premoli Silva and Sliter, 1999; Leckie et al., 2002). Fraass et al. (2015; fig. I.1) highlighted connections from planktic foraminifera evolution to the Ocean Anoxic Events (Cretaceous), the Paleocene Eocene

Thermal Maximum (Paleogene), the Oi-1 event (Eocene/Oligocene boundary), for example.

Planktic foraminiferal evolution occurred in three main phases; the Cretaceous, the Paleogene, and the Neogene (Tappan and Loeblich, 1988; fig. I.2 Fraass et al., 2015). The Cretaceous can be subdivided between the diversification before and after the Aptian/Albian boundary as well (Huber and Leckie, 2011). Intervals of high diversity (Maastrictian, Eocene, and Pliocene-Pleistocene) are separated by the K/Pg mass extinction and the Oligocene. The K/Pg extinction is recovered from quickly, but the Oligocene stands out as an extended interval of low diversity (Fraass et al., 2015). The Oligocene is also the only interval in the planktic foraminiferal evolutionary record that does not covary with the macrostratigraphic pattern of marine sedimentation, making it profoundly different (Peters et al., 2013). While part of the low diversity and disconnection from sedimentary cycles may be a primary signal (Peters et al., 2013; Fraass et al., 2015), it also may be due to a problematic taxonomy through that interval. The foraminifera through the Oligocene are difficult to work with, as they have frequently convergent morphologies leading to a gnarled taxonomy (see Chapter 2).

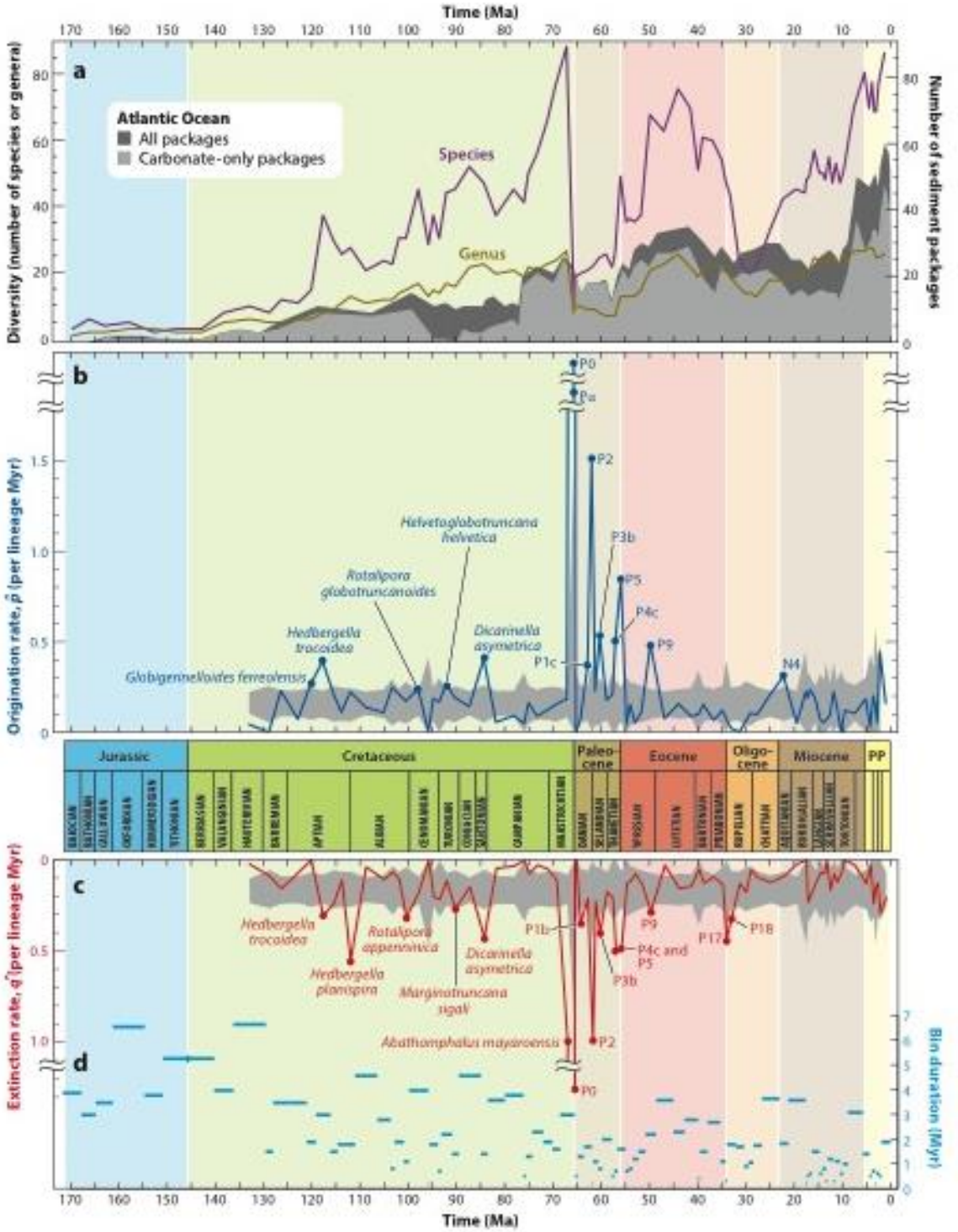

Figure I.2 Macroevolution in the planktic foraminifera. Reproduced from Fraass et al. (2015). Fig. 2a Number of sedimentary packages against number of planktic foraminifer genera and species during each foram biozone. Figure 2b. Rate of origination (per lineage per million year) depicted against time (Ma). Figure 2c. Rate of extinction (per lineage per million year) depicted against time (Ma). Figures 2b and 2c. Grey bar represents a

Monte Carlo simulation of purely stochastic macroevolutionary rate (see Fraass et al., 2015 for details). Intervals noted with their biozone name are deemed significant rate excursions, as they exit the grey stochastic evolutionary model. Figure 2d. Length of the biozone against time. Note: This analysis used the N & P zones employed in Pearson et al. (1999), rather than the zonation scheme (Wade et al., 2011) used in this study.

I.1 Chronostratigraphy

One of the most important types of data in any science that studies the rock record is age. Without a detailed understanding of the age of a piece of rock, or layer of sediment, it is not possible to talk about rates or the global context of deposition, for example. A primary concern in this dissertation is chronostratigraphy, or the study of the depositional age of sediments. Chapter 1 tests a recent biostratigraphic correlation (Wade et al., 2011), after developing an intergrated bio-magneto-astro-chemostratigraphy for IODP Site U1396 in the Caribbean Sea. Chapter two uses revised biostratigraphic calibrations to update the sedimentation rate estimates at Site 803, but also lays groundwork for developing more Oligocene biostratigraphic datums. Lastly, chapter three employs several scientific ocean drilling sites to investigate the Mi-1 glaciation event. Much of that chapter deals with updating the age models produced for those sites to modern chronostratigraphic systems.

Biostratigraphy is a well established tool for defining the relative ages of sediments, with a profound connection to ocean drilling science. Leg 3 of the Deep Sea Drilling Project tested the hypothesis of Plate Tectonics, using biostratigraphy and paleomagnetic reversals (The Shipboard Scientific Party, 1970). Many workers through the years have developed zonation schemes, with primary and secondary datums adding a high degree of control for both the Cenozoic and Mesozoic (e.g., Berggren et al., 1985; Wade et al., 2011). As biostratigraphy has advanced, the implication in later studies has

been higher accuracy and higher precision. Wade et al. (2011) for example, implies 10-kyr precision with their calibrations. The use of biological organisms to date sediments is rife with inherent problems, for example, a shift in the local climate or oceanography at a site could move a species ecological niche elsewhere, making it go prematurely extinct at a site. Chapter one takes the 0-4.5 Ma record of a tropical Integrated Ocean Drilling Project (IODP) site and tests the recent Wade et al. (2011) calibration in recently recovered sediments.

The Oligocene, in particular, stands out as a problematic epoch for biostratigraphy. To illustrate, the Miocene has 63 datums with an average of ~3.5 datums/myr, the Eocene has 37 datums with an average of ~1.7 datums/myr, and the Paleocene has 29 datums with an average of ~3.6 datums/myr. The Oligocene, on the other hand, has 11 datums, thus an average of 1 datum/myr, sitting within the nadir in diversity between the Eocene high and Neogene diversification. It also has the fewest secondary datums, just 5. Biostratigraphic control is therefor the weakest within the Oligocene in the planktic foraminifera. The problem is compounded by homeomorphy, with many species resembling others even in different genera, making the Oligocene difficult to study with respect to planktic foraminifera. Chapter 2 is a step toward fixing both the taxonomic and biostratigraphic issues by outlining key features able to be identified under a binocular microscope, and by determining the top and bottom occurrences of several species within the relatively continuous sedimentation at Ocean Drilling Program (ODP) Site 803 in the western equatorial Pacific.

I.2 Paleoceanography

Chapters 1 and 3 deal primarily with paleoceanographic problems, including ocean gateway and circulation changes in the context of global climate change; chapter 1 in the Pliocene and Pleistocene (last 4.5 myr), and chapter 3 with the Oligocene/Miocene boundary (~23 Ma). The Plio-Pleistocene is a key interval to understand with respect to anthropogenic climate change. One important use for paleoceanography is to develop detailed histories of ancient climate records on which to test models. To test climate sensitivity, events recording both cooling and warming are important. We essentially strive to flip uniformitarianism: the past is the key to the present. The Pliocene offers us an excellent opportunity. Due to its relatively recent nature (2.58-5.33 Ma) there are a great deal of sedimentary archives available. It was also warmer than the present (e.g., Dowsett and Robinson, 2009). It presents one of the best opportunities to study a warm climate with paleogeography very similar to today. There are still outstanding questions though, like the impact that closing one of the last ocean gateways, the Central American Seaway (CAS), had on local, regional, and global oceanography and climate.

Chapter 1 examines the history of sedimentation near Montserrat Island in the Caribbean Sea, with respect to the closure of the CAS. As Site U1396 only recovered sediments younger than ~4.5 Ma, much of the closure was done by the time U1396 was recording the local paleoceanography. The final closure history, which alters the salinity contrast between the Pacific and Atlantic Oceans (e.g., Haug and Tiedemann et al., 1998) has implications on the thermohaline circulation, and thus bottom water flow in the region. The increase in bottom water flow possibly impacted the rates of sedimentation at Site U1396.

Chapter 3 investigates the 'Mi-1' event, which roughly occurs at the Oligocene Miocene boundary at 23 Ma. The Mi-1 glaciation is a substantial, but transient, ice growth event on Antarctica, recorded by a ~1‰ oxygen isotope excursion in deep-sea benthic foraminifera. After the initial rapid glaciation of Antarctica at the Eocene/Oligocene boundary (33.9 Ma), called the Oi-1 event, most oxygen isotope records demonstrate strong eccentricity forcing (fig. I.3; Pälike et al., 2006b). Some records have shown similar findings for Mi-1 (Sites 926/929; Pälike et al., 2006a). In chapter three, Deep Sea Drilling Project Site 78, and Ocean Drilling Program Sites 744 and 803 are used to explore the lead up to Mi-1 in the Southern Ocean (744) and equatorial Pacific Ocean (78 and 803). The sites allow investigations on the possible influence that orbital geometry had on productivity (Diester-Haass et al., 2011), sedimentation, and current strength. Through the use of a recent R-package ('astrochron'; Meyers, 2014) an analysis of the various frequencies recorded in the sediment by a variety of data-types is undertaken, resolving largely eccentricity forcing, even at the high latitude Site 744. Lastly, the many proxy records at previously published sites distributed through the global ocean are discussed in an attempt to establish the timing of events in the different ocean basins and explore a possible trigger for the onset of the Mi-1.

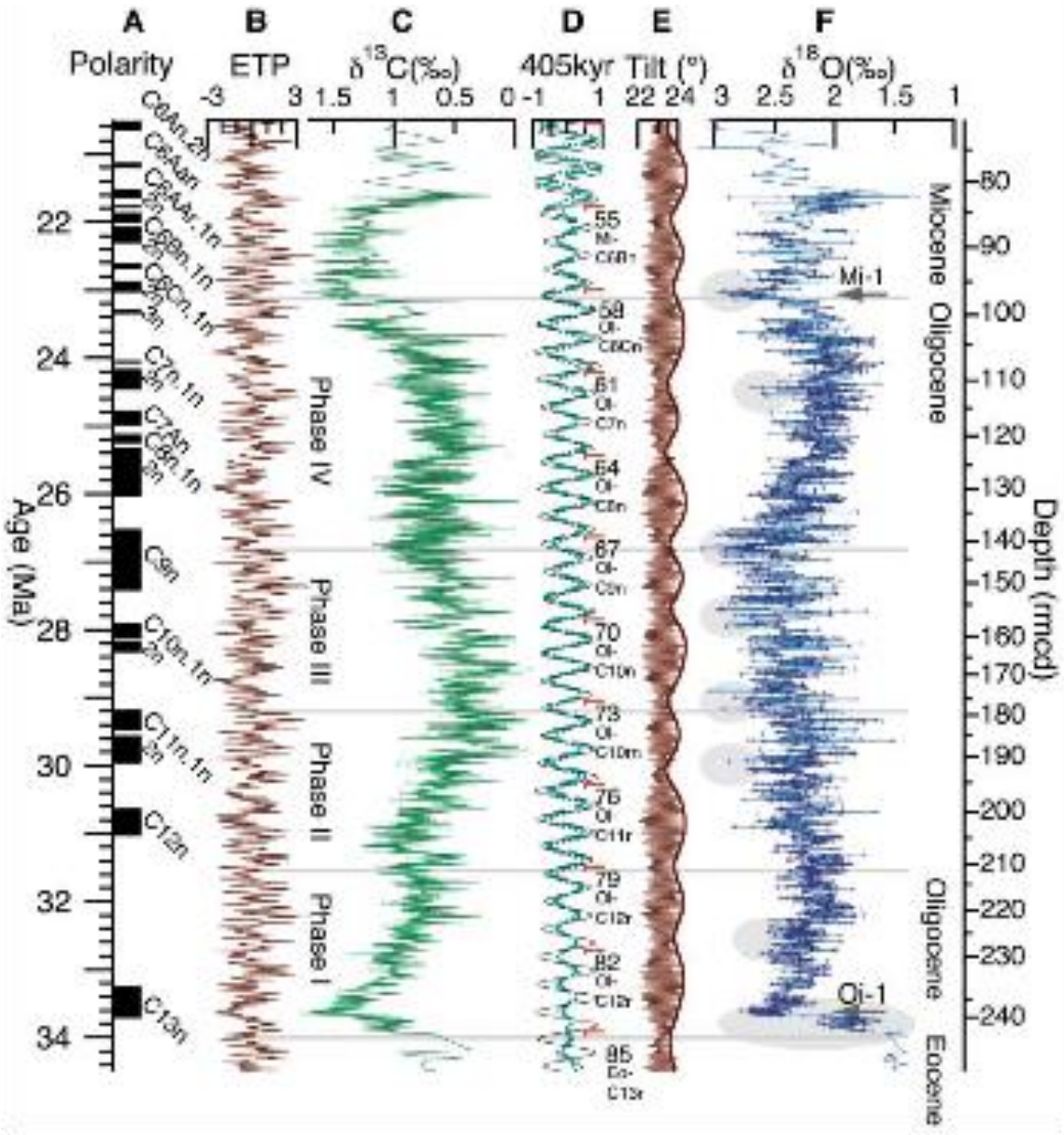

Figure I.3 Oligocene stable isotope and orbital configuration. Reproduced from Pälike et al., 2006b. Key portions of this plot for the discussion here are Panels C, D, E, and F. Carbon (C) and Oxygen (F) isotopes are from ODP Site 1218 benthic foraminifera. Panel D is the ~405 kyr eccentricity cycle, which is suggested to control Oligocene climate, along with the ~1.2 Ma obliquity amplitude cycle represented in E as the thicker brown line (Wade and Pälike, 2004).

CHAPTER 1

SEDIMENT ACCUMULATION AND PALEOCEANOGRAPHY OF THE NORTHEASTERN CARIBBEAN: IODP SITE U1396 OFF MONTSERRAT, LESSER ANTILLES

1.1 Abstract

Site U1396 was drilled as a part of Integrated Ocean Drilling Project Expedition 340 to establish a longer record of Lesser Antilles volcanism than previously known. A ~150 m sediment succession was recovered from three holes cored on a bathymetric high ~33 km southwest of Montserrat. A series of shipboard and newly generated chronostratigraphic tools (biostratigraphy, magnetostratigraphy, astrochronology, and stable isotope chemostratigraphy) were employed to generate an integrated age model. Two possible chronostratigraphic interpretations for the Brunhes chron are presented, with hypotheses to explain the conflicting chronostratigraphic markers observed between this study and Wall-Palmer et al. (2014). The recent Wade et al. (2011) planktic foraminiferal biostratigraphic calibration is tested, with significant mismatches between calibrated ages of secondary datums, while primary datums are observed largely as expected. Lastly, sedimentation rates are calculated, both including and excluding the contribution of discrete volcanic sediment layers in the succession. Rates are found to be 'pulsed' or highly variable within the Pliocene interval, declining through the 1.5-2.4 Ma interval, and then lower through the Pleistocene. Possible explanations for the observed trends in the sedimentation rates include orbitally-forced biogenic production spikes, elevated contributions of cryptotephra (dispersed ash), and changes in bottom waters and flow rates with increased winnowing in the area of Site U1396 into the Pleistocene. This

study provides an integrated chronostratigraphic framework for further paleoceangraphic and other studies.

1.2 Introduction

Montserrat is within the Lesser Antilles chain of islands in the Caribbean Sea. The Lesser Antilles has a history of volcanism dating back to the mid-Oligocene, though the western arc has been active since the early Miocene (Macdonald et al., 2000). Montserrat, one of the youngest islands in the arc, has built by three different phases of volcanism, all younger than ~2,600 ka (Harford et al., 2002). The current phase of volcanism began in 1995, resulting in both loss of life and evacuation of many settlements on the island. The eruption has produced numerous volcanic deposits, from pyroclastic material deposited on land and in the surrounding ocean, to substantial marine debris flows mapped using bathymetric surveys (Le Friant et al., 2010). With ~65% of volcanically-extruded material being emplaced in the ocean (Le Friant et al., 2010), the need to establish a robust geologic record from an offshore prospective is vital.

The history of Montserrat volcanism has been extended by the use of offshore sediments and has been an area of active research (e.g., Cassidy et al., 2013, 2014; Le Friant et al., 2008, 2010; Trofimovs et al., 2010; Shipboard Scientific Party, 2012; Wall-Palmer et al., 2014). This history has primarily been examined with respect to the hazard posed to the surrounding communities. Debris flows, in particular, have been a source of concern as potential tsunamogenic events, emplacing substantial amounts of material (>380 X 10^6 m^3) in the ocean, as seen both in the modern (e.g., Herd et al., 2006) and geological record (~14 ka; Trofimovs et al., 2010). While some local modern flows are clearly associated with the Soufrière Hills volcano (e.g., Herd et al., 2006), debris flows

within the geological record have not been clearly associated with volcanic activity, but rather the rapid sea-level rise associated with transitioning from glacial to interglacial conditions (Trofimovs et al., 2010). Understanding the past history of volcanic activity in the Lesser Antilles, and the frequency and composition of previous debris flows, is therefore of importance to the local communities. With that in mind, IODP Expedition 340: Lesser Antilles Volcanism and Landslides drilled several sites to examine the composition and history of the surrounding sediments. Sediments from four sites were recovered around Montserrat, allowing the shipboard scientific party to examine the heterogeneity of the surrounding sediments.

The Caribbean Sea during the Pliocene and Pleistocene is also of tremendous interest, as differences between Pacific and Atlantic Oceans indicate the presence or absence of the Panamanian Isthmus (e.g., Groeneveld et al., 2014). That closure history remains a deeply complicated subject without a simple obvious solution (see discussion in Molnar, 2008). The impact the closure had on the oceanography of the Caribbean Sea is unclear. Some authors suggest that closure increased meridional overturning circulation (e.g., Keigwin, 1982; Haug and Tiedemann, 1998; Osborne et al., 2014) while others suggest a profound shift to oligotrophic waters (e.g., Chaisson, 2003; Jain and Collins, 2007), as just two example implications. While these are not mutually exclusive, and could be intertwined, the timing of these various studies do not seem to line up, as some modeled implications for closure occur separated by more than a million years. The addition of another deep-sea site, within the eastern edge of the Caribbean Sea, with a high-resolution chronology, would be able to possibly elucidate questions of Central

American Seaway closure. The first step, however, is to generate a high-resolution chronology.

Biostratigraphy is inherently imprecise, as all of the data are biological, they are filtered through various 'noisy' processes, both during life and after death. Planktic foraminifera, for example, are prone to ecological and climatological fluctuations, and regional distributions controlled by oceanographic processes (Bé & Tolderlund, 1971), all of which can affect the stratigraphic level of highest and lowest appearances in a single sediment core. Taphonomic processes, such as winnowing or differential preservation, for example, can also change the true 'Top' (last appearance or highest occurance) or 'Bottom' (first appearance or lowest occurance) of a species. Despite inherent difficulties, the utility and value of planktic foraminiferal biostratigraphy is well established. Most biostratigraphic calibrations use meridional zonation schemes, divided into 'tropical' or 'tropical-subtropical' zonation schemes, while additional subdivisions (Atlantic vs. Pacific Ocean calibrations) alleviate some of the regional differences. The recent Wade et al. (2011) calibration has refined existing datums from Berggren and Pearson, 2006 (and references therein) and established a number of new datums. Wade et al. (2011) also used the Cande and Kent (1995) geomagnetic polarity timescale, as well as more recent astrochronologically calibrated timescales (Pälike et al., 2006; Lourens et al., 2004) to produce robust datum ages. However, while these dates are robust within a single site or among closely-situated sites, it is not commonplace to define an 'error' for the datums. Biostratigraphic originations, ideally in quickly spreading species, are at best only geologically instantaneous, as organisms cannot spring into being simultaneously around the world. Similarly, true biological extinctions are likely a series of regional

extinctions that finally culminate in the elimination of the entire species, after the rest of the areas where the species persisted are decimated. One reason that planktic foraminifera persist as a premier biostratigraphic system is their enormous, largely homogenous biogeographic ranges (Bé & Tolderlund, 1971), thus, their 'regional' originations and extinctions at the scale of tropical-subtropical subdivisions.

Site U1396 (fig. 1) presents an excellent opportunity to verify the last 4.5 myr of the Wade et al. (2011) calibration. Shipboard analysis suggests that the sediments from Site U1396 represent relatively continuous sedimentation and an excellent paleomagnetic stratigraphy was recovered (Expedition 340 Scientists, 2013). Shipboard planktic foraminiferal biostratigraphy determined that all primary datum species and the majority of the secondary datum species were present at the site. The same was true for nannofossil datum species. Detailed shipboard core description established five main units (A-E). Unit A was roughly 40 cm of bioclastic sand near the sediment water interface, possibly deposited from the recent 1995 eruption on Montserrat, recovered at Holes A and C. Unit B is a ~110-m thick sequence of hemipelagic mud interrupted by layers of tephra. Unit C is likely the result of 'inflow' from a pumice layer, producing a distorted stratigraphy. Unit D is a volcanic breccia, while Unit E is similar to Unit B (Expedition 340 Scientists, 2013). Units B and E represent the vast majority of sedimentation at this site.

The aim of this study is two fold. The first aim is to produce a robust age-model at the sub-chron level. This site has the potential to answer important questions about the volcanic history of Montserrat and surrounding islands, as well as the paleoceanographic history of the Caribbean Sea. While the recovered sediments cannot address much of the

Panamanian Isthmus closure history, which occurred largely in the Miocene (Keigwin, 1982; Haug and Tiedemann, 1998), it can answer questions about the final closure (~3-4 Ma) and its impacts on the biota, productivity, and circulation (e.g., Jain and Collins, 2007). With ~150 m representing 4.5 myr of sedimentation, a high resolution record of paleoceanographic, evolutionary, and climatic changes is possible from Site U1396. A robust age-model is the first step towards addressing those questions, continuing the data collection of Wall-Palmer et al. (2014). Second, this site presents a good opportunity to test the newly-established datums from Wade et al. (2011). To those ends, several chronostratigraphic tools were employed. Astrochronological tuning was performed on the color reflectance parameter L* (Brightness) from shipboard physical properties data using the 'astrochron' package within the R programming environment (Meyers, 2014; R Core Team, 2015). A ~9-kyr resolution benthic foraminiferal $\delta^{18}O$ record was generated and compared to the LR04 benthic foraminifera stack (Lisiecki & Raymo, 2005). Planktic foraminiferal biostratigraphy was also carried out at the same resolution (~9 kyr), to provide support for the other chronostratigraphic techniques and to be checked against the calibrations.

1.3 Methods

1.3.1 Geologic Setting and Shipboard Results

Site U1396 is located at 16°30.49′N, 62°27.10′W at ~800 m water depth (Figure 1.1). It is roughly southwest from the island of Montserrat sitting atop a bathymetric high. Coring on the high was hypothesized to limit the occurrence of turbidites, allowing for a more continuous record of volcanism than possible at other Expedition 340 sites. In addition, the sedimentation rates determined for the nearby CARMON-2 site (Le Friant et

al., 2008) suggested it would be possible to extend the existing geologic history to 4-5 Ma (Expedition 340 Scientists, 2013). Three holes were drilled at Site U1396, Hole B was to replace a single damaged core (U1396A/2H) from Hole A. Lithostratigraphy between the holes correlates well (see below), excluding a single unit (Unit C) in Hole C, a substantial interval of pumice flow-in which does not occur in the same thickness in Hole A. Shipboard age determination suggested that the base of Hole C was older than Hole A, and so Hole C was selected as the main hole for biostratigraphic and stable isotope work. Hole A was used to fill coring gaps or to avoid coring disturbances.

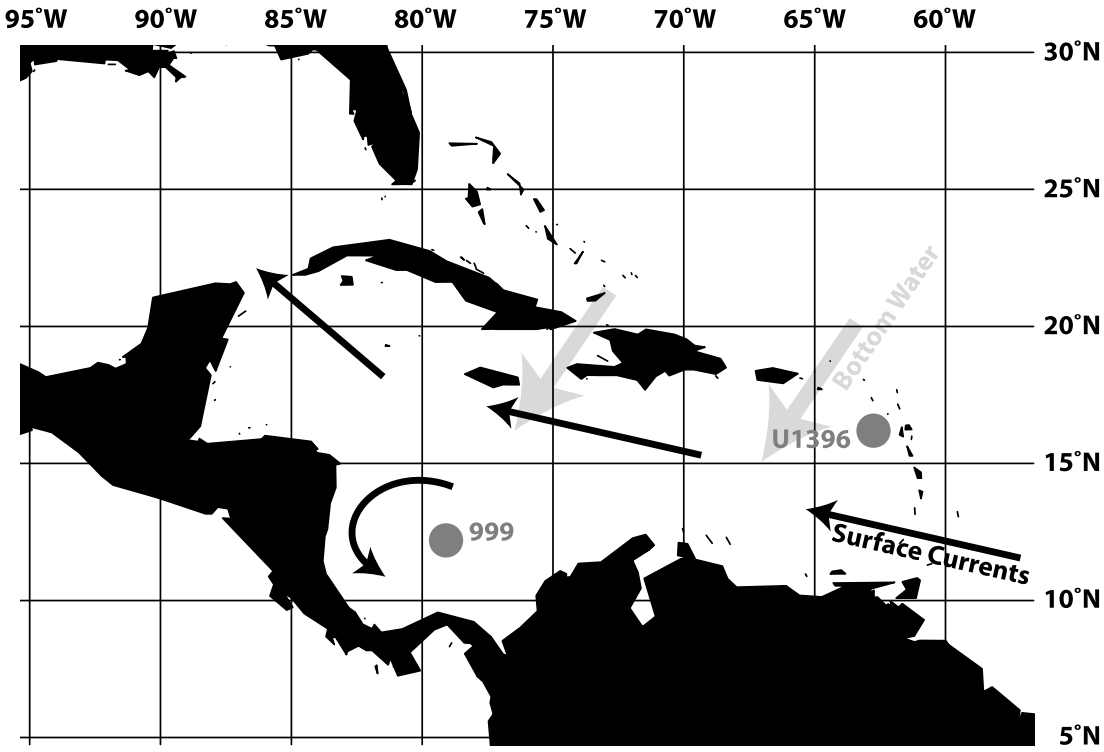

Figure 1.1. Site Map. Map showing surface currents (black), as well as entry points for bottom waters (grey) in the Caribbean Sea. ODP Site 999 and IODP Site U1396 are highlighted as well. Base map from R-package 'maps'.

Description of the core, preliminary calcareous nannofossil and planktic foraminiferal biostratigraphy, and physical properties data collection (e.g., color reflectance) were all performed shipboard. The initial shipboard age model sedimentation

rates for the Pliocene of ~4 cm/kyr and ~2 cm/kyr in the Pleistocene, largely determined by the paleomagnetic reversal stratigraphy and supported by nannofossil and planktic foraminiferal biostratigraphy (Expedition 340 Scientists, 2013). A revised splice was created to alleviate issues not captured in the shipboard correlation, creating composite core depth below seafloor scales (CCSF-A, CCSF-D; Hatfield, *in press*). This splice used magnetic susceptibility to correlate Holes A, B, and C, largely relying on Hole A. Tools for the R computing environment was created by the first author to splice all preexisting and newly generated data onto the new CCSF-D scale (see Appendices A and B). Several CCSF scales are used here, CCSF-A denotes the composite depth within Holes U1396A, B, or C individually, while CCSF-D is the depth within the composite section. Figure 1.2 depicts the process of splicing the color reflectance data and lithostratigraphic data from the initial CSF depth scale to the CCSF-D scale. The correlation of magnetic susceptibility across the holes appears to be robust; there is good agreement between the both L* (brightness) and lithostratigraphy in the CCSF-A scale (Figure 1.2b). An additional reassessment of the paleomagnetic datums was undertaken (Hatfield, *in press*), and that age-depth relationship is used here. One small adjustment was made for Core U1396A/2H. The oriented core liner for Core U1396A/2H was shattered during drilling resulting in unoriented and disturbed sediments, and so was not used in the composite section. Both core description and core photos show several correlatable tephra deposits, and so a simple lithostratigraphic correlation was used to place U1396A/2H on the CCSF-A scale. An offset of 1.71 m appears to correlate the U1396A/2H to U1396C/1H and U1396C/2H without any need for compression.

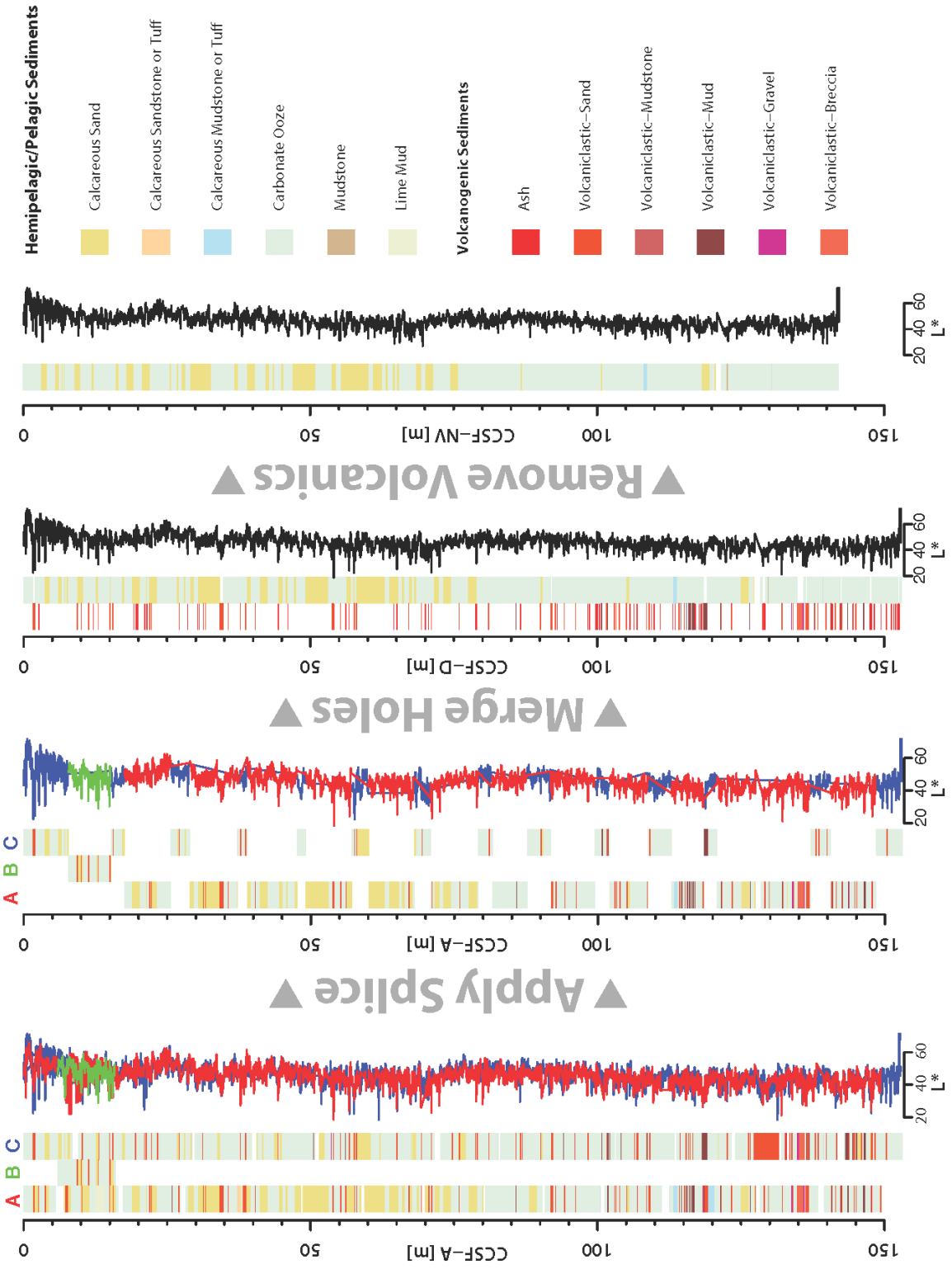
Hemipelagic/Pelagic Sediments
Calcareous Sand
Calcareous Sandstone or Tuff
Calcareous Mudstone or Tuff
Carbonate Ooze
Mudstone
Lime Mud
Volcanogenic Sediments
Ash
Volcaniclastic–Sand
Volcaniclastic–Mudstone
Volcaniclastic–Mud
Volcaniclastic–Gravel
Volcaniclastic–Breccia
▲ Remove Volcanics ▲
▲ Merge Holes ▲
▲ Apply Splice ▲
CCSF–NV [m]
CCSF–D [m]
CCSF–A [m]
L*
A
B
C
0
50
100
150
20
40
60

Figure 1.2. Stratigraphic data transformation process. First panel depicts major lithology for each hole (A, B, C), with Color Reflectance Brightness (L*) for each hole. Hole A is depicted as red, Hole B is green, and Hold C is Blue. Key to the colors for the major lithology is shown on the far right. Depths for this panel are all on CCSF-A. Second panel depicts the spliced stratigraphy, with each hole as a distinct column. L* in this panel only includes data included from the splice. Depths for this panel are all on CCSF-A. Third panel depicts the composite section, with volcanic units and hemipelagic/pelagic sediments in distinct columns. L* in this panel is the spliced L* sequence. Depths for this panel are all on CCSF-D. Fourth panel depicts the composite section removing all sediments with a volcanic major lithology. Both lithostratigraphic column and L* in this panel are not depicted as true depth, but are depicted on the CCSF-NV non-volcanic depth scale (See text).

Volcanic sedimentation occurring with an eruption (syn-eruptive *sensu* Carey and Schneider, 2011) is geologically instantaneous. Ash fallout, in particular, settles within vertical gravity currents faster than normal particles (Carey, 1997). The instantaneous introduction of cm-scale units of volcanic material interfere with the expected cyclic bands of sediment produced by Milankovitch or glacial-interglacial periodicity. Ash deposits, for example, are frequently darker in color than hemipelagic material, and so impart stochastic noise (from a cycle perspective) to an analysis of the frequencies within color reflectance. Also, hemipelagic material would be deposited at an entirely different sedimentation rate than the 'instantaneous' ash deposits. Removal of the discrete volcanic deposits, such as volcanic ashes, should result in a cleaner hemipelagic stratigraphic column, and hence a series of frequencies less dominated by noise. Therefore, removing the volcanically-derived sediments from stratigraphic column is reasonable prior to attempting astrochronologic tuning. However, this does not alleviate the issue of dispersed ash, as documented by ODP Leg 165 in the Caribbean (Sigurdsson et al., 1997) and within the upper several meters of Hole U1396C (McCanta et al., *in review*). Again, a tool in R was created by the first author to remove the volcanic sediments from the stratigraphy (see supplemental information). Figure 1.2 depicts this process. This tool

identifies the volcanic sediments, isolates them, removes them from the stratigraphic column, and then reassesses the depths to create a CCSF-NV (No Volcanics) scale. This CCSF-NV scale allows the comparison of three distinct sedimentation rates, the composite sedimentation rate, a hemipelagic sedimentation rate, and a volcanic sedimentation rate.

1.3.2 Astrochronology

Astrochronologically tuning the sediments from Site U1396 was not done independently of the previous age model. Employing roughly half the paleomagnetic datums, a hemipelagic sedimentation rate (linear sedimentation rate - thickness of volcanically sourced sediments) was applied. Astrochronological analysis was performed using 'astrochron', a package developed for R (Meyers, 2014). Tuning was performed in intervals roughly 0.5 myr in length. L* was interpolated to 3-kyr, prior to the evolutive harmonic analysis (EHA). The stratigraphic sequence was padded to roughly double the number of points in the interpolated. The window size for the EHA was 140-kyr with a step of 3-kyr. EHA results (e.g., fig 1.3) suggest tunable frequencies, despite the still substantial component of noise.

Tuning was performed so that there was as good an agreement between age diagnostic criteria and orbital or glacial-interglacial frequencies as possible; however, as previously noted, the signal is prone to substantial noise. This is likely due to a number of factors, both human and sedimentological. A slight offset between the correlation in the splice could result in a missed portion of a cycle at splice points, for example. If the sedimentation rate were 4 cm/kyr, an offset in the splice of 2.5 cm would result in a loss of ~1/4 of the 41-kyr obliquity cycle. This would manifest in the EHA diagram by

splitting the observed frequency into two pieces, one higher frequency and one lower, with a gap in the middle (Meyers and Sageman, 2014). If an inaccurate thickness or depth of a volcanic unit were in the core description, it would also similarly impact the cyclicity. It is also possible that removing all sediments with any volcanoclastic origin is overly cautious; some of those sediments may not be geologically instantaneous and may be from redeposition of volcanic components (post-eruptive *sensu* Carey and Schneider, 2011). The presence of cryptotephra (dispersed ash) would change the L* value of the sediments away from the predicted orbital or glacial-interglacial pattern. The use of such a wide window (140-kyr) was to account for this increase in noise. It does, however, induce a lag. An example of this is the smearing of frequencies about the employed paleomagnetic datums. In Figure 1.3 the white lines above and below the black anchor datum are where the EHA will begin to 'feel' the sedimentation rate change; the smearing is a result of the change from one linear sedimentation rate to the next. The window size was a compromise between accounting for this noise and creating an age model responsive to sedimentation rate changes.

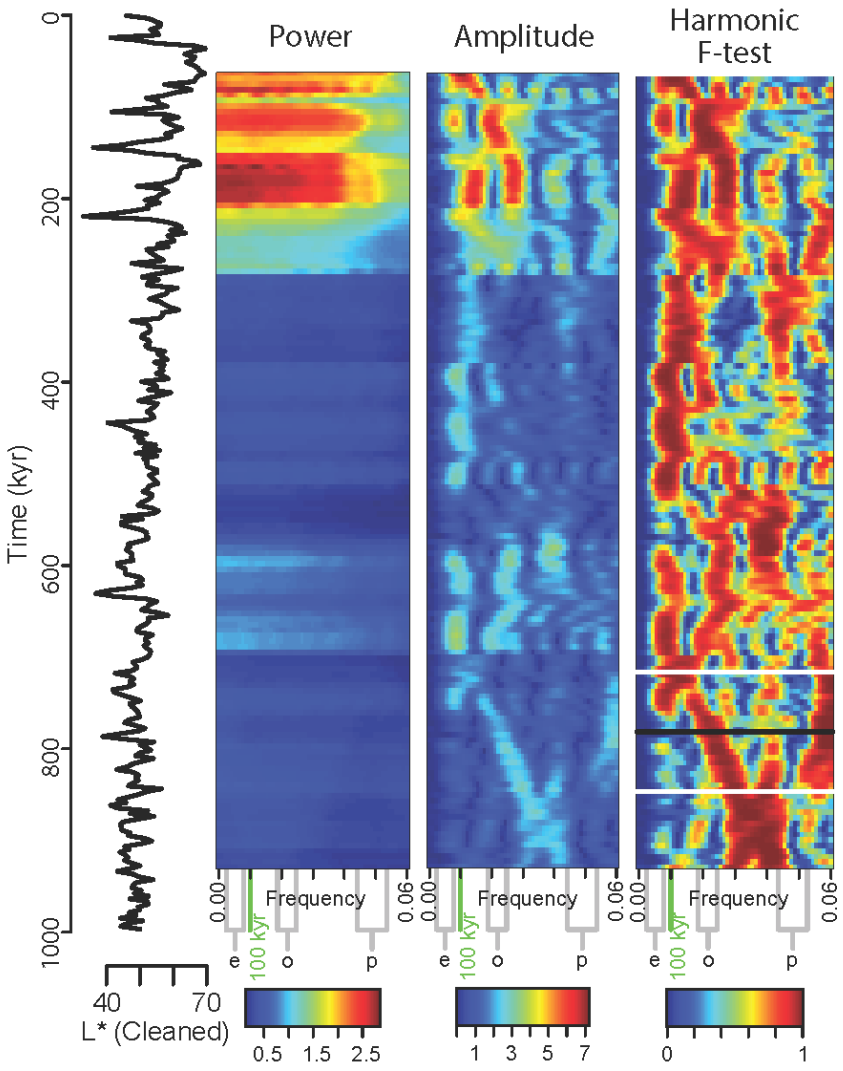

Figure 1.3. Results of 0-1 Ma Evolutive Harmonic Analysis (EHA). Left most panel is the L* brightness record, cleaned of volcanic sediments and put on a paleomagnetic timescale. Second panel is the spectral power (hotter colors denote higher power). Third panel is amplitude of spectra (hotter colors denote larger amplitude at depicted frequency). Final panel is the results of the harmonic F-test, depicting where there is significant spectral power. The results of the harmonic F-test were used to tune. The horizontal black line on the final depicts a paleomagnetic sedimentation rate control point. White lines above and below depict the earliest that the EHA 'feels' the abrupt sedimentation rate change which occurs at the paleomagnetic datum. Note the 'smearing' about that point seen in the changing frequencies throughout the highlighted interval. Grey lines depict expected orbital frequencies (e eccentricity, o obliquity, p procession), if the sedimentation rate were to be constant. The green line depicts the frequency described by a 100-kyr period.

1.3.3 Micropaleontology

A total of 596 samples were examined for biostratigraphically-important species. Two different strategies were used for sample choice. Within the upper 7 m of Site U1396, a sample spacing of 5 cm (~0.5-2 kyr) was used (these samples were previously used in Wall-Palmer et al., 2014). Below 7 mbsf a sampling resolution of ~9 kyrs was used, based on the shipboard age model but excluding volcanic sediments. All samples were checked against the Jutzeler et al. (*in press*) coring disturbance compilation and were found to be outside of all intervals with coring disturbances. For samples below 7 meters, samples were dried for ~24 hours, then soaked in a mild Sparkleen solution for 24-72 hours, a step necessary to free foraminifera from surrounding sediment. Sediment was washed over a 63 μm sieve before being dried for ~24 hours in a 40-50°C oven. Prior to being inspected, the samples were dry-sieved over a 150 μm sieve. All identification was performed at the >150 μm size fraction, following the taxonomy of Kennett & Srinivasan, 1983. Ages for the biostratigraphic datums follow the Wade et al. (2011) astrochronological calibration (and references therein).

Samples within the upper Pleistocene-Holocene Brunhes chron were inspected for *Globorotalia menardii* and *G. tumida*, as those taxa have been shown to fluctuate in response to glacial-interglacial cycles (e.g., Ericson and Wollin, 1968; Kennett and Huddlestun, 1972). This biozonation scheme has been employed globally and locally with success (e.g., Reid et al., 1996). Here it was used to continue the data collection of Wall-Palmer et al., 2014, extending their record of %*G. menardii-tumida* (undifferentiated) to the first geomagnetic reversal (i.e., base of the Bruhnes chron). Samples were dry-sieved over a 355 μm sieve, then a split to ~300 individuals was

performed using a microsplitter. Total planktic foraminifera and *G. menardii-tumida* were counted.

Individual foraminifera were imaged on a Carl Zeiss EVO 50 XVP scanning electron microscope near the top or bottom of their range to corroborate the positions of the datums described within this work. The desired foraminifera were placed on a piece of carbon tape, then coated with a 4 nm thick coating of carbon or platinum prior to imaging.

1.3.4 Stable Isotopes

Three species of benthic foraminifera (*Planulina wuellerstorfi, Cibicidoides mundulus,* and *Cibicidoides robertsonanius*) and one species of planktic foraminifera (*Globigerinoides ruber*) provide a stable isotope chemostratigraphy for U1396. *P. wuellerstorfi* was most common until 25 CCSF-A (~1.5 Ma), but absent in some samples throughout. Primarily *C. mundulus* was used in place of *wuellerstorfi*, but within the upper ~10 m *mundulus* was also scarce, and *C. robertsonanius* was used. Within the top 7 m sample volume was reduced (to alleviate the depletion of the core with the 5-cm resolution), and so a mixture of all three species were used when a single species was not possible. *Globigerinoides ruber* was used through the Brunhes chron to address low variability within the benthic $\delta^{18}O$ record (see below).

Preservation was variable through the study interval. Specimens were graded on a ‘pristine’ - ‘frosty’ - ‘bad’ scale. Pristine individuals were glassy, with no infilling. Frosty individuals were opaque, or had mild infilling. ‘Bad’ individuals, which were only used in rare instances where there was no other choice, had overgrowth, broken final chambers, or moderate infilling. The best-preserved individuals were used for isotopic

analysis, though generally were ‘frosty’ throughout the study interval, though there were intervals of exceptionally good preservation, and several intervals affected by diagenesis. A table of $\delta^{18}O$ values, ages, species, and preservation grade can be found in the supplemental information. The only general trends identified in preservation was a gradual decrease in the frequency of well preserved benthic foraminifera with increasing depth, though good preservation was still found near the base of Site U1396.

Planulina wuellerstorfi was typically used over either *Cibicidoides* species, though preservation of the individuals used for analysis occasionally required the use of *Cibicidoides*. 41 samples had enough adequate individuals from two species and so were used to generate offsets between the species. The number of individuals dissolved for each measurement varied (see Appendix E), but was typically only three to four, due to the large mass of the benthic tests. Roughly nine individuals of planktic *Globigerinoides ruber* were used in the analysis. The majority of samples were run at the University of Massachusetts Amherst Stable Isotope Laboratory on a Finnigan Delta XL+ with a Kiel III automated carbonate preparation system (>7 mbsf; these are in black, red, and brown on Figure 4). The rest of the samples were run at the National Oceanography Centre, Southampton using a Europa GEO 20-20 mass spectrometer with an automatic carbonate preparation system (0-7 mbsf; orange on fig. 1.4).

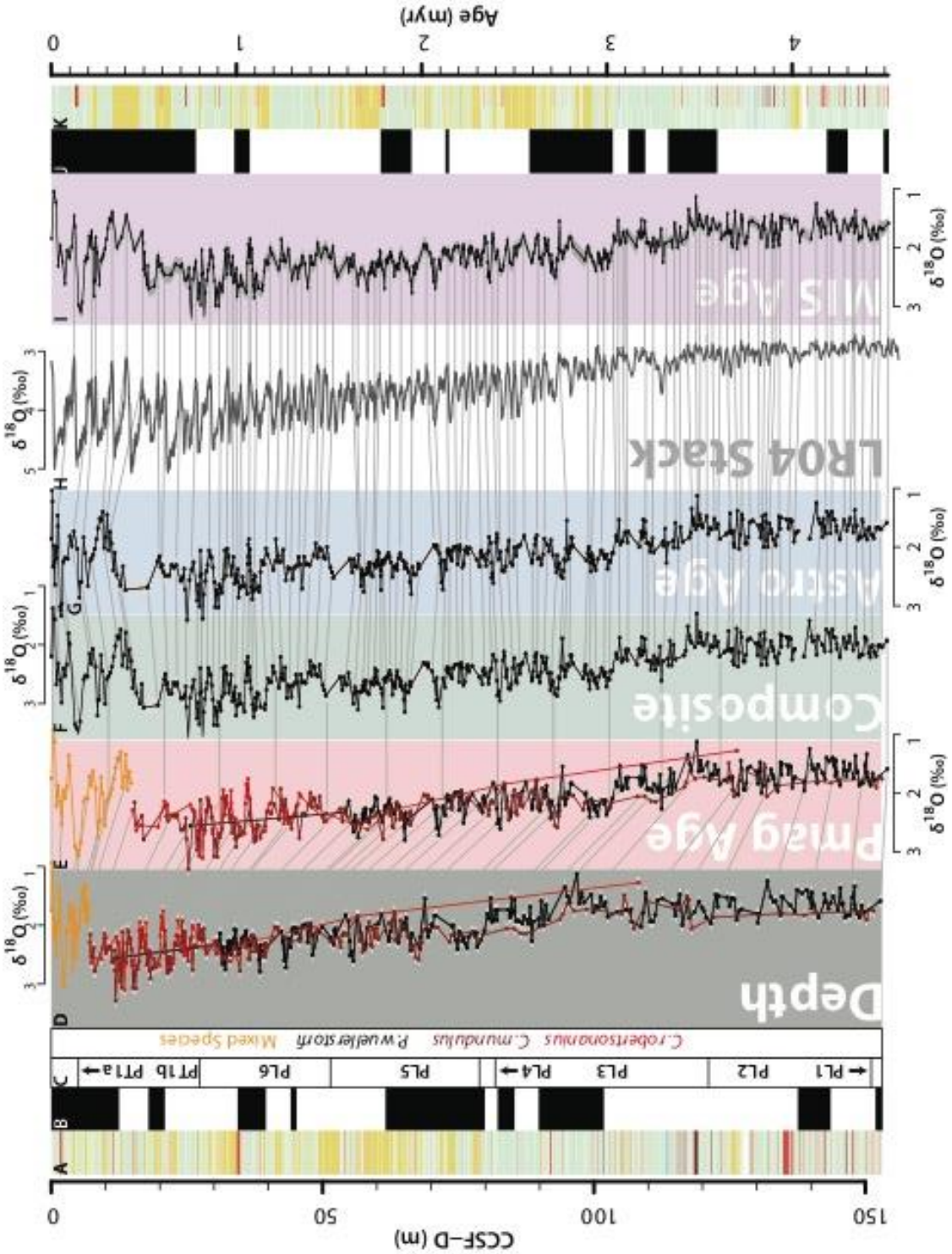

Figure 1.4. Summary of transformations from depth (CCSF-D) to Marine Isotope Ages for $\delta^{18}O$ record. 1.4.A lithostratigraphic column is spliced core description lithostratigraphy, on the CCSF-D depth scale. 1.4.B Paleomagnetic stripe is from Hatfield, *in press* (CCSF-D). 1.4.C Planktic foraminiferal biozonation is from this study,

CCSF-D, using the Zones from Wade et al. (2011). 1.4.D $\delta^{18}O$ record separates the individual species (red is *Cibicidoides robertsonanius*, brown is *Cibicidoides mundulus*, black is *Planularia wuellerstofi*, orange is mixed) and plots them on the CCSF-D depth scale. 1.4.E Pmag Age is the separated $\delta^{18}O$ records with ages as defined by a linear sedimentation rate from paleomagnetic datums. 1.4F Composite is the composite $\delta^{18}O$ record on the Pmag Age scale (see Methods). The light grey polygon behind the $\delta^{18}O$ values is the error associated with the $\delta^{18}O$ measurements (0.1‰ for P. *wuellerstofi*, and 0.14‰ for other species, see Methods). 1.4.G Astro Age employs the astrochonology generated in this study for ages. 1.4.H LR04 Stack is from Liesecki & Raymo, 2005. 1.4.I MIS Age are the ages from correlations between the composite record (1.4.G, Astro Age) to the LR04 benthic stack. Individual grey lines of correlation cannot be traced across the entire figure, instead they were chosen to elucidate the individual transformations they connect. Lines from Astro Age to LR04 Stack to MIS Age are continuous, however. 1.4.J paleomagnetic stripe is ages from Ogg et al., 2012. 1.4.K first lithostratigraphic column is the hypothetical 'no volcanics' lithostratigraphic column with age, while the second column is the true lithostratigraphic column with age. All colors follow figure CCSF-CCSFNV. All $\delta^{18}O$ scales are the same width.

1.4 Results

1.4.1 Astrochronology

Brightness (L*) in the shipboard color reflectance dataset (Expedition 340 Scientists, 2013) was found to have orbital signals. Figure 1.3 presents the entire spliced U1396 record. There is noise present throughout the record. Tuning resulted in mild offsets from the paleomagnetically derived sedimentation rate, and suggests a mostly continuous record of sedimentation at this site. It should be noted that tuning was performed attempting to fit all available chronostratigraphic information and attempting to match the results of Wall-Palmer et al. (2014) (See Discussion). Most of the deviations from paleomagnetically derived ages were modest, within the 0-50 kyr range.

1.4.2 Benthic Isotope Values

Stable isotope results largely agree with the expected glacial-interglacial cycles (Fig. 1.4.D). Variability decreases with depth. There is a gradual trend towards increasing $\delta^{18}O$ values, with a mean value of ~2‰ for 100-150 CCSF-A, increasing to ~2.5‰ for

50-10 CCSF-A. Strong >1‰ variability is seen beginning around 30 mbsf until 0 mbsf. A strong step towards higher values is observed at ~80 CCSF-A.

The offset in $\delta^{18}O$ values between the three species was calculated. Figure 1.5 depicts histograms for those values. Most $\delta^{18}O$ offsets were within the propagated instrumental error for the two $\delta^{18}O$ measurements (~0.1‰ for each measurement therefore ~0.14‰ for offsets). The mean offset between *Planulina wuellerstorfi* and *Cibicidoides mundulus* was ~0.062‰ (n=25), while *Cibicidoides mundulus* and *Cibicidoides robertsonanius* was ~-0.011‰ (n=14). Only two samples had both *Planulina wuellerstorfi* and *Cibicidoides robertsonanius*, with a mean offset of -0.105‰. No stratigraphic trends were noted with respect to the offsets, several samples with multiple species were adjacent and fell on either side of the mean values.

An effort was made to primarily use *Planulina wuellerstorfi* for the time series. It was most commonly used within 150-80 CCSF-A, with *Cibicidoides mundulus* and *C. robertsonanius* largely used until ~7 mbsf, and, due to smaller sample sizes, a mix of benthic all three species above 7 mbsf. When *P. wuellerstorfi* was not available (above 80 CCSF-A), *Cibicidoides mundulus* was used to supplement, using the offset value generated in this study (~0.062‰). In the case where *Cibicidoides roberstonanius* was the only possible choice, the offsets from *P. wuellerstorfi* to *C. mundulus* and *C. mundulus* to *C. robertsonanius* were used to calculate the composite value (green line, fig. 1.5A).

Benthic foraminiferal $\delta^{18}O$ results follow the trends established by the LR04 benthic foram stack (Lisiecki and Raymo, 2005). While the sampling resolution within this study is lower than Wall-Palmer et al. (2014), similar trends can be identified

between the planktic and benthic $\delta^{18}O$ records. Figure 1.4 presents the correlations between the astrochronologically-derived ages and the LR04 stack (grey lines). Several intervals were not correlated, either due to data-resolution issues most likely, or due to the obscuring of MIS cycles through some other means (see discussion about low benthic $\delta^{18}O$ variability below). Those include around MIS 55 (~1.6 Ma) and around KM2 (~3.1 Ma). There are several suggested changes to the interval correlated by Wall-Palmer et al. (2014), which are discussed below.

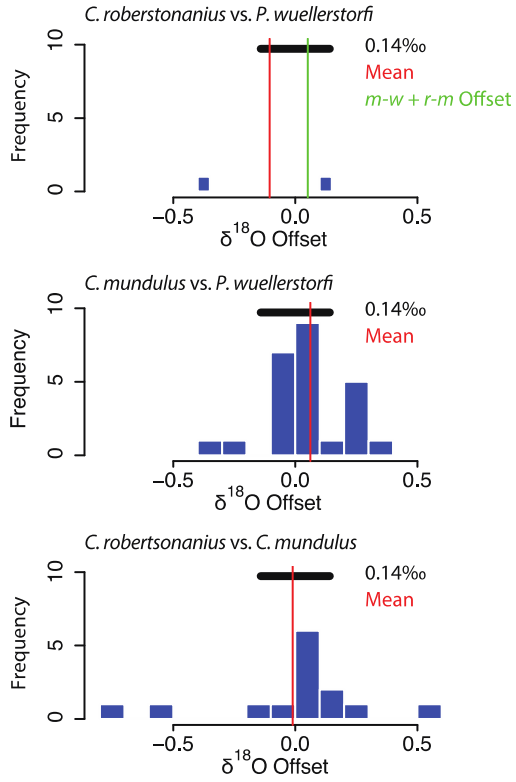

Figure 1.5. Histogram of $\delta^{18}O$ offsets between benthic species. Top panel depicts the offset between *Cibicidoides robertsonanius* and *Planulina wuellerstorfi*. For all panels, lthe arge black line depicts the combined machine errors for two measurements. The red line depicts the mean for the values within the histogram. Because there were only two samples with both species, the green line depicts the expected offset between *C. robertsonanius* to *P. wuellerstorfi* using *Cibicidoides mundulus* as an intermediary. Middle panel depicts the offset between *Cibicidoides mundulus* and *Planulina wuellerstorfi*. Bottom panel depicts the offset between *Cibicidoides robertsonanius* and *Cibicidoides mundulus*.

1.4.3 Biostratigraphy

The majority of the datums from Wade, et al. (2011) were found within the sediments at Site U1396 (Table 1.1, Figure 1.6). Only *Globorotalia hirsuta, Globoralia hessi, Globorotalia excelsa, Globoturborotalia apertura, Globoturborotalita woodi,* and *Globoturborotalita decoraperta* were not found, or were found in such sporadic occurrences they had limited biostratigraphic utility. *Pulleniatina* was not split into distinct species, instead only the presence or absence of *Pulleniatina* spp. was noted. The order of primary datums was found as expected from youngest to oldest: Top *Globorotalia tosaensis,* T *Globigerinelloides fistulous,* T *Globorotalia miocenica,* T *Dentoglobigerina altispira,* T *Sphaeroidinellopsis seminulina,* T *Globorotalia margarita,* and lastly T *Globoturborotalita nepenthes. G. fistulosus* was found only sporadically and was found above the expected range by a substantial amount of time (~0.5 myr). *G. tosaensis* appears to roughly correspond to the expected age, with ~100 kyr difference between the U1396 top and the calibrated age, but otherwise the few biostratigraphic species within the Pleistocene are found well outside their expected ranges (see discussion). Within the Pliocene, the ranges of *G. miocenica, D. altispira, S. seminulina, G. margarita,* and *G. nepenthes* all fit very closely to their expected ranges as calibrated by Wade et al. (2011).

Species Datum	Age (Ma)[a]	Age (Ma)[b]	Sample	Sample Depth CSF-B	T [CCSF-D]	B [CCSF-D]	T PMag	B PMag	T Astro	B Astro	T MIS	B MIS	Offset
T *Globorotalia flexuosa*	0.07	0.07	U1396C/1H/1, 1-2cm	0.015	-	-	-	0.000	-	0.000	-	0.000	0.070
T *Globigerinella. calida*	0.22	0.22	U1396C/4H/6, 125-127 cm	35.764	38.59	38.77	1.914	1.919	1.951	1.955	1.951	1.955	1.733
B *Globorotalia flexuosa*	0.40	0.40	U1396C/4H/3, 47-49 cm	30.723	33.31	33.33	1.724	1.724	1.742	1.742	1.754	1.754	1.354
B *Globorotalia hirsuta*	0.45	0.45	*Not present at Site*										
T *Globorotalia tosaensis*	**0.61**	**0.61**	**U1396C/1H/5, 90-91 cm**	6.905	**-**	**-**					**0.494***	**0.495***	**0.116**
B *Globorotalia hessi*	0.75	0.75	*Not present at Site*										
B *Globorotalia excelsa*	1.00	1.00	*Not present at Site*										
T *Globoturborotalita. obliquus*	1.30	1.30	U1396C/3H/3, 21-23 cm	20.953	22.01	22.51	1.129	1.154	1.106	1.124	1.116	1.140	0.172
T *Goides. fistulosus*	**1.88**	**1.88**	**U1396C/3H/6, 51-53 cm**	25.504	**27.13**	**27.31**	**1.398**	**1.407**	**1.428**	**1.438**	**1.436**	**1.456**	**0.434**
B *Globorotalia truncatulinoides*	1.93	1.93	U1396C/5H/2, 110-112 cm	39.353	43.21	43.81	2.092	2.116	2.113	2.126	2.073	2.092	0.152
T *Globigerinoides extremus*	1.99	1.98	U1396C/3H/3, 85-87 cm	21.560	22.97	23.15	1.179	1.188	1.144	1.152	1.164	1.172	0.812
B *Pulleniatina finalis*	2.05	2.04	*Pulleniatina not split*										
T *Globorotalia exilis*	2.10	2.09	U1396C/5H/2, 110-112 cm	39.353	42.96	43.23	2.082	2.092	2.108	2.113	2.064	2.073	0.022
Reappearance of *Pulleniatina*	2.26	2.26	U1396C/5H/6, 3-5 cm	43.986	48.16	48.43	2.226	2.233	2.219	2.228	2.237	2.244	0.019
T *Globoturborotalita woodi*	2.30	2.30	*Not present at Site*										
T *Globorotalia pertenius*	2.60	2.60	U1396C/6H/3, 112-114 cm	50.312	55.33	55.64	2.416	2.424	2.382	2.387	2.362	2.367	0.236
T *Globorotalia miocenica*	**2.39**	**2.39**	**U1396A/6H/2, 125-127 cm**	46.178	**49.91**	**51.46**	**2.273**	**2.313**	**2.261**	**2.297**	**2.270**	**2.288**	**0.111**
T *Globorotalia limbata*	2.39	2.39	U1396C/6H/5, 20-22 cm	52.282	57.36	57.72	2.470	2.479	2.435	2.445	2.421	2.433	0.037
T *Globoturborotalita decoraperta*	2.75	2.75	*Not present at Site*										
T *Globorotalia multicamerata*	2.99	2.98	U1396C/6H/7, 34-36 cm	55.257	60.26	60.86	2.546	2.562	2.532	2.553	2.529	2.548	0.442
T *Dentoglobigerina altispira*	**3.13**	**3.13**	**U1396C/8H/5, 27-29 cm**	71.335	**78.49**	**78.91**	**2.998**	**3.007**	**3.004**	**3.014**	**3.003**	**3.010**	**0.124**
T *Sphaeroidinellopsis seminulina*	**3.16**	**3.16**	**U1396C/8H/7, 14-16 cm**	74.080	**81.51**	**81.82**	**3.090**	**3.101**	**3.085**	**3.098**	**3.077**	**3.085**	**0.079**
B *Globigerinoides fistulosus*	3.33	3.33	U1396C/8H/5, 115-117 cm	72.165	79.77	80.37	3.029	3.049	3.035	3.049	3.025	3.035	0.300
B *Globorotalia tosaensis*	3.35	3.35	U1396A/9H/2, 19-21 cm	73.741	82.17	82.19	3.114	3.114	3.115	3.115	3.105	3.105	0.245
Disappearance of *Pulleniatina*	3.41	3.41	U1396C/9H/5, 124-126 cm	81.801	89.93	90.27	3.333	3.340	3.361	3.370	3.570	3.365	0.058
B *Globorotalia pertenuis*	3.51	3.52	U1396C/13H/2, 30-32 cm	114.688	125.84	125.86	3.993	3.993	4.000	4.000	4.025	4.025	0.505
T *Pulleniatina primalis*	3.65	3.65	*Pulleniatina not split*										
B *Globorotalia miocenica*	3.76	3.77	U1396C/13H/1, 48-50 cm	113.384	124.52	124.54	3.971	3.971	3.971	3.971	3.985	3.985	0.215
T *Globorotalia plesiotumida*	3.76	3.77	U1396A/12H/3, 38-40 cm	103.950	115.79	115.88	3.827	3.828	3.841	3.842	3.850	3.852	0.081
T *Globorotalia margaritae*	**3.84**	**3.85**	**U1396C/12H/5, 135-137 cm**	110.696	**89.85**	**89.83**	**3.331**	**3.341**	**3.359**	**3.370**	**3.355**	**3.365**	**0.490**
B *Globorotalia crassaformis* s.l.	4.30	4.31	*Present in last sample*	139.110	152.75	152.77	4.514	-	4.513	-	4.520	-	
T *Globoturborotalita nepenthes*	**4.36**	**4.37**	**U1396C/15H/6, 62-64 cm**	137.540	**150.64**	**151.10**	**4.465**	**4.475**	**4.454**	**4.466**	**4.466**	**4.475**	**0.101**
B *Globorotalia exilis*	4.44	4.45	U1396C/15H/4, 139-141 cm	135.473	148.88	148.99	4.424	4.426	4.405	4.408	4.426	4.429	0.022
B *Sphaeroidinellopsis kochi*	4.52	4.53	U1396C/14H/6, 60-62 cm	128.202	140.06	140.08	4.234	4.234	4.232	4.232	4.232	4.232	0.298

Table 1.1. Table of planktic foraminifera biostratigraphic datums. Bolded lines denote datums used as primary zonal markers, unbolded lines denote secondary datums. Age columns are from Wade et al., 2011. a denotes an age calibrated to the Cande and Kent, 1995 time scale, while b denotes calibration to the Lourens et al., 2004 astrochronological timescale. Sample is the highest or lowest sample in which the species was found. Sample depths CSF-B uses the midpoint of the sample depths, and the shipboard composite depth scale. T [CCSF-D] and B [CCSF-D] is the possible range in depths for each datum. T PMag and B PMag is the range in age for each datum, derived from the

linear paleomagnetic ages. T Astro and B Astro is the range in age for each datum, derived from the astrochronological tuning. T MIS and B MIS is the range in age for each datum, derived from the correlation to the LR04 benthic $\delta^{18}O$. Offset is the difference between the midpoint MIS age and the astrochronologically tuned calibrated age (Wade et al., 2011). * denotes ages presented in Wall-Palmer et al. (2014). *Globorotalia flexuosa* was found in the first sample, while *Globorotalia crassaformis* s.l. was found in the last sample, and so neither datum has a true top or bottom, respectively.

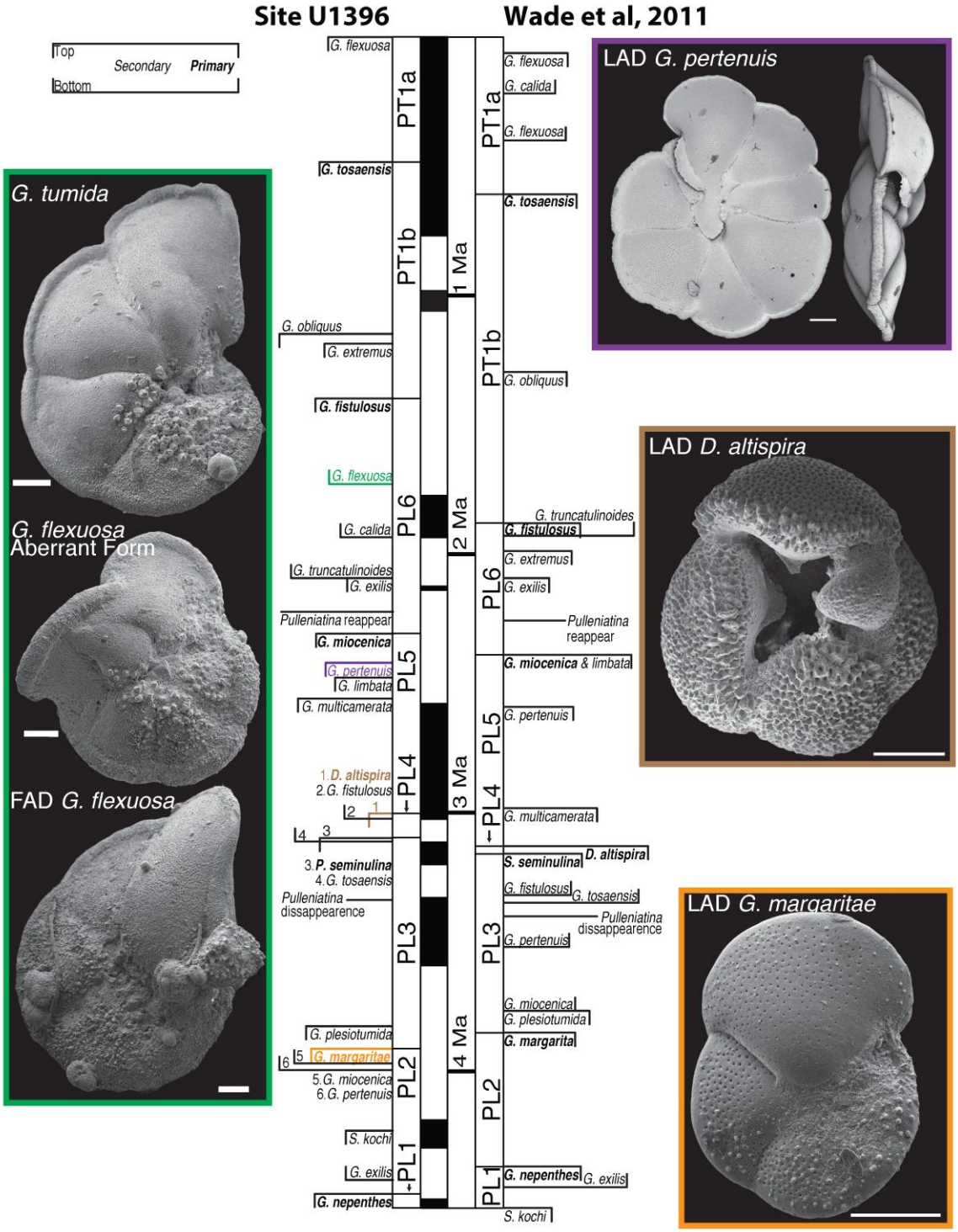

Figure 1.6. Summary of differences between Wade et al., 2011 age datums and findings at U1396 with important Scanning Electron Micrographs (SEM). Ages for the biostratigraphic datums are presented as MIS ages, with the horizontal line corresponding to the chronostratigraphic position of the top or bottom. Primary datums are bolded. Colored datums correspond to the SEMs at the sides of the figure. SEMs are either from

the sample in which the datum was recorded (*Globorotalia pertenuis*) or nearby core catcher samples. Core catchers are not the precise bottom, as cc samples were not included in the splice. They are close, however. All scale bars are 100 µm. *Globorotalia tumida*, G. flexuosa (Aberrant form), and *G. flexuosa* are from sample U1396C/3H/cc. *Globorotalia pertenuis* is from sample U1396C/6H/3, 112-114 cm. *Dentoglobigerina altispira* is from sample U1396C/8H/cc.

Secondary datums T *G. obliquus*, T *G. exilis*, B *G. truncatulinoides*, T *G. limbata*, T *G. pertenuis*, B *G. tosaensis*, B *G. miocenica*, T *G. plesiotumida,* and B *G. exilis* were all found close to their calibrated ages. The bioevents Reappearance and Disappearance of *Pulleniatina* were also extraordinarily close to their calibrated ages. In particular, several of the menardellid species (e.g., *G. exilis*) were subject to substantial fluctuations in population, and so their adherence to the calibrated ages is surprising, but a positive indicator of robust planktic foraminiferal datums.

Several secondary datums, as could be expected, did not conform as precisely to the expected ages as the above. T *G. flexuosa* was observed within the top sample, and its base (B *G. flexuosa*) was found ~1.3 myr earlier than expected. The local top for *G. extremus* was 800 kyr younger than it was expected. T *G. multicamerata* was ~400 kyr younger than the expected age, but as mentioned previously, all menardellids were subject to substantial fluctuations in population. B *G. miocenica* appears within the U1396 sediments ~200 kyr older than its calibrated age, while B *G. pertenuis* appears 500 kyr older than the calibrated base. T *S. kochi* occurs ~300 kyr younger than the calibrated age.

1.4.4 Hiatuses

Shipboard chronostratigraphy suggested a gradually decreasing sedimentation rate towards the present (Expedition 340 Scientists, 2013). It also suggested a largely continuous section, with minimal hiatuses. Biostratigraphy largely agrees with the

paleomagnetically derived sedimentation rates, and clustering of biostratigraphic datums, as would be characteristic of a hiatus, is not observed in the U1396 sequence. While hypothetically evolutive harmonic analysis can be used to identify hiatuses (Meyers and Sageman, 2004), the use of such a large window (140-kyr) and the amount of noise within the signal makes this not possible at Site U1396. Astrochronology does suggest that there are instances of lowered sedimentation rate. In the absence of strong evidence for hiatuses, the U1396 benthic and planktic $\delta^{18}O$ isotope time series was correlated to marine isotope stages as if there were no hiatuses. If strong sedimentological, biostratigraphic, or other evidence were uncovered within these sediments for hiatuses, this would change the correlations to the marine isotope stages, and thus the inferred ages of the sediments themselves.

1.5 Discussion

This study continues much of the data collection begun in Wall-Palmer et al. (2014). In doing so, some conflicting age diagnostic criteria were revealed within 10's of cm from the base of the Wall-Palmer study, suggesting a revision of that chronostratigraphy may be necessary. For example, Wall-Palmer et al. (2014) used the %*Globorotalia menardii* zonation scheme (Ericson & Wollin, 1968; Kennett and Huddlestun, 1972), successfully employed repeatedly in the region (e.g., Reid et al., 1996; Le Friant et al., 2008). This scheme relies on the relative abundance of *Globorotalia menardii* or *Globorotalia tumida* (the majority of the flat keeled planktic foraminifera within these sediments). The zonations are described as abundant (Z, X, V, and T) or not abundant (Y, W, and U). Determining between 'abundant' and 'not abundant' is not always distinct, as they are in these sediments (Figure 1.7, W to early V).

Here we continued the %G. *menardii-tumida* counts down to the Brunhes-Matuyama reversal, identifying distinct proportion changes centimeters below the lowest sample analyzed by Wall-Palmer et al. (2014). These changes in %*G. menardii-tumida* place the chronostratigraphy suggested by Wall-Palmer et al. (2014) in doubt.

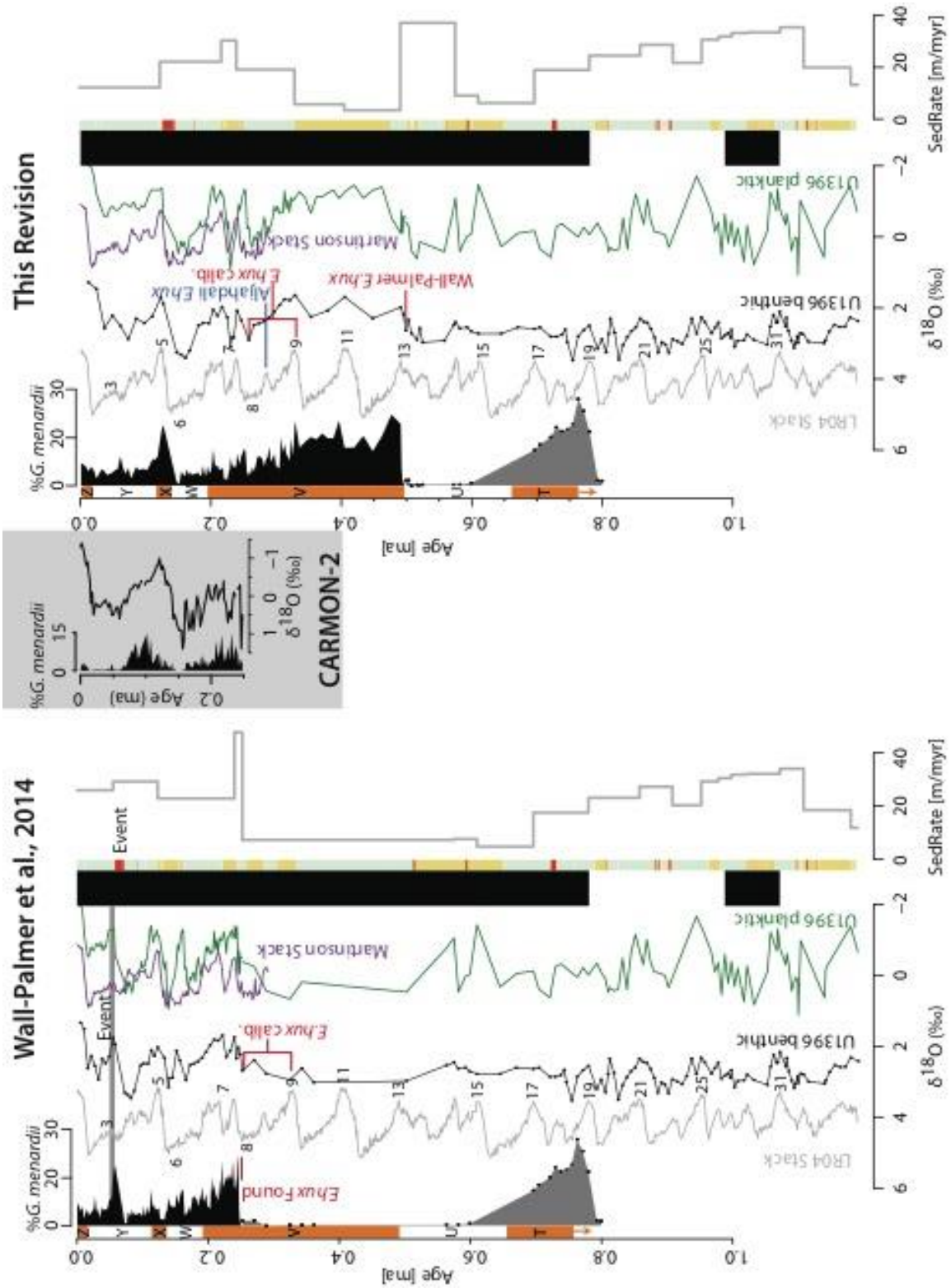

Figure 1.7. Summary of the two contrasting interpretations for the Brunhes chron chronostratigraphy. The left panel depicts the Wall-Palmer et al. (2014) interpretation, with this revisions correlations starting at MIS 15. The right panel depicts the proposed

revision to the stratigraphy. Orange *Globorotalia menardii* zonation scheme is depicted as correlated to the marine isotope stages by Reid et al. (1996) which ends within zone T around MIS 19. LR04 Stack in grey is the Liseicki and Raymo (2005). The purple line is the planktic foraminiferal oxygen isotope stack of Martinson et al., 19XX. Black polygon is the % *G. menardii* from Wall-Palmer et al. (2014), while the grey is the newly generated data from this study (points denote samples counted). The *Emiliana huxleyi* FAD datum within the left panel is the datum employed in Wall-Palmer et al. (2014), with the calibrated ages from Ogg et al. (2014), roughly correlates to MIS 8 in the Mediterranean Sea. Blue line refers to the new *E. huxleyi FAD* (Aljahdali; unpublished Masters Thesis). Green line is the *Globigerinoides ruber* data from Wall-Palmer et al. (2014), with new data starting at roughly MIS 8 on the left panel, and MIS 13 on the right panel. Black rectangles are the paleomagnetic chron interpretation from Hatfield, *in press*. Sedimentation rates are calculated as m/myr. Stratigraphic columns follow figure STRAT CCSF-D. Slight offset in event bed from Wall-Palmer et al. (2014) is due to the calculation of sediment ages and slight misfit in the correlated ages. The event bed is the same as topmost volcanic unit.

The most important chronostratigraphic control used by Wall-Palmer et al. (2014) in the lower part of their study interval was the base (B) of *Emiliana huxleyi*. The B *E. huxleyi* globally occurs within MIS 8 (~0.27 Ma) or MIS 9 (~0.29 Ma; Ogg et al., 2014). It was identified at ~6.9 m with SEM imaging (Wall-Palmer et al., 2014), but other studies (Aljahdali, 2013, unpublished Masters Thesis, Florida State University) place the first occurrence much higher (~3 m). In addition, the planktic foraminifera datum for Biozones PT1a/1b, T *G. tosaensis* (~0.61 Ma; Wade et al., 2011), was determined to be slightly below the *E. huxleyi* datum. Within the original publication, this was suggested to be a regional difference in extinction, with T G. *tosaensis* occurring at MIS ~8 (0.27 Ma), which is ~340 kyr offset from its calibrated age (Wade et al., 2011).

Three possibilities remain to explain these discrepancies. First, if the revised stratigraphy proposed in fig. 1.7 is incorrect and Wall-Palmer et al. (2014) is correct, the Aljahdali datum is 3 m too high, and there is a condensed section encompassing MIS 13 to 9. This then suggests that MIS 3, 5, and 6 $\delta^{18}O$ values are roughly equivalent, rather than the substantially glacial-interglacial change magnitudes normally associated with

those stages. Also, the %*G. menardii-tumida* zonation then has a much weaker connection to the glacial-interglacial cycles, in particular the predicted abundances through zone V are absent. It should be stated, however, that B *E. huxleyi* is a well-established datum, with a consistently robust MIS 8 appearance within the tropics (Thierstein et al., 1977; Ogg et al., 2012), and as such, should have a higher chronostratigraphic priority than a comparably rougher abundance-based zonation scheme.

Second, if the Wall-Palmer et al. (2014) datum is valid and the Aljahdali datum is incorrect, and the rest of the Wall-Palmer et al. stratigraphy is not, then this would represent a >100 kyr earlier origination for *E. huxleyi* than previously identified. As stated above, B *E. huxleyi* has a remarkably globally synchronous first appearance at MIS 8 (Thierstein et al., 1977). Here, it would have to occur within MIS 13. This scenario to solve the discrepancy seems unlikely.

Lastly, if the Wall-Palmer et al. (2014) B *E. huxleyi* datum is skewed by downhole contamination, then the Aljahdali B *E. huxleyi* is the first *in situ* occurrence. The sample cited for the B *E. huxleyi* by Wall-Palmer et al. (U1396/1H/5 90-91 cm) only contained rare *E. huxleyi*, while the only other samples examined above (U1396/1H/1 1-2 cm, U1396/1H/1 30-31 cm) contained abundant *E. huxleyi*. The sediments used for SEM analysis were procured in the proper fashion (sample edges were trimmed to minimize down-hole contamination, for example; Wall-Palmer, pers. comm. 2015), the rarity of the nannofossil within those sediments possibly suggests that they were not in place, and were a product of downhole contamination. This could account for the ~3 m difference between the two studies. By removing the Wall-Palmer B *E. huxleyi* control on the

chronostratigraphy, we can then fit to several other chronostratigraphic systems. For example, *G. menardii* Zones X and V fit. MIS 6 no longer has a negative $\delta^{18}O$ excursion (MIS 6.4 in Wall-Palmer et al., 2014; MIS 7 in this revision). B *G. tosaensis* has a smaller offset to the calibrated age. The remainder of this work employs this last hypothesis as the age model, though we appeal for further chronostratigraphic work within the Brunhes chron at Site U1396 to help solve this dilemma.

1.5.1 Biostratigraphy

The Pleistocene has only a couple of the datums found where they expected at Site U1396 relative to the calibration by Wade et al. (2011). *G. tosaensis* and *G. obliquus* appear to have a robust calibration from the Caribbean perspective. This is perhaps a function of the limited number of datums within the Pleistocene, relative to Pliocene. Both of the youngest datums, T *G. flexuosa* and B *G. calida,* appear to have substantially different ranges than calibrated. For B *G. calida,* this is possibly due to regional differences between the Pacific Ocean (the calibration is from DSDP Leg 135; Chaproniere et al. 1994) and the Caribbean Sea. *G. flexuosa* is also found far earlier than expected. The most diagnostic feature of *G. flexuosa* is a ~90° twist on the final chamber, with the rest of the gross morphology resembling an intermediate form between *Globorotalia menardii* and *Globorotalia tumida.* Figure 1.6 (green box) depicts *G. tumida* and *G. flexuosa,* from the sample containing Base *G. flexuosa.* Also within that sample, very rarely, was an aberrant form of *G. flexuosa* or *G. tumida* with a final chamber appearing to start at 90° to the coiling axis, then twisting back equatorially. This could speculatively be seen as evidence that the '*flexuosa*' form is a simple mutation from the *Globorotalia menardii* sensu stricto, one which induces ~90° torsion in the

growth of the final chamber and is not a true biological species. Further work could elucidate if there is an ecological affinity to the '*flexuosa'* form, or if it has a stochastic appearance in the fossil record, as would be expected of a random mutation of the form. Both of these species, *G. flexuosa* and *G. calida,* have recognition issues as they progress through ontogeny. An adult *calida* resembles a juvenile *Globigerinella aequilateralis,* while *G. flexuosa* without the final chamber would be identified as a *G. tumida* or *G. menardii.* As impoverished as the Pleistocene is for datums, these are still poor characteristics for biostratigraphic marker taxa.

These two biostratigraphic datums were used repeatedly shipboard during Exp. 340. The majority of the sites recovered were younger than any primary planktic foram marker datum, and so these secondary datums had to be regularly employed. Finding these two taxa outside of their expected ranges at Site U1396 calls into question many of the biostratigraphically-derived ages for other sites drilled during Exp. 340. Many of those other sites, however, have nannofossil biostratigraphic datums as well, and those are more robust through this interval. Those ages, which were supported by the B *E. huxleyi,* for example, the nearest nannofossil datum to B *G. calida* (calibrated age), are still valid.

There are comparatively more datums within the Pliocene than the Pleistocene that conform to expectations. Closest to the Pliocene/Pleistocene boundary is B *G. truncatulinoides,* which perhaps should be employed as the PL6/PT1b zonal marker, instead of T *G. fistulosus.* The difference between the Pliocene/Pleistocene boundary and the top of PL6 would only change ~120 kyr, and *G. truncatulinoides* is more common, at least in these sediments, than *G. fistulosus.* Both taxa are easily recognizable, the only

advantage that *fistulosus* has over *truncatulinoides* is that the projections from a *fistulosus* test are readily identifiable even when broken. Most of the menardellid top calibrations were accurate at U1396, excluding T *G. multicamerata.* The spacing between the events at U1396, however, were somewhat condensed, all taking place within Chron C2r. The B *G. fistulosus* occurs later than expected, within the wrong biozone. This species is very sporadic throughout its entire range (including the upper portion of the range), making both the first and last occurrences suspect. The T and B *G. exilis* were observed in close proximity of the expected age, though not always within the biozone expected, due to deviations in other marker taxa.

ODP Site 999 is a nearby location within the Caribbean Sea, making it a good comparison for this study. This study replicates the order of bioevents determined at Site 999 (Chaisson & D'Hondt, 1999) with few differences, though this study uses more datums (as more datums have been calibrated since 1999). The order of T *G. miocenica* and T *G. limbata* were reversed relative to U1396. This is not a substantial issue, as calibrations suggest these two occur within <10 kyr of each other. T *G. fistulosus* appears to have occurred closer to the expected age at Site 999, suggesting the persistence of *G. fistulosus* may simply be a local issue. *G. pertenuis* occurs closer to the calibrated age at Site 999 than it does at U1396, based on bioevent order. This again suggests a local mismatch in found age vs. calibrated age. Lastly, either *G. nepenthes* occurs later than it does at U1396, or both *G. exilis* and *G. plesiotumida* occur earlier. While *G. nepenthes* is the primary marker, *G. exilis* and *G. plesiotumida* are both found at almost precisely their calibrated ages, suggesting perhaps a local mismatch at Site 999, rather than Site U1396.

Largely, however, the order of bioevents at Site 999 corroborates the findings of Site U1396, and the order of datums found within it.

1.5.2 Sedimentation

1.5.2.1 Age Scheme Mismatch

This study employs three different age models, purely-paleomagnetic, astrochronologic (between paleomagnetic datums), and marine isotope stage correlations. These different methods have individual strengths and weaknesses. Paleomagnetic ages are precise, as the ages of the reversals are well known, but the accuracy is increasingly poor as time between reversals increases. Astrochronology provides variable accuracy and precision. The analysis utilizes a number of different parameters, like window size or interpolation step, that all change how responsive the resulting age model is to hiatuses or changes in sedimentation rates, or the upper and lower limits of detectable frequencies. Lastly, MIS correlation is generally precise, and provided all marine isotope stages are present, is difficult to do incorrectly. It also has the advantage, if the data-resolution is high enough to detect them, that extremely abrupt sedimentation rate changes can be observed. The same hypothetical abrupt sedimentation rate would be missed by paleomagnetic ages if it were within a single normal or reverse chron. Similarly, the change in sedimentation rate would be smoothed by astrochronology if the window size were not small enough to detect it. However, if all marine isotope stages are not present, or if data density is poor, then correlation becomes less accurate. Because of the three different characteristics of these age models, it is possible to demonstrate the advantages of the different models of age estimations by looking at their offsets.

The three non-biostratigraphic age schemes agree well as seen in the Figure 1.8, when excluding the Brunhes chron (see discussion of Wall-Palmer et al., 2014 above). Figure 1.9 presents the differences in ages between the various methods of age estimation, paleomagnetically-derived minus marine isotope stage (Mag-MIS) and paleomagnetically-derived minus astrochronologically-derived (Mag-A). When not considering the Brunhes chron, the Mag-MIS offset is typically larger than Mag-A. This suggests that the astrochronology is underestimating high sedimentation rates and overestimating low sedimentation rates, if we assume that the MIS ages are near-instantaneous estimates of the sedimentation rate. In intervals where Mag-MIS is smaller than Mag-A, the MIS age seems to be reacting to changes in sedimentation rate more quickly than the astrochronologically-derived ages. Again, this is a weakness of this particular astrochronologic age model, likely due to the large window size, which imparts a 'lag' on the changes in sedimentation rate. A larger window size would mix frequencies over a larger interval, and so react more slowly to changes in sedimentation rate while a smaller window size would react more quickly. Again, the larger window-size was used here to account for the noise in the dataset.

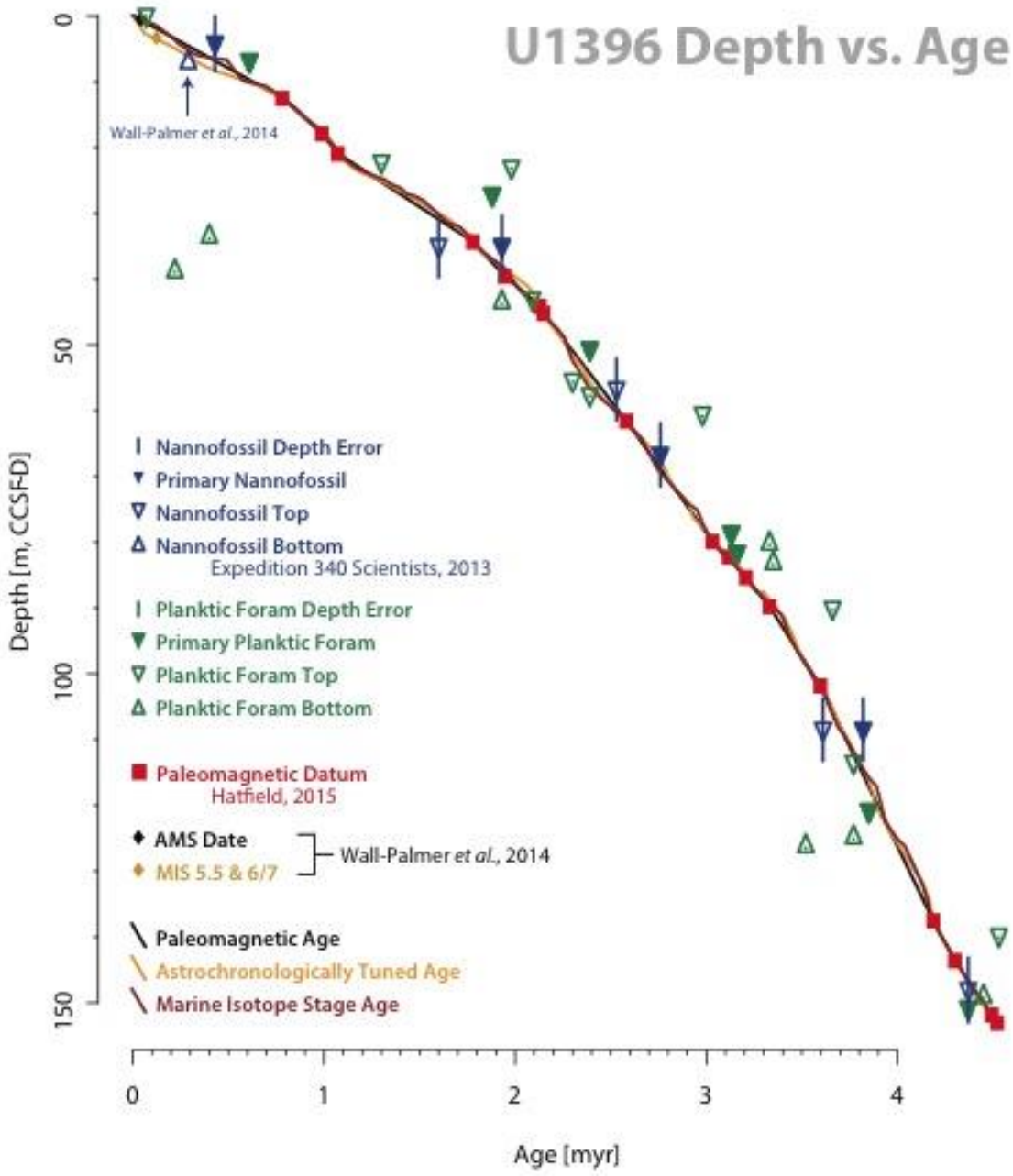

Figure 1.8. Summary of the age vs. depth relationship of the Site U1396 sediments. Paleomagnetic datums are depicted in red squares, depths are from Hatfield, *in press*, ages from Ogg et al. (2012). The nannofossil datums are depicted in blue triangles, open for secondary and closed triangles for primary. Depths for nannofossil datums are from Expedition 340 Scientists (2013) unless noted as being from Wall-Palmer et al. (2014), ages are from Backman et al. (2012). The vertical blue line denotes uncertainty in true stratigraphic position of datum. Planktic foraminifera datums are depicted in green triangles, open for secondary and closed triangles for primary. Depths are from this study, ages are from the Wade et al. (2011) astrochronological calibration. Vertical line denotes uncertainty in true stratigraphic position of datum. The black diamond denotes a ^{14}C date

(Accelerator Mass Spectrometry AMS), and yellow diamond denotes MIS 5.5 & 6/7, identified within Wall-Palmer et al. (2014). The black line depicts a linear interpolation for sediment age between paleomagnetic datums. The orange line depicts the ages from the astrochronological tuning. The brown line depicts the ages from the $\delta^{18}O$ correlation to the Marine Isotope Stages (MIS) within the LR04 benthic $\delta^{18}O$ stack (Liesecki and Raymo, 2005).

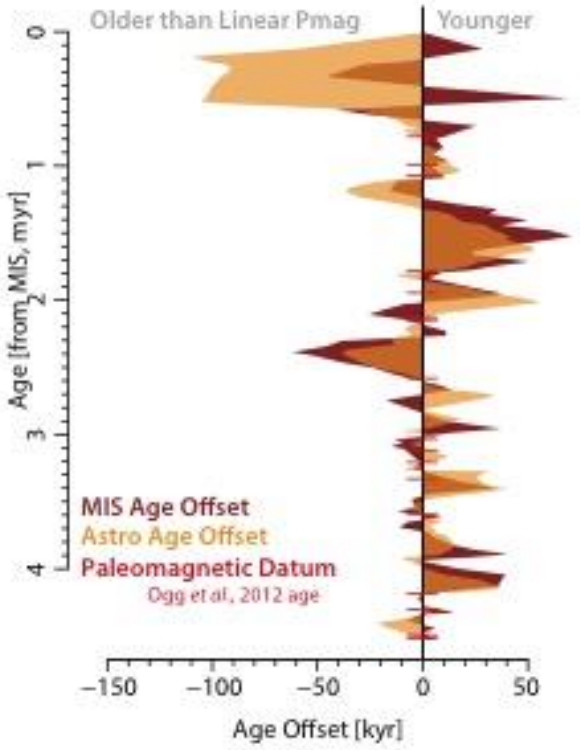

Figure 1.9. Summary of differences in different methods of age calculation. The orange polygon represents the difference between the astrochronological ages and the paleomagnetic age for each sample included in the isotope record. The brown polygon represents the difference between the Marine Isotope Stage ages and the paleomagnetic age for each sample included in the isotope record. The red horizontal lines correspond to the ages of paleomagnetic reversals (Ogg et al., 2012).

All offsets between the various age models were minimal, and generally smaller than time between isotope stages. This suggests that while the above discussion is valid, the paleomagnetically-derived ages are quite robust, and skipping the 'tuning' step within the methods would likely have not changed the MIS-correlations. This also strongly suggests that this is a fairly continuous section, excluding perhaps some portion of the Brunhes chron.

1.5.2.2 Sedimentation Rates

The sedimentation rate is calculated in several different forms. First, a linear sedimentation rate was calculated from the paleomagnetic datums, both including volcanics (red) and without (blue) (Figure 1.10). The difference between these two, or a volcanic accumulation rate, is in purple. The non-volcanic, or hemipelagic, sedimentation rate is somewhat different than previous studies. Shipboard chronostratigraphy described a roughly monotonic decrease in sedimentation rate from 0 Ma to ~4.5 Ma (Expedition 340 Scientists, 2013), which is seen in the total sedimentation rate (red line, fig. 10). When the thickness of the volcanically sourced sediments is removed (blue line, fig. 10), the monotonic decrease in rate disappears and the sedimentation rates resemble a step-function. When viewed as a step function, sedimentation rates are ~4 cm/kyr until ~2.2 Ma and ~2 cm/kyr after, partially owing to the increasing thickness of the volcanically sourced beds from ~3.5-4.5 Ma (purple line, fig. 10), which account for ~1 cm/kyr of the sedimentation rate. Alternatively there is a gradual decline in sedimentation rate from ~3.5 to ~2.1 Ma, with higher rates before and lower rates after. Either interpretation removes the monotonic increase seen in the sedimentation rate, which includes both volcanic and hemipelagic sedimentation.

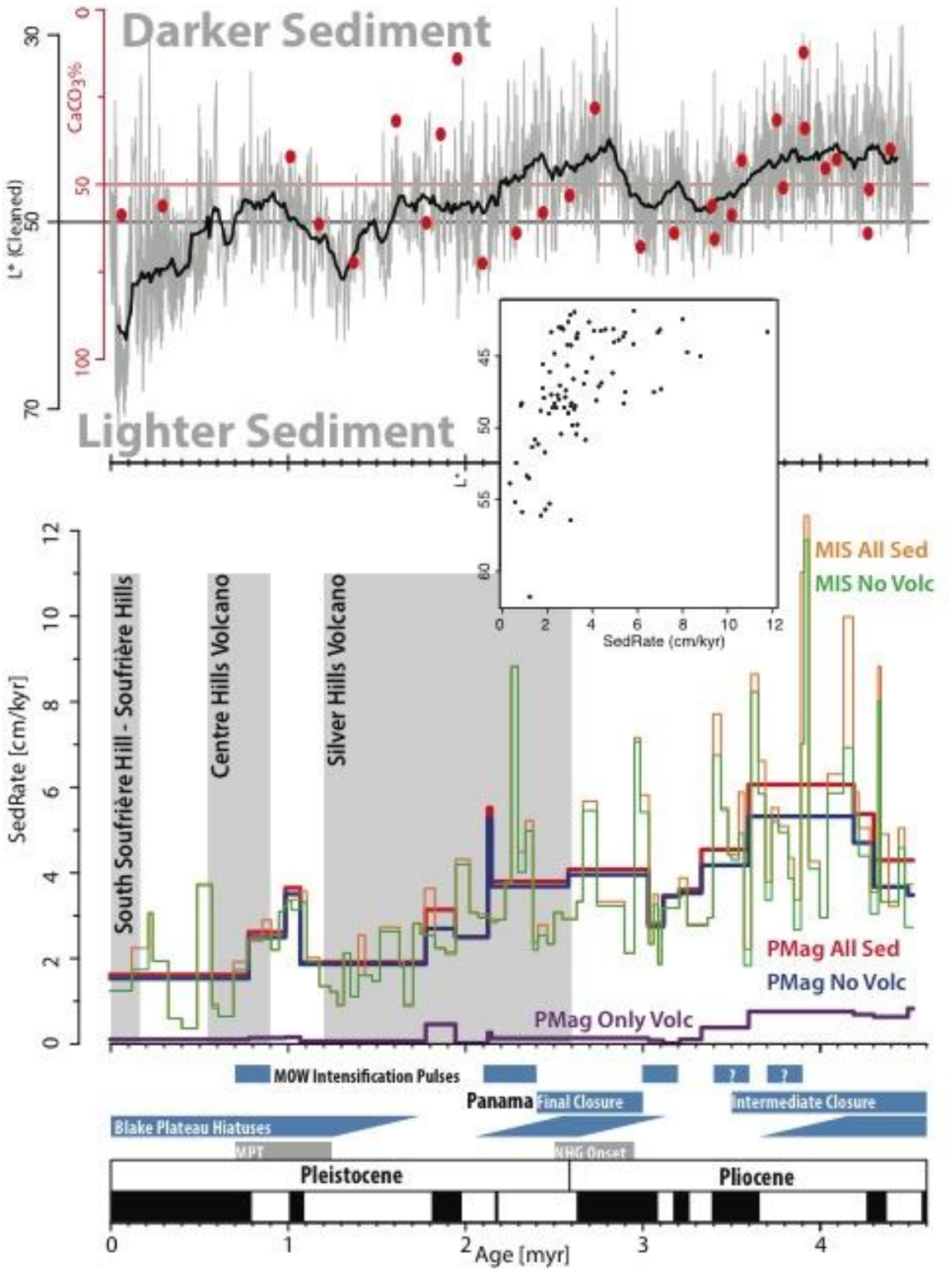

Figure 1.10. Summary of sedimentation rates, paleoceanographic events, and sediment character. Upper panel depicts the L* (brightness) parameter from shipboard measurements. Black line represents a 100-kyr running mean. Red dots are discrete

$CaCO_3$% measurements from shipboard geochemistry. In the bottom panel, paleomagnetically derived sedimentation rates are in red (all sediment types), blue (no volcanic sediments), and purple (only volcanic sediments). MIS-age derived sedimentation rates are in orange (all sediment types) and green (no volcanic sediments). Inset depicts the correlation between L* and MIS No Volc sedimentation rates. Blue boxes represent several pertinent paleoceanographic events (see discussion for citations and numerical dates), while grey depict climatic events.

The sedimentation rate constructed from the marine isotope correlations is much more volatile than the paleomagnetically-derived sedimentation rates, but still follows the rough trends laid out by the paleomagnetic rates. The rates are particularly volatile prior to 2 Ma. Rates are ~6 cm/kyr until ~3.65 Ma, then drop to ~4 cm/kyr from ~2.15-3.65 Ma. There is a slow decline in the rates from ~4 cm/kyr to ~2 cm/kyr from ~2.5- ~1.5 Ma. There is a pulse of sediment roughly coincident with the middle Pleistocene Transition (MPT), with rates varying between ~4 and <1 cm/kyr afterwards. Brightness (L*) shows a particularly good agreement with the sedimentation rates. Figure 1.10 depicts the sedimentation rates, with the black line representing a running mean of L* with a 100 kyr window to remove higher frequency glacial-interglacial cycles and examine only the longer-term trends. There is a strong significant correlation between sedimentation rate and L* (See fig. 1.10 inset, p value < 0.001). This connection demonstrates the lighter sediments (higher L* values) were deposited at a slower rate than the darker sediments (lower L* values). $CaCO_3$% data, from shipboard geochemistry, shows a weak correlation to the L* values throughout the entire record, however qualitatively there are intervals where it appears sediment carbonate content may be driving the L* changes (e.g., 3-4 Ma). While geochemical sampling attempted to avoid the influence of volcanic sediments and sample purely hemipelagic sedimentation, the distinct possibility that carbonate-free volcanic material, in the form of cryptotephra

(dispersed ash), may be influencing the $CaCO_3$% data was suggested by Expedition 340 Geochemistry.

1.5.2.3 Local Volcanism / Regional Effects

There are several possible explanations for the L* to sedimentation rate correlation. First, the additional input of dispersed volcanogenic sediment could strongly affect sedimentation rate. The 3.5-4.5 Ma interval has ~1 cm/kyr observed volcanic sedimentation, while overall the sedimentation is ~4 cm/kyr. If we assume, for the sake of discussion, that the flux of purely hemipelagic sediment is constant throughout the entire interval at ~2 cm/kyr (~0-2 Ma rough average sedimentation rate), there is ~1 cm/kyr of unaccounted for sedimentation in the 3.5-4.5 Ma interval. As the observed volcanically-derived sedimentation is highest throughout this interval, it seems possible that the undetected dispersed ash, or cryptotephra, throughout that interval might be high as well. The lower L* value agrees with elevated cryptotephra, as dispersed ash would darken the sourrounding sediments. There are pulses of volcanic sediment at ~1.9 Ma which also coincide with inflections in the brightness. This hypothesis, however, breaks down when considering the local volcanic history. The Silver Hills Volcano on Montserrat was active ~ 2.6 to ~1.2 Ma, and the general trend through this interval at Site U1396 is one of increasing brightness and presumably less volcanic ash and other volcaniclastic sediments. While the volcanic sediments could be sourced from elsewhere, it seems likely that the growth of Montserrat should have a substantial impact on U1396. If this hypothesis of sedimentation rate changes being purely volcanically driven is true, then one would expect that the growth of the nearest volcano to have an impact. Rather, the data suggest less volcanic influence as Montserrat grows.

1.5.2.4 Gateway Changes

The closure of the Isthmus of Panama had a profound effect on the oceanography of the Caribbean Sea. Bottom water closure was completed by ~4.5 Ma (Keigwin 1982; Haug and Tiedemann, 1998). Other portions of the Central American Seaway (CAS) history are somewhat controversial (for a discussion see Molnar, 2008), owing somewhat to the prolonged nature of the closure, or the idea that sea level changes derived from glacial-interglacial cycles could have closed and opened the gateway repeatedly (e.g., Groeneveld et al., 2014). At ~4.2 Ma there is evidence that there is no more oceanographic exchange through the CAS (e.g., Jain and Collins, 2007), though other authors place 'final closure' later (~3.2-3.6 Ma; Haug and Tiedemann, 1998). At the most extreme, land animal exchange between continents is observed at 2.7 Ma, offering a youngest-limit to the closure history. At 4.2 Ma there is a substantial drop in productivity, observed in multiple lines of evidence from benthic foraminiferal assemblages and $\delta^{13}C$ time series at Site 999 (Jain and Collins, 2007). Chaisson (2003) observed a distinct change in menardellid evolution between the Atlantic and Pacific Oceans, the Caribbean Sea forms occupying higher and more oligotrophic conditions. Both productivity and menardellid evolution are linked the CAS closure, which is thought to displace the locus of productivity and upwelling to the Pacific Ocean while the Caribbean Sea experiences the growth of oligotrophic conditions. This expansion of oligotrophic conditions is seen during the interval of highly variable, or 'pulsed' sedimentation rates at U1396. The sediments at U1396 are largely biogenic so there must be a link between productivity and sedimentation rate. This link is not as simple as higher productivity equals higher sedimentation rate though, as factors like bottom water corrosiveness, siliceous vs.

carbonate productivity, or bottom water current strength, among many others, alter the sedimentation rate as well. The confluence of oligotrophic indicators from Site 999 and pulsed rates at Site U1396 suggest a possible, though counter intuitive, link.

The closure date of ~3.2-3.6 Ma comes from an examination of $\delta^{13}C$ benthic records and % sand content of carbonate. Between 4.6-3.6 Ma the lysocline appears to have lowered, and Caribbean bottom water shows an affinity to values seen in the deep Atlantic Ocean (Haug and Tiedemann, 1998). This deepening in lysocline is viewed, in the Haug and Tiedemann (1998) model, to be due to increase North Atlantic Deep Water formation and increased thermohaline circulation, driven by increased salinity contrast from the Pacific to Atlantic Oceans. Changes in bottom water and lysocline position could explain higher sedimentation rates, provided the lysocline or bottom water were fluctuating enough to explain the more variable rates. There is also no obvious change in preservation as would be expected if dissolution were controlling the sedimentation rate. There is only the trend of fewer well preserved foraminifera with depth, as is expected.

The lower L* values with higher sedimentation rates suggest that biogenic silica could be driving the sedimentation in the lower Pliocene of Site U1396. The sedimentation rate also appears to possibly contain obliquity-forced cycles during the volatile interval, obliquity cycles having been previously seen in productivity indicators at other locations during the Plio-Pleistocene (e.g., Bolton et al., 2010). The link at Site U1396, however, is highly speculative. The correlations between the $\delta^{18}O$ U1396 data and the MIS LR04 stack is, through the highly volatile sedimentation rate interval, based on smaller changes in $\delta^{18}O$ because of the smaller glacial-interglacial changes at those times. The time between correlation points is also fairly small, and so minor changes in

the points used for correlations could produce substantial impacts on sedimentation rates. The high variability is, however, still seen in the astrochronologically-derived sedimentation rates (not shown). The extreme swings in sedimentation rate also suggest that even if MIS stages were moved by 10's of cm the magnitude of the pulses in rate may change, the pulses would remain. The high rates also do not correspond to either extreme glacials or interglacials. Indeed, indicators for high seasonality were observed in the benthic analysis at Site 999 (Jain and Collins, 2007) prior to the final closure at ~4.2 Ma. The pulses in sedimentation may indicate that Site U1396, closer to the equatorial Atlantic Ocean, experienced elevated productivity longer than at the more central Caribbean Sea Site 999, or that a long term trend toward more oligotrophic conditions was punctuated by intervals of higher productivity.

There are several ways to test if these two scenarios of pulsed sedimentation rate driven by pulses of productivity. Assemblage counts of the biota, either foraminifera or nannofossil, should respond to changes in the upper water column. Mixed-layer to benthos $\delta^{13}C$ gradients should also depict changes in production, provided the longer term trends were removed from the analysis, as well as changes due to glacial-interglacial intervals. Examination of the magnetic susceptibility data could determine if there were periods of increased terrestrial input, which could drive the pulsed productivity. Lastly, if siliceous diatoms or calcareous nannofossils were the driver of the pulsed sedimentation, a series of smear slides during several high and low intervals could determine changes in their abundance.

There are other gateway changes that could have played a role in controlling sedimentation at Site U1396. Mediterranean Outflow Water (MOW) enters the Atlantic

Ocean through the Strait of Gibraltar and is an important component of Atlantic Ocean circulation patterns. Evidence from the Gulf of Cadiz, off the Portugal coast, suggests periods of intensification in MOW strength at 0.7-0.9, 2.0-2.4, and 3.0-3.2 Ma (Hernández-Molina et al., 2014). If this water were to flow into the Caribbean Sea at times, MOW would be the deepest water-mass in the Caribbean Sea due to its high salinity, and thus high density. There is an established glacial-interglacial control on the water entering the Caribbean over the past 200 kyr, with more corrosive Antarctic Intermediate Water (AAIW) during the interglacials and less corrosive glacial North Atlantic Intermediate Water (or upper North Atlantic Deep Water) during the glacials (Haddad and Droxler, 1996).

Kaneps (1979) suggested increases in Gulf Stream strength throughout the Plio-Pleistocene, interpreting a series of hiatuses on Blake Plateau as intervals of high Gulf Stream velocity. The precise timing of the hiatuses, however, is suspect as the ages are based on 1970-era biostratigraphic calibrations (hence the 1-myr error bars in figure 1.10). If Blake Plateau hiatuses and MOW intensifications were roughly synchronous, then MOW flowing into the Caribbean Sea contributed to a strengthened Gulf Stream flow. At Site U1396 there are intervals of elevated carbonate deposition, very roughly coincident, with the Blake Plateau hiatuses and MOW intensifications. This seems counter to the expectation from the literature (e.g., Haddad and Droxler, 1996), as the bottom water bathing Site U1396 would likely be AAIW, a nutrient rich but corrosive water mass. MOW, on the other hand, would be less corrosive, nutrient poor, and warm. The lithostratigraphy from Site U1396 agrees somewhat with different water masses bathing throughout the Plesitocene. At ~600 ka and again at ~400 ka there are calcareous

sand intervals, which are associated with lower sedimentation rate suggesting extensive winnowing removing the fine fraction. Removing fine sediment would lower the sedimentation rate. These sandy intervals appear to be associated with MIS 15-16 and MIS 10-12. Directly preceding these sandy intervals, the interval from 0.55 to 0.75 Ma is one of low $\delta^{18}O$ variability in the benthic record. A change in Caribbean Sea bottom water may explain the decreased benthic $\delta^{18}O$ variability, if it were episodic, only bathing benthic organisms in warm water during glacials, and a relatively cooler water mass during interglacials. This would have the effect of flattening the curve, effectively removing the benthic glacial-interglacial differences in $\delta^{18}O$ while retaining the observed high planktic $\delta^{18}O$. While the dates for MOW intensification do not agree with the lower variability in benthic $\delta^{18}O$, MOW dates are at present poorly constrained (Hernández-Molina et al., 2014). Currently MOW intensification occurs at ~0.7-0.9 Ma (Hernández-Molina et al., 2014). Our low $\delta^{18}O$ variance interval is ~150 kyr younger, with low sedimentation rate and winnowing occurring at ~0.7-0.6 Ma and ~0.5-0.35 Ma, but the mismatch could simply be due to poorly constrained dates from the MOW outflow studies. It should be noted that geochemical evidence points to limited MOW influence in the Caribbean during the Plio-Pleistocene (Osborne et al., 2014), that evidence is only from after 2 Ma, well after the hypothesis described above.

A second pulse of winnowing coincides with MIS 11. However, low benthic $\delta^{18}O$ variability through this interval is likely due to a limited number of $\delta^{18}O$ values, as the sample resolution shrinks to ~50 kyr. While there is similarity between the winnowing pulse at MIS 15 and MIS 11, we cannot rule out a data density issue at MIS 11. The planktic record suggests that while MIS 15 benthic variability is limited, MIS 10 and MIS

12 may be missing in a hiatus, as the typical glacial $\delta^{18}O$ values are missing from both benthic and planktic records.

Perhaps a more likely connection from gateway changes to rates of sedimentation is thermohaline circulation. Haug and Tiedemann (1998) demonstrated a link between the salinity contrast, formed by CAS closure, between Pacific and Atlantic Ocean. This contrast, with saltier Atlantic Ocean water, helps to boost formation of North Atlantic Deep Water (NADW), which in turn boosts thermohaline circulation. Several studies have demonstrated this link (e.g., Osborne et al., 2014; Zhang et al., 2012) both in proxy reconstruction and inter-model comparison. Proxy reconstructions, especially the geochemical reconstructions both from oxygen isotope gradients between Pacific and Atlantic basins and other methods (e.g., Osborne et al., 2014), suggest that this was not a simple single increase, that in fact there were multiple fluctuations in the strength superimposed on the long-term trend of increased thermohaline circulation. These fluctuations in thermohaline circulation were of varying duration, but had ~100-kyr scale durations, and so could be some of the variability that is seen in the sedimentation rates at Site U1396.

Realistically, the observed changes in sedimentation rate and brightness are a mixture of different factors: volcanic input, carbonate and siliceous productivity, and thermohaline circulation. The period from ~3-4 Ma could have been a period of highly variable productivity, driven by obliquity and incomplete construction of the CAS. Thermohaline circulation, as the CAS had not completely closed, could also have been uneven, and sped up and slowed down in fits, as seen in Osborne et al., 2014, leading to the highly volatile rates observed through that interval. Volcanic input cannot be ruled

out as a contributing factor, but it is not likely to be the only source of higher sedimentation rates through this interval. As CAS closure became more and more final the increase in thermohaline circulation drove quicker bottom water circulation over Site U1396, leading to increased winnowing and lower sedimentation rates, resulting in the gradual decline in rates observed. Lastly, the low sedimentation rates, with pulses of winnowing, could have been due to the lower productivity, increased thermohaline circulation, and variation in bottom water character during the 0-2 Ma interval. All of the changes above are testable. Sediment smear slides would be able to identify if there is a period of changing opal - carbonate dominance, while planktic and nannofossil assemblage changes would elucidate both surface water mass changes and productivity shifts. An examination of the gradients between $\delta^{18}O$ and $\delta^{13}C$ could identify the influence of changing surface and bottom water masses, while examining the relative proportion of different size fractions would address current strength. Careful geochemical investigation, conscious of the diverse volcanic input within the sediments, could elucidate how stable the trends identified at Site 999 are relative to the rest of the Caribbean Sea. Lastly, identification of cryptotephra through the record would allow a more detailed study of the influence of volcanic sediments through this interval.

1.6 Conclusions

1. Site U1396, drilled ~33 km southwest of Montserrat, contains a relatively continuous sequence of Pliocene and Pleistocene sedimentation. There is a general trend to decreasing sedimentation rate towards the present, both in volcanic and non-volcanic sedimentation.

2. The chronostratigraphy of Site U1396 is based on planktic foraminifer biostratigraphy, calcareous nannofossil biostratigraphy, magnetostratigraphy, astrochronology, and oxygen isotope chemostratigraphy (marine isotope stages). The resulting chronostratigraphy provides a detailed framework to reconstruct the paleoceanography and record of sediment accumulation in the northeastern Caribbean.

3. Two biostratigraphic datums used extensively shipboard (B *Globigerinella calida* and T *Globorotalia flexuosa*) were found to be unreliable at Site U1396, but at several other Exp. 340 sites these datums agreed with calibrated ages as supported by nannofossil biostratigraphy.

4. There is a strong correlation ($p < 0.001$) between sedimentation rate and L* (brightness). There is weak correlation between ($p < 0.1$) brightness and $CaCO_3$ content throughout the entire record, but some intervals of L* qualitatively appear to be controlled by carbonate content. This suggests that the main phases of Montserrat volcanism may not be contributing strongly to the sedimentation at U1396, as the growth of Montserrat (<2.6 Ma) occurs during times of lower sedimentation rates at Site U1396.

5. Sedimentation rate at Exp. 340, Site U1396 is likely controlled by a mix of factors, including volcanogenic, lithogenic, and biogenic sediment sources. A series of hypotheses to explain highly volatile rates were explored, with connections to Site 999, a more centrally located Caribbean Sea ODP Site, with suggestions for future work to elucidate the direct causes. Highly variable, but consistently elevated, rates of sedimentation are intriguingly high during a period normally considered to be

oligotrophic within the Caribbean Sea. Therefore, it is suggested that a more likely connection is to bottom water conditions, including episodic changes in bottom water flow rates in the Pliocene and increased winnowing into the Pleistocene, due to CAS closure through the study interval.

CHAPTER 2

OLIGOCENE PLANKTIC FORAMINIFERAL TAXONOMY AND EVOLUTION: AN ILLUSTRATED REVISION OF OCEAN DRILLING PROGRAM SITE 803

2.1 Abstract

The Oligocene (33.9 – 23.0 Ma) has historically proven to be a difficult interval to examine with respect to planktic foraminifera; the tendency for many of the taxa to be basically globigerine in shape, with four or five chambers in the final whorl means differences between species are limited. Recently, an international working group has been attempting to clarify the Oligocene planktic foraminiferal taxonomy, with the goal of establishing phylogenetically-consistent generic and species concepts. A relatively expanded and continuous Oligocene section recovered at Ocean Drilling Program Site 803 in the western equatorial Pacific was previously studied by Leckie et al. (1993) using fairly conservative species concepts. Since 1993, foraminiferal biostratigraphic datum age calibrations have changed, and so revised sedimentation rates for the 220-m thick Oligocene sequence are actually more constant than previously thought. As a part of the recent taxonomic revision, this site was reevaluated and numerous additional taxa are noted to exist at this location. Macroevolutionary rates are calculated from the occurrences, and increased extinction is found within the late Oligocene, counter to the expectations laid out in broader-scale macroevolutionary studies. An effort is made to describe the diagnostic features, which can be used to distinguish all taxa under a standard binocular microscope. Finally, several figures of scanning electron microscope photomicrographs (from Site 803 and tropical Atlantic Ocean ODP Site 628) depict

features used to describe and differentiate important, but difficult or homeomorphic taxa, with the hope that these figures can be used by other workers at the microscope attempting to do Oligocene-based studies. The results of this study demonstrate that further taxonomic investigation of Oligocene planktic foraminifera is warrented.

2.2 Introduction

Planktic foraminiferal evolution is comprised of three main diversification phases; the Cretaceous (K), the Paleogene (Pg), and the Neogene (Ng; Cifelli, 1969; Norris, 1991; Fraass et al., 2015). Each of these diversification phases is accompanied by a large increase in the variety of forms present (Cifelli, 1969). The K and Pg are separated by the end-Cretaceous mass extinction which caused the extinction of >95% of all planktic foram species, followed immediately by high rates of origination (Fig. 1; Fraass et al., 2015). The Pg diversification ended largely by global cooling and the glaciation of Antarctica (Oi-1 event), as well as a major reorganization of ocean circulation, and changes in water column structure and productivity at the Eocene-Oligocene boundary (Wade and Pälike, 2004; Coxall and Pearson, 2007; Wade and Pearson, 2008; Cramer et al., 2009). In contrast to the relatively quick recovery in the early Paleogene, planktic origination is low with minimal cumulative increase in diversity throughout the Oligocene. The first several biozones in the Miocene, however, have statistically significant increases in the origination rate compared to a stochastic macroevolutionary model (Wei and Kennett, 1986; Fraass et al., 2015). Throughout the Oligocene, a prevalence of inflated to compressed globigerine forms persists, somewhat similar to the ‘disaster fauna’ found after the K-Pg impact (Smit, 1982; Liu and Olsson, 1964; Olsson et al., 1999; Coxall et al., 2006; Koutsoukos, 2014), or the low diversity, simple forms

found after the Aptian-Albian turnover event associated with Oceanic Anoxic Event 1 b (e.g., Leckie et al., 2002; Huber and Leckie, 2011; Petrizzo et al., 2012). This delayed Oligocene recovery, then dramatic diversification during the early Miocene, is intriguing. Why do the planktics evolve so little throughout the Oligocene?

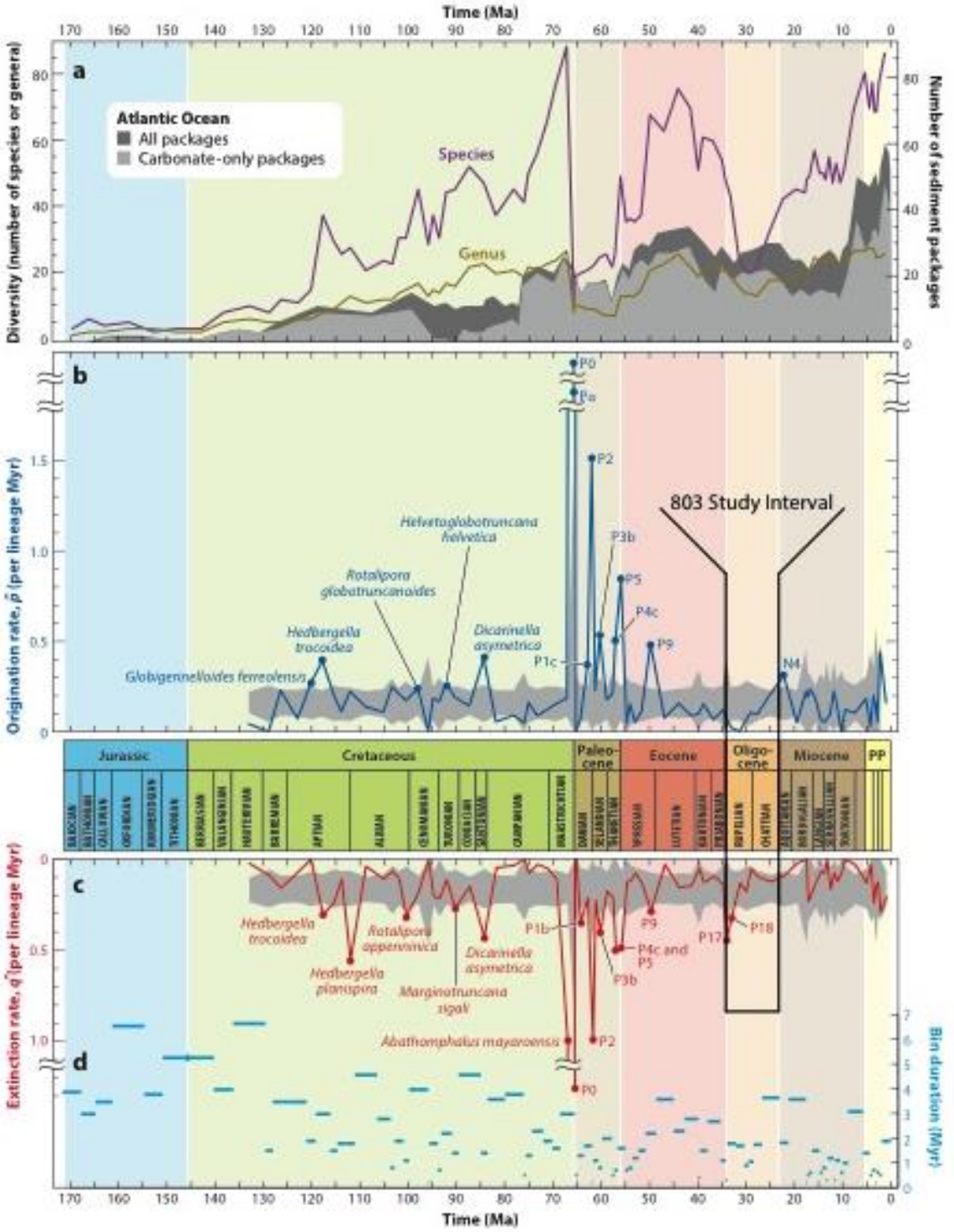

Figure 2.1. Evolutionary context for Chapter 2. Figure reproduced from Fraass et al. (2015). Figure 1a. Number of sedimentary packages against number of planktic foraminifer genera and species during each foram biozone. Figure 1b. Rate of origination (per lineage per million year) depicted against time (Ma). Figure 1c. Rate of extinction (per lineage per million year) depicted against time (Ma). Figures 1b and 1c. The grey bar represents a Monte Carlo simulation of purely stochastic macroevolutionary rate (see

Fraass et al., 2015 for details). Intervals noted with their biozone name are deemed significant rate excursions, as they exit the grey stochastic evolutionary model. Figure 1d. Length of the biozone against time. Note: This analysis used the N & P zones employed in Pearson et al. (1999), rather than the zonation scheme (Wade et al., 2011) used in this study.

Climatically, the Oligocene was relatively stable following the rapid glaciation of Antarctica (DeConto and Pollard, 2003; Zachos et al., 2008; Cramer et al., 2009), which lowered the calcite compensation depth (Lyle et al., 2002 – ODP Leg 199 IR vol.) and caused the extinction of a variety of species and genera (e.g., *Hantkenina*; Coxall and Pearson, 2007; Wade and Pearson, 2008), as the climate system entered an 'ice-house' state. Oxygen isotopes suggest ~7 myr of generally cool conditions, with ~5 additional glacial events superimposed (Pälike et al., 2006). Following the glaciation at ~27 Ma (Oi-2b), there was a gradual warming (see Pekar et al., 2006 for a discussion), ending in a short-lived Antarctic glaciation near the Oligocene Miocene boundary (Mi-1 event; Miller et al., 1991). It may seem counterintuitive that an interval with generally stable cool conditions would so hinder the recovery of the planktic foraminifera so dramatically. Unfortunately, the difficulty of species-level identification in the Oligocene has hindered an understanding of this odd interval in planktic foraminiferal evolutionary history; producing an unwieldy and gnarled taxonomy. Prior to statistical interrogation of the inner workings of the Oligocene, this taxonomy must be refined and the originations and extinctions of various taxa must be more robust.

Planktic foraminiferal taxonomy is undergoing a reorganization and standardization as a part of the Paleogene Planktonic Foraminiferal Working Group, a subcommittee of the International Submission on Paleogene Stratigraphy. This group has most recently focused on genera primarily extant during the Oligocene (e.g., Fox and Wade, 2013). The Oligocene has historically been difficult to study due to the

overwhelming degree of convergence between species and between genera. Unlike many other intervals of time, planktic foraminifera of the Oligocene are generally composed of 3-5 globose chambers with cancellate walls. They simply lack the more flamboyant variety of forms found in the Maastrictian, the Eocene, or the Neogene.

The prevalence of globigerine forms has led to some species being assigned to numerous genera since initially described (e.g., *Globoturborotalita euapertura* has also been classified as *Globigerina* and *Turborotalia*), resulting in tangled systematics. An effort has been made within this revision to acknowledge the phyletic history of these taxa, and to resolve taxonomic concepts into both a usable and phyletically-robust system. Concepts for genera, like *Dentoglobigerina*, have to be shifted to accommodate the phyletic transitions observed within these groups. In the case of *Dentoglobigerina*, the umbilical tooth is no longer the key definition, as certain species within *Subbotina* also possess teeth, while some *Dentoglobigerina* lack them. It is the hope that these subtly altered generic definitions will be more robust and useful than the un-emended originals.

The larger taxonomic revision by the working group has also erected a number of new species. This study takes a previous work (Leckie et al., 1993), which employed a conservative taxonomic approach, and utilizes the new taxonomy to revise the species present. The diversity through the Oligocene section of Ocean Drilling Program (ODP) Site 803 has roughly doubled. An emphasis has been placed on establishing strict and usable delineations between species that closely resemble one another to aid in the use of the new taxonomic scheme (See Systematics). The goal of many of the illustrations herein is to present systematics in a visual manner, to highlight the key features defining these species. Due to sometimes-poor preservation at Site 803, ODP Site 628 was also

used for illustration and for comparing taxonomy within different ocean basins. Biostratigraphic species, those whose top or bottom occurrences are used as datums, are reexamined. The species concepts of the biostratigraphically useful zonal taxa have remained mostly unchanged, and therefore the zonation scheme, as presented in Wade et al. (2011), has remained fairly stable. However, the age-depth relationship established at ODP Site 803 has changed as datums have been recalibrated to astrochronologic timescales (Wade et al., 2011), resulting in a new age-depth relationship and revised sedimentation rates.

2.3 Methods

2.3.1 Site Description

In their original study, Leckie et al. (1993) compared two low latitude Ocean Drilling Program sites; one from the Pacific (ODP Hole 803D) and one from the Atlantic (ODP Hole 628A). ODP Site 803 is located at 2°25.98'N, 160°32.46'E on the Ontong Java Plateau in the western equatorial Pacific Ocean. Currently, it is at 3,412 meters water depth (Kroenke et al., 1991). While initial stratigraphy suggested that there were several hiatuses throughout the chalk deposition (Shipboard Scientific Party, 1991), this was later revised as higher resolution biostratigraphy suggested continuous sedimentation (Leckie et al., 1993). Previous work at Site 803 has established a diverse assemblage of planktic foraminifera, especially the *Dentoglobigerina,* with moderate to good preservation. Site 803 was employed here for identifying species ranges and occurrences.

ODP Site 628 is located at 27°38.10'N, 78°18.95'W on the Little Bahama Bank in the tropical North Atlantic Ocean. It currently sits at 966 meters water depth (Austin et al., 1986). Both shipboard and subsequent stratigraphy has shown that there are a number

of hiatuses throughout the Oligocene (Leckie et al., 1993). Because of these hiatuses, Site 628 will be used only for specimen illustrations. A full taxonomic revision of the specimens found at Site 628 has not been undertaken here.

2.3.2 Sample Preparation

All samples were previously washed and picked (Leckie et al., 1993). A mild Calgon and dilute hydrogen peroxide solution was used to soak the samples to aid in disaggregating the chalk. Some samples were also ultrasonicated for 10-15 seconds to further disaggregate. After soaking for several hours or overnight, samples were washed over a 63 μm sieve. Samples were then dried in a low-temperature (<60°C) oven. Most samples had to undergo this process twice to be clean enough for study.

2.3.3 Biostratigraphy

We follow the Cenozoic tropical planktic foraminiferal zonation of Wade et al. (2011). This revision integrates previous zonation schemes and datums (Berggren et al., 1995; Berggren & Pearson, 2005) into a tuned astronomical framework, while augmenting it with additional datums. The Oligocene zonation remained relatively static through this revision, with no additional datums, although datum ages have been recalibrated. Here we present both the original zonation (P Zones; Berggren et al., 1995) and the newer zonations (O & M Zones; Berggren & Pearson, 2005; Wade et al., 2011).

2.4 Discussion

2.4.1 Biostratigraphy

Primary and secondary biostratigraphic datums and species occurrences were all rechecked in the light of the new taxonomic system (Figure 2). The concepts of biostratigraphic species, those used to define zones or as secondary markers, are fairly

stable by necessity. Modifying the concept of a biostratigraphic species would render interpretation of subsequent use of that datum complicated at best and useless at worst. As such, biostratigraphic taxa are hopefully constant from biostratigrapher to biostratigrapher and have not changed much through this revision. This is evident in the relative stability of the stratigraphic ranges of the biostratigraphic taxa used in Leckie et al. (1993) and this current study. This current study also adds datums, zones, and ages not employed in Leckie et al. (1993).

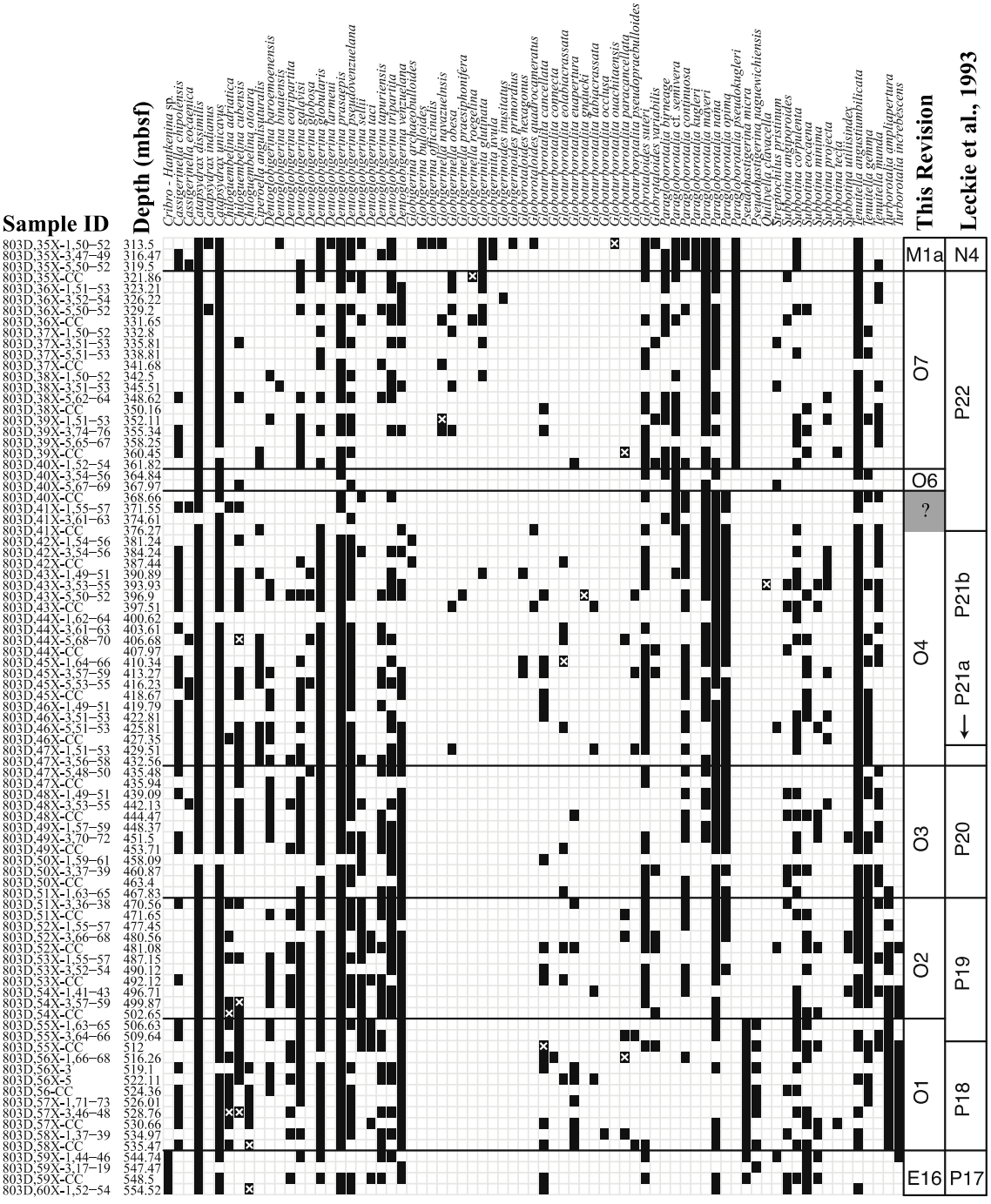

Figure 2.2. Graphic representation of species occurrences at Hole 803D. A black box denotes a species present within a sample, while a white X denotes an SEM image used in this publication. The grey box within the This Revision Zonation scheme is discussed within the text (see Biostratigraphy, TC *Chiloguembelina cubensis*)

The Oligocene is relatively impoverished for biostratigraphic control in the planktic foraminifera. While biostratigraphic zones are of similar length to the rest of the

Paleogene, there are far fewer secondary marker taxa than in other intervals (Wade et al., 2011). In addition, several taxa, including a primary zonal taxon, are found to have anomalous ranges at Site 803. TC *Chiloguembelina cubensis* (Top Common occurrence of *Chilloguembelina cubensis*) datum does not work well at Site 803. TC *Chiloguembelina cubensis* marks the boundary between zones O4 and O5, while T *Paragloborotalia opima* (Top of *Paragloborotalia opima*) marks the O5 and O6 boundary (Berggren and Pearson, 2005; Wade et al., 2011). Within the sediments at Site 803, the last common occurrence of *C. cubensis* is too high, occurring above both the T *P. opima* and B *Paragloborotalia pseudokugleri* (Bottom of *Paragloborotalia pseudokugleri*). While the utility of TC *C. cubesis* has been demonstrated at other locations (e.g., Wade et al., 2007; Coccioni et al., 2008), care must be taken when employing it, with explicit definitions for what defines a 'common' occurrence. Though sporadic, *C. cubensis* has been shown to range up to the Oligocene/Miocene boundary at both Pacific Site 803 and Atlantic Site 628 (Leckie et al., 1993). There are several elevated abundances of *Chiloguembelina cubensis* within sediments from Site 803. The last two samples with higher numbers of *C. cubensis* are 803D/43X/1 49-51 cm and 803D/44X/5 68-70 cm. Both samples occur within Zone O4, meaning both could potentially be the true TC of *C. cubensis.* If one of those samples represents the typically recorded TC *C. cubensis*, then higher resolution sampling of other sites might show a highly restricted final pulse of *C. cubensis* abundance in Zone O6, which is possibly the case (Wade, *communication 2014*), then this has simply been frequently missed by normal sampling resolutions. Here we tentatively use sample 803D-44X-5, 68-70 cm as the TC *C. cubensis*, as it fits closest to the rest of the age-diagnostic data. This is not for

age interpretation, but more to stress the apparent continuous sedimentation at this site, which would be obscured if Zone O5 were skipped.

The B and BC (Bottom Common occurrence) of *Globigerinoides primordius* are both anomalously high at Site 803 compared with Site 628 in the Atlantic (Leckie et al., 1993). *Globigerinoides* is simply not present at this site prior to the Oligocene/Miocene boundary (O7/M1a boundary). As such, we cannot employ either of the *G. primordius* datums at Site 803.

Figure 3 represents a summary of age depth relationships and presents the variety of changes from Berggren and Miller, 1988 to a more recent calibration. Figure 3A presents this recalibration in an Age-Depth context for Hole 803D. Rates were calculated between biostratigraphic datums taking into account the sampling resolution. Because the sampling was done roughly every other section, there is uncertainty to the actual stratigraphic position of the biostratigraphic datum, and so a maximum or minimum possible sedimentation rate can be calculated, if the B/T is allowed to vary within the last found sample and the first absent sample. The light, mid-, and dark grey rectangles depict these minimum and maximum sedimentation rates. The various lines correspond to the original sedimentation rate (mid-grey), primary datums (except TC *Chiloguembelina cubensis*, light grey), and all datums (except *C. cubensis* and *G. primordius*, dark grey).

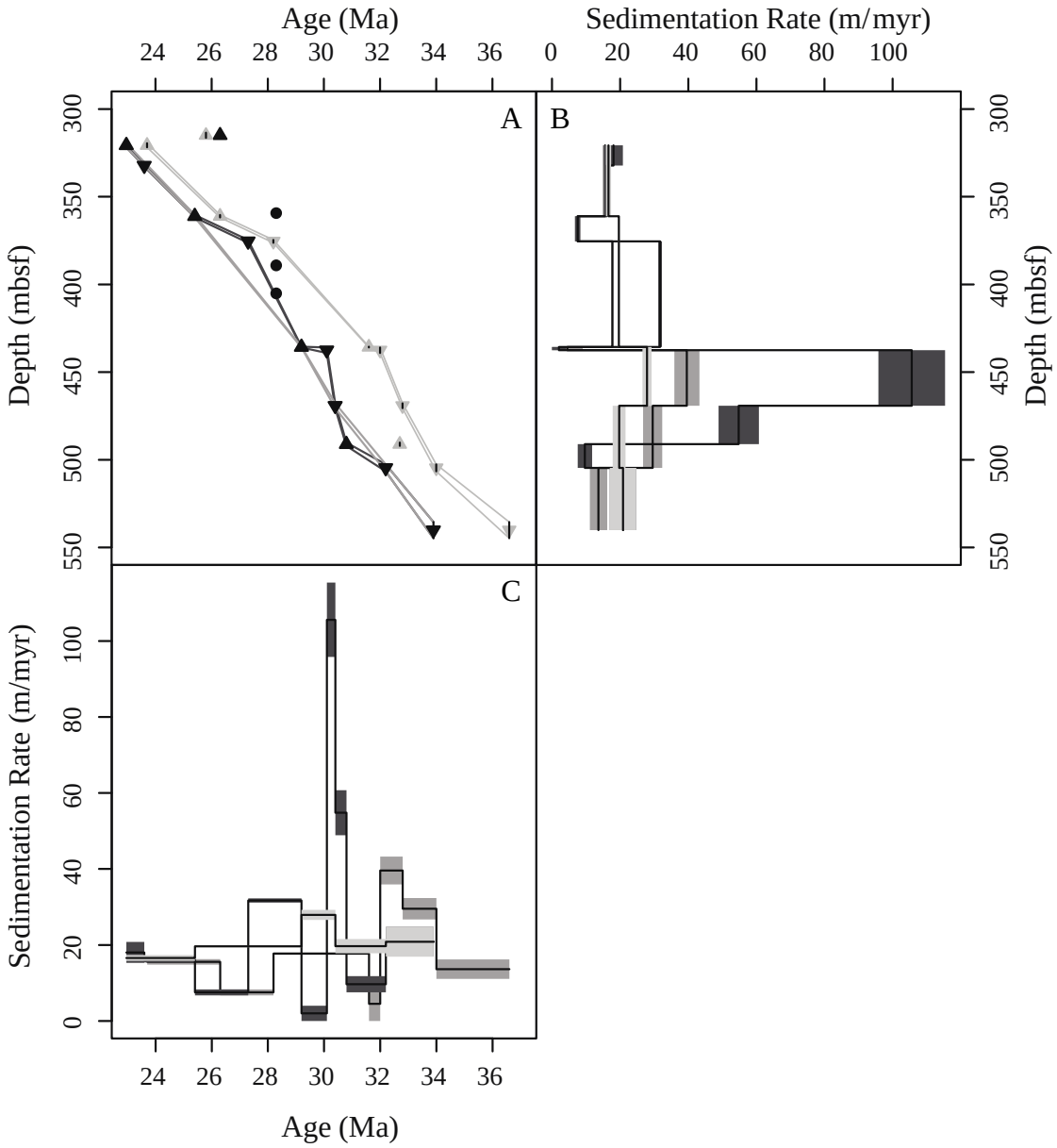

Figure 2.3. Age, depth, and sedimentation rate changes. Figure 1A. Age v. Depth at Site 803. Upwards-pointed triangles correspond to a B, while downwards-pointed triangles correspond to a T. Circles are a TC (see text for discussion). Grey denotes the Berggren et al. (1985) and Berggren and Miller (1988) calibration used in the Leckie et al. (1993) study, while black denotes datums used in this work employing the Wade et al. (2011) astrochronological ages. Each pair of lines denotes the highest and lowest possible stratigraphic position of the datums, given the sampling resolution. Light grey lines denote the Leckie et al. (1993) sedimentation rate, mid-grey denotes use of only primary datums (except TC *C. cubensis*, see text), while dark grey denotes the use of all datums (except TC *C. cubensis*, and B *G. primordus*, see text). Figure 1B. Sedimentation Rate v. Depth at Site 803. Light grey polygons denote the Leckie et al. (1993) sedimentation rate, mid-grey polygons denote use of only primary datums (except TC *C. cubensis*, see text), while dark grey polygons denote the use of all datums (except TC *C. cubensis*, and B *G.*

primordus, see text). The black vertical lines denote the midpoint of each sedimentation rate section. Figure 1C. Sedimentation Rate v. Age at Site 803. Light grey polygons denote the Leckie et al. (1993) sedimentation rate, mid-grey polygons denote use of only primary datums (except TC *C. cubensis*, see text), while dark grey polygons denote the use of all datums (except TC *C. cubensis*, and B *G. primordus*, see text). The black lines denote the midpoint of each sedimentation rate section.

Figure 4 represents the precise changes in the age of each calibrated datum (Wade et al., 2011) compared with the ages used in Leckie et al. (1993), which were based on Berggren et al. (1985) and Berggren and Miller (1988). Note that the earliest Miocene and late Oligocene recalibrated to roughly 0.5 to 1 myr older, while the early Oligocene datums are roughly 1.75 to 2.75 myr older. The substantial break in age differences likely is due to revisions in paleomagnetic ages from Berggren et al. (1985) to Pälike et al. (2006). These changes have a significant effect on the ages assigned to the sediments at Site 803.

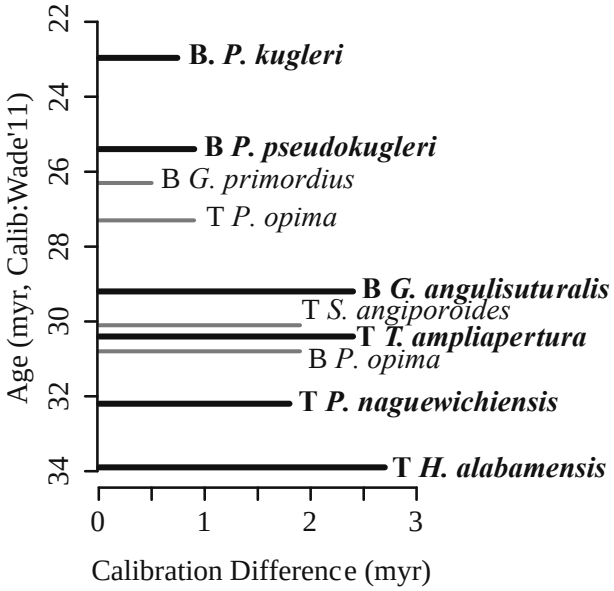

Figure 2.4. Differences in datum ages from the Berggren et al. (1985) and Berggren and Miller (1988) time scales to the Wade et al. (2011) calibration. Primary datums are represented by thicker black lines, while secondary datums are thinner and grey.

If we accept the premise that Site 803 represents nearly constant and continuous sedimentation, then this suggests that there are some issues with the secondary datum

calibrations. For example, the secondary datum T *Subbotina angiporoides* is later at Site 803 than other sites, if only primary datums are used to estimate age. T *Tenuitella gemma*, on the other hand, falls directly on the 'primary-only' age estimate line. There are no major sedimentological changes in the study interval that would suggest the major changes in the sedimentation rate as suggested by the anomalous T *S. angiporoides* (Shipboard Scientific Party, 1991).

2.4.2 Evolutionary Metrics

Figure 5 shows several evolutionary metrics at Site 803. There is a small trend of increasing simple diversity from low values (~25 species in the first few samples in this interval), to moderate values for most of the Oligocene (~35 species). The substantial difference between the per-sample (grey) and the per-myr (black) lines suggest that there are a large number of very rare taxa recognized through this interval. These taxa appear within single samples, inflating the per-myr values, as those amalgamate ~7 samples. The overall trends within the more volatile per-sample data and the per-myr data are roughly equivalent.

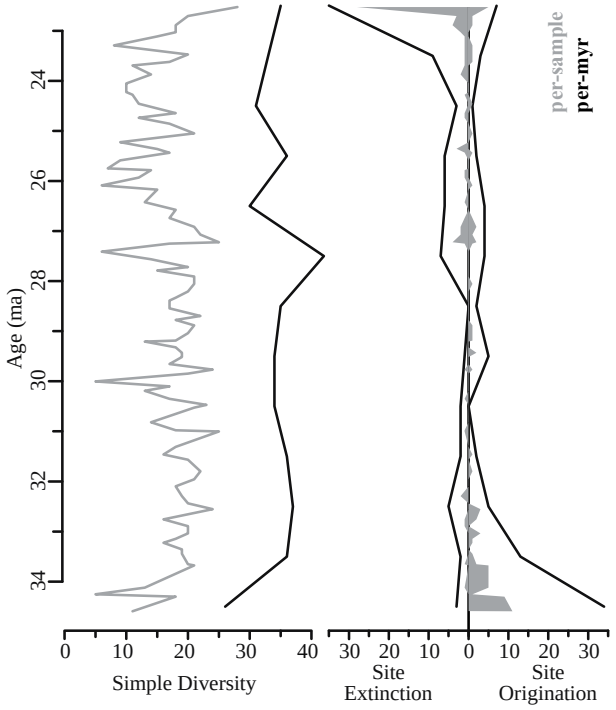

Figure 2.5. Evolutionary metrics with time. All data are plotted as per-sample (grey) and as per-myr (black). All data plotted with the 'primary only' biostratigraphic age model.

The evolutionary rate data at Site 803 is strongly biased by the 'edge effect' (Foote, 2000). This artificially increases the site originations (SO) at the lower limit of the interval and site extinctions (SE) at the upper limit. It tends to impose a 'smeared' look to those artificial increases, as seen within the first and last myr at this site. Thus, the substantial SO at >32 Ma and the SE at <24 Ma are not real, but rather artifacts of the taxa having 'first appeared' at the lower limit of the record, and 'last appeared' at the upper limit. This site does not seem to demonstrate the significant extinctions seen at other locations associated with the Eocene/Oligocene boundary (Wade and Pearson, 2008; Pearson et al., 2008; Aze et al., 2013; Fraass et al., 2015), but the low simple diversity at the base of the record records the classic E/O turnover. There is an intriguing pulse of origination seen within the first few samples within basal Miocene Zone M1a, near the top of the interval. The last bin is, in fact, smaller than the rest (3 samples), and

so is likely underestimating the true evolutionary activity through this interval, which has been noted as substantial (e.g., Wei and Kennett, 1986; Chaisson and Leckie, 1993; Fraass et al., 2015).

The bulk of the record is fairly featureless, like the Oligocene Epoch itself, except for the mild increase in extinction seen in the late Oligocene. This is also associated with a number of rare taxa going extinct (Fig. 2), seen with the dramatic increase in the per-myr diversity. While this is artificially increasing the rate of extinction through this interval ('singletons' *sensu* Foote, 2000), the offset between the SO (which should also be increased by higher numbers of singletons) and SE suggests that the extinction increase through this interval is real. Several of the taxa that had persisted from the Eocene (like the *Subbotina* and *Chiloguembelina*) last appear through this interval, following the global trend of weakly elevated rates of extinction through the later portion of the Oligocene (Fraass et al., 2015). Not observed here is the increased rate of origination in the last biozone in the Oligocene, which coincides with previously observed deep-sea warming. The flipped nature of the evolutionary trends near the end of the Oligocene, which are here locally extinction-dominated, while globally origination-dominated, maybe explained by several hypotheses.

One hypothesis is that the taxonomic revision has increased the number of taxa restricted to the Oligocene. These taxa would go extinct in the late Oligocene, inflating the number of extinctions at this site, while Miocene taxa have not been revised, and so have not been more thoroughly split. This is the case, but the local lack of origination is more severe than just additional splitting could likely account for. Another explanation is biogeographic. If instead of true extinction at Site 803, the local increase in extinction

could be due to migration events. The late Oligocene is sometimes thought to be an interval of some warming, at least in the deep-sea (e.g., Pekar et al., 2006). Oligocene taxa, like *Catapsydrax* for example, are better adapted for cooler thermocline waters (Pearson et al., 1997). If the tropics warmed in the late Oligocene, the cooler adapted taxa may have migrated to higher, cooler latitudes, causing a local extinction at Site 803. Further work at other Sites could demonstrate this, if their ranges were found to be extended, relative to Site 803. Lastly, this could be an example of taxonomic revision modifying our understanding of macroevolutionary rates. While this study cannot say that, if this is a true signal, that would have consequences for the validity of previous macroevolutionary study (e.g., Ezard et al., 2011; Lloyd et al., 2012; Fraass et al., 2015). If these revisions do impact the overall macroevolutionary trends, then previous studies would be invalidated by shifting taxonomic concepts. However, as many of the diversity curves in these previous studies, for example, despite being generated with entirely different methods, are obviously similar, macroevolutionary study is probably stable through revisions of individual epochs like the Oligocene. Further work on Oligocene taxonomy at multiple sites, preferably at other latitudes, would allow for more explicit conclusions.

2.4.3 Homeomorphy

The Oligocene is a time of severe homeomorphy between several, independent taxa. Figures 5-10 illustrate many of these taxa, which most closely resemble each other. The individuals presented represent the end-members of the species and are as close in morphology as possible. The aim here is to illustrate the frequently subtle distinguishing features between homeomorphic species with key annotations. It is the hope that these

illustrations are of use for other workers when trying to differentiate these species through this frequently frustrating interval of Earth history. An effort has been made to define species using characteristics, which can be observed with a typical binocular microscope, rather than those found within a taxonomy requiring the use of a Scanning Electron Microscope. This effort was occasionally unsuccessful (e.g., *Chiloguemelina* and *Globoturborotalita).* Further discussion of those differences can be found below in Systematics.

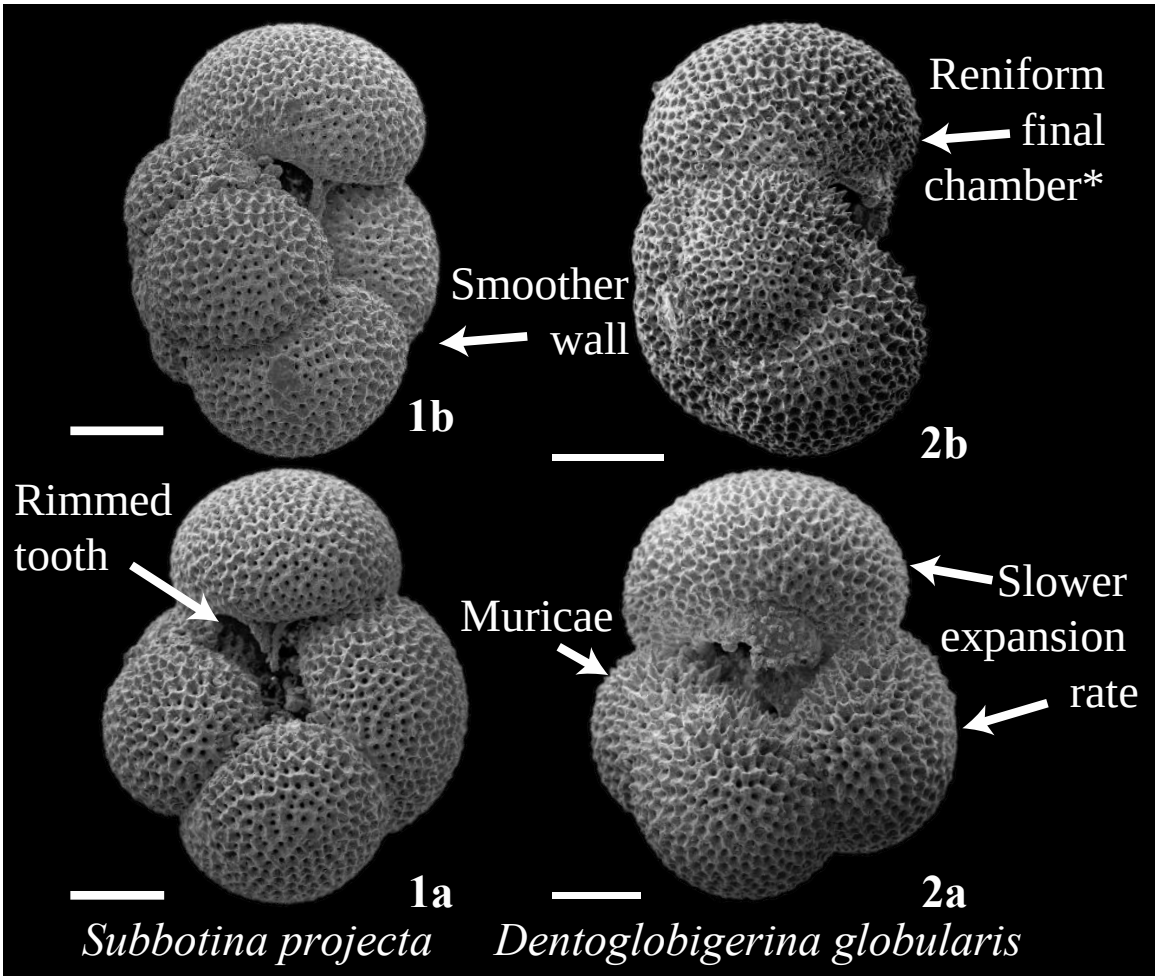

Figure 2.6 Key taxonomic differences between homeomorphs *Subbotina projecta* and *Dentoglobigerina globularis*. 1. *Subbotina projecta* Sample ODP 628A-17H-CC. 2. *Dentoglobigerina globularis* Sample ODP 628A-19H-3, 100-102 cm. *While the reniform final chamber of *D. globularis* is a key distinguishing feature, rare *S. projecta* can posses a compressed final chamber, as the figured specimen does. See Figure 10 for

specimens of *S. projecta* with spherical final chambers. This specimen is illustrated here to demonstrate the profound similarity between some specimens of these two species. Scale bar = 100 µm.

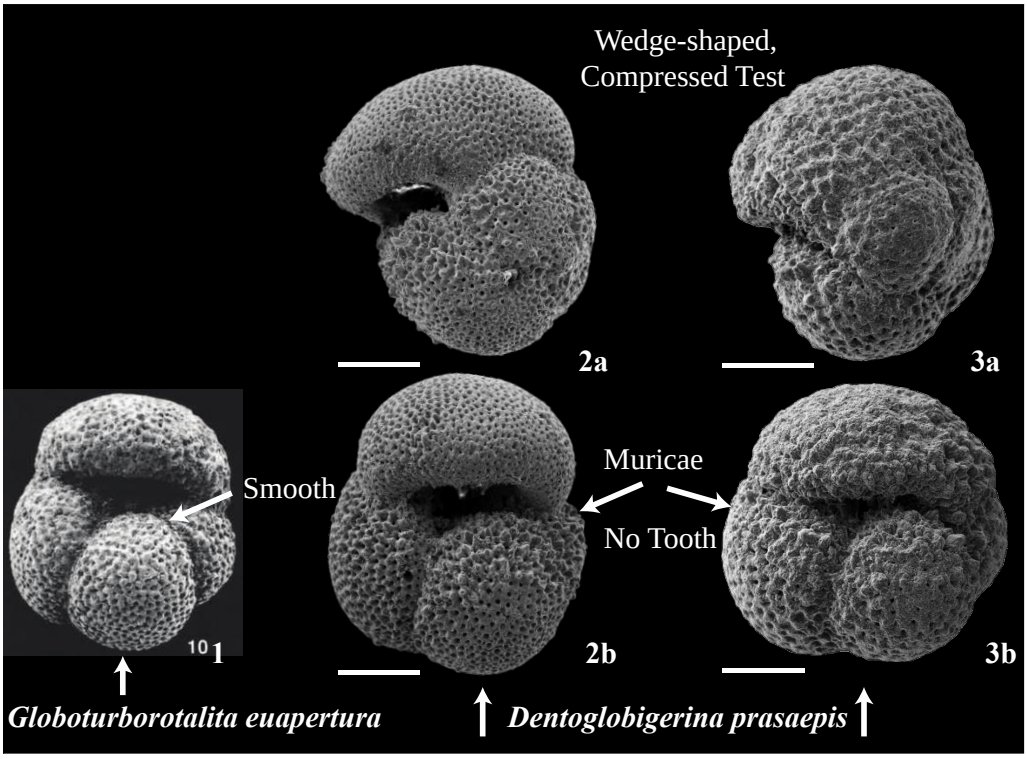

Figure 2.7 Key taxonomic differences between homeomorphs *Dentoglobigerina prasaepis* v *Globoturborotalita euapertura.* 1 *Globoturborotalita euapertura* Image reproduced from Leckie et al. (1993). 2 *Dentoglobigerina prasaepis* Sample ODP 628A-26X-1, 74-76 cm. 3 *Dentoglobigerina prasaepis* Sample ODP 628A-18H-1, 100-102 cm. Scale bar = 100 µm.

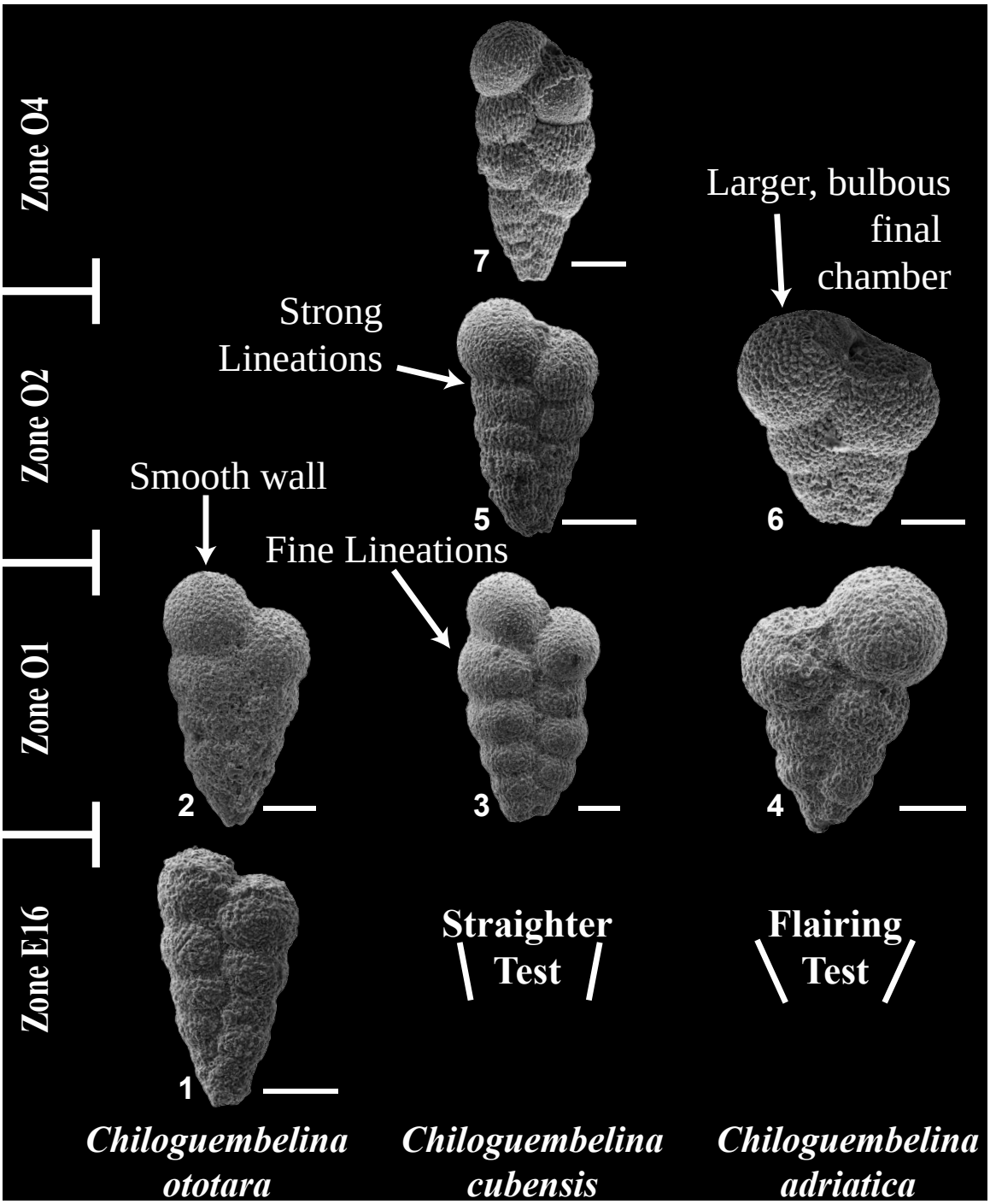

Figure 2.8 Key taxonomic differences between *Chiloguembelina cubensis*, *C. adriatica*, and *C. ototara*. 1 *C. ototara* Sample ODP 803D-60X-1, 52-54 cm Zone E16. 2 *C. ototara* Sample ODP 803D-58X-CC Zone O1. 3 *C. cubensis* Sample ODP 803D-57X-3, 46-48 cm Zone O1. 4 *C. adriatica* Sample ODP 803D-57X-3, 46-48 cm Zone O1. 5 *C. cubensis* Sample ODP 803D-54X-3, 57-59 cm Zone O2. 6 *C. adriatica* Sample ODP 803D-54X-CC Zone O2. 7 *C. cubensis* Sample ODP 803D-44X-5, 68-70 cm Zone O4. Scale bar = 50 µm.

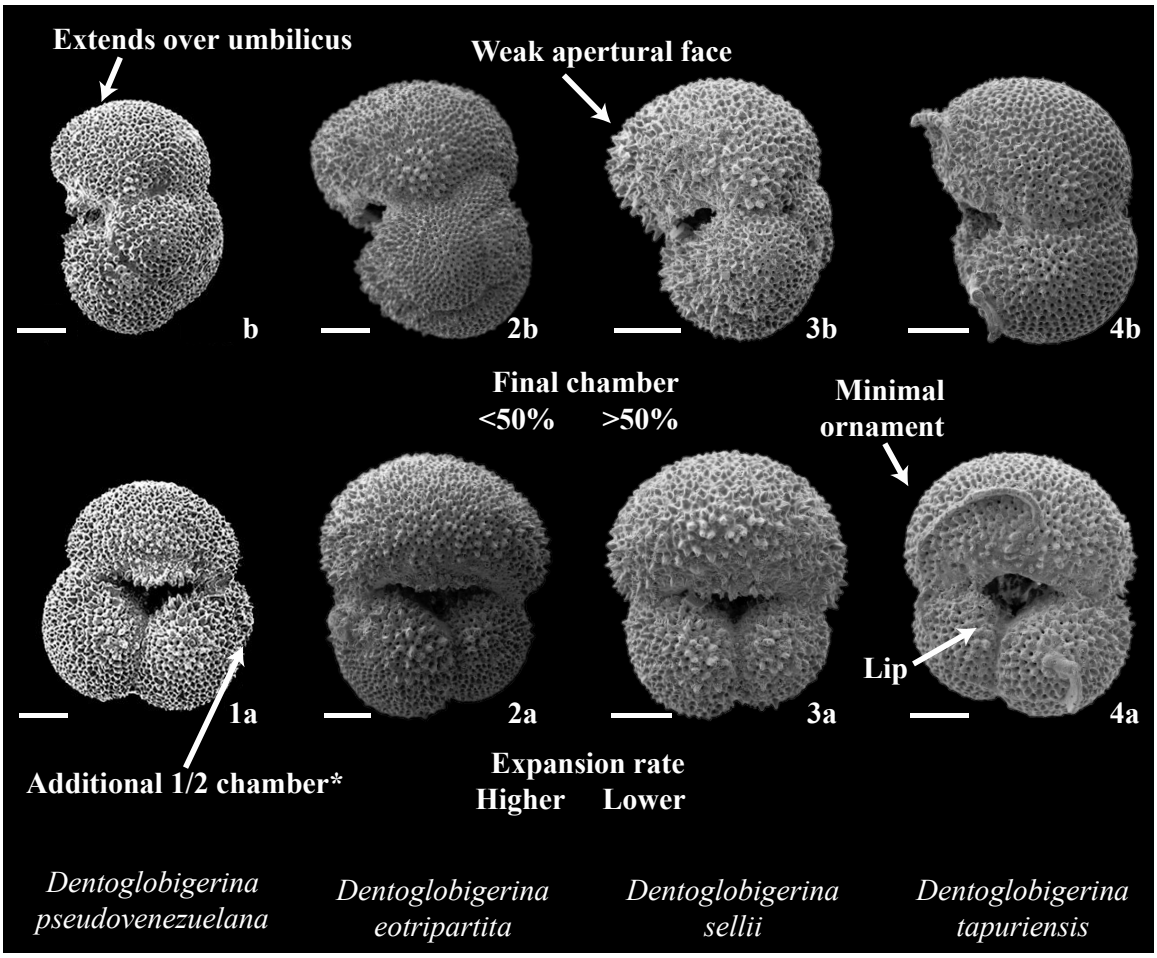

Figure 2.9 Key taxonomic differences between *Dentoglobigerina pseudovenezuelana, D. eotripartita, D. sellii,* and *D. tapuriensis.* 1 *Dentoglobigerina pseudovenezuelana* Holotype reproduced from Pearson et al. (2006), Sample FCRM 1923, Lindi, Tanzania middle Upper Eocene *Cribrohantkenina danvillensis* Zone. 2 *Dentoglobigerina eotripartita* Sample ODP 628A-18-1, 100-102 cm Zone P22. 3 *Dentoglobigerina sellii* Sample ODP 628A-26X-1, 100-102 cm Zone P18. 4 *Dentgolobigerina tapuriensis* Sample ODP 628A-18-1, 100-102 cm Zone P22. Scale bar = 100 µm.

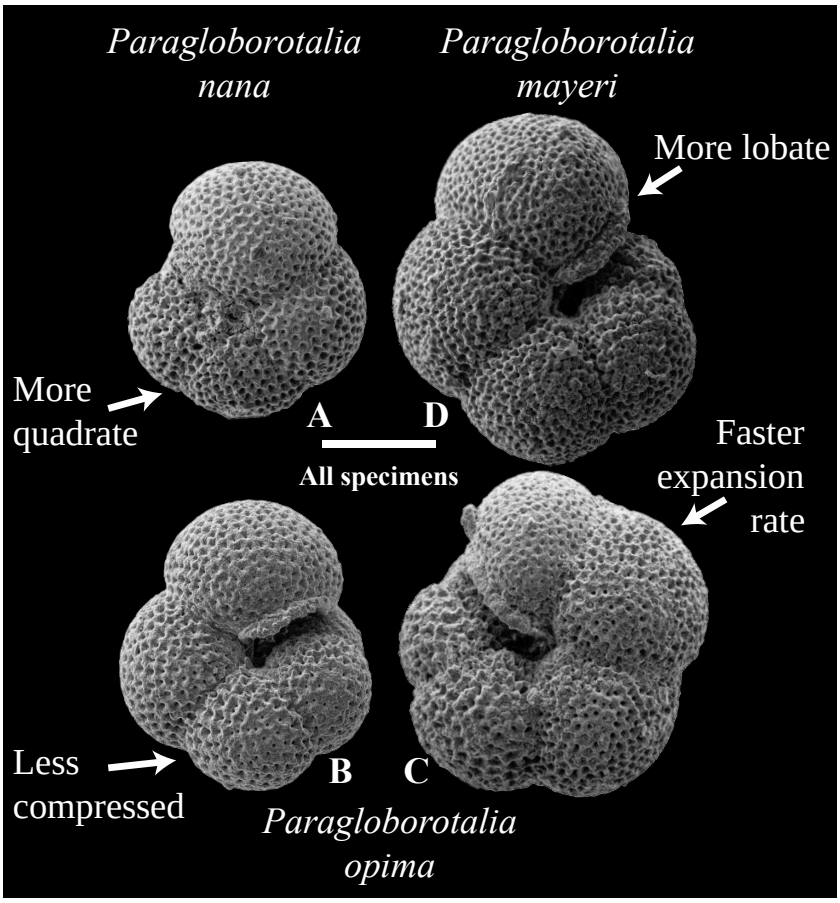

Figure 2.10 Key taxonomic differences between *Paragloborotalia nana*, *P. opima*, and *P. mayeri*. 1 *Paragloborotalia nana* Sample ODP 628-24-1, 100-102 cm Zone P21a. 2 *Paragloborotalia mayeri* Sample ODP 628-17-CC Zone P22. 3 *Paragloborotalia opima* Sample ODP 628-18-1, 100-102 cm Zone P22. 4 *Paragloborotalia opima* Sample ODP 628-16-5, 100-102 cm Zone P22. Scale bar = 100 µm.

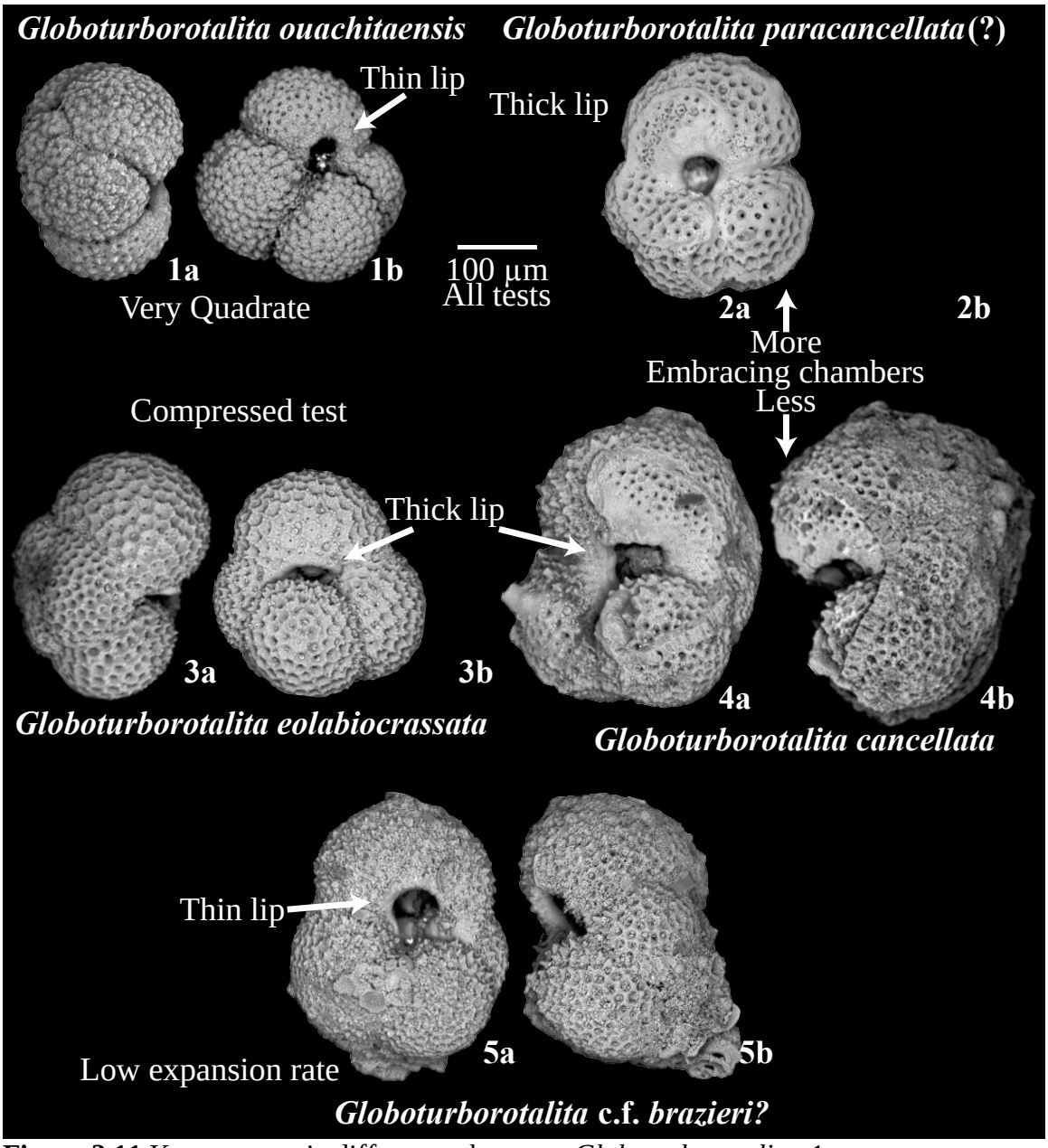

Figure 2.11 Key taxonomic differences between *Globoturborotalita.* 1 *Globoturborotalita ouachitaensis* Sample ODP 803D-35X-1, 50-52 cm Zone M1a. 2 *Globoturborotalita paracancellata* Sample ODP 803D-39X-CC Zone O6. 3 *Globoturborotalita eolabiocrassata* Sample ODP 803D-45X-1, 64-66 cm Zone O4. 4 *Globoturborotalita cancellata* Sample ODP 803D-56X-1, 66-68 cm Zone O1 5 *Globoturborotalita paracancellata/brazieri?* Sample ODP 803D-56X-1, 66-68 cm Zone O1. Scale bar = 100 µm.

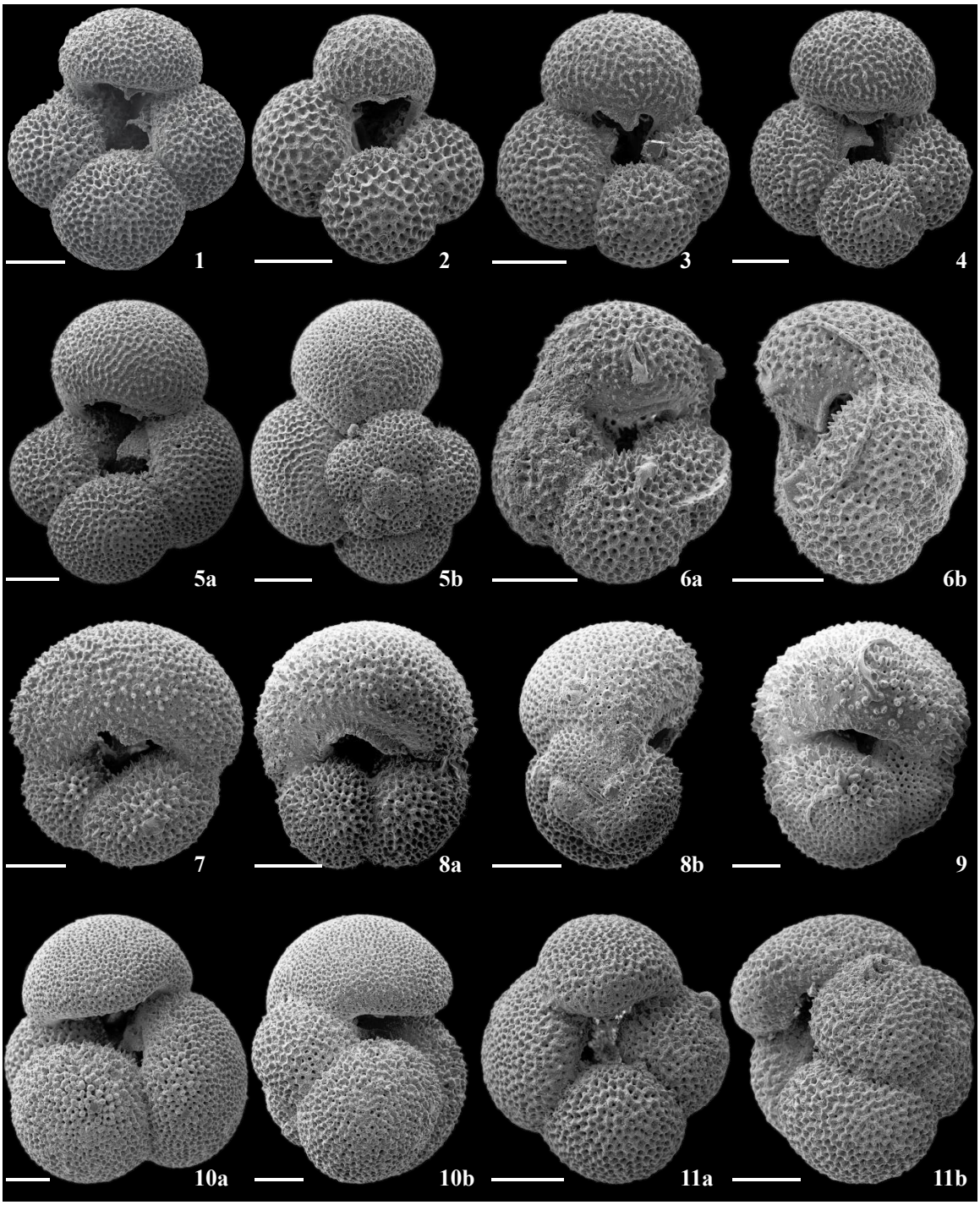

Figure 2.12 Variability within the genera *Dentoglobigerina* and *Subbotina.* 1 *Subbotina projecta* Sample ODP 628A-18-1, 100-102 cm. 2 *Subbotina projecta* Sample ODP 628A-18-1, 100-102 cm Zone O6. 3 *Dentoglobigerina globularis* Sample ODP 628A-17-3, 100-102 cm Zone O6. 4 *Dentoglobigerina globularis* Sample ODP 628A-17-3, 100-102 cm Zone O6. 5 *Subbotina projecta* Sample ODP 628A-147-CC Zone O6. 6 *Dentoglobigerina larmeui* Sample ODP 628A-16-5 Zone O6. 7 *Dentoglobigerina selli* Sample ODP 628A-17H-CC Zone O6. 8 *Dentoglobigerina tapuriensis* Sample ODP 628A-16-5-CC Zone O6. 9 *Dentoglobigerina selli* Sample ODP 628A-16-5-CC Zone O6.

10 *Dentoglobigerina venezuelana* Sample ODP 628A-17X-3, 100-102 cm. 11 *Dentoglobigerina venezuelana* Sample ODP 628A-17-1, 100-102 cm. Scale bar = 100 µm.

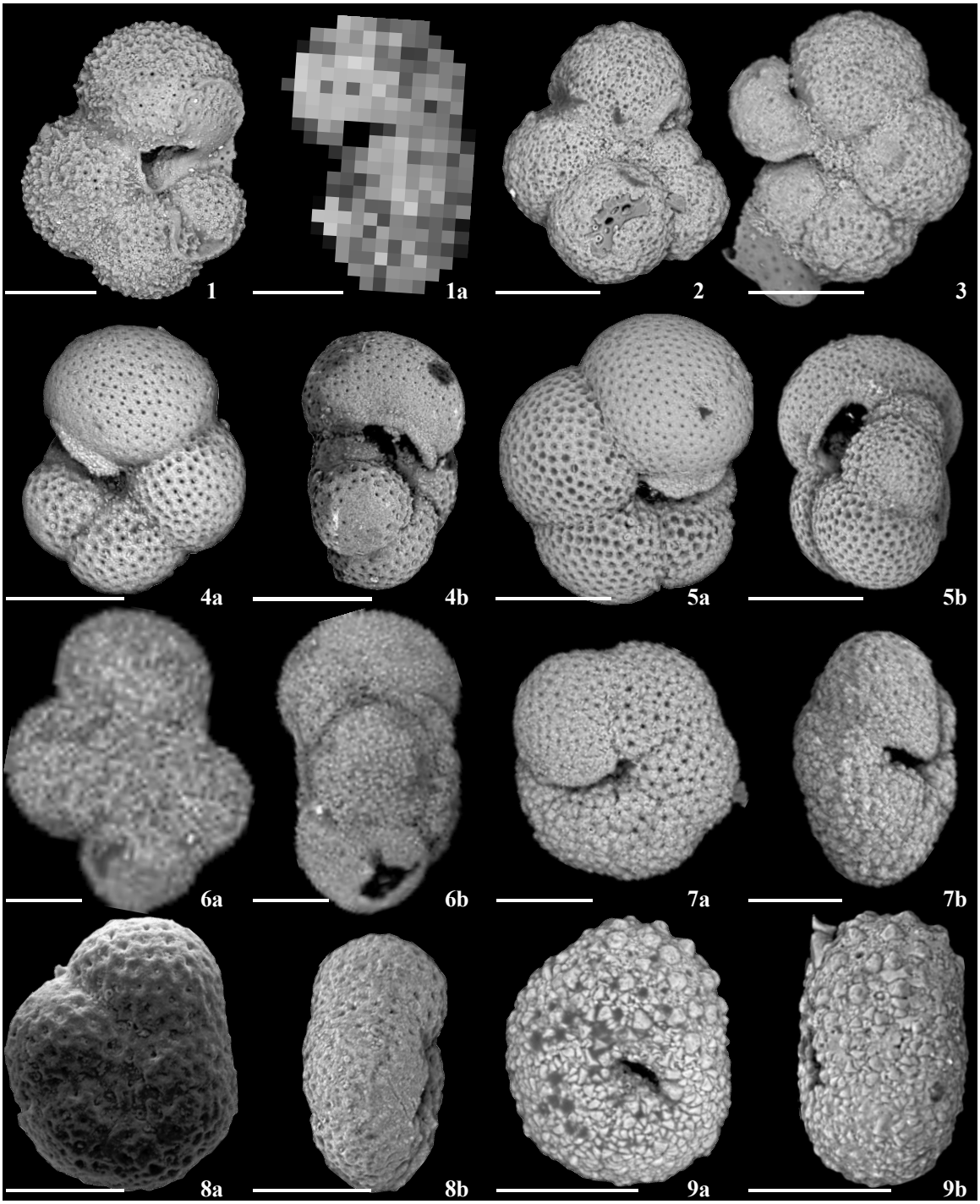

Figure 2.13 Oligocene taxa. 1 *Globoturborotalita gnaucki* Sample ODP 803D-43-5, 50-52 cm Zone O4. 2 *Globigerinella roegelina* Sample ODP 803D-35-CC Zone O6. 3 *Globigerinella navazuelensis* Sample ODP 803D-39X-1, 51-53 cm Zone O7. 4 *Paragloborotalia nana* Sample ODP 628A-18H-3, 100-102 cm Zone O6. 5

Paragloborotalia nana Sample ODP 628A-22-CC Zone O6. 6 *Quiltyella clavacella* Sample ODP 803D-43-3, 53-55 cm Zone O6. 7 *Paragloborotalia birnageae* Sample ODP 803D-35-6, 39-41 cm Zone O6. 8 *Paragloborotalia birnageae* Sample ODP 803D-51-1, 36-38 cm Zone O6. 9 *Paragloborotalia birnageae* Sample ODP 803D-35-6, 75-77 cm Zone O6. Scale bar for specimens 1-5 = 100 µm, 6-9 = 50 µm.

2.5 Systematics

The systematics section that follows attempts to follow the taxonomic divisions laid out by the Atlas of the Oligocene Planktic Foraminifera (Wade et al., in prep.). Citations are not made within the individual species descriptions and discussions, which follow except in cases where there are important distinctions because they would be redundant and excessive. Citations for genera used are as follows: *Globorotaloides, Catapsydrax,* and *Protentelloides* (Coxall & Spezzaferri, in prep.); *Paragloborotalia* (Leckie et al., in prep.); *Globigerina, Globigerinella,* and *Quityella* (Spezzaferri et al., in prep.); *Ciperoella* n. gen. (Olsson et al., in prep.); *Globoturborotalita* (Spezzaferri et al., in prep.); *Subbotina* (Wade et al., in prep); *Globigerinoides* (Spezzaferri et al., in prep.); *Dentoglobigerina* and *Globoquadrina* (Pearson et al., in prep.); *Turborotalia* (Pearson et al., in prep.); *Tenuitella* (Pearson et al., in prep.); *Cassigerinella* (Pearson et al., in prep.); *Streptochilus* (Smart & Thomas, in prep.).

Genus *Paragloborotalia* Cifelli 1982

Type species: *Paragloborotalia opima* (Bolli, 1957)

The genus *Paragloborotalia* is characterized by low trochospire coiling, a cancellate wall texture, and greater than four chambers in the final whorl. More derived forms of this genus tend to have a greater number of chambers, a trend which persists

even when considering a single species (e.g., *Paragloborotalia mayeri*). This genus most closely resembles *Globorotaloides,* but lacks the strong cancellate wall texture, and the tendency for bulla. *Paragloborotalia* also tend towards more inflation, and *Globorotaloides* is truly planispiral, while *Paragloborotalia* is low-trochospirally-coiled.

Paragloborotalia kugleri (Bolli,1957)

Diagnosis. Small test with roughly 6 chambers in the final whorl. Curved sutures on spiral side, and an angular periphery in edge view.

Discussion. It can be distinguished from *Paragloborotalia pseudokugleri*, the direct ancestor, by an angular periphery in edge view, curved spiral sutures, and the addition of a chamber. It should be noted, this is a gradual transition and *P. kugleri* sensu stricto is typically first seen in the >63 µm size fraction, and appears later in the >125 µm. It can be distinguished from *Paragloborotalia mayeri* and *P. siakensis* by having less inflated chambers and an angular margin in edge view.

Paragloborotalia pseudokugleri (Blow, 1969)

Diagnosis. Small test with roughly 5 chambers in the final whorl. Straight sutures on the spiral side and a curved peripheral margin in edge view.

Discussion. It can be distinguished from *P. kugleri* by lacking the angular margin, by having straight sutures on the spiral side, and by possessing one fewer chamber than is

typical of *P. kugleri*. It can be distinguished from *P. mayeri* and *P. siakensis* by having less inflated chambers.

Paragloborotalia opima (Bolli, 1957)

figs. 10.3, 10.4

Diagnosis. Large four-chambered test with cancellate wall texture. High rate of chamber expansion, giving it a quadrate appearance in equatorial outline. Prominent lip on the umbilical-extraumbilical aperture with a low arch.

Discussion. Historically, *Paragloborotalia opima* is distinguished from *Paragloborotalia nana* (originally a subspecies of *P. opima*) primarily by size: any specimen larger than 390 µm (or 320 µm depending on the author) is a *P. opima,* while smaller is *P. nana* (e.g., Bolli, 1957). While this is a biostratigraphically-useful, if tremendously utilitarian, species concept, it eschews all biological sense of what a species should be. With this definition, any juvenile *P. opima* is placed into *P. nana,* essentially growing into a different species throughout its ontogeny. While this remains the quickest and easiest tool for identifying these two species, other differences have been described (e.g., Spezzaferri, 1994). Those differences are apparently unsupported when addressed with a morphometric approach (Wade et al., *in review*). This creates what could be viewed as a philosophical conundrum: Are we dividing up foram morphospace as a stratigraphic tool or are we dividing it to approximate as close to true biological reality as possible? If we simply want to use planktic forams as chronostratigraphic tools, then subdividing species concepts on the basis of size makes sense. *P. opima* is a good

chronostratigraphic datum in an interval with few reliable datums. However, if we view them as biological species then the subdivision between these two species is at least questionable. One solution would be to re-erect them as subspecies as they were originally described, with *P. opima opima* and *P. opima nana.* This is still unsatisfactory, as *P. nana* is the long-ranging root-stock for many of the *Paragloborotalia.* The best solution may be to adopt *P. nana opima* and *P. nana nana*. This then relies on the longer-ranging, more important taxon as the species, with the brief probable ecophenotype as the subspecies. This also simplifies the ontogenetic problem, which is that currently an individual is a *nana* until it grows large enough to gain the prestige of an '*opima*'.

Either way, it remains prudent therefor to maintain the primary use of the size criterion for biostratigraphy until it can be definitively established that *opima* is an ecophenotype. Changing the definition of biostratigraphic datums has implications for subsequent works, and the size criterion has proven a useful, consistent, and simple-to-use datum.

It can be distinguished from *P. mayeri, P. siakensis,* and *P. pseudokugleri* by a smaller number of chambers, a quicker chamber expansion rate, and a more quadrate appearance. It can be distinguished from *P. kugleri* by the features stated above and by having a curved periphery in edge view.

Paragloborotalia nana (Bolli, 1957)

Figs. 10.1, 13.4, 13.5

Diagnosis. Small four-chambered test with a cancellate wall texture. Moderate rate of chamber expansion, giving a quadrate appearance in equatorial outline. Prominent lip on the umbilical-extraumbilical aperture, which is a low arch.

Discussion. See *Paragloborotalia opima* for a discussion on how to distinguish *P. nana* from *P. opima*.

It can be distinguished from *P. mayeri, P. siakensis, P. pseudokugleri* by a smaller number of chambers, a quicker chamber expansion rate, and a more quadrate appearance. It can be distinguished from *P. kugleri* by the features stated above, and by having a curved periphery in edge view.

Paragloborotalia mayeri (Cushman & Ellisor, 1939)

Fig. 10.2

Diagnosis. Moderate to large six-chambered test with a cancellate wall texture and inflated chambers.

Discussion. Much disagreement has occurred in the literature about the division between *P. mayeri* and *P. siakensis*. No *P. siakensis* could be identified at Site 803, so this work cannot illustrate the possible differences. It can be distinguished from *P. pseudokugleri* by possessing more inflated chambers. It can be distinguished from *P. kugleri* by lacking an angular periphery in edge view, by possessing more inflated chambers.

Paragloborotalia continuosa (Blow, 1959)

Diagnosis. Moderate-sized test with roughly four rapidly-expanding chambers in the final whorl. Cancellate wall texture.

Discussion. Paragloborotalia continuosa is grossly similar to the *P. nana - P. opima* group, with roughly four chambers in the final whorl. It can be distinguished from that group with a larger aperture and a higher expansion rate. This higher expansion rate gives the chambers a more inflated and spherical appearance.

Family CASSIGERINELLIDAE Bolli et al., 1957, emend. Li, 1986

Genus *Cassigerinella* Pokorný, 1955, emend. Li, 1986

Type species: *Cassigerinella boudecensis* Pokorný, 1955

Cassigerinella is readily distinguished by a microperforate wall and a unique coiled-biserial coiling style. Two species range through the Oligocene, *Cassigerinella chipolensis* and *Cassigerinella eocaenica*.

Cassigerinella chipolensis (Cushman and Ponton, 1932)

Discussion. Cassigerinella chipolensis is more common within the sediments than its parent species *C. eocaenica.* They can be distinguished by the degree of inflation within their chambers. *C. chipolensis* has more inflated chambers, which also gives the aperture a more rounded appearance.

Cassigerinella eocaenica Cordey, 1968

Discussion. C. eocaenica can be distinguished by a more compressed overall shape and chambers, which give it a thinner profile in edge view. It also has a more elongate aperture, due to the compressed final chamber. *Cassigerinella eocaenica is* rare within the sediments at Site 803, and only appearing sporadically within the upper Oligocene.

Family CHILOGUEMBELINIDAE Reiss, 1963

Genus *Chiloguembelina* Loeblich and Tappan, 1956

Type species: *Guembelina midwayensis* Cushman, 1940

Chiloguembelina is a small biserial genus. Species within it have varying degrees of ornament. It can be distinguished from *Streptochilous* by having rougher walls, and by lacking the 'drooping' chamber shape found in *Streptochilus*.

Chiloguembelina cubensis (Palmer, 1934)

Figs. 8.5, 8.7

Diagnosis. Biserial, costate test with a slow chamber expansion rate.

Discussion. Chiloguembelina cubensis differs from *C. adriatica* by having a slower expansion rate, which gives its test a straighter appearance. It can be distinguished from *C. ototara* by possessing costae, either continuous or discontinuous. While the

distinction between *C. cubensis* and *C. adriatica* can be done without the aid of an SEM, the distinction between *C. ototara* and *C. cubensis* is difficult (Huber et al., 2006).

T: 803D-37-3, 51-53 Zone O7

B: 803D-56-5 Zone PO1-2

Chiloguembelina adriatica Premec-Fućek et al., 2015

Figs. 8.4, 8.6

Diagnosis. Biserial test with a rapid expansion rate and a 'flaring' appearance to its test. The final and penultimate chambers in particular, are large relative to the preceding chambers.

Discussion. Chiloguembelina adriatica can be distinguished from *C. cubensis* by a strong 'flaring' appearance, with a much faster expansion rate. The final chamber in *C. adriatica* is large and spherical. *C. adriatica* is a rare species within the sediments at Site 803. It is more common within the lower Oligocene. This species is readily identified from the *C. ototara - cubensis* plexus with a binocular microscope.

T: 803D-41-1,55-57 Zone O6

Chiloguembelina ototara (Finlay, 1940)

Figs. 8.1, 8.2

Diagnosis. C. ototara is a small biserial species with a pustulose wall.

Discussion. It can be distinguished from *C. cubensis* by lacking costae. Due to the small size of the specimens, and the fine costae *C. cubensis* possesses early in this gradual transition (Figs. 7), the determination between these two species is best done through the use of SEM images, rather than light microscopy. It can be distinguished from *C. adriatica* by lacking the 'flaring' appearance of *C. adriatica.*

T: 803D-56-3 Zone O1-2

Family Chiloguembelinidae Reiss, 1963

Genus *Streptochilus* Brönnimann & Resig, 1971, emend. Smart & Thomas, 2007

Type species: *Bolivina tokelauae* Boersma, 1969

Streptochilus is a small biserial genus. Only one representative species was found at Site 803. *Streptochilus* possesses a smoother wall texture and has more embracing chambers than *Chiloguembelina.*

Streptochilus pristinum Brönnimann & Resig, 1971

Diagnosis. Small biserial test, with embracing chambers and smooth walls.

Discussion. It can be distinguished from *Chiloguembelina* by possessing a smooth wall and sutures which point down at the edge. This 'drooping' chamber shape is the most useful feature, as it can be determined through simple light microscopy.

Family GLOBANOMALINIDAE Loeblich & Tappan, 1984, emend. Pearson et al., 2006

Genus *Pseudohastigerina* Banner & Blow, 1959

Type species: *Nonion micrus* Cole, 1927

Pseudohastigerina is a very small planispiral genus with 6-9 chambers in the final whorl. The aperture is equatorial with a lip. Two species of this genus range into the lower Oligocene sediments at Site 803.

Pseudohastigerina micra (Cole, 1927)

Discussion. It can be distinguished from *P. naguewichiensis* by possessing a more rapid chamber expansion rate, leading to a less circular and more ovate test shape in umbilical view.

T: 803D-55-1, 63-65 Zone O1/O2 boundary

Pseudohastigerina naguewichiensis (Myatliuk, 1950)

Discussion. It can be distinguished from *P. micra* by possessing a less rapid chamber expansion, leading to a more circular test.

T: 803D-55-1, 63-65 Zone O1/O2 boundary

Genus *Turborotalia* Cushman & Bermúdez, 1949

Type species: *Globorotalia centralis* Cushman & Bermúdez, 1937

Turborotalia is a moderately-sized, moderately-compressed genus with a weakly cancellate wall texture. In the Oligocene most turborotalids has 4 chambers in the final whorl and lacks the keels prevalent during the Eocene. Both species present at Site 803 have large apertures, and small umbilical areas.

Tubrorotalia ampliapertura (Bollii, 1957)

Diagnosis. Moderately-sized test with large, umbilical-extraumbilical aperture. 4 chambers in the final whorl with a moderate expansion rate.

Discussion. It can be distinguished from *T. increbescens* by a more umbilically-pointed aperture and a less compressed test. There is, however, a high degree of intergradation between *T. ampliapertura* and *T. increbescens*.

T: 803D-51-3, 36-38 Zone O2/O3

Turborotalia increbescens (Bandy, 1949)

Diagnosis. Turborotalia increbescens is a moderately-sized species with a large, umbilical-extraumbilical aperture. It can be very compressed and tightly coiled, though not always.

Discussion. It can be distinguished from *T. ampliapertura* by its aperture, which points toward the edge, and can be a smaller, more compressed arch. It also can have a more compressed, less lobate test. There is a high degree of intergradation between *T. increbescens* and *T. ampliapertura*. This leads to some difficulty as *T. ampliapertura* is a

biostratigraphic marker species, and so a sensu stricto (s.s) delineation must be made, as it has been below.

T s.s.: 803-54-3,57-59 Zone O2

T cf.: 803-52-CC Zone O2

Family GLOBIGERINIDAE Carpenter et al., 1862

Genus *Catapsydrax* Bolli et al., 1957

Type species: *Globigerina dissimilis* Cushman & Bermüdez, 1937

Catapsydrax is one of the few predominantly bullate genera in the Oligocene. Species within this genus are moderate to large, bullate, 3.5-4 chambered macroperforate foraminifera. They have a heavily cancellate wall texture. There are 3 species of Catapsydrax within the sediments at Site 803, one of which is newly erected since the original publication.

Catapsydrax dissimilis (Cushman & Bermüdez, 1937)

Diagnosis. Large bullate test with a heavily cancellate wall and four chambers in the final whorl. The bulla, which most adult specimens possess, has two to four infralaminal openings.

Discussion. It can be distinguished from *C. unicavus* by having two to four infralaminal openings, not one, and from *C. indianus* by having up to four openings, and by lacking the ‘barbell’ shape bulla which *C. indianus* possesses.

The ranges of *Catapsydrax unicavus* and *Catapsydrax dissimilis* were not revised from the original publication, as those concepts have not changed.

Catapsydrax unicavus Bolli et al., 1957

Diagnosis. Large bullate species with a heavily cancellate wall and 3.5-4 chambers in the final whorl. The bulla, which most adult specimens possess, has one infralaminal opening and a lip.

Discussion. It can be distinguished from *C. dissimilis* by possessing only one infralaminal opening, rather than two to four openings. It can be distinguished from *C. indianus* by having only one infralaminal opening, and lacking the 'barbell' shaped bulla with five infralaminal apertures which *C. indianus* possesses.

The ranges of *Catapsydrax unicavus* and *Catapsydrax dissimilis* were not revised from the original publication, as those concepts have not changed.

Catapsydrax indianus Spezzaferri & Pearson, 2009

Diagnosis. Large bullate test with four chambers in the final whorl.

Discussion. The bulla takes the form of a 'barbell' shaped covering over the umbilical area, with five infralaminal apertures. As with the previous two species, the key to identification is the number of infralaminal apertures, as only *C. indianus* has five. The rare specimens at Site 803 also have a tendency to be more globular with deeper sutures, but it is difficult to generalize as so few *C. indianus* were observed.

B*:* cf. 803D-36-5, 50-52 Zone P22

Genus *Globorotaloides* Bolli, 1957

Type species: *Globorotaloides variabilis* Bolli, 1957

Globorotaloides is a moderately-size genus with between 3.5-6 chambers in the final whorl. It has a distinct cancellate wall texture and many species have a tendency to have bulla. It is very similar to *Catapsydrax* but can be differentiated on the basis of flatter coiling and typically smaller tests.

Globorotaloides hexagonus (Natland, 1938)

Diagnosis. Small species with roughly five chambers in the final whorl, flat coiling, and an umbilically-restricted aperture.

Discussion. It can be distinguished from *G. variabilis* by a lack of the bullate-like final chamber and by an umbilically-restricted aperture. We do not record any first or last occurrence, due to the rarity of this species within the sediments at Site 803.

Globorotaloides quadrocameratus Olsson et al., 2006

Diagnosis. Moderately-sized test with 4 chambers in the final whorl. It has a distinctly cancellate wall texture and a flat spiral side.

Discussion. It has a rapid chamber expansion rate and higher inflation, giving it a characteristic lobate shape that the other species of *Globorotaloides* lack. It can be distinguished from other *Globorotaloides* by lobate chambers. *Globorotaloides quadrocameratus* is a very rare species within the sediments at Site 803.

Globorotaloides suteri Bolli, 1957

Diagnosis. *S*mall- to medium-sized test with 3.5-4 chambers in the final whorl and a heavily cancellate wall. It can have a bulla, though does not always. Chambers expand at a moderate-to-high rate.

Discussion. Catapsydrax unicavus and *C. dissimilis* have a higher trochospire in late whorls, a more centered bulla, and more spherical test shape, distinguishing them from *G. suteri*. The juvenile tests of *C. unicavus* and *G. suteri* appear remarkably similar, and should be split on the basis of flatter coiling.

Globorotaloides variabilis Bolli, 1957

Diagnosis. Globorotaloides variabilis was found at this site to be a small species, with five chambers in the final whorl. It typically, but does not always, possess a bulla.

Discussion. The final, bulla-like, final chamber extends over the umbilicus, and is much larger than in many other *Globorotaloides* species, when present. It can be distinguished from *G. suteri* by possessing an additional chamber. It can be distinguished from *G. hexagonus* by a slightly smaller chamber expansion rate.

Family GLOBIGERINIDAE Carpenter et al., 1862

Genus *Ciperoella* Olsson et al., in prep.

Type species: *Ciperoella ciperoensis* Bolli, 1954

Ciperoella angulisuturalis (Blow, 1969)

Diagnosis. Moderately-sized test with a heavily cancellate wall texture. It has 4.5-5 chambers in the final whorl. It has a deep umbilicus with an umbilical aperture. It has a low to moderate trochospiral coiling style.

Discussion. Most distinct about *Ciperoella angulisuturalis* are the sutures, which are sharply depressed, forming a series of interconnected 'U' shaped channels around the specimen. Besides being moved to a new genus, this species concept was not revised, nor are there other species with similar features, and so the occurrences have not been reinvestigated.

Family GLOBIGERINIDAE Carpenter et al., 1862

Genus *Dentoglobigerina* Blow, 1979; emend. Pearson et al., in prep.

Type species: *Globigerina galavisi* Bermúdez, 1961

The genus *Dentoglobigerina* is unified by a distinct, cancellate wall texture, globular chambers, and a final chamber which typically projects over the umbilicus. This is a revised definition from the original, with the presence of an umbilical tooth no longer a generic-level trait. Species and specimens range from small (e.g., *D. prasaepis*) to some

of the largest in the Oligocene (e.g., *D. venezuelana*). Within the Oligocene, species typically have between three to four chambers, with two exceptions (*D. globosa* and *D. sellii*).

Several species first appear within Biozone O1, the first biozone within the study interval. Due to the scattered occurrences of several species within the first core (Core 59) in the study interval, the first appearance datum for species identified within those samples has not been interpreted.

Dentoglobigerina globularis (Bermúdez, 1961)

Figs. 6.2, 12.3, 12.4

Diagnosis. Large test with cancellate wall texture. It possesses 4 inflated globular chambers and an open and deep umbilicus with an umbilical tooth. Final chamber is reniform and projects over the umbilicus.

Discussion. In the original publication (Leckie et al., 1993) the species currently recognized as *D. globularis* was considered as *Globigerina gortanii*. *G. gortanii* was 'characterized by its bulla-like final chamberlet and variable dorsal convexity.' (Leckie et al., 1993). These remarks still describe many of the features of the '*G. gortanii*' shown in the illustrations. However, with the broadened description of the *Dentoglobigerina* genus, the 'parachute-like' final chamber fits within the *Dentoglobigerina* description, as dentoglobigerinid final chambers project over their umbilicuses.

Dentoglobigerina globularis is distinguished from *D. galavisi* by having four, rather than 3.5 chambers in the final whorl, and having an umbilical tooth that projects

toward the antepenultimate chamber when present, rather than to the suture. It also has a more inflated final chamber compared to *D. galavisi*.

Dentoglobigerina globularis is distinguished from *D. baroemoenensis* by having more globular chambers, a slightly more closed umbilicus. The more compressed chambers of *D. baromoenensis* gives it a more quadrate appearance and a more compressed final chamber in edge view.

Dentoglobigerina globularis is similar to *Subbotina projecta*, see *S. projecta* discussion and Figure 5 for how to distinguish these two homeomorphs.

Dentoglobigerina galavisi (Bermúdez, 1961)

Diagnosis. D. galavisi has 3.5 weakly oppressed chambers and a final chamber that projects over the umbilicus. It can be weakly ornamented with pustules around the umbilicus, and it has an umbilical tooth which points toward the suture.

Discussion. D. galavisi is distinguished from *D. sellii* by having more discrete chambers, a less spherical test, and by having 3.5 rather than three or less chambers in the final whorl. It is distinguished from *D. globularis* by having 3.5 rather than 4 chambers in the final whorl, and a less open and deep umbilicus. The umbilical tooth in *D. globularis* also points toward a chamber, while in *D. galavisi* it points toward a suture.

Dentoglobigerina prasaepis (Blow, 1969)

Figs. 7.2, 7.3

Discussion. D. prasaepis was not recognized within the original publication. This form is an extreme homeomorph with *Turborotalia euapertura*. *D. prasaepis* is a small compressed dentoglobigerinid. It has no tooth but retains a *Dentoglobigerina* wall-texture. Both *D. prasaepis* and *T. euapertura* have 3.5-4 chambers in their final whorls, with low broad arched apertures containing a rim or a lip. *D. prasaepis* tends to be smaller than *Turborotalia euapertura*, with the rougher wall typical of the dentoglobigerinids. The umbilical and apertural areas of *D. prasaepis* also tends to be somewhat pustulose, while *T. euapertura* is smooth. These homeomorphs are difficult to split without the aid of an SEM. The use of smooth vs. rough wall seems to be the most useful feature with a binocular microscope, though it is still difficult. *D. prasaepis* can also appear similar to *D. venezuelana*, but can be distinguished by a typically smaller size, the consistent lack of an umbilical tooth, smaller umbilical/apertural opening, and a more compressed appearance (see fig. 6).

Dentoglobigerina tripartita (Koch, 1926)

Diagnosis. Dentoglobigerina tripartita has a large spherical test, with three chambers in the final whorl. It can be found with, or without, a large tooth. The final chamber can also project into the umbilicus, though there are several examples of final chambers that appear more bulla-like, and are straight, rather than pointed, across the umbilicus. The area around the umbilicus is frequently heavily ornamented and pustulose.

Discussion. The concept employed for *"Globigerina tripartita"* in Leckie et al. (1993) has now been split into *D. tripartita* and *D. eotripartita* (Pearson et al., in prep.). *Dentoglobigerina tripartita* is distinguished by the overwhelmingly spherical test. This 'ball' like test shape is approached within *D. eotripartita*, and though useful, does not provide a sharp dividing line on which to delimit a species. In edge view, *D. tripartita* still has a spherical appearance, and while *D. eotripartita* has a projecting final chamber, it still has an open umbilicus, and very distinct chambers, which are lacking in *D. tripartita*. *Dentoglobigerina tripartita* also is only seen with 3 chambers in the final whorl, while *D. eotripartita* sometimes has 3.5 in less advanced forms.

D. tripartita is distinguished from *D. sellii* by its spherical test, and in having no apertural face. *D. sellii* can also have 2.5 chambers, while *D. tripartita* has 3 by definition.

Dentoglobigerina tapuriensis (Blow & Banner, 1962)

Figs. 9.4, 12.8

Diagnosis. Large test with cancellate wall texture. 3-3.5 chambers in the final whorl, with a large inflated final chamber and a high rate of chamber expansion.

Discussion. Only found at Site 628, this species is distinguished from *D. sellii* by lacking an umbilical tooth, by possessing 3-3.5 chambers, and by a final chamber that is <50% of the test in edge view. It also has a tendency to have less ornament on the apertural face, though the face is not always well developed. The aperture, most importantly, is a low-arched aperture, rather than resembling *D. sellii* with a tooth or lip

on a large aperture. It can be distinguished from *D. taci* by having a larger aperture and a larger test.

Dentoglobigerina eotripartita Pearson et al., in prep.

Figs. 9.2

Diagnosis. Large test with 3 to 3.5 chambers in the final whorl. Has a small- to medium-sized umbilicus. Can possess a very weakly developed apertural face, though frequently there is no apertural face. Final chamber projects over the umbilicus, and can have pustulose umbilical shoulders.

Discussion. Dentoglobigerina eotripartita is the ancestor of *D. tripartita*, and is descended from *D. galavisi*. It approaches, but does not reach, circularity in chambers similar to *D. tripartita*. As in *D. galavisi*, the umbilical tooth, when present, points to a suture.

D. eotripartita is distinguished from *D. galavisi* in having more oppressed chambers, typically 3 chambers in the final whorls. *D. eotripartita* is distinguished from *D. tripartita* by having a less circular outline in umbilical and edge view, and having a typically more open aperture. *D. eotripartita* is distinguished from *D. sellii* in the size of its final chamber. While the final chamber of *D. sellii* is more than 50% of the area of the test in umbilical view, the final chamber of *D. eotripartita* is smaller. Also, *D. sellii* can have less than 3 chambers in the final whorl, due to the increase in expansion rate in the final chamber.

Dentoglobigerina larmeui (Akers, 1955)

Figs. 12.6

Diagnosis. Moderately-sized test with four chambers in the final whorl and a cancellate wall texture. Umbilicus is moderately open and deep, with a quadrate appearance. Weakly developed apertural face with fewer perforations than the surrounding test.

Discussion. Dentoglobigerina larmeui was misidentified as *Globoquadrina dehiscens* within the original publication. Both species are distinctly quadrate, with 4 chambers in the final whorl. They have tight, rectangular umbilicuses, with umbilical teeth. The feature that distinguishes these two very similar species is best seen in edge view. They are distinguished on the development of a sharp, imperforate apertural face in *G. dehiscens*, while *D. larmeui* has a less developed perforate and rounded face. *D. dehiscens* also frequently has pustules at the top of the apertural face, *D. larmeui* is rounded. The umbilical tooth is also exaggerated in *G. dehiscens*, while it is subtle in *D. larmeui*. Lastly, the gross morphology of the test as seen from the umbilical side is different; *D. larmeui* is more rounded, while *G. dehiscens* is sharply quadrate. *D. larmeui* is best described as a transitional form between *D. galavisi* and *G. dehiscens*. Within the sediments at this location, B *D. larmeui* occurs at the M1a to O7 zone boundary with B *P. kugleri*.

B: 803D-35-1, 50-52 Zone M1a

Dentoglobigerina sellii (Borsetti, 1959)

Figs. 9.3, 12.7, 12.9

Diagnosis. Moderate to large test with 2.75-3 chambers in its final whorl. Rapid chamber expansion rate with a strongly apressed final chamber that is >50% of the test in umbilical view. Weakly developed apertural face. Test has a spherical overall appearance.

Discussion. Grossly similar to *D. galavisi,* but can be distinguished by a more closed umbilicus, more embracing chambers, especially the final chamber, and a higher expansion rate. This expansion rate gives *D. sellii* a more spherical appearance, while *D. galavisi* is more lobate in appearance. *Dentoglobigerina sellii* is distinguished from *D. tripartita* by having less embracing chambers, a weakly developed apertural face, and a less spherical test. *Dentoglobigerina sellii* is distinguished from *D. binaiensis* by lacking the sharp, imperforate apertural face of *D. sellii,* and by having up to three chambers, while *D. binaiensis* can have up to four.

B: 803D-55-CC Zone O1or2

Dentoglobigerina venezuelana (Hedberg, 1937)

Figs. 12.10, 12.11

Diagnosis. Large test with four very compressed and embracing chambers in the final whorl. The umbilicus is deep, but with a very tight opening. It has umbilical teeth, but these are frequently difficult to see within the umbilicus due to the small opening.

Discussion. *Dentoglobigerina venezuelana* can be readily distinguished from *D. tripartita* by having four chambers instead of three. *Dentoglobigerina venezuelana* is distinguished from *D. pseudovenezuelana* by having 4 chambers instead of 3.5-4 in its final whorl, and by its more compressed chambers. *Dentoglobigerina venezuelana* can be distinguished from *D. prasaepis* by its large size and by the presence of umbilical teeth. *Dentoglobigerina prasaepis* also has a different, more compressed apertural opening and a more compressed overall appearance.

Dentoglobigerina pseudovenezuelana (Blow & Banner, 1962)

Figs. 9.1

Diagnosis. Large 3.5-4 chambered test. Chambers range from embracing, seen typically in the final chamber, to subspherical, seen typically in the penultimate and previous chambers.

Discussion. It is generally a large species, though typically slightly smaller than the substantial *D. venezuelana.* It can be distinguished from *D. venezuelana* by a more quadrate appearance,and less embracing chambers. It can be distinguished from *D. tripartita* by having four chambers, with a large inflated final chamber. It can also appear similar to *D. eotripartita*, and can be distinguished by having four chambers and the more closed umbilicus, compared to the more open umbilical area of *D. eotripartita*.

Dentoglobigerina baroemoensis (LeRoy, 1939)

Diagnosis. Large test with four compressed chambers in the final whorl. It has a moderately wide and deep umbilicus.

Discussion. It can be distinguished from its ancestor *D. globularis* by the presence of compression in the final chamber, leading to a slightly wider and rectangular-shaped umbilical area. The umbilical tooth in the more derived specimens, which develop a more quadrate shape, can be larger than those typical of *D. globularis*. *D. baroemoensis* can be distinguished from its daughter species, *D. larmeui*, by the absence of the distinct quadrate appearance. *D. baroemoensis* is only loosely quadrate, while *D. larmeui* is sharply quadrate. *D. larmeui* is also flattened on the spiral side in edge view, while *D. baroemoensis* is curved. *D. larmeui* has created compression on the chambers as well, giving it a larger umbilical area than *D. baroemoensis.*

B: 803D-56-CC Zone O1 or 2

Dentoglobigerina globosa (Bolli, 1957)

Diagnosis. Moderately large globular test with 4.5-6 sub-spherical chambers in the final whorl.

Discussion. It strongly resembles its ancestor, *D. globularis*, but can be differentiated by the addition of at least half a chamber. This changes the outline of *D. globosa* from the ‘diamond’ shape of *D. globularis* to a more open and evolute test shape. The specimens within the study interval only vary from 4.5 to 5 chambers in their final whorl and are only seen very rarely.

B*:* 803D-47-5, 48-50cm Zone O4

Dentoglobigerina taci Pearson & Wade, 2009

Diagnosis. Moderately-sized 3-3.5 chambered test. Small umbilical aperture with a lip.

Discussion. It can be distinguished from *D. sellii* by possessing a very restricted aperture, and a smaller size. It can be distinguished from *D. tapuriensis* by possessing a smaller aperture and only three chambers in the final whorl.

Family GLOBIGERINIDAE Carpenter et al., 1862

Genus *Globigerina* d'Orbigny, 1826

Type species: *Globigerina bulloides* d'Orbigny, 1826

The genus *Globigerina* has, in the Oligocene, roughly four chambers in the final whorl with a *bulloides*-type wall. It possesses only a rimmed aperture if any apertural ornament is present. It also lacks any of the supplemental apertures of *Globigerinoides*, and is more trochospirally-coiled than *Globigerinella.*

Globigerina archaeobulloides Hemleben & Olsson, in prep.

Diagnosis. Moderately-sized test with a *bulloides*-type wall texture and 4-4.5 globular chambers in the final whorl. Low-arched aperture with a thin rim.

Discussion. It can be distinguished from *G. bulloides* by possessing a lower aperture, and a smaller umbilical area.

Globigerina bulloides d'Orbigny, 1826

Diagnosis. Large test with a *bulloides*-type wall texture with four embracing and very inflated chambers in the final whorl. It has a large, but moderately high aperture with a large umbilical area.

Discussion. It can be distinguished from *G. officinalis and G. archaeobulloides* by possessing a large umbilical area, a large aperture, and inflated chambers. It can be distinguished from *Globigerinella praesiphonifera* by possessing a moderately trochospiral test, an umbilical aperture, and a slower chamber expansion rate.

Globigerina officinalis Subbotina, 1953

Diagnosis. Moderate-size test with a *bulloides*-type wall texture and 3.5-4 chambers in the final whorl. It possesses a small- to moderately-sized aperture with a rim or lip. It has low trochospiral coiling.

Discussion. It can be distinguished from *G. bulloides* by possessing a smaller aperture and umbilical area, and a lower trochospire. It can be distinguished from *G. archaeobulloides* by possessing a smaller aperture and more compressed chambers.

Genus *Globigerinella* Cushman, 1927

Type species: *Globigerinella aequilateralis* (Brady, 1879)

The genus *Globigerinella* strongly resembles the genus *Globigerina*, in that members possess roughly four chambers in their final whorls, globular chambers, minimal ornament around the aperture, and a *bulloides*-type wall. It differs, however, in that they have a more planispiral coiling than *Globigerina*'s trochospiral coiling, and more derived forms (e.g., *Globigerinella roegelina*) possess several characters not found in *Globigerina*.

Globigerinella praesiphonifera (Blow, 1969)

Diagnosis. Moderately large test with a *bulloides*-type wall texture and 4-4.5 chambers in the final whorl. It has an extremely low trochospiral coiling style. It has a very quick expansion rate with inflated chambers. It has a large aperture which does not extend quite to the periphery and has a large umbilical area.

Discussion. It can be distinguished from *G. bulloides* by possessing a near-planispirally coiled test and a quicker chamber expansion rate. It can be distinguished from *Globigerinella obesa* by a quicker expansion rate and a more lobate test.

Globigerinella obesa (Bolli, 1957)

Diagnosis. Moderately-sized test with a *bulloides*-type wall texture. It has low trochospiral coiling, and four moderately inflated chambers in the final whorl. It has an umbilical-extraumbilical aperture with a moderate arch and a tight umbilicus.

Discussion. It can be distinguished from *Globigerinella praesiphonifera* by lacking the rapid expansion of chambers seen in that species, and by having a low trochospire, rather than a near-planispiral one. It is distinguished from *Globigerina officinalis* by having an umbilical-extraumbilical and moderately arched aperture and more inflated chambers, compared to *G. officinalis'*s more compressed chambers.

Globigerinella navazuelinsis (Molina, 1979)

Figs. 13.3

Diagnosis. Small test with a *bulloides*-type wall texture and five to six chambers in the final whorl. It has a planispiral coiling style. It has an aperture with a thick rim, which can be equatorially or umbilically positioned. It has a slow rate of chamber expansion.

Discussion. It can be distinguished from *Globigerinella roegelina* by possessing more chambers in the final whorl, a slower chamber expansion rate, a more compressed test, and less clavate chambers.

Globigerinella roegelina Spezzaferri & Coxall, in prep.

Figs. 13.2

Diagnosis. Small test with a *bulloides*-type wall texture and roughly four chambers in the final whorl. It has extremely low trochospiral coiling. Aperture typically a moderately high arch with a thick lip. The aperture is sometimes equatorial, extending to past the periphery. The final, and sometimes the penultimate, chamber(s) are distinctly clavate while earlier chambers are more spherical.

Discussion. It can be distinguished from *Globigerinella navazuelensis* by a more lobate test, possessing fewer chambers in the final whorl, having a trochospiral coiling style to *G. navazuelensis*'s planispiral style and by the clavate final chamber.

Genus *Globoquadrina* Finlay, 1947

Type species: *Globorotalia dehiscens* Chapman et al., 1934

Globoquadrina dehiscens (Chapman et al., 1934)

Diagnosis. Large four-chambered test with a cancellate wall texture. Umbilicus deep and open. Chambers distinctly compressed into a quadrate shape.

Discussion. *Globoquadrina dehiscens* was originally described in sediments from Site 803, but this investigation determined those to be the species *Dentoglobigerina larmeui*. *Globoquadrina dehiscens* can be distinguished from *Dentoglobigerina larmeui* by possessing a more quadrate test and a more open and deep umbilicus. Most importantly, when viewed in edge view, there is a substantial difference in the curvature of the chambers. *Dentoglobigerina larmeui* is rounded, whereas *G. dehiscens* possesses sharp umbilical shoulders, which have an imperforate apertural face below them.

Family GLOBIGERINIDAE Carpenter et al., 1862

Genus *Globoturborotalita* Hofker, 1976

Type species: *Globigerina rubescens* Hofker, 1956

Globoturborotalita is a moderately-sized genus with a heavily cancellate wall texture. Chambers are typically globular and embracing. Apertures are umbilical, and generally small in the early Oligocene, with some species taking on larger apertures in the upper Oligocene. Individuals within the genus *Globoturborotalita* were rare within the sediments at Site 803 so B/T were not determined for this genus.

Globoturborotalita ouachitaensis (Howe & Wallace, 1932)

Diagnosis. Small test with a heavily cancellate wall-texture. It has four evenly-spaced chambers in the final whorl, giving it a characteristic diamond shaped test. It also has an umbilically-restricted aperture with a lip.

Discussion. It can be distinguished from *G. eolabiacrassata* and *G. labiacrassata* by possessing a more quadrate outline, and a smaller lip. *Globoturborotalita ouachitaensis* is very rare at this site, only appearing in the top sample of this study.

Globoturborotalita euapertura (Jenkins, 1960)

Figs. 7.1

Diagnosis. Small species with four chamber in the final whorl, and a coarsely cancellate wall texture. It has an umbilical aperture with a small rim. It has a "wedge-like" shape in edge view.

Discussion. Globoturborotalita euapertura is frequently misidentified as *Dentoglobigerina prasaepis*, due to the severe homeomorphy between the two species. Both species have compressed tests with a rimmed umbilical aperture. *Dentoglobigerina prasaepis* can be pustulose around the umbilical area and has somewhat inflated chambers, while *G. euapertura* does not have pustules and is more 'wedge-shaped' in edge view. *Globoturborotalia euapertura* also possesses a more circular aperture, a more compressed test, and is typically smaller than *D. prasaepis*. It should be noted that these are all very fine, and frequently difficult to see, differences. These species both possess characteristics atypical for their genera, *D. prasaepis* lacks the umbilical tooth of the dentoglobigerinids while *G. euapertura* has a final chamber which projects across the umbilicus, as typical in the *Dentoglobigerina*.

Globoturborotalita euapertura can be distinguished from *G. labiacrassata* and *G. eolabiacrassata* by lacking the thick lip typical of those two species, and having a less lobate periphery. *Globoturborotalita labiacrassata* also possesses a more open umbilical area.

Globoturborotalita labiacrassata (Jenkins, 1966)

Diagnosis. Moderately-sized test with four subglobular chambers in the final whorl. It possesses an umbilical aperture, with a thick rim.

Discussion. It can be distinguished from *G. eolabiacrassata* by possessing a higher arched aperture, a more open umbilicus, and a more lobulate test. It can be distinguished from *G. ouachitaensis* by possessing a less quadrate test, a thinner lip, and less lobate appearance.

Globoturborotalita eolabiacrassata Spezzaferri et al., in prep.

Figs. 11.3

Diagnosis. Moderately-sized test with a thickly cancellate wall texture and four chambers in the final whorl. It possesses a characteristic thick lip around the umbilically-restricted aperture.

Discussion. It can be distinguished from *G. labiacrassata* by a generally smaller size, more compressed chambers, and a smaller umbilical area. It also possesses a lower aperture. It can be distinguished from *G. ouachitaensis* by possessing a thick lip, more compressed chambers, and lacking the characteristic quadrate appearance of *G. ouachitaensis.*

Globoturborotalita cancellata (Pessagno, 1963)

Figs. 11.4

Diagnosis. Large test with a heavily cancellate wall and 3.5 to 4 chambers in the final whorl. It has a small umbilically-oriented aperture, with a thickened lip or rim, and a small umbilical area.

Discussion. It can be distinguished from *G. ouachitaensis* by possessing a lighter lip or rim, not being as quadrate, possessing less lobulate chambers. It can be distinguished from *G. labiacrassata* and *G. eolabiacrassata* by possessing a lighter lip or rim, and generally a larger test. It can be distinguished from *G. paracancellata* by having more embracing chambers, and a final chamber that is roughly the same size, or slightly smaller, than the penultimate chamber. *Globoturborotalita cancellata* and *G. paracancellata* are very similar, and distinguishing them, especially as their ranges are similar, can be challenging.

Globoturborotalita paracancellata Olsson & Hemleben, in prep.

Figs. 11.5

Diagnosis. Large test with a heavily cancellate wall and 3.5 to 4 chamber in the final whorl. It has a small umbilically-oriented aperture, with a thickened lip or rim, and a small umbilical area.

Discussion. It can be distinguished from *G. ouachitaensis* by possessing a lighter lip or rim, not being as quadrate, possessing less lobulate chambers. It can be distinguished from *G. labiacrassata* and *G. eolabiacrassata* by possessing a lighter lip or rim, and generally a larger test. It can be distinguished from *G. paracancellata* by having a more lobulate periphery, and a final chamber that is larger than the penultimate. *Globoturborotalita cancellata* and *G. paracancellata* are very similar, and distinguishing them, especially as their ranges are similar, can be challenging.

Family GLOBIGERINIDAE Carpenter et al., 1862

Genus *Subbotina* Brotzen & Pozaryska, 1961, emend. Olsson et al., 1999

Type species: *Globigerina triloculinoides* Plummer, 1926

Subbotina is a lobate, weakly cancellate genus with three to four chambers within the final whorl during the Oligocene. Representative specimens typically have an umbilical aperture with some degree of apertural ornament. It is differentiated largely by more distinct chambers than *Dentoglobigerina* and a weaker wall texture than *Globoturborotalita*.

Subbotina angiporoides (Hornibrook, 1965)

Diagnosis. Small- to moderately-sized test with three to four chambers in the final whorl. It has a thick rim around the aperture, which is a low slit which extends across the antepenultimate chamber. It has compressed chambers, and a smooth, macroperforate wall.

Discussion. It can be distinguished from *Globoturborotalita labiacrassata* and *G. eolabiacrassata* by the size of the aperture, both *G. labiacrassata* and *G. eolabiacrassata* have a visible umbilical area, while *S. angiporoides* does not, and by the degree to which the chambers are compressed. Both *G. labiacrassata* and *G. eolabiacrassata* have less compressed chambers, while *S. angiporoides* has more compressed and more embracing chambers. It can be distinguished from *S. minima* by possessing a lower aperture, by

having an umbilical, rather than an umbilical-extraumbilical aperture, and by having four, rather than 3.5, chambers in the final whorl. It can be distinguished from *S. utilisindex* by having four, rather than three, chambers in the final whorl, and by having an umbilical, rather than umbilical-extraumbilical aperture, and a thicker lip.

Subbotina corpulenta (Subbotina, 1953)

Diagnosis. Large test with four inflated chambers in the final whorl. The umbilicus is frequently covered with an inflated bulla.

Discussion. It can be distinguished from the genus *Catapsydrax* by possessing the less cancellate and smoother wall typical of the subbotinids, and by the more inflated bulla, which tends to appear 'balloon-like' over the umbilicus. The bulla present in *Catapsydrax* also have lips and smaller apertures. The aperture on *S. corpulenta* tends to extend over a larger area, and tends to extend higher. It can be distinguished from *Globorotaloides* by lacking the characteristic wall texture of the *Globorotaloides* and by possessing a higher trochospire and a more inflated bulla and chambers. It can typically be distinguished from *S. eocaena* by possessing a bulla.

Subbotina eocaena (Gümbel, 1868)

Diagnosis. Moderate to large test with 3.5-4 chambers in the final whorl. It has a umbilical aperture with a moderately high arch, bordered by a lip. It has inflated lobate chambers.

Discussion. *Subbotina eocaena* is very similar to *Globoturborotalita paracancellata*. Both species have 3.5-4 chambers in the final whorl, a moderately high arched aperture, with embracing, lobate chambers. The distinguishing difference between the two species is the presence of a lip in *Subbotina eocaena* and a rim in *Globoturborotalita paracancellata.* This is frequently a difficult split to make, even in well-preserved material, but it was attempted in these sediments. Both species were rare, and so no discussion of further morphological features can be made, as any identification could be in the range of variability not fully observed within the sediments at Site 803.

Subbotina eocaena can be distinguished from *Dentoglobigerina globularis* by lacking an umbilical tooth. This is not always a useful distinction, as *Subbotina eocaena* has a prominent lip, which can be unevenly distributed around the aperture, giving it the appearance of a weak tooth. It can also be distinguished by more spherical chambers, a smaller umbilical area, and by not having a final chamber that projects over the umbilicus. Those features are also more useful than distinguishing between an uneven lip and a tooth under a binocular microscope.

It can be distinguished from *S. projecta* and *S. tecta* by possessing only a lip for apertural ornament, rather than *S. tecta*'s shield-like projection, and *S. projecta*'s umbilical tooth. It also possesses more tightly coiled chambers with a small umbilicus.

Subbotina minima (Jenkins, 1965)

Diagnosis. Small- to moderately-sized test with a weakly cancellate wall texture. It has a small umbilical area, with a low-arched aperture. It has roughly three and a half slowly inflating chambers in its final whorl, giving it a compressed, subspherical form.

Discussion. It can be distinguished from *Subbotina angiporoides* by possessing fewer chambers, and lacking the prominent lip possessed by *S. angiporoides*. It can be distinguished from *Globoturborotalita eolabiacrassata* and *Globoturborotalita labiacrassata* by lacking a prominent lip, possessing more compressed chambers, and a more closed umbilicus.

Subbotina projecta Olsson et al., in prep.

Figs. 6.1, 12.1, 12.2, 12.5

Diagnosis. Large test with a cancellate wall texture and 3.5-4.5 subspherical to globular chambers in the final whorl. It has a large umbilicus and aperture ornamented with a large tooth. The tooth tends to be off-center and curved, with elevated sides, like a tooth-rim.

Discussion. Figure 6 illustrates the differences between *Subbotina projecta* and *Dentoglobigerina globularis.* The key difference between these two species, and that which clearly places *projecta* in *Subbotina* rather than *Dentoglobigerina* is the wall texture, which is clearly subbotinid. Besides that single difference, difficult to see using a binocular microscope, there is no single clean criterion upon which to distinguish these two species. *S. projecta* is not muricated about the umbilicus, though this is not always strong in *D. globularis*. *Dentoglobigerina globularis* has a slower expansion rate, which

gives it a somewhat more quadrate appearance, though again, this is subtle. *Dentoglobigerina globularis* also possess four chambers, while *S. projecta* can have between 3.5-4.5. The final chamber in *S. projecta* is more variable, in *D. globularis* the final chamber is always reniform, and projects over the umbilicus slightly, while in *S. projecta* the final chamber can be very subspherical to compressed, as in Figure 6. Coiling tends to be somewhat looser in *S. projecta* and tighter in *D. globularis*.

It can be distinguished from *Subbotina eocaena* by the presence of an umbilical tooth and by a larger umbilicus. It can be distinguished from *Subbotina corpulenta* by a smaller expansion rate, less embracing chambers, presence of an umbilical tooth, and the lack of a bulla.

Subbotina utilisindex (Jenkins & Orr, 1973)

Diagnosis. Small to Moderate-sized test with a weakly cancellate wall texture. It has a small umbilical area, with a low-arched aperture. It has roughly three and a half slowly inflating chambers in the final whorl, giving it a compressed, sub spherical form.

Discussion. It can be distinguished from *Subbotina angiporoides* by possessing fewer chambers, and lacking *S. angiporoides* prominent lip. It can be distinguished from *Globoturborotalita eolabiacrassata* and *Globoturborotalita labiacrassata* by lacking a prominent lip, possessing more compressed chambers, and a more closed umbilicus.

Family GLOBIGERINIDAE Carpenter et al., 1862

Subfamily GLOBIGERININAE Carpenter et al., 1862

Genus *Globigerinoides* Cushman, 1927

Type species: *Globigerina rubra* d'Orbigy, 1839

Globigerinoides is a genus similar to *Globigerina* or *Globigerinella*, but all species possess a supplemental aperture. Species within *Globigerinoides* possess a *bulloides*-type wall texture.

Globigerinoides primordius (Blow & Banner, 1962)

Diagnosis. Large test with a cancellate wall texture and 3-3.5 subspherical to spherical chambers the final whorl. It has a umbilical aperture with a thick rim, and a small supplemental aperture on the spiral side. It has a high rate of chamber expansion, with the final chamber close to 50% of the test in umbilical view.

Discussion. It can be distinguished from most other foraminifera not within *Globigerinoides* by simply possessing a supplemental aperture. It most closely resembles a *Globigerina bulloides* with the small addition of a supplemental aperture.

Globigerinoides inusitatus Jenkins, 1966

Diagnosis. Large foraminifera with a cancellate wall texture and 3-4 chambers in the final whorl.

Discussion. It possesses a range of morphologies from *G. primordius*-like to *G. trilobus*-like, but is unified by the small primary, umbilical aperture, and a far larger

supplemental aperture on the spiral side with a rim. That larger supplemental aperture distinguishes this species from others in the *Globigerinoides.* No further comments can be made about the general morphology of *Globigerinoides inusitatus*, as only one specimen was found.

Family GLOBIGERINITIDAE Bermúdez, 1961, revised Li, 1987, revised, Pearson & Wade, 2009

Genus *Globigerinita* Brönnimann, 1951

Type species: *Globigerinita naparimaensis* Brönnimann, 1951

Globigerinita is a small microperforate genus. As the taxonomy of this genus has not changed in the recent Oligocene revision, the identifications were verified but not revised through this interval.

Genus *Tenuitella* Fleisher, 1974, emend. Li, 1987, Huber et al., 2006

Type species: *Globorotalia gemma* Jenkins, 1966

Tenuitella is a small, trochospiral, microperforate genus. Within the Oligocene, there are three species, with between four to five chambers in the final whorl.

Tenuitella angustiumbilicata (Bollii, 1957)

Diagnosis. Small 4.5-5 chambered test with microperforate walls. The wall texture can be ornamented with small pustules.

Discussion. It can be distinguished from *T. gemma* by slightly higher coiling, a more compact test, and a tendency to have 4.5 chambers. That coiling is most obvious in the final chamber, which has a tendency to stand out in edge view, away from the previous chambers. It can be distinguished from *T. munda* by possessing at least 4.5 chambers to the four found in *T. munda*.

Tenuitella gemma (Jenkins, 1966)

Discussion. It can be distinguished from *T. angustiumbilicata* by slightly lower trochospire coiling, typically a smoother test, and a tendency to have 5 rather than 4.5 chambers. It can be distinguished from *T. munda* by possessing 4.5-5 chambers in the final whorl, while *T. munda* has 4.

The original Leckie et al., 1993 publication employed *T. gemma* as a species, illustrated with in Plate 6, but did not list the range within Figure 6 as an oversight.

T: 803D-37-1, 50-52 Zone O7

Tenuitella munda (Jenkins, 1966)

Discussion. It can be distinguished from other tenuitellids by possessing only 4 chambers.

Family HANTKENINIDAE Cushman, 1927

Genus *Hantkenina/Cribrohantkenina*

Discussion. Hantkenina alabamensis was originally listed within the samples at Site 803. However, within those sediments, only tubulospines were found. No full tests were seen. As we are here following the revised taxonomy of the Paleogene Planktonic Working Group, there are five possible species within the last biozone of the Eocene. Determination to species level is not possible, so the species leaving test debris could have been *H. primitiva, H. compressa, H. alabamensis, H. nanggulaensis,* or *Cribrohantkenina inflata.*

CHAPTER 3

THE MI-1 EVENT: ORBITAL AND SECULAR CHANGES FROM LOW AND HIGH LATITUDES

3.1 Abstract

The Oligocene/Miocene boundary is characterized by a ~1.0‰ oxygen isotope excursion, the Mi-1 event (23.0 Ma), representing an abrupt and transient glaciation on Antarctica. This study produces three records of the event: DSDP Site 78 and ODP Site 803 in the eastern and western equatorial Pacific Ocean, respectively, and ODP Site 744 on the Kerguelen Plateau in the Southern Ocean. Paloeceanography of these sites is elucidated through sediment particle counts, stable isotopes, and size fraction analyses. The study reveals the influence of both secular and orbital controls on the records. Changes in the depth of the lysocline at Sites 744 and 803 are shown to be global and caused by eccentricity forced changes in carbonate productivity. Site 744 displays a strong connection to the ~1.2 Ma obliquity amplitude cycle. Increased wind driven upwelling ~300-kyr prior to the Mi-1 peak oxygen isotope values drew warmer intermediate waters up to the surface, increasing local productivity. About 150-kyr of the Mi-1 excursion is missing in a hiatus at Site 744, which agrees with other data showing increased bottom water flow of the Antarctic Circumpolar Current. Progressively higher rates of productivity during the last 1.2-1.3 myr of the Oligocene, timed at ~405-kyr eccentricity band, sequestered CO_2 and preconditioned Antarctica for glaciation across the Oligocene/Miocene boundary, which was itself driven finally by orbital conditions. Thus, we conclude that Mi-1 is driven by a mix of long-term and orbital changes.

3.2 Introduction

In the broadest terms, the Oligocene was an 'ice-house' world, and while parts of the Miocene were a brief respite of warmth, much of the Miocene was cool (Zachos et al., 2001a). As with most geological boundaries, the Paleogene/Neogene boundary was defined first on paleontological data. The Neogene was used first as a term to group Miocene and Pliocene mollusks as distinct from Eocene (Hörnes, 1853). Evolutionary and ecological distinctions have since been codified by subsequent research, not just in mollusks, but in the evolution of grass (e.g., Kellog, 2001; Strömberg, 2005) and grazers (e.g., MacFadden et al., 1991), corals (e.g., Edinger and Risk, 1994; Budd and Johnson, 1999), foraminifera (e.g., Cifelli, 1969; Fraass et al., 2015) and other microfossils (Kamikuri et al., 2005) among others, though some of this evolutionary activity is dispersed throughout the early Miocene.

While many of the changes between the Oligocene to the Miocene are gradational, there are punctuations in this transition. One such transition is the Mi-1 (Miocene isotope) event. Mi-1 was first described in Miller et al. (1991) as an 'isotope zone' to be used for global correlation, though with an eye to its presumed paleoclimatic significance. Mi-1 is a ~1.0‰ oxygen isotope excursion in benthic foraminifera seen globally (Miller et al., 1991; Zachos et al., 2001a, 2001b). It is the first of several 'Mi' events, similar to the 'Oi' (Oligocene isotope) events from the Oligocene (Miller et al., 1991). Typically, the ~1‰ $\delta^{18}O$ excursion is believed to be ~50% ice-volume change and ~50% deep-sea temperature shift (Paul et al., 2000). Evidence for glaciation at Mi-1 is not exclusively isotopic; it coincides with major sequence boundaries on the New Jersey Margin (Miller et al., 1996; Kominz et al., 2008), glacial marine sediments (Leckie and

Webb, 1986; Birkenmajer, 1987; Naish et al., 2001, 2008; Wilson et al., 2009), as well as more positive $\delta^{18}O$ benthic values than can be accounted for by the change in the Mg/Ca paleothermometer (Cramer et al., 2011; Mawbey and Lear, 2013).

3.2.1 Chronostratigraphy

The Chattian-Aquitanian Global Standard Stratotype-section and Point (and therefore the Paleogene-Neogene and Oligocene-Miocene boundaries) is defined at the Lemme-Carrosio section (Italy) at the reversal between subchrons C6Cn.2n and C6Cn.2r (Steinger et al., 1997). The stratigraphic position of the boundary is corroborated in marine settings by planktic foraminifer *Paragloborotalia kugleri* (Base of biozone M1) and calcareous nannofossil *Reticulofenestra bisecta* (Base of biozone NN1), along with several other secondary markers (Steinger et al., 1997). As ~1‰ oxygen isotope excursions in the marine realm are generally interpreted as globally synchronous events (though see Results-Chronostratigraphy), Mi-1 provides an important check on the bio-magnetostratigraphy.

The most recent date for Mi-1, based on an integrated magento-astrochronology age model at ODP Site 1264 (Liebrand et al., 2011) is 23.0 Ma (corroborating previously established dates by Shackleton et al., 2000), directly following the base C6Cn.2n (Cycle $58_{OI\text{-}C6Cn}$; *sensu* Wade and Pälike, 2004; Fig. 3.1). The inflection point with increasing values for Mi-1 starts at ~23.3-23.2 Ma, depending on the section considered (~23.3 Ma, Site 926/929, Zachos et al., 2008; ~23.2 Site 1090, Billups et al., 2002). In a broad sense, the inflection can be seen as roughly coincident with subchron C6Cn.3n. There are large changes in benthic foraminiferal $\delta^{13}C$ as well (Figs. 3.1, 3.2), with 3-4 increasingly large eccentricity paced variation beginning at ~24.2 Ma. The series of events culminating in

the glaciation are the reason that this interval of Earth history is frequently referred to by UK authors as the 'OMT' or Oligocene Miocene Transition. OMT will be used hereafter to denote the interval from 24.5-22 Ma, the lead up and recovery to glaciation, while Mi-1 denotes the ~1‰ excursion in benthic foraminiferal $\delta^{18}O$ values. While there is a distinction, Mi-1 will also be used as the name for the glaciation implied by the isotopic values, to ease the nomenclatural burden on the reader.

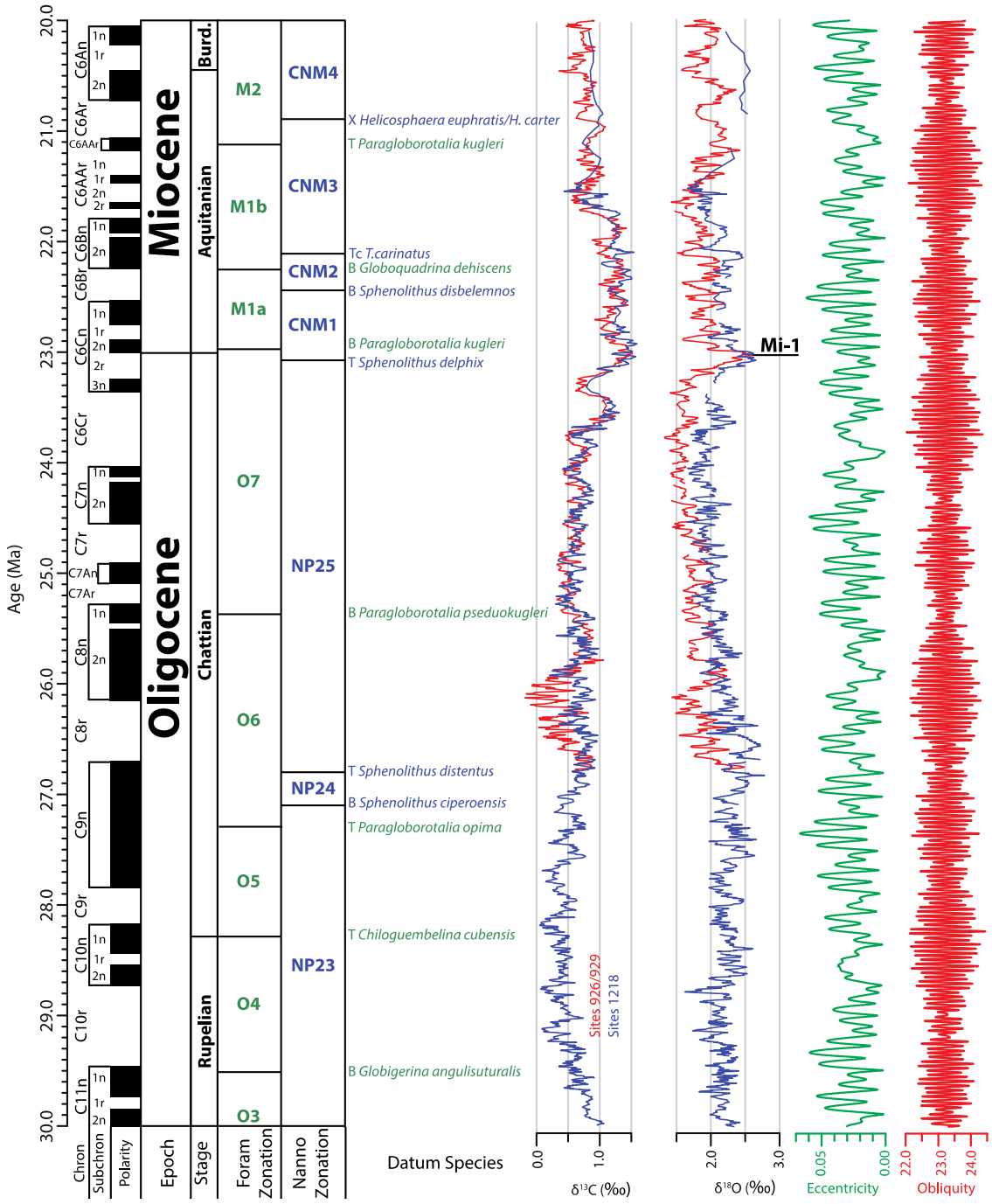

Figure 3.1 Summary of Chronostratigraphic data. Chron, subchron, and polarities are from Pälike et al. (2006b). Planktic Foraminiferal zonation scheme from Wade et al. (2011). Calcareous nannofossil zonation scheme from Expedition 320/321 Scientists (2010) (NP Zones) or Backman et al. (2012) (CN Zones). Blue datum species are the primary datums for calcareous nannofossil zonations while green are primary datums for planktic foraminiferal zonation. T = Top, B = Bottom, Tc = Top Common occurrence, while X refers to a change in dominance. Stable isotope data was compiled in Zachos et

al. (2008) from Pälike et al. (2006b) for Site 1218 (blue lines) and Zachos et al. (2001) for Sites 926/929 (red lines). All stable isotope data are presented as a 5-point running mean. Orbital parameters (eccentricity and obliquity) are from the Laskar et al. (2004) solution.

There are four 'standard-bearer' sites for examining Mi-1 (Fig. 3.1). ODP Sites 929 and 926 are typically examined together, as they are closely spaced on the Ceara Rise, off the north coast of Brazil in the western equatorial Atlantic, with minimal differences in the $\delta^{18}O$ values (Zachos et al., 2001b; Pälike et al., 2006a). ODP Site 1218 is in the eastern equatorial Pacific Ocean, and the time series demonstrate similarity in stable isotope values to Sites 929/926. ODP Site 1090 is within the subantarctic southern South Atlantic Ocean, and while Mi-1 has a very clear expression at this location, the correlation with paleomagnetic datums records a slightly different timing (fig. 3.2).

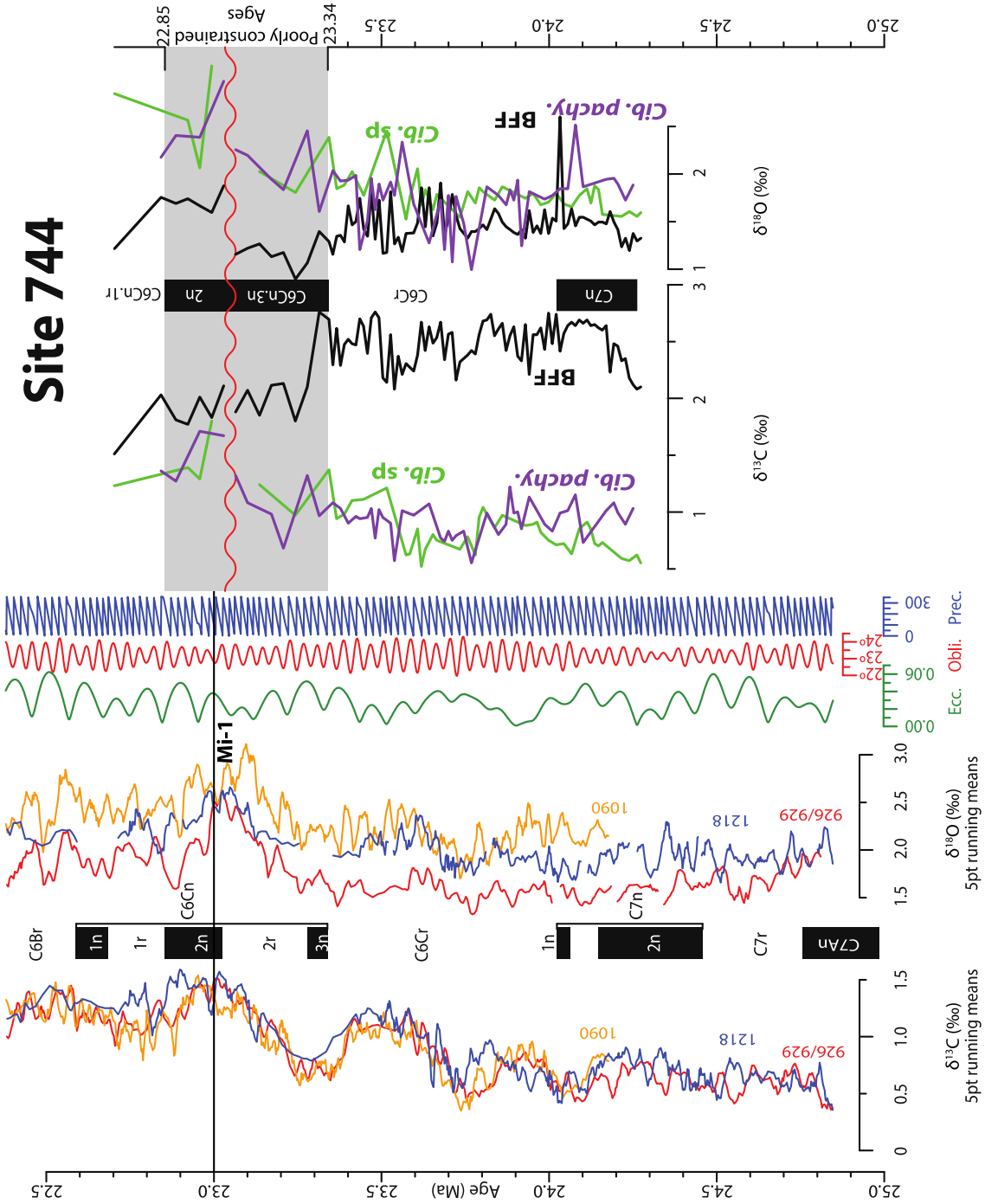

Figure 3.2 Stable isotope stratigraphy. Left panel depicts $\delta^{13}C$ and $\delta^{18}O$ records (5-pt running means) from Sites 926/929 (red), 1090 (orange), and 1218 (blue). Data were compiled in Zachos et al. (2008). In-between stable isotope time series is paleomagnetic polarity stripe with chron and subchron designations. Green, red, and blue lines in the middle of the figure represent orbital parameters eccentricity, obliquity (tilt), and procession, respectively (Laskar et al., 2004). Right panel is stable isotope values from Site 744, bulk fine fraction (black), *Cibicidoides pachyderma* (purple), and *Cibicidoides*

sp. (green). All *Cibicidoides* data have been adjusted to equilibrium values (+0.5‰) to aid in comparison to the Zachos et al. (2008) compilation.

3.2.2 Possible Causes of Mi-1

The current leading hypothesis for the cause of the Mi-1 glaciation is climatic forcing due to favorable orbital parameters. Zachos et al. (2001b) suggested a cold-favorable node, dominated by low eccentricity and low obliquity, triggered Mi-1. Since that publication there have been revisions to the calculations of the orbital parameters (Laskar et al., 2004; Laskar et al., 2010), which put the strong obliquity node at ~24.2 Ma, while 23.0 Ma is not as strong. Modeling investigations suggest that that there are thresholds for atmospheric pCO_2 that must be reached for glaciation to occur, despite orbital configurations favorable for ice growth (DeConto et al., 2008). Subsequent investigations into orbital pacing and glaciations suggest that the climate system must be 'pre-conditioned' by low obliquity, then triggered by low eccentricity (Wade and Pälike, 2004; Pälike et al., 2006b). The orbital driver hypothesis usually draws upon the carbon cycle to force glaciations. One consequence is deepening-shoaling cycles in the lysocline at eccentricity periods (Pälike et al., 2006b). At Sites 926/929 there is some suggestion of increased current strength or lysocline changes at the ~1.2 myr modulated-obliquity period (Zachos et al., 1996), but it may not be a direct linkage (Pälike et al., 2006a). This ~1.2 myr obliquity period appears throughout the Oligocene, frequently prior to Oi (Oligocene isotope) events (Wade and Pälike, 2004).

Various measures of paleoproductivity peak around 23.0 Ma, with increasing values starting earlier with higher latitude (~24.6 Ma, Site 1090; ~23.7 Ma, Site 1265; Diester-Haass, et al., 2011) and later at low latitude Sites 926/929 (U/Ca 23.2 Ma;

Mawbey and Lear, 2013; BFAR 23.4 Ma; Diester-Haass et al., 2011). Paleoproductivity indicators are high throughout the OMT (as defined here) within southern latitude marine sites. Carbonate accumulation rates also strongly increase in these intervals at roughly equivalent timing as the benthic foraminiferal accumulation rate (BFAR), suggesting a link between the BFAR and carbonate accumulation. This link, however, is only seen at the mid- to higher latitude sites, not at the low latitudes (Diester-Haass, et al., 2011; Florindo et al., 2015). Rates of biogenic opal and organic carbon deposition increase prior to the Mi-1 event at Site 1090 (Anderson and Delaney, 2005). DSDP Site 516 in the western South Atlantic Ocean, also records increasing sedimentation rates leading up to a peak coinciding with Mi-1 (Florindo et al., 2015). Productivity proxies and $\delta^{13}C$ were both found to track both the short and long eccentricity cycles (Diester-Haass et al., 2011). Coherence in these cycles has previously been taken to suggest that eccentricity-paced productivity is controlling the $\delta^{13}C$ values, and that increased paleoproductivity drew down atmospheric CO_2 to levels triggering glaciation (Diester-Haass et al., 2011; Florindo et al., 2015). CO_2 levels, however, are generally stable in most reconstructions for the latest Oligocene (e.g., Zhang et al., 2013). Possible explanations include issues with CO_2 proxies or temporal resolution issues (e.g., Zhang et al., 2013). If CO_2 was stable throughout the latest Oligocene, more of an onus is put on orbital and other drivers to glaciate Antarctica.

Studies of the Eocene Oligocene Transition (EOT) and OMT both invoke carbonate burial mechanisms to drive glaciation (see below). As such, changes in bottom water are of interest when discussing these periods. Late Oligocene and early Miocene deep water was typically sourced from the Southern Ocean as suggested by low-

resolution $\delta^{13}C$ gradient data from a variety of sites (e.g., Woodruff and Savin, 1989; Wright and Miller, 1992). Evidence from Site 1090 suggests that the Antarctic Circumpolar Current (AAC) operated differently in the past; the shallower ACC may have facilitated organic carbon burial in the Southern Ocean (Anderson & Delaney, 2005). The Oligocene CCD was ~1 km or more deeper than during much of the Eocene (Pälike et al., 2012), but evidence from Site 1090 suggests that an important control on the local CCD in the Southern Ocean is the productivity and flux of calcareous plankton (Anderson & Delaney, 2005). In addition, evidence from Site 1090 suggests that organic carbon burial during the late Oligocene to early Miocene was more efficient with higher biosiliceous productivity, rather than during times dominated by carbonate sedimentation (Anderson & Delany, 2005), counter to modern hydrography. Opal and phosphorus burial leads the $\delta^{13}C$ changes at Site 1090 by ~80-kyr, which Anderson and Delaney (2005) view as a biogenic opal flux driver for the carbon cycle changes proceeding Mi-1. There is some discussion of increased weathering and/or upwelling through the OMT leading to the productivity changes, but differentiating the two processes has proven difficult (Anderson and Delaney, 2005; *and references therein*).

Largely distinct from the paleoproductivity drawdown model is the 'missing sink' model of Lear et al. (2004). At Site 1218 in the eastern equatorial Pacific Ocean there is an interpreted cooling step of ~2°C based on benthic foraminiferal Mg/Ca at ~23.8 Ma, followed by a gradual warming of bottom waters of ~2°C until 23.3 Ma (Lear et al., 2004). The authors explained the warming as a negative feedback of glacial ice growth covering the Antarctic bedrock, lowering global weathering rates (the 'missing sink' model; also see Scher et al., 2011). A second cooling event at ~23.3-23.1 Ma is the

second advance of the ice sheet in their model, leading to another warming step after 23.1 Ma. The 'missing sink ' mechanism attempts to explain the observed two-step ice growth and cooling at Mi-1, and is supported by $\delta^{18}O$ leading $\delta^{13}C$ (Lear et al., 2004). Similar, but higher resolution evidence at Sites 926/929 in the western equatorial Atlantic demonstrate orbital control to the cooling steps around Mi-1. Organic carbon burial then acted as a feedback to help cool the climate, as evidenced by an increase in the U/Ca and BFAR proxies (Mawbey and Lear, 2013), in lock-step with eccentricity. They also find two cooling steps prior to the maximum $\delta^{18}O$ values (~23.0 Ma) though with different timing, at ~23.24 and ~23.14 Ma (Mawbey and Lear, 2013).

The Mi-1 event is similar to the major glaciation near the Eocene/Oligocene boundary (Oi-1 event) in several respects. For one, both anomalies occur in two steps separated by several hundred thousand years (Miller et al., 1991; Paul et al., 2000; Zachos et al., 2001b; Lear et al., 2004; Coxall et al., 2005; Pälike et al., 2006b; Coxall and Wilson, 2011; Mawbey and Lear, 2013). Like Mi-1, there is abundant evidence that the Oi-1 is coincident with cold-orbit parameters and productivity increases (e.g., Pälike et al., 2006; Coxall and Wilson, 2011). Carbonate records across the EOT depict a dramatic ~1 km drop in the Calcite Compensation Depth (CCD; Van Andel, 1975; Coxall et al., 2005; Pälike et al., 2012). The CCD drop has been interpreted as either a consequence of shifting the main carbonate deposition centers from shelf to deep sea with a drop in sea level, or from changes in weathering flux (Coxall et al., 2005). The EOT also records a fundamental change in thermohaline circulation with the permanent establishment of the psychrosphere and dominance of Antarctic-sourced cold deep waters associated with the transition from the 'greenhouse' climate state of the Late Cretaceous-

Eocene to the 'icehouse' climate state of the Oligocene-Quaternary (e.g., Benson, 1975; Kennett and Shackleton, 1976; Corliss, 1979; Miller et al., 1987; Kennett and Stott, 1990). By contrast, the OMT shows no similar depression of the CCD (Pälike et al., 2012), perhaps in part due to the prior establishment of the psychrosphere and the transient nature of Mi-1.

This study aims to test the hypothesis of increased productivity at higher latitudes, as well as the importance of different orbital parameters through the late Oligocene early Miocene interval. Counts of the sediment and stable isotope data from Site 744 (southern Kerguelen Plateau) permit a discussion of the orbitally controlled changes in regional biota and oceanography, as well as secular shifts. Low latitude Sites 78 and 803 (equatorial Pacific Ocean) test the previous suggestion that the tropical sea surface temperature records exhibited little to no change at this time. They also test the paleoproductivity hypothesis as it pertains to the low latitudes. Finally, we test the Pälike et al. (2006b) model of eccentricity-controlled lysocline position as it responds to orbital and carbon forcing at both high and low latitude sites.

3.3 Methods

3.3.1 Geological Setting

DSDP Site 78, Leg 9, was cored in 4,363 meters water depth near the Clipperton Fracture Zone in the eastern equatorial Pacific at 7°57.37'N, 127°21.39'W (fig. 3.3). Extensive biostratigraphic work was completed on siliceous and calcareous microfossils, including radiolarians, calcareous nannofossils, and planktic foraminifers (The Shipboard Scientific Party, 1972; fig. 3.4). The Oligocene/Miocene boundary is contained within the Grey Unit of the Marquesas Formation and described as a mix of foram nanno ooze and

chalk, and foram-rad-nanno Ooze. *Paragloborotalia kugleri* was found in Section 1 of Core 16, as well as other biostratigraphic data suggesting the Oligocene/Miocene boundary was within Cores 15 or 16 (fig. 4). Site 78 is equatorial during the OMT, so paleomagnetic declinations cannot be used in the age model.

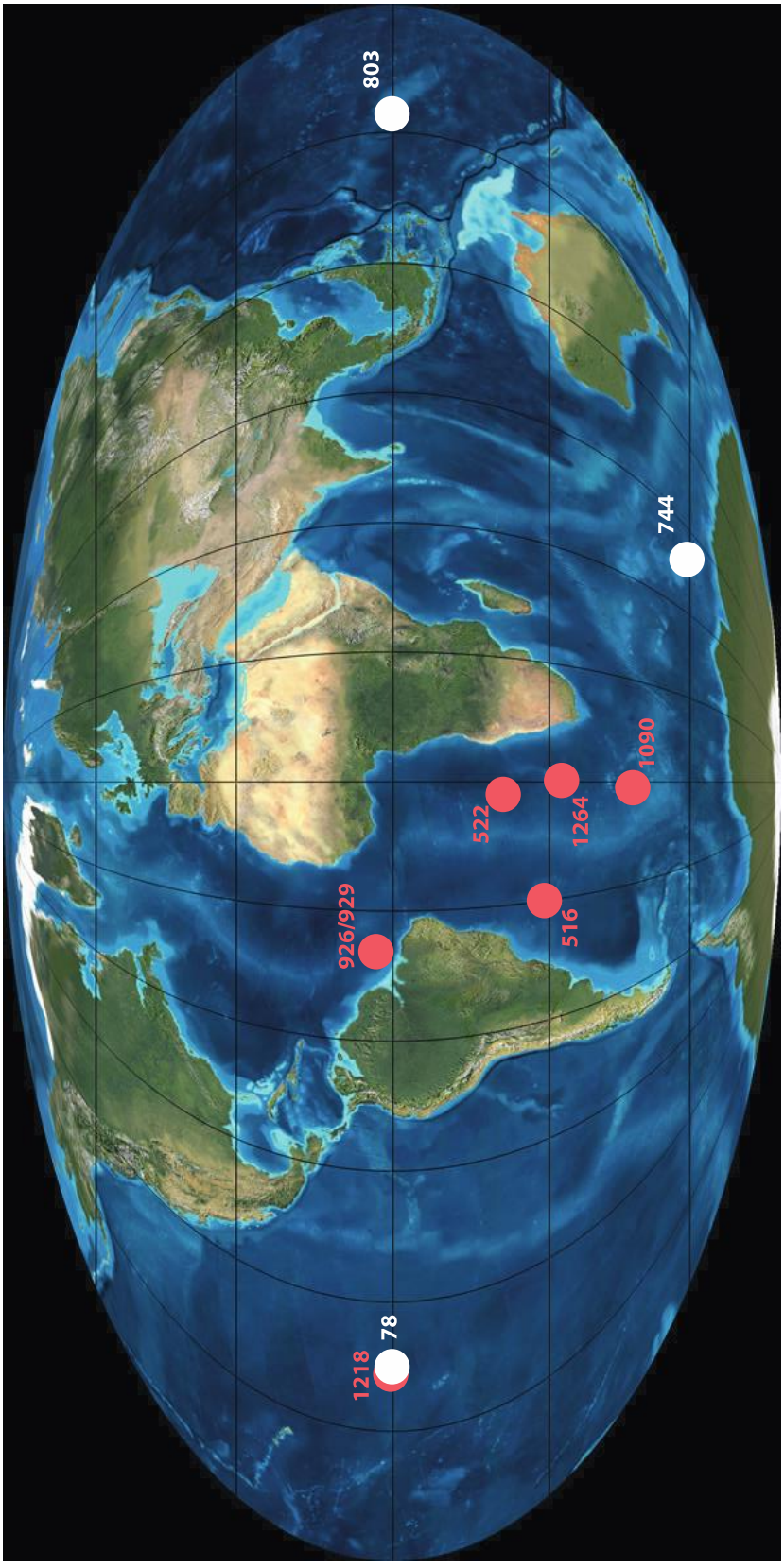
803
744
1090
1264
522
516
926/929
78
1218

Figure 3.3 Site Map. Sites discussed within this study and approximate paleoposition. Sites in white are studied here, while sites in red are from other publications. Map from Blakey, CPGeosystems.

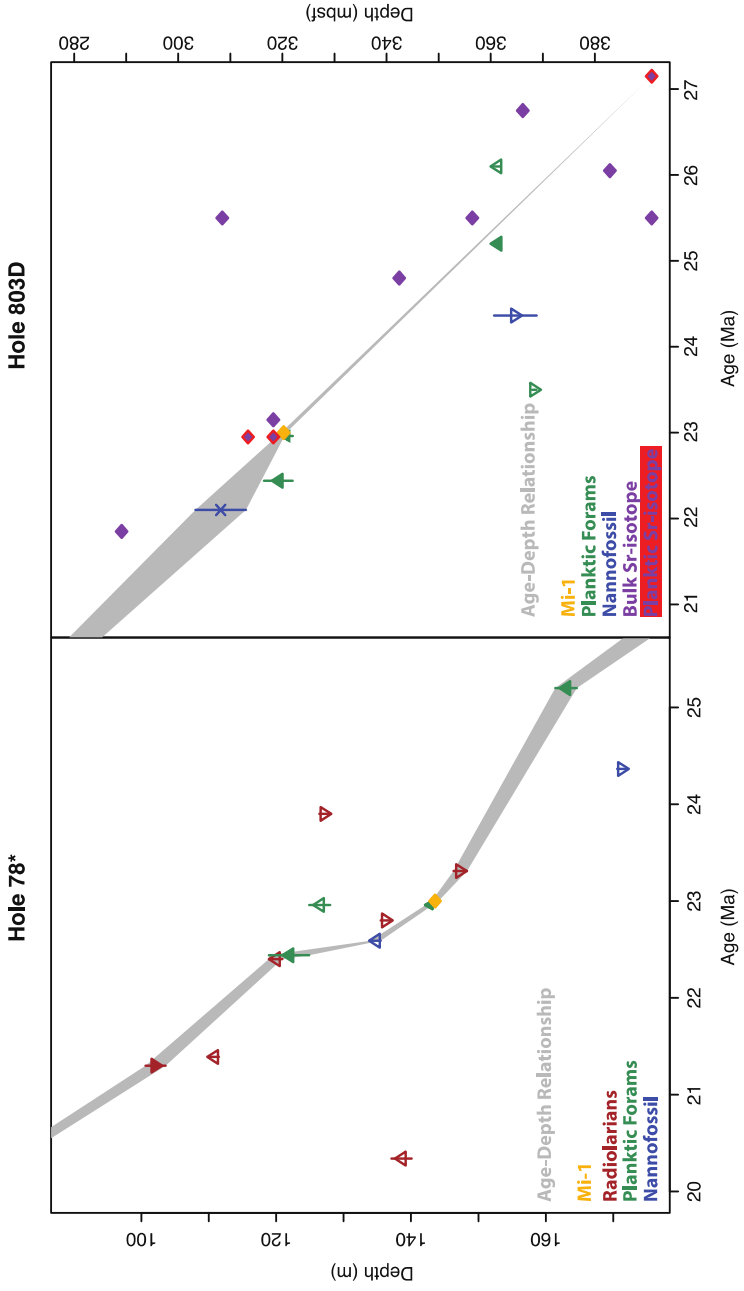

Figure 3.4 Depth vs. Age, Sites 78 and 803. - Left panel depicts age diagnostic criteria vs. depth (m) for DSDP Hole 78*, right panel for ODP Hole 803D. Grey band depicts the error in age model designation, based on linear sedimentation between diagnostic criteria. Mi-1 is represented by a yellow diamond, while Sr-isotope data is purple (bulk) or purple with red outline (planktic). For biostratigraphic base datums, triangles are upward

pointing, while tops are downward pointing. Primary datums are filled, while secondary are open. Biostratigraphic datums are as follows; radiolarians are brown, nannofossils are blue, and planktic foraminifera are green. Sources for all data are in text.

ODP Site 744, Leg 119, was cored at ~2,300 meters water depth on the southern end of the Kerguelen Plateau in the southern Indian Ocean at 61°34.66'S, 80°35.46'E (fig. 3.3). Hole 744A, Core 12H was originally thought to contain the latest Oligocene, while the base of Core 11H was interpreted as lower Miocene, with a ~1.5 m core gap in between, suggesting that the boundary was not recovered in the gap. Unit II spans the Eocene-Miocene and consists of a soft nannofossil ooze, with calcareous nannofossils making up >70% of the sediments (Shipboard Scientific Party, 1989). Paleolatitude calculations (via paleolatitude.org; van Hinsbergen et al., 2015) suggest a position 64°S±2° at the time of Mi-1.

ODP Site 803, Leg 130, was cored at 3,424 meters water depth on the Ontong Java Plateau in the western equatorial Pacific at 2°25.98'N, 160°32.46'E (fig. 3.3). The Oligocene/Miocene boundary was originally interpreted in Core 35X based on calcareous nannofossil and planktic foraminiferal biostratigraphy (fig. 3.4). Lithologic Unit IB is a nannofossil chalk to nannofossil chalk with foraminifers (Shipboard Scientific Party, 1991). Site 803, like Site 78, is equatorial during the study interval, so paleomagnetic declinations cannot be used in the age model.

3.3.2 Analytical Methods

3.3.2.1 Micropaleontological Methods

Standard micropaleontological samples sizes of ~20 cc were used for this study. For most sites, samples were soaked in either a weak Sparkleen solution or simple tap water for 2-3 days to aid disaggregation. The majority of Site 744 samples were dried

then weighed prior to soaking to generate a dry-bulk mass. Samples were then washed over a 63 μm sieve. After washing, samples were dried in a warm oven (50°-60° C). Lastly, samples were sieved and weighed in different size fractions (>250 μm, 250-150 μm, and 150-63 μm).

All counts were made at the >63 μm fraction after splitting the sample using a standard microsplitter. Sediment particles were separated into categories (planktic foram, benthic foram, planktic foram fragment, radiolarian, sponge spicules and echinoderm spines, diatom, and 'other'). Planktic foraminifer fragments and whole tests were split at ~50%, <50% of a test was considered a fragment, and >50% was considered an intact test. 'Other' included anything that was not a part of any of the other defined categories, but remained a very minor component of the sediment in all samples. Most particle component data are based on picking >300 planktic foraminifera while counting the rest of the sediment particles (details about counting practices are in the supplemental information).

Estimated error values for counts were calculated via this expression (e.g., Fatela and Taborda, 2002):

$$CI=1.96\sqrt{(g(1-g)/n}$$

These values (CI) express the 95% confidence interval of the counts estimating the true proportion of the particle category within the sediment, and are a function of the number of individual grains counted (n), and the number of grains within the group in question (g). These errors are depicted by the width of the 'ribbon' in Figures 3.5, 3.6, and 3.7

with the observed value at the center of the ribbon, and either edge representing the 95% confidence limits.

The fragmentation index has been shown to be a good recorder of the position of the lysocline (Peterson and Prell, 1985), and is calculated as:

p/{p+f}*100=FI

where (p) is the number of whole planktic tests (>50% of the test remaining), while (f) is the number of fragmented tests (<50% of test remaining). Counting errors for both planktic foram and fragments were propagated through to these indexes, resulting in the ribbons depicted in Figures 3.5, 3.6, 3.7, and 3.8.

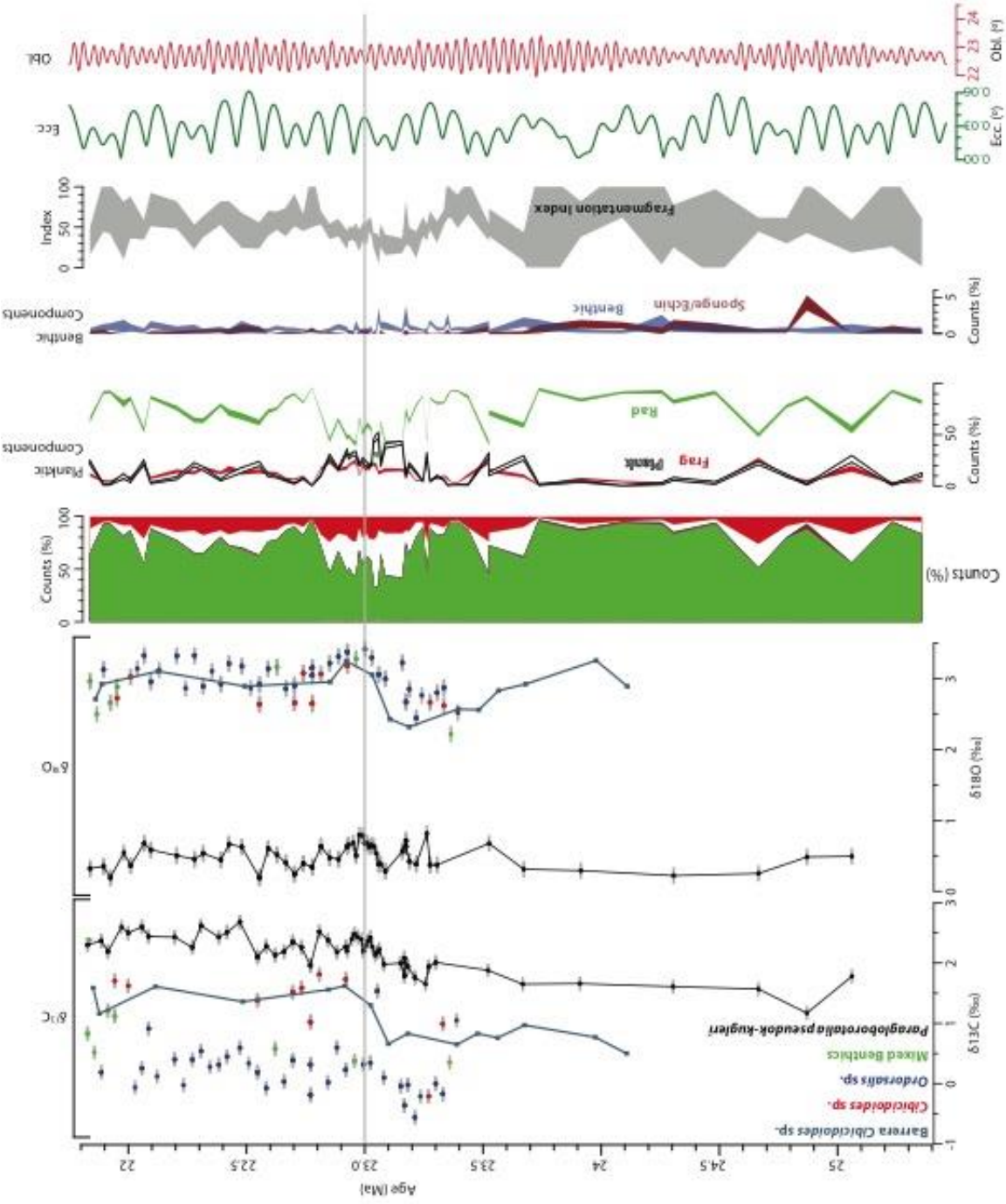

Figure 3.5 Summary of data for ODP Site 803. Isotopic data are plotted with ~0.1‰ error associated with mass spectrometers (grey bar). *Cibidicoides* sp. is red (this study) and light blue (Barerra et al., 1993). *Ordorsalis* sp. is dark blue, mixed benthic green, and *Paragloborotalia pseudokugleri-kugleri* is black. Sediment particle counts are represented both as cumulative and separated. Colors are as follows: green radiolarian, brown sponge spicules and echinoderm spines, blue benthic foraminifera, white whole planktic foraminifera tests, red fragments of planktic foraminifera tests. Width of 'ribbon'

in separated count data is the confidence interval, calculation of which is described in text. Fragmentation index is grey, width of 'ribbon' is again the confidence interval. Lastly, green and red line represent eccentricity and obliquity (tilt) respectively, from Laskar et al., 2004 solution.

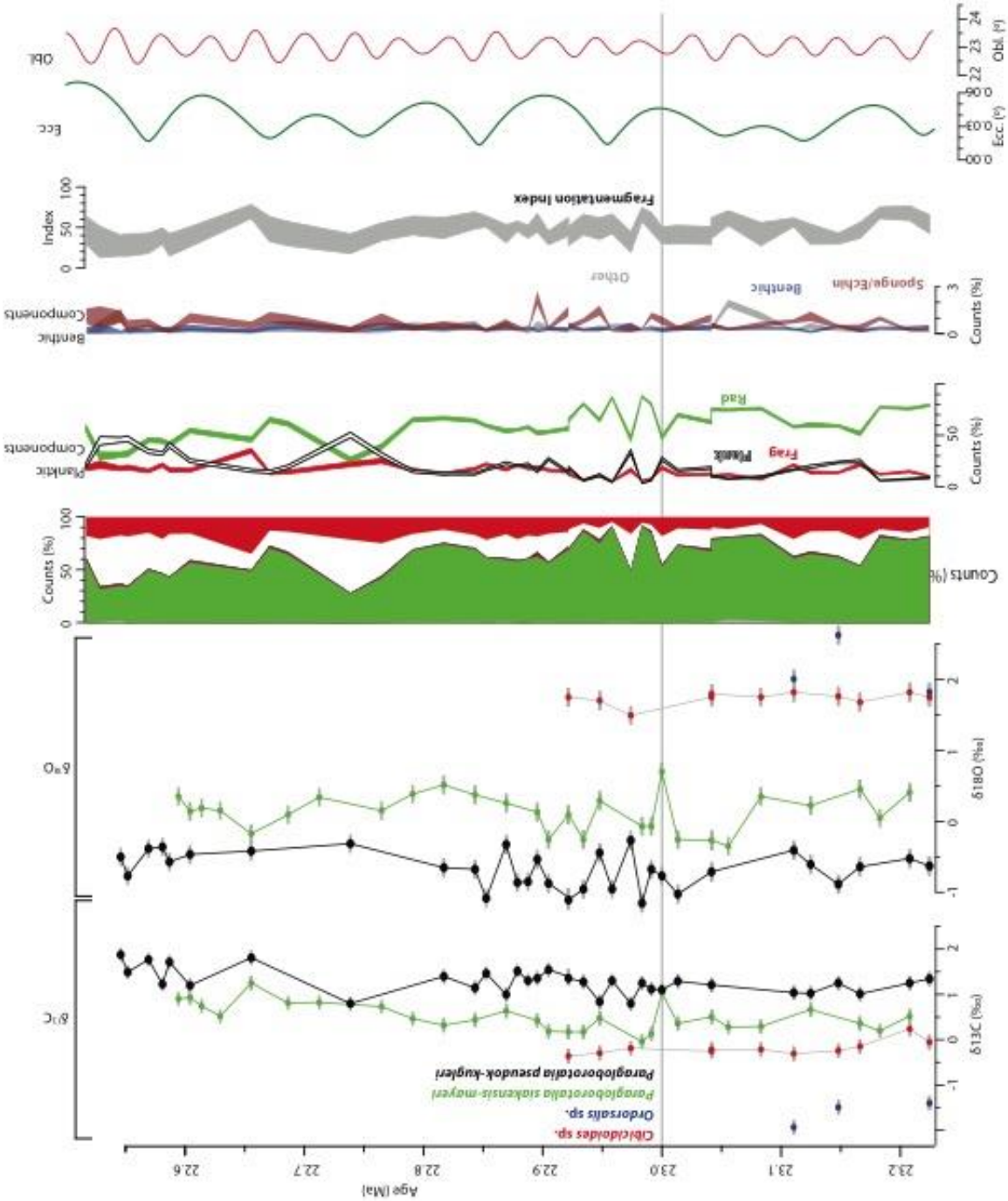

Figure 3.6 Summary of data for DSDP Site 78. Isotopic data are plotted with ~0.1‰ error associated with mass spectrometers (grey bar). *Cibidicoides* sp. is red, *Oridorsalis* sp. is blue, *Paragloborotalia siakensis-mayeri* is green, and *Paragloborotalia pseudokugleri-kugleri* is black. Sediment particle counts are represented both as

cumulative and separated. Colors are as follows: green radiolarian, brown sponge spicules and echinoderm spines, blue benthic foraminifera, white whole planktic foraminifera tests, red fragments of planktic foraminifera tests. Width of ‘ribbon’ in separated count data is the confidence interval, calculation of which is described in text. Fragmentation index is grey, width of ‘ribbon’ is again the confidence interval. Lastly, green and red line represent eccentricity and obliquity (tilt) respectively, from Laskar et al., 2004 solution.

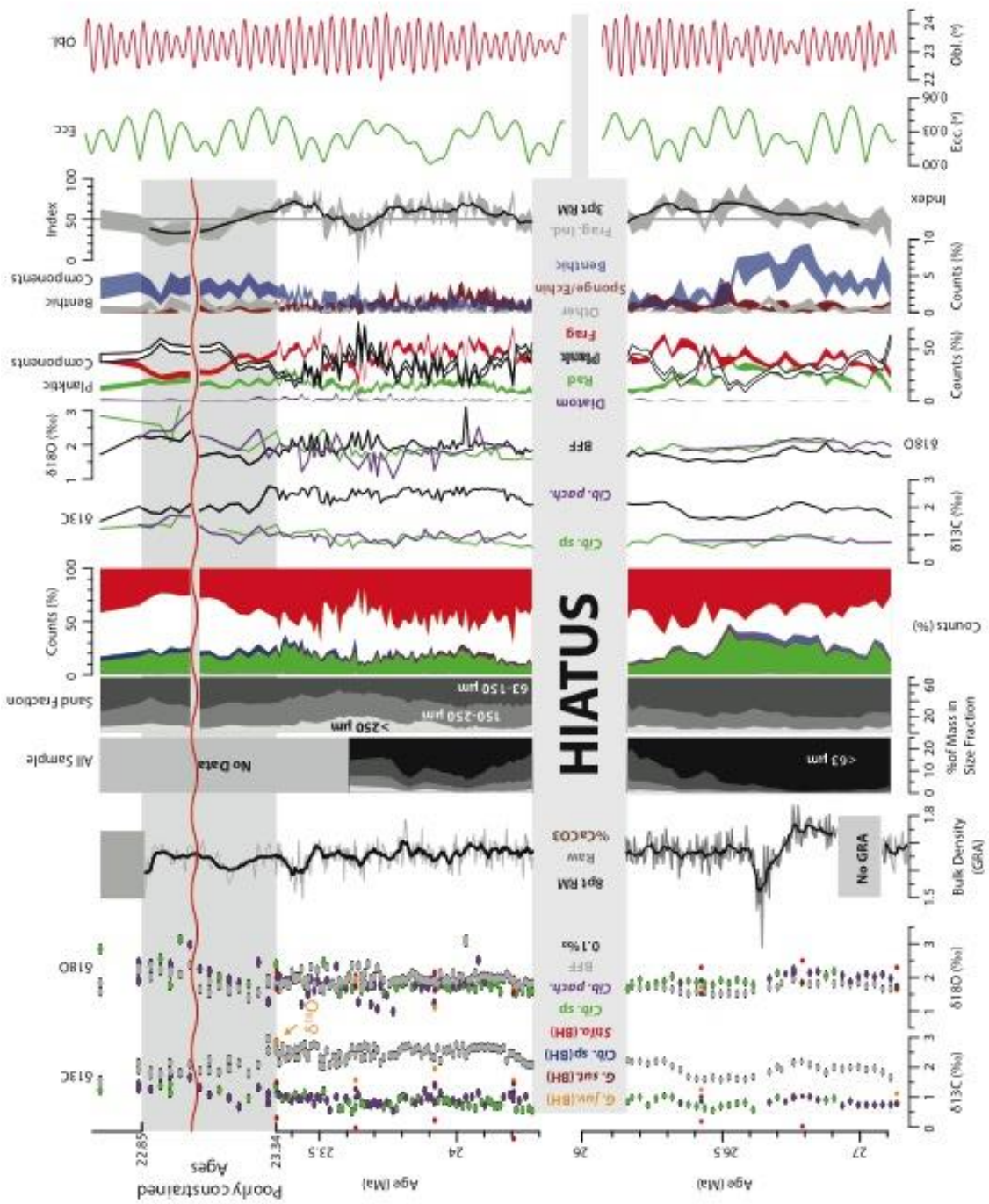

Figure 3.7 Summary of data for Site 744. Raw $\delta^{13}C$ and $\delta^{18}O$ values for each analysis, the black bar represents the ~0.1‰ error associated with mass spectrometers. Colors are as depicted on the figure. Grey (raw) and black (8 point running mean) lines represent the bulk density (g/cm^3) measured by the GRA (Gamma Ray Attenuation) tool shipboard. Brown circles denote a percent carbonate (%$CaCO_3$) measurement taken on the fine fraction sediment used for isotopic measurement. Shaded rectangles refer to the fraction of sediment composed of particles from specific size fractions; black is the <63 µm size fraction. Note the scale. This data is only available for some of the samples. The second

rectangle is the same analysis, but without the influence of the <63 µm size fraction. Dark grey is the 53-150 µm size fraction, mid-grey is the 150-250 µm size fraction, and light grey is the >250 µm size fraction. Last block diagram is the counts of the >63 µm size fraction particles. Red is the fraction of the sediment composed of planktic foram fragments (<50% of test remaining), while white is the percent composed of whole planktic tests (>50% of test remaining). Blue represents benthic foraminifera, purple diatoms (>63 µm), green radiolarians, brown is sponge spicules and echinoderm spines, and grey is any particle not already included. Other is typically small broken carbonate shells, and is rarely over 3% of the sediment. $\delta^{13}C$ records are represented by green (*Cibicidoides* sp.), purple (*Cibicidoides pachyderma*), and bulk fine fraction (dominated by calcareous nannoplankton). Some samples have multiple analyses which have been averaged in these lines. Count 'ribbons' represent the count for each sediment type, with an estimate of the error associated with the counts (See Methods). Planktic and benthic components are plotted separately on different scales to accentuate the trends. Grey and brown ribbons represent the fragmentation index and planktic-to-benthic index respectively. The width of the ribbon represents the error propagated through to the index from the counting error. The black line running through each ribbon represents a 3-point running mean. Green and red lines are the Laskar (2004) solution for eccentricity and obliquity (tilt), respectively, plotted with degrees.

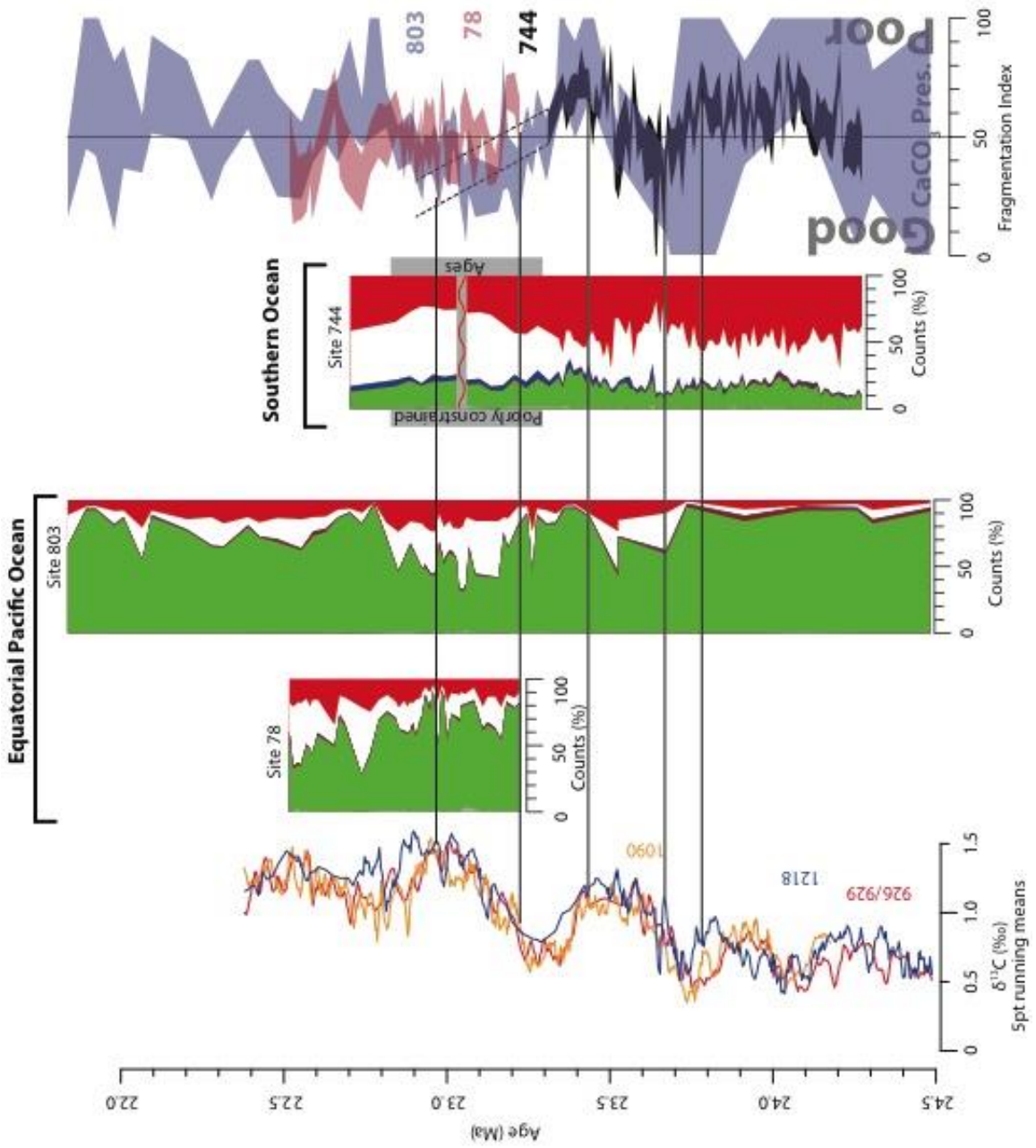

Figure 3.8 Carbon cycle and biota. Summary of $\delta^{13}C$ time series from Zachos et al. (2008) and sediment counts and fragmentation from Sites 78, 803, and 744. Horizontal lines are intervals discussed in text as important changes in carbon cycle dynamics and lysocline position. Colors for fragmentation are blue for Site 803, red for Site 78, and black for Site 744. Color for count blocks follow previous figures.

3.3.2.2 Stable Isotope Methods

Stable isotope time series were generated for Sites 78, 803, and 744 (fig. 3.5-7). At all sites the genus *Cibicidoides* (epifaunal) was the first choice for benthic time series, to allow for easy comparison to other composite records (Zachos et al., 2008). Site 78 had extremely low benthic abundance and little coarse sediment fraction, so data within that time series is sparse (fig. 3.6). Site 803 has an existing *Cibicidoides* sp. record (Barerra et al., 1993), which was supplemented at a higher resolution here. In several samples, *Cibicidoides* sp. was not available in high enough abundance, and so *Oridorsalis* sp. (infaunal) was employed to supplement. If *Oridorsalis* sp. was rare as well, mixed benthic foraminifera were amalgamated into a single measurement. Several samples with both *Cibicidoides* and *Oridorsalis* were analyzed to establish a consistent offset between the genera. Benthic foraminifera were rare within the sediments from Site 744, but generally well preserved. Isotopic values were generated from *Cibicidoides pachyderma* or *Cibicidoides* sp., if there were not enough *C. pachyderma* to reach the mass required for analysis. Benthic foraminifera were from a restricted size fraction (250-355 μm for Site 744, as noted in appendix H for Sites 78 and 803). All samples were either run on the University of Massachusetts - Amherst Finnigan Delta XL+ Mass Spectrometer with a Kiel III Automated Carbonate Preparation System, using between 80 and 150 μg of foraminifera, or at University of California - Santa Cruz ThermoScientific MAT-253 with a Kiel IV carbonate device. The number of foraminifera that make up this mass of calcium carbonate varies, and has been noted in the appendix H. *Cibicidoides* $\delta^{18}O$ values were adjusted to equilibrium values (0.5‰ offset) to facilitate comparison with the global compilation (Zachos et al., 2008; figs. 3.1, 3.2, 3.8).

Planktic foraminifera were employed at Sites 78 and 803 to generate time series representing mixed-layer and thermocline water properties. *Paragloborotalia pseudokugleri* and *P. kugleri* are mixed-layer dwellers, while *Paraglobrotalia siakensis-mayeri* live within the upper thermocline. For Site 744, the decanted residue of the soaked samples from the initial washing stages was used for bulk isotopic measurements. This residue is the <63 μm size fraction (bulk fine fraction; BFF), and so was largely calcareous nannoplankton and juvenile planktic foraminifera (see smear slide analysis below). The mass of those samples was ~80-150 μg. Standard machine error (~0.1‰) is plotted at all times.

Several smear slides were made to qualitatively identify the components of the fine fraction sediments. Samples selected for smear slide analysis were 744A/12H/1 18-20, 66-68, 102-104, 132-134; 744A/12H/2 42-44; 744A/12H/4 60-62. Samples were dominantly calcareous nannoplankton with relatively minor contributions of siliceous microfossils (sponge spicules, diatoms, and silicoflagellates) and juvenile planktic foraminifers, as well as extremely rare lithic components (~<0.1%). Within the samples identified, there appeared to be a general trend for higher silicate contribution to the fine fraction relative to the calcareous content in the low density intervals (e.g., ~23.4 Ma), which agrees with studies of the density-fine fraction relationship at nearby sites (Nobes et al., 1991). Even within intervals of relatively higher silicate contribution, calcareous nannoplankton remain the dominant component of the fine sediment. Thus, our BFF isotope data is largely recording a mixed layer signal, and we should ideally only expect a minimal influence on $\delta^{13}C$ and $\delta^{18}O$ values due to foraminifera.

The relationship of calcareous nannoplankton $\delta^{13}C$ and $\delta^{18}O$ values to planktic foraminiferal values in bulk fine fraction isotope analyses is complex, and a current matter of debate (Reghellin et al., 2015, *and references therein*). There is disagreement of the precise offset, if there are species- or genus-specific vital effects, growth rate changes, stability and preservation of the values with depth and carbonate saturation state, and so on. There is also some evidence that while absolute values in nannoplankton stable isotopes are not in precise equilibrium with seawater, the offset driven by fractionation during nannoplankton calcification is *relatively* constant. Evidence from the tropics (e.g., Reghellin et al., 2015) demonstrates bulk carbonate values record a mixed-layer signal, though with some 'vital effects' from the differing biology of the calcareous nannofossils generating the carbonate. We here use the stable isotope values from the BFF as a generally good recorder of mixed-layer values, though offset from both foraminiferal and equilibrium values. These results are compared with the low-resolution multi-species foraminifer isotope record from Site 744 (Barerra and Huber, 1991; fig. 3.7).

3.4 Results

3.4.1 Chronostratigraphy

There are several isotopic events in the published records (largely known from Sites 296/929, 1090, and 1218) compiled in Zachos et al. (2008), which appear strongly correlative (fig. 3.2). The Mi-1 $\delta^{18}O$ excursion begins coeval at all sites at ~23.3 Ma, increasing from ~23.3 to 23.0 Ma, with peak values at ~23 Ma (though timing is different at Site 1090, see below). In the uppermost Oligocene, there are three, possibly four, intervals of successively higher $\delta^{13}C$ values, with lows in-between. $\delta^{13}C$ is enriched high at ~24.2 Ma, ~23.9 Ma, ~23.5 Ma, and most enriched at 23.0 Ma. With respect to

paleomagnetic polarity, C6Cn.3n occurs coeval with low $\delta^{13}C$, and the initiation of the Mi-1 $\delta^{18}O$ excursion, while $\delta^{13}C$ and $\delta^{18}O$ both rise through C6Cn.2r, and both $\delta^{13}C$ and $\delta^{18}O$ peak (in the tropics) during C6Cn.2n (Fig. 3.1, 3.2). $\delta^{18}O$ values, however, at Site 1090 rise, peak, and then begin to fall all within C6Cn.2r (Fig. 3.2; orange line). The offset in peak $\delta^{18}O$ values marking the Mi-1 event at Site 1090 compared with the other sites is only seen in the $\delta^{18}O$ values; $\delta^{13}C$ values between the three sites are roughly synchronous. The maximum $\delta^{18}O$ values are typically recorded at 23.0 Ma, seen at Sites 926/929 and 1218.

While Mi-1 originally was described in the literature as an 'isotopic zone', referring to the interval between subsequent peak $\delta^{18}O$ values (Miller et al., 1991), it has come to specifically refer to the peak $\delta^{18}O$ value at the boundary. At Site 1090 (high resolution), and at DSDP Site 522 on Walvis Ridge in the southeast Atlantic (low resolution), where Mi-1 was originally defined (Miller et al., 1991), there is a ~100 kyr earlier peak in $\delta^{18}O$ values, occurring in subchron C6Cn.2r rather than C6Cn.2n (Miller et al., 1988; Billups et al., 2002). ODP Site 1264, also cored on Walvis Ridge, $\delta^{18}O$ peak Mi-1 values (Liebrand et al., 2011) are slightly different from all of the above, and contain a ~100 kyr plateau, fitting between the Site 1090 peak and Sites 926/929 peak. This discrepancy between Sites 1090 and 522, and Sites 926/929 and 1218 is an important chronostratigraphic feature, discussed later, but it also represents an esoteric nomenclatural issue as well. The Oligocene/Miocene boundary occurs at the base of C6Cn.2n (Steinger et al., 1997), which is stratigraphically above the peak values of $\delta^{18}O$ at Site 522 (Miller et al., 1988; Miller et al., 1991). Thus, at the 'type locality', Mi-1 actually occurs in the uppermost Oligocene, and should in fact be called Oi-3. We,

however, retain the name Mi-1 in deference to the preponderance of literature referring to it as such. It, however, is interesting that peak $\delta^{18}O$ values are time-transgressive feature, rather than synchronous, which is discussed later.

The sites studied here were all drilled prior to the advent of modern astrochronologically-tuned biostratigraphic calibrations (e.g., Wade et al., 2011). As such, the age models developed shipboard are in need of updating. What follows is a discussion of the various modifications employed to adjust the age models to modern standards. In general, however, the following was done. Tropical biostratigraphic datums now use modern age calibrations, such as Wade et al. (2011) for planktic foraminifera, Backman et al. (2012) for calcareous nannofossils, and Kamikuri et al. (2011) for radiolarians. Dates collected for the Pacific Equatorial Age Transect (PEAT) Exp. 320/321 supplement those not published in Wade, Backman, or Kamikuri (Expedition 320/321 Scientists, 2010). Paleomagnetic reversal dates use a mix of ages from Pälike et al. (2006b) and Lourens et al. (2004). The more recent publication of Gradstein et al. (2012) was not used, as it would be more difficult to compare against the stable isotope compilation of Zachos et al. (2008), which uses the Pälike et al. (2006) and Lourens et al. (2004) dates. Site 744 has had more recent chronostratigraphy studies (Roberts et al., 2003; Florindo et al., 2013), and we follow those age models, with a slight modification discussed below. Other chronostratigraphic tools (astrochronology, Sr-isotopes) are discussed below as necessary.

3.4.1.1 ODP Site 744

Site 744 has been the subject of multiple chronostratigraphic studies spanning many decades since the original shipboard biostratigraphy (Shipboard Scientific Party,

1989) to, most recently, a recent integrated bio-magnetostratigraphy (Florindo et al., 2013). Florindo et al. (2013) suggested there are a series of hiatuses which are likely correlative to early Miocene Mi events within Cores 10H and 11H, a speculation made without isotopic evidence for a direct link. Other studies deal directly with the paleomagnetic stratigraphy of Core 12H, our study interval. A summary of the previous studies (Shipboard Scientific Party, 1991; Keating and Sakai, 1991; Roberts et al., 2003; Florindo et al., 2013) is presented in figure 3.9. The ages of the reversals in the geomagnetic polarity time scale (e.g., Berggren et al., 1985a, b; Gradstein et al., 2012), and the paleomagnetic interpretation of Core 12H sediments have changed significantly since the site was originally cored in 1989; for example, the normal polarity at ~100 mbsf has been attributed to C7An, C6Cn.3n, and C6Cn.2n.

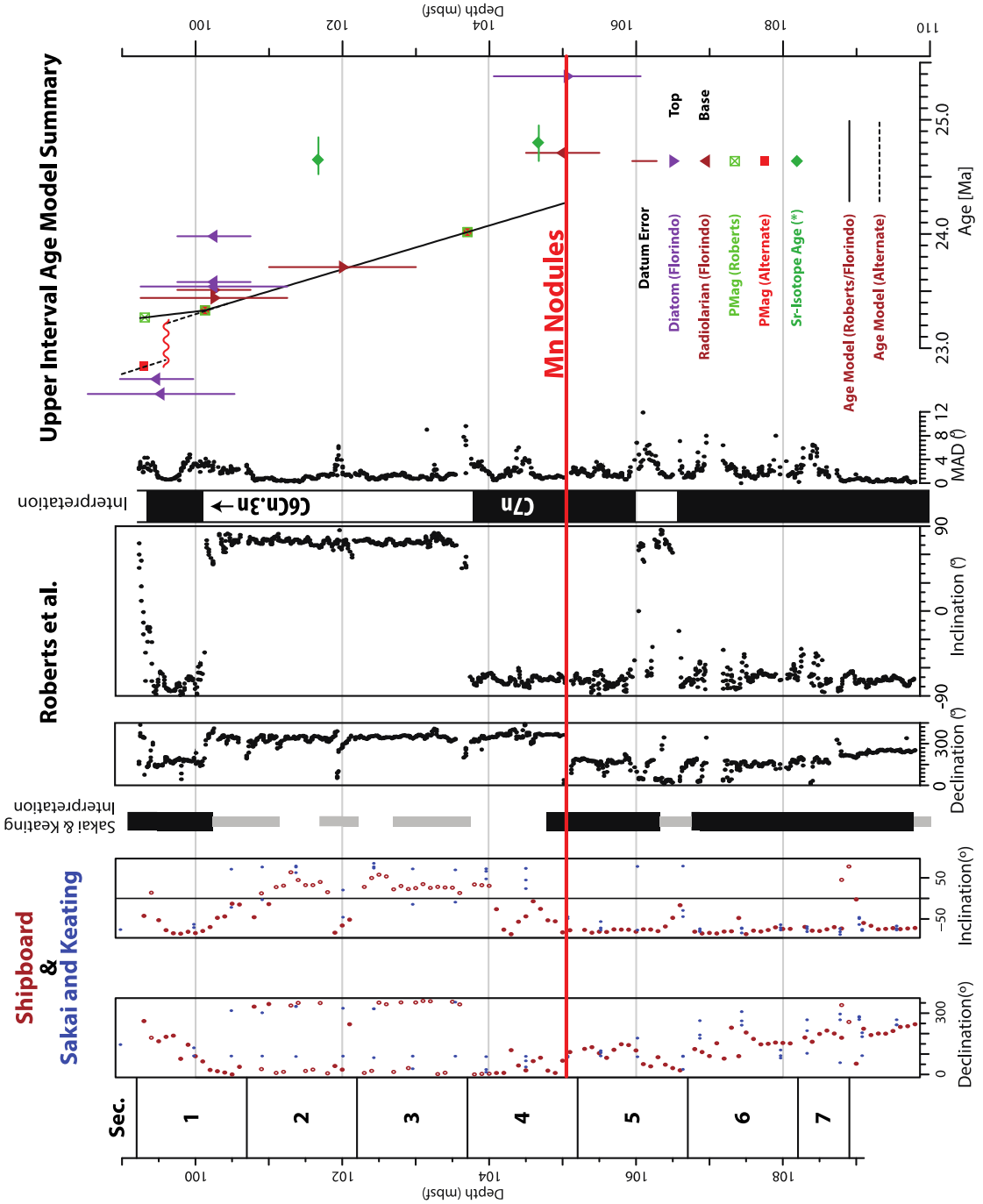

Figure 3.9 Site 744 age diagnostic criteria. Summary of paleomagnetic studies through Site 744 Core 12. Leftmost two panels depict the shipboard (brown) and Keating and Sakai (1991; blue) paleomagnetic delination and inclination. The Keating and Sakai (1991) interpretation is represented by black (normal polarity), white (reverse polarity), and ambiguous (grey). The Roberts et al. (2003) study largely supports the Keating and Sakai (1991) interpretation with some changes to the depths of various reversals. These four panels (declination, inclination, interpretation, and MAD) are modified from Roberts et al. (2003). MAD refers to maximum angular deviation, a measure of the polarity

strength. Far right is the age model for the upper interval of Core 12. Colors denote various biostratigraphic systems (purple, diatoms; brown, radiolarians) from Florindo et al. (2013) while green boxes represent the paleomagnetic interpretation of Roberts et al. (2003). Solid black line is the Roberts et al. (2003) age model for the Core 12 upper interval samples, while the dashed line and red box denote the revision in this study. Green diamonds represent the Sr-isotope data, discussed in the text. Horizontal red line represents the Manganese nodules found at 105.05 mbsf.

There is sedimentological evidence for a hiatus in Core 12H, via a manganese nodule at 744A/12H-4/135 cm (~ 105 mbsf; Shipboard Scientific Party, 1989) suggesting a prolonged interval at the sediment water interface. Above that hiatus there is generally good agreement between the Shipboard (Shipboard Scientific Party, 1989), Keating and Sakai (1991), and Roberts et al. (2003) inclinations. Directly above the Mn nodule horizon at 105.05 mbsf there is a normal polarity, though the duration of the normal is not always agreed upon (fig. 3.9). There is a polarity reversal at ~103.9 mbsf (Roberts et al., 2003 interpretation), followed by a ~4 m interval of reversed polarity. There is then a short normal interval <1 m in length, followed by a reverse polarity at the very top of the core. There are no significant increases in the maximum angular deviation (MAD; Roberts et al., 2003); a substantial increase would indicate an abrupt change in inclination between samples, suggesting an altered paleomagnetic signal (Roberts et al., 2003). The paleomagnetic polarity interpretation from Roberts et al. (2003) suggests that chrons C7n, C6Cr, C6Cn.3n, and the very bottom of C6Cn.2r were recovered in Core 12H. These interpretations are supported by diatom and radiolarian biostratigraphy (Florindo et al., 2013; fig. 3.9).

Sr-isotope data (Barrera and Huber, 1991), with recent age calibrations (McArthur et al., 2014), suggest substantially older (~1 myr) ages (fig. 3.9). This discrepancy has been noted several times before, most recently by Roberts et al. (2003). There is a ~1 myr

difference in the Sr-isotope dates straddling the hiatus, a hiatus which should be ~2 myr according to the Roberts et al. (2003) bio-magnetostratigraphic age model. Additionally, the upper Sr date (101.67 mbsf, ~24.65 Ma) would put that portion of sediment in the normal polarity chron C7n, rather than the reverse polarity recorded in the sediment at 101.67 mbsf. One possible explanation for the Sr discrepancy could be due to higher frequency fluctuations in Sr-isotope values than are accountable for in the spline fit model used for the Sr-isotope lookup tables (McArthur et al., 2012; 2014). Because of the agreement between the paleomagnetic stratigraphy, the biostratigraphy, and the stable isotope stratigraphy through that interval, we have chosen to disregard the contrarian Sr-isotope ages.

In the Site 744 record some of the global isotopic trends are observed, with some important differences (fig. 3.2, 3.10). There are two intervals with higher benthic $\delta^{13}C$ values (~23.8, ~23.4 Ma; fig. 3.2). There is also a series of lower $\delta^{18}O$ values in the *Cibicidoides pachyderma* record (~23.7 Ma; fig. 3.2), roughly correlative to the 0.6‰ decrease observed in the global compilation. There is a rise in the $\delta^{13}C$ benthic, $\delta^{18}O$ benthic, and $\delta^{18}O$ BFF values within the normal polarity interval at the top of Core 12H (within 'Poorly Constrained Ages'; fig. 3.2), interpreted in Roberts et al. (2003) as C6Cn.3n. If the Roberts et al. (2003) magnetostratigraphic interpretation is correct, then the Site 744 isotope values do not fit with the global compilations, which show relatively steady $\delta^{18}O$ values and falling $\delta^{13}C$ values through C6Cn.3n (Zachos et al., 2008; fig. 3.2); this is not the pattern of $\delta^{18}O$ and $\delta^{13}C$ values observed.

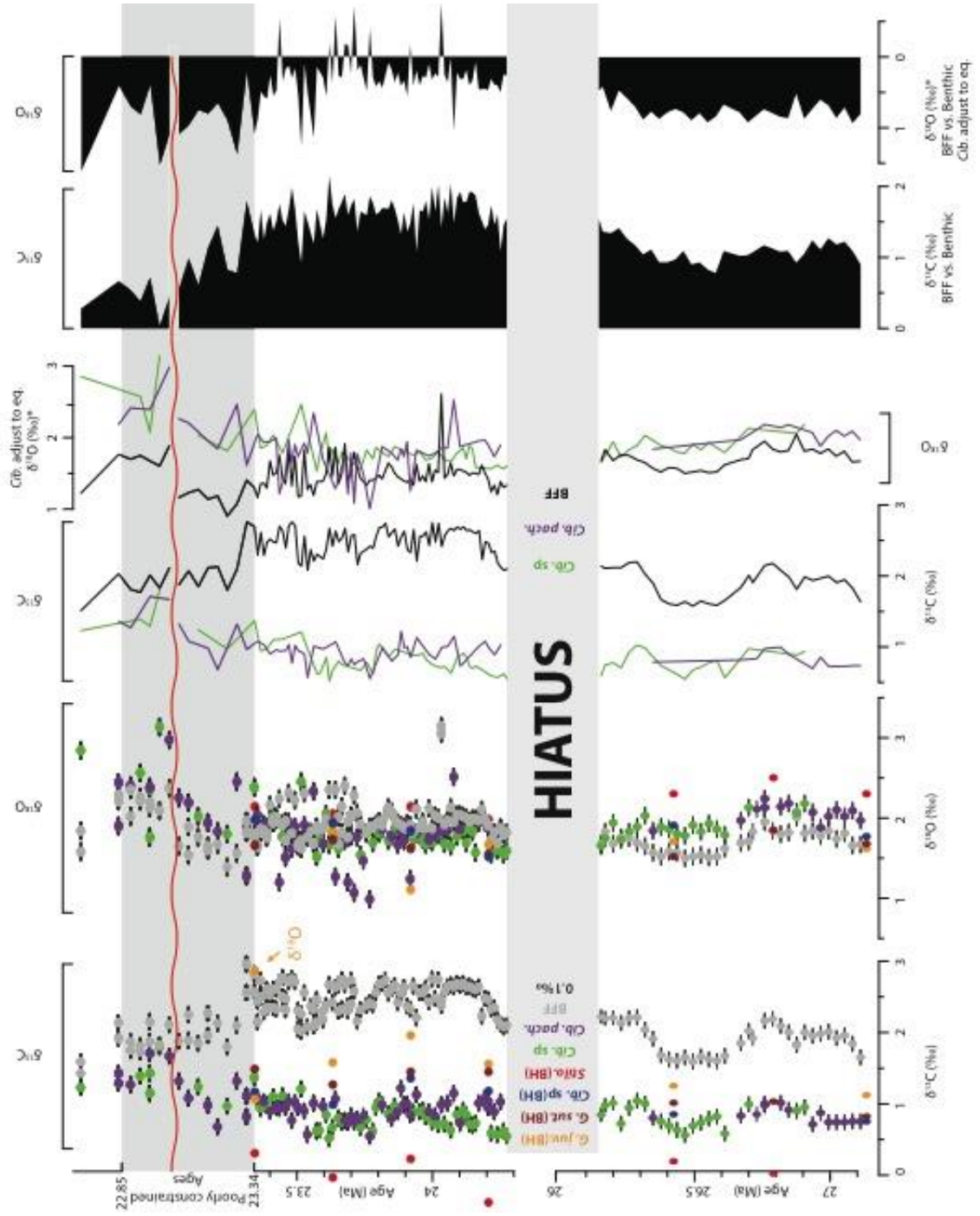

Figure 3.10 Site 744 Stable Isotope Data. Expanded view of stable isotope data from Site 744, colors follow figure 6. Right most panel is the gradient between bulk fine fraction (BFF) data and benthic data.

A multitude of different age model permutations were attempted to remedy the discrepancies between Site 744 and global isotope values. If we move the age model up so that C6Cn.3n, 2r, and 2n are the interpretation of the sediment polarity, this makes the peak $\delta^{18}O$ values occur ~100 kyr after the peak at Site 926/929. It also makes what should be gradual increases in $\delta^{13}C$ and $\delta^{18}O$ into intervals with essentially no change until just prior to maximum $\delta^{18}O$ and $\delta^{13}C$ values. Lastly, it violates the biostratigraphic data, which suggests an age ~500 kyr younger than that scenario. Sliding the age model down (C7n.2n, 1r, and 1n) makes less sense because the biostratigraphic data are then far too young, and the same issue of having this sharp excursion suggesting a ~1‰ shift in both $\delta^{13}C$ and $\delta^{18}O$ in multiple records within what is a relatively flat interval globally. Maintaining a hypothesis of relatively continuous sedimentation and moving the paleomagnetic interpretations does not fit the existing chronostratigraphic data any better than the Roberts et al. (2003) age model.

Another possible explanation for the BFF C-isotope excursion near the top of Core 12H is diagenesis. Were the excursion simply a diagenetic feature, we would expect the gradient in the isotopic values to collapse. The $\delta^{13}C$ gradient does collapse during the excursion, but the benthic values appear to rise to the relatively invariant BFF values. The converse would be expected if this were a single horizon dominated by diagenesis. The BFF values, which are largely calcareous nannoplankton (see smear slide analysis below), should record a mixed-layer signal. Diagenesis should drive the $\delta^{13}C$ values to be more similar to the bottom water signal (benthics). The observed collapse is precisely the opposite of what a single diagenetic horizon would predict. In addition, carbonate preservation appears to be substantially more favorable near the interpreted Mi-1

excursion (see count data below). Lastly, the $\delta^{18}O$ gradient actually increases during the excursion, rather than decreases. $\delta^{18}O$ should be a less faithful recorder of original values than $\delta^{13}C$ if affected by diagenesis (Pearson et al., 2001), strongly suggesting that the C-isotope excursion is not simply a diagenetic problem.

Another possible remedy to age model discrepancies is a condensed section within the top of Core 12H. There are numerous reasons this might be the case. There are subtle color changes in the top of Core 12H, which may suggest that there is a change in the style of sedimentation. The change from fairly bright to slightly darker calcareous ooze may indicate that there is a decrease in the $CaCO_3$% in the sediments. Other evidence for a change in sedimentation rate is the tight clustering of biostratigraphic datums at roughly the same depth as the C6Cr to C6Cn.3n reversal (fig. 3.9). Biostratigraphy, however, has fairly low resolution at the base of the Florindo et al. (2013) study, with datums having 1 or 2 m of uncertainty due to sampling resolution. The clustering of biostratigraphic datums (~100 mbsf) may be due to very low sedimentation rates in uppermost part of Core 12H. The above offers good support that abrupt isotopic shift in BFF C-isotopes records paleoceanographic changes, rather than diagenesis. The problem with this interpretation is the well-constrained and robust paleomagnetic data, without a reversed interval (which would be C6Cn.2r). The complete absence of subchron 2r, while assuming constant deposition, is difficult to explain.

As stated previously, Mi-1 is not a synchronous $\delta^{18}O$ excursion. Sites 1090 and 522, both in the South Atlantic Ocean, record peak $\delta^{18}O$ values within C6Cn.2r, rather than in 2n as the tropical sites do. Using the Roberts et al. (2003) age model, unmodified, would put the 'Mi-1' excursion within 3r, ~300-kyr prior to the tropical Mi-1 excursion,

and ~200-kyr prior to the South Atlantic Ocean Mi-1 excursion. While an early excursion is a possibility, it would mean that the Southern Ocean cooled dramatically (>4°C throughout the entire water column, assuming no salinity change) prior to the rest of the globe. It would require, as well, the local carbon signal to be dramatically different from the global signal. While local temperature records could be changed by shifting water masses, for example, interpreting a ~1‰ shift in the carbon isotopes typically requires invocation of global carbon cycling, rather than local phenomena. Thus, the Roberts et al. (2003) age model for the top of Core 12H is likely flawed, as the stable isotope values cannot be explained adequately with respect to known paleoceanographic mechanisms for shifting stable isotope values by such large magnitudes.

The last possibility is that there is a hiatus within Section 1 of Core 12H (e.g., fig. 3.1). In between samples 744A, 12H-1, 48-50 cm and 54-56 cm there is a shift in several of the isotopic records, particularly all three oxygen isotope records (~1.0‰ BFF, ~0.7‰ Benthic; fig. 3.9). If there were a hiatus between those two samples, with 54-56 cm in C6Cn.3n, 48-50 cm in C6Cn.2n, skipping C6Cn.2r, the Site 744 isotope values would roughly square with the global trends. After eliminating all other stratigraphic possibilities as implausible (see above), a hiatus resolves the issue relatively simply. We propose a small adjustment to the Roberts et al. (2003) age model, given the new stable isotope data (fig. 3.9, alternate age model line).

Mi-1 is a very short excursion, with peak oxygen isotope values only occurring for ~100-kyr at most. The elevated values within 744A, 12H-1, 48-50 cm suggest that is the peak of the Mi-1 excursion, with the recovery followed after; this assertion is backed up by the paleomagnetic reversal at the top of Section 1 (C6Cn.2n to 1r). With the ~0.7-

0.5‰ $\delta^{18}O$ increase during the hiatus, and the consistent shared slope between all of the Mi-1 high resolution records, an rough estimate of 150-kyr is missing in the hiatus. As that is a rough calculation, with considerable issues, it is not used on the figures. Site 744 data is presented with substantially different age designations through the interval of 'Poorly Constrained Ages' (PCA) between C6Cn.3n base and C6Cn.2n top, highlighted on each figure. This is to stress the limited chronostratigraphic data through the interval, and to allow for more detailed examination of the initial portion of the excursion.

3.4.1.2 ODP Site 803

Site 803 was located very close to the equator during the Oligocene and early Miocene. As such, low inclination values and very low magnetic susceptibility precluded any paleomagnetic data through the OMT interval (Shipboard Scientific Pary, 1991). Biostratigraphic datums were employed to develop an age model, as well as the $\delta^{18}O$ apex of Mi-1 set at 23.0 Ma (Liebrand et al., 2011). Biostratigraphic data suggest a roughly linear sedimentation rate throughout much of the Oligocene (Leckie et al., 1993; Fraass and Leckie, *in prep.* Chapter 2). Sr-isotope data from Barrera et al. (1993) were normalized to a value of 0.71014 for the NBS-987 standard, current practice is to normalize to the NIST-987 (McArthur et al., 2001). Thus, 0.0001 was added to Sr-isotope values from Barrera, then we employed Sr-isotope lookup tables (McArthur et al., 2012) to evaluate the ages. Unlike Site 744, Sr-isotope ages at Site 803 agree well with the biostratigraphic and stable isotope data. Age-diagnostic data are summarized in fig. 3.4.

Several attempts at generating an astrochronologically-tuned age model were performed at Site 803. Using the 'astrochron' R-Package (Meyers, 2014) evolutive harmonic analyses (EHA) and average spectral misfit (ASM) analyses were employed to

detect orbital frequencies. While the EHA appeared to show intervals of strong orbital forcing, the ASM analyses were never statistically significant enough to validate the more qualitative interpretation of the EHA. Despite not resolving a robust sedimentation rate (likely owing to the core breaks throughout the section), the sedimentation rate resolved was roughly the same as interpreted by the biostratigraphic age model.

3.4.1.3 DSDP Site 78

Site 78 similarly has no paleomagnetic declination stratigraphy due to its equatorial position through the study interval (The Shipboard Scientific Pary, 1972). Biostratigraphic data includes radiolarians, calcareous nannofossils, and planktic foraminifera. There is substantial spread in secondary datum taxa (fig. 3.4), however, this could be expected when using decades old species distribution table and modern chronostratigraphic calibrations. However, there is good agreement in the primary datums (see fig. 3.4), which were used to construct the age model. Lastly, the $\delta^{18}O$ apex was defined at 23.0 Ma.

3.4.2 Paleoceanography

3.4.2.1 ODP Site 744

Within the lower interval (~27.1-26.15 Ma) there are moderate changes in the benthic $\delta^{13}C$ from ~1‰ to 0.5‰ (fig. 3.7), mimicking the roughly 0.5‰ drop in the $\delta^{13}C$ bulk fine fraction. This same trend, with the lowest value at ~26.5 Ma, appears in the $\delta^{18}O$ values in both benthic and bulk isotopes. The offset from benthic to BFF in $\delta^{18}O$ is only ~0.2‰ (fig. 3.10). This offset between BFF and benthic foraminifera changes after the hiatus. The upper interval has a larger $\delta^{13}C$ gradient between the benthic and mixed layer records, with the benthic $\delta^{13}C$ values between 0.5‰ to 1‰, while the BFF is

between 2‰ to 2.5‰. Although the benthic $\delta^{13}C$ values are variable, there are two intervals of lower values at ~24.2 Ma and ~23.7 Ma. There is a ~1‰ to 0.7‰ shift in benthic values at the top of the record. BFF $\delta^{13}C$ values after the hiatus rise to ~2.7‰, with several temporary drops (~24.0, ~23.7, ~23.6 Ma) and a final drop near the C6Cn.3n base (~23.34 Ma) roughly coincident with the onset of the benthic Mi-1 excursion.

$\delta^{18}O$ values are also different after the hiatus, with benthic values slightly lower than the BFF values, though the gradient is not always consistent (fig. 3.10). Roughly coincident with the last drop in $\delta^{13}C$ mixed layer values there is a slightly lowering of $\delta^{18}O$ values (early C6Cn.3n, in the interval of 'Poorly Constrained Ages', PCA), followed by a ~0.6‰ increase (C6Cn.2n, PCA). Benthic $\delta^{18}O$ values are relatively constant through the 24.2-23.4 Ma interval, with a slight decrease in $\delta^{18}O$ values in the *Cibicidoides pachyderma* record at ~23.8 Ma. This decrease is seen in roughly four non-consecutive samples, and is not observed in the *Cibicidoides* sp. values. There was no observed preservational defect observed in the benthic foraminifera ran in those analyses, but a diagenetic signal cannot be entirely ruled out. The decrease at 23.6 Ma at Site 744 does, however, coincide with a similar ~0.4‰ decrease in the $\delta^{13}C$ records seen at Site 1090 (Southern Atlantic Ocean), which stay low for ~200 kyr, suggesting $\delta^{18}O$ values may preserve a robust signal. At the top of the record (early C6Cn.3n, PCA) there is a benthic excursion of ~1.0‰ in both the *Cibicidoides* sp. and *Cibicidoides pachyderma* records. This excursion occurs simultaneously with the BFF $\delta^{18}O$ excursion and the benthic $\delta^{13}C$ excursion. We interpret this as the initiation of the Mi-1 excursion, a hiatus removing part of the excursion, and the very end of the Mi-1 peak values. No excursion is

observed in the BFF $\delta^{13}C$ values, which is probably recording the local near-surface environment (fig. 3.7, 3.10).

The bulk density record was generated shipboard during Expedition 119 (Shipboard Scientific Party, 1991). The gamma ray attenuation (GRA) values record a mix of changes in both porosity and density within the sediments. There are two intervals of low density/porosity in Core 12H, a dramatic drop at ~26.65 Ma and two smaller decreases at ~23.4 and the middle of the C6Cn. 3n (PCA) and near the top of the PCA (fig. 3.7). The substantial drop in the lower interval is ~100 kyr prior to the change in benthic foraminiferal percentage and radiolarian percentage seen at ~26.7 Ma. Bulk density appears to demonstrate strong cyclically at Milankovtich frequencies (see Cyclicity below).

There are two strong changes in the size fraction masses, one during the hiatus and one at broadly at 23.6 Ma (fig. 3.7). Both before and after the hiatus there is a large decrease in the mass of the <63 μm size fraction, down to ~20% from >90% at ~27 Ma. There is very little change in the structure of the >63 μm mass, though there is a long-term trend toward the >250 μm being a larger contribution to the overall mass. The recovery after the hiatus in <63 μm mass takes ~200 kyr. The other large change in the structure of the size fraction mass occurs broadly, with the largest size fraction (>250 μm) increasing in importance until ~23.6 Ma, then decreasing steadily up to the top of the core. The >250 μm size fraction contributes roughly the same percentage of mass to the sample at the directly post-hiatus as it does at the top of the core. In general, the <63 μm and 63-150 μm fractions broadly track the biosiliceous components (radiolarians and diatoms).

The sediment component counts depict a typical open ocean site, with nearly pure biogenic sedimentation. The >63 μm fraction of the sediment is generally dominated by the planktic foraminiferal tests and fragments, with radiolarians as the second most important components (fig. 7). The earliest portion of the record (27.1-26.5 Ma) is the time with the most equitable distribution of radiolarian to foraminiferal tests, with ~50% radiolarian and highly fragmented planktic tests. Benthic foraminifers are more abundant through the earlier portion than the later, nearing 10% of the sample ~26.9-26.6 Ma. There is a sharp drop in both radiolarian and benthic foraminiferal contribution at 26.6 Ma, with an increase in planktic foraminifers (tests and fragments). The hiatus does not contain an abrupt change in counts, instead there a gradual increase in radiolarian tests until ~24.1 Ma with a corresponding decrease in the planktic foraminifer contribution. There is a long-term gradual drop in radiolarian percentage until ~23.6 Ma, where it begins to rise again until ~23.4 Ma. At ~23.4 Ma there is a sharp drop of ~10%, and values are roughly steady after. Large diatoms (>63 μm) were very rare through the lower interval. In the upper section they are never a major component, but they exceed 5% of the sample during several samples. Peaks in diatom abundance are generally confined to the 23.9-23.4 Ma interval. Within the PCA, benthic foraminifera become more abundant, though not more than 5% of the sample.

The fragmentation index is a generally a recorder of relative lysocline depth, here it suggests major changes in the solubility of calcium carbonate at the seafloor. The fragmentation index scores samples from 0 (good preservation, 100% whole tests) to 100 (poor preservation, 100% fragments). The index in Core 12H stays roughly between 25 and 75 (figs. 3.7, 3.8). Moderately poor planktic foraminifer preservation (and therefore

less stable calcium carbonate and a shallower lysocline) is seen at ~26.5, 24.2-23.8, and 23.4 Ma, while preservation appears to be better at ~27 and ~23.7 Ma, and within the PCA, as well as before and after the hiatus.

Isotopic gradients between the mixed-layer bulk fine fraction and benthic foraminifera are depicted in figure 3.10. There is a roughly 1.0‰ $\delta^{13}C$ difference between the benthos and the mixed-layer in the lower interval, which increases slightly near the hiatus. The gradient continues to increase after the hiatus until it peaks at ~1.5‰ at ~24.1 Ma. There are fluctuations in *Cibicidoides* sp.-BFF and *C. pachyderma*-BFF, but these are rarely synchronous. There is a rapid decline in BFF and benthic $\delta^{13}C$ gradient values from ~23.4 Ma until the Mi-1 hiatus, which is represented as a nearly complete collapse in the $\delta^{13}C$ gradients. The $\delta^{18}O$ values prior to the hiatus are ~1.0‰ higher in the benthic foraminifers, though ~100 kyr prior to the hiatus the gradient begins to switch. Post-hiatus the gradient in $\delta^{18}O$ is variable but much less, generally <0.5‰, until a sharp increase initially at ~23.5 Ma, and more sustained gradient increase at ~23.4 Ma, peaking at ~1.5‰ offset between BFF and benthic $\delta^{18}O$ at the Mi-1 excursion.

3.4.2.1.1 Frequency Analysis

Data was also investigated for Milankovitch cyclicity. Datasets vary in sampling resolution and quality. Bulk density (GRA), for example, can be analyzed at a high resolution, resolving high frequency variations (e.g., precession), while others are lower resolution and can only resolve obliquity or eccentricity. Two analyses were employed to investigate the changing orbital periodicity in the data, a simple periodogram (not shown) and the more complicated evolutive harmonic analysis (fig. 3.11). Because of the drastic sedimentation rate change at the base of chron C6Cn.3n, data above this polarity reversal

were excluded. Similarly, the lower interval was not investigated due to the limited length of the section, and thus limited ability of the analysis to detect frequencies.

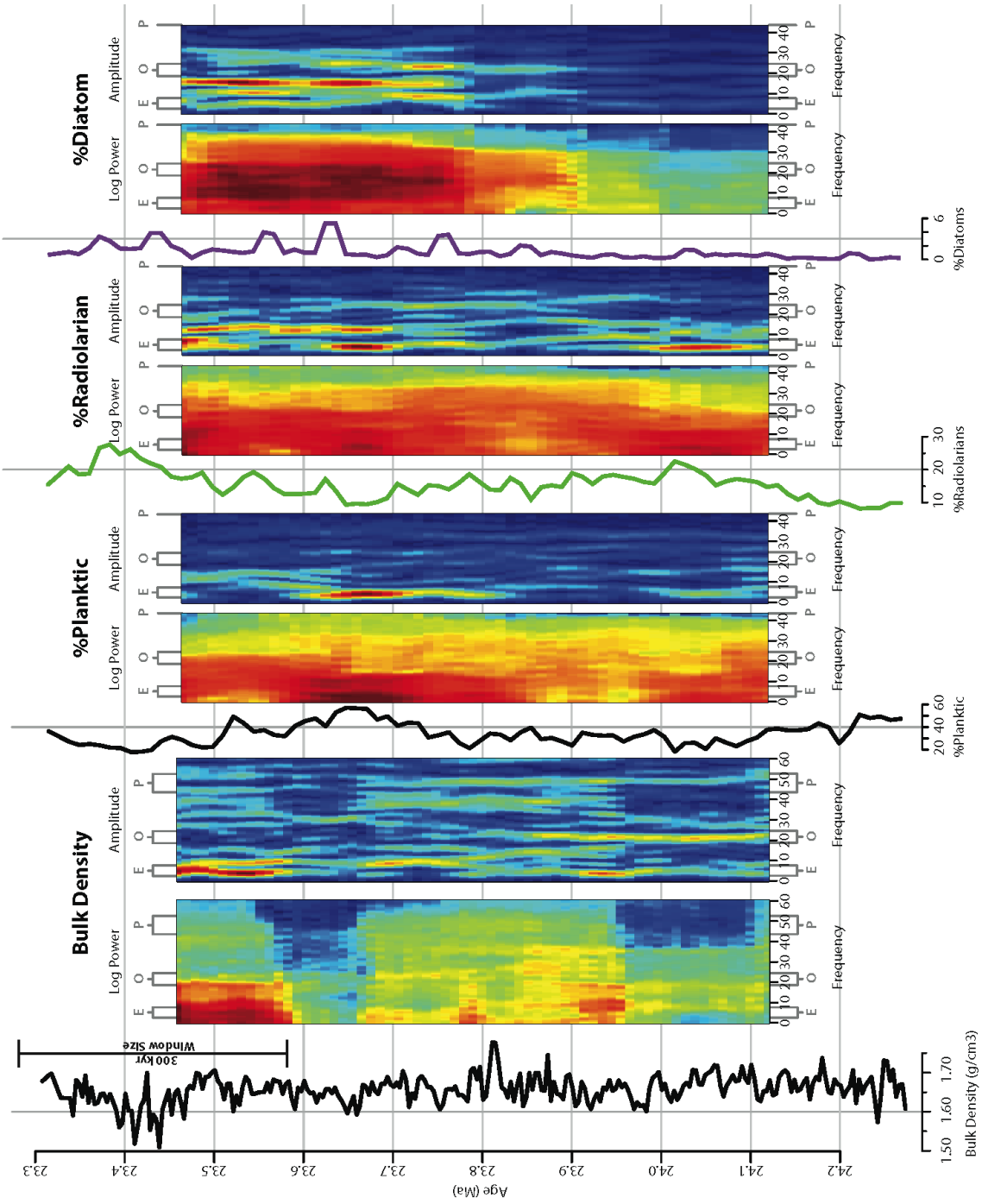

Figure 3.11 Site 744 key evolutive harmonic analyses. Evolutive Harmonic Analyses (EHA) were performed in the R 'astrochron' package (Meyers, 2014). An EHA requires evenly spaced data, so an interpolation at ~3.4 kyr was performed, while count data was interpolated at ~11.5 kyr. All data was padded to roughly 2 times the number of data

points, with a 300 kyr window (depicted at left), and a 10 kyr step. Cooler colors indicate small amplitude changes (or low power) in a given frequency at a given time, while warmer colors indicate large amplitude changes (or higher power). E, O, and P stand for eccentricity, obliquity (tilt), and precession, respectively.

Bulk density was interpolated at ~3.5 kyr (the median sampling interval) in the upper interval. The periodogram depicts orbital periodicities within the predicted bands for this time period. Both periods, short and long, in both eccentricity and obliquity are merged into one single band. Merged periodicities are likely due to the untuned nature of the record, as there are likely changes in sedimentation rate not accounted for in the paleomagnetically-derived age model. Intriguingly, the power/amplitude in the obliquity is low, while the other two parameters are high. Weak obliquity is the opposite of what is expected at a high-latitude location. The EHA (see fig. 3.11 caption for details) depicts similar patterns for the orbital periods, with a consistent precession peak with the majority of the power in eccentricity and obliquity changes. Obliquity is strong at the beginning of the record, up until ~23.8 Ma where it greatly diminishes in strength. Eccentricity begins to strengthen then, with a moderate amplitude at 23.7 Ma, then the largest changes in bulk density occur starting at ~23.6 Ma, with two clear eccentricity parameters, merging to one at 23.5 Ma to the top of the record.

Sediment composition count data was all interpolated at roughly the same resolution (~11 kyr). At this resolution, the long precession cycle is just at the cusp of detection, and so will not be commented on. These data are also limited by being percentage data. As percentages, substantial changes in one variable, for example radiolarians, would force other variables, say foraminifera, to respond to that same frequency, whether or not it was driving changes in planktic foraminifer abundance or not.

The %planktic record appears to vary with eccentricity from 23.8 Ma to the top of the record (fig. 3.11). There is an interval from ~23.6-23.5 Ma in which eccentricity appears to wane in importance. Weaker eccentricity could be due to either a real signal or to slowing sedimentation rate prior to the reversal boundary. %radiolarian results show similar changes; there are large (though not as strong as in the %planktic) amplitude changes at eccentricity frequencies (fig. 3.11). Amplitude seems highest at ~24.5 and 23.7 Ma, with a higher frequency signal appearing at 23.7 Ma. It is possible the higher frequency is obliquity, however it is slightly too low to be unequivocal.

The %diatom record is substantially different from the previous records (fig. 3.11). Diatoms (>63 μm) appear to fluctuate strongly (both in amplitude and in power) to the obliquity through this interval, with substantial amplitude variation at the ~15 frequency. While the %diatom changes are quite small (maximum ~9%), these changes observed to be larger than the error estimates for these samples (fig. 3.7). Again, this frequency is not quite precisely obliquity, however it is certainly higher than eccentricity, and far lower than procession. Given the limited nature of the age model, it seems probable (though not certain) that this is obliquity.

The fragmentation index is constructed from the %planktic and %fragment values. As a ratio, it should not have the 'overdubbing' effect observed in the other count data. However, EHA results for the fragmentation index is very similar to the %planktic EHA results, with strong eccentricity forcing and relatively weak obliquity forcing (Fig. 3.12). The sediment size fraction masses were also investigated in the same way (not shown) and demonstrated the same eccentricity frequency domination.

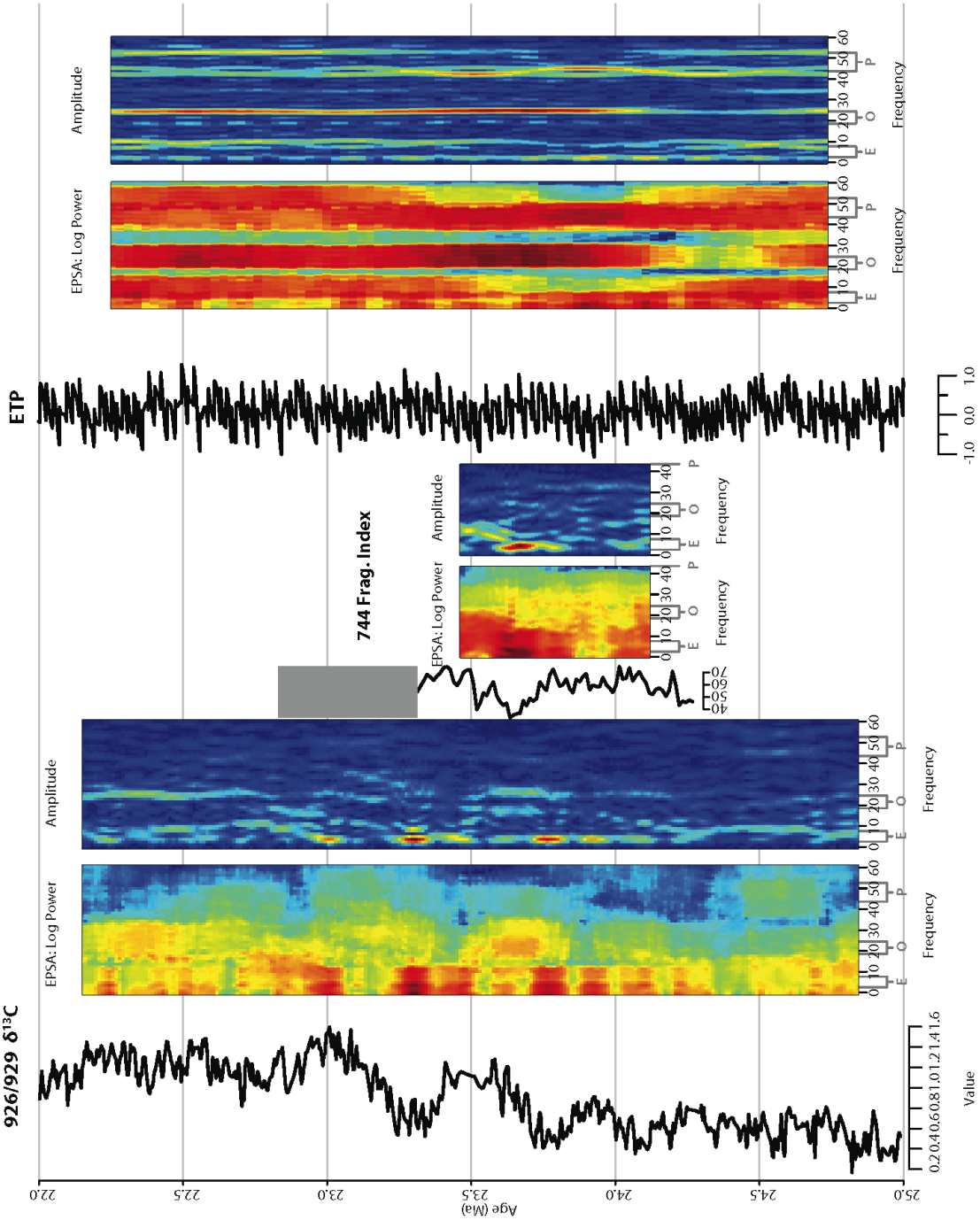

Figure 3.12 Mi-1 key evolutive harmonic analyses. Sites 926/929 carbon isotope time series against Site 744 Fragmentation Index and 'ETP' from Laskar et al. (2004). Sites 926/929 were interpolated to the median sampling interval, as was Site 744.

Throughout the entire analysis of frequencies eccentricity was most prominent cycle (figs. 3.11, 3.12). Only %diatom and possibly %radiolarian depict other frequencies with appreciable power (fig. 3.11, 3.12).

3.4.2.2 ODP Site 803

Benthic stable isotopes (both *Cibicidoides* sp. and *Oridorsalis* sp.) generally agree with the global compilation records through the study interval, as well as the existing Barrera et al. (1993) *Cibicidoides* sp. record (fig. 5). The Mi-1 $\delta^{18}O$ excursion is ~1.0‰, as expected both from the Barrera et al. (1993) data and the multi-site compilations of Zachos et al. (2008), and is roughly the expected duration, with acknowledgement that the age model is predominately biostratigraphic. There is a roughly constant offset in *Cibicidoides* sp. to *Oridorsalis* sp. as well (0.27‰ $\delta^{18}O$, 1.24‰ $\delta^{13}C$; n=5). $\delta^{18}O$ corroborate the more detailed study of Katz et al. (2003), which has a ~0.28‰ offset, while the $\delta^{13}C$ is 0.24-0.53‰ more offset than Katz et al. (2003) or Shackleton et al. (1984).

Planktic foraminifer isotope records also agree with tropical trends seen at other sites (e.g., Paul et al., 2000). There is a smaller change (~0.5‰) across Mi-1 in the mixed-layer (*Paragloborotalia kugleri-pseudokugleri*) $\delta^{18}O$ time series relative to benthic data (fig. 3.5). Neither planktic nor benthic records depict the pre-Mi-1 $\delta^{13}C$ eccentricity-forced shifts seen globally, but there is, in both, a shift to more positive values across Mi-1. The absence of the $\delta^{13}C$ signal is likely due to the lower resolution relative to the global compilations.

Counts of the >63 μm sediment record purely biotic sedimentation at Site 803. Throughout the study interval radiolarians (~40% to >90%) and planktic foraminifers

(<50%) dominate the assemblage (fig. 3.5). There is a substantial component of both whole and fragmented planktic foraminiferal tests, suggesting that this site occupied a water depth above the CCD and below the lysocline. Minor contributions are made from benthic foraminifera (<3%) and echinoderms and sponges components (<6%). There are instances with noticeable increases (>20%) in the planktic foraminifer fraction, ~25, ~24.7, ~23.6, and 23.2-22.8 Ma, with several instances post-Mi-1 with modest increases. Increases, however minor, in benthic foraminifera, occur during the Mi-1 centered increase in planktic foraminifera.

There are substantial swings (30-80) in the fragmentation index (figs. 3.5, 3.8). Inflection points in carbonate preservation occur at ~23.6 Ma (peak good preservation), ~23.45 Ma (peak poor preservation), ~23.1 Ma (good), and 23.75 Ma (poor). After ~23.75 Ma the preservation is moderate for the rest of the record.

3.4.2.3 DSDP Site 78

Benthic foraminifers were rare at Site 78, making the stable isotope record poor (fig. 6). Due to the discontinuous record of benthic $\delta^{18}O$, the traditional method of detecting Mi-1, we must rely on biostratigraphic markers (both radiolarian and planktic foraminifera) or planktic stable isotopes, which do not contain as large an excursion in the tropics. There is a small shift in planktic isotopes, roughly where B *Paragloborotalia kugleri* occurs. Biostratigraphy is obviously not the ideal method for detecting an isotopic excursion, but it is the best proxy available to identify the Oligocene/Miocene boundary and Mi-1 at this site.

As with Site 803, planktic isotopes record minimal change through the upper Oligocene and lower Miocene at Site 78. They depict a minor increase in $\delta^{18}O$ values

across the interpreted Mi-1 excursion of ~0.5‰. The change is larger in the deeper dwelling *P. siakensis-mayeri* plexus. The excursion also seems dramatically shorter at Site 78 than at all other sites, due in large part to the paucity of benthic foraminifera at this site. Counts at Site 78 record purely biological sedimentation, dominated by radiolarians, with a much more minor contribution of calcium carbonate. There are seemingly pulsed-increases in radiolarians during and after Mi-1, with slight increases in carbonate prior as well, and in the ~50 kyr lead up to the event. After Mi-1, a much larger increase in carbonate content is noted. The benthic components at Site 78 contribute very little to the sediment, with all components <3% in each sample. Benthic foraminifers only once exceed 1% of the sample, near the top of the study interval.

There are minor changes in the fragmentation index, and thus the lysocline, at Site 78 relative to the other two sites (fig. 3.8). The smaller changes are perhaps due to the smaller interval of time encompassed by the study interval at Site 78, missing the early lead up to Mi-1. There is a moderate decrease in carbonate preservation after the interpreted stratigraphic position of the Mi-1 event.

3.4.2.4 Linear Correlations

There should be an obvious correlation between the number of whole planktic tests in a sample and the number of fragments. Fig. 3.13 depicts this correlation in all three sites in this study. Both low and high latitude sites demonstrate very good correlations between the fragmentation index and the number of whole planktic tests in the sediment. While this is not surprising, as the fragmentation index is simply fragments divided by whole tests plus fragments, it suggests that higher flux of planktic tests can suppress the lysocline. This appears to be particularly strong at the high latitude site,

which shows a stronger correlation between the two variables. This pattern suggests that an increase in the number of planktic foraminifera to the seafloor may suppress the lysocline by shear flux of $CaCO_3$, leading to fewer fragments per foraminiferal test. Such a mechanism is similar to the Berger et al. (1982) model of equatorial carbonate fluxes during high productivity.

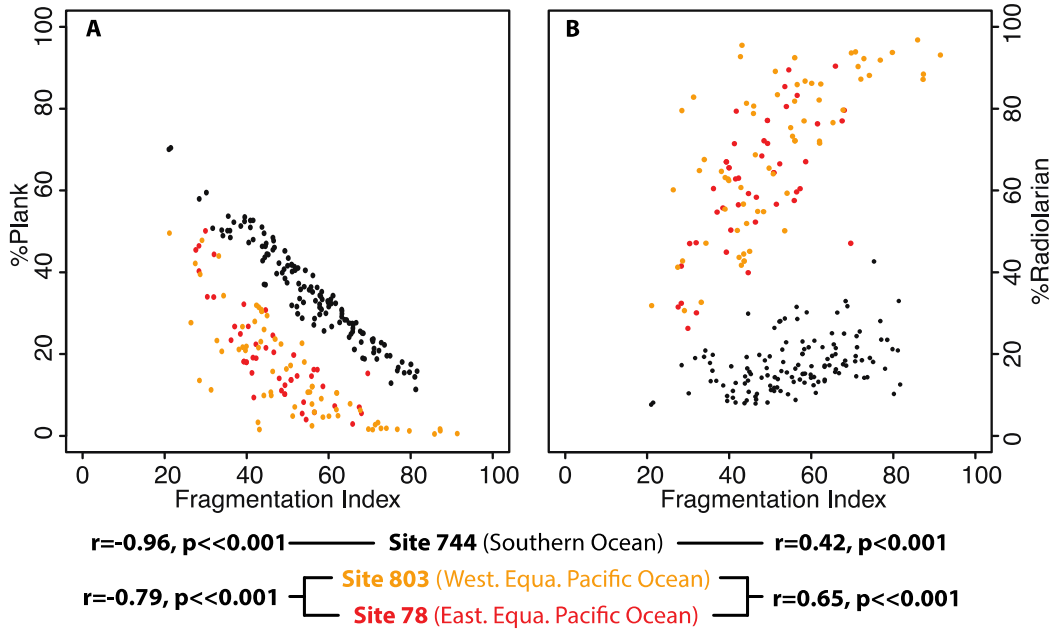

Figure 3.13 Linear correlations. Comparison of %planktic and fragmentation index, and %radiolarians and the fragmentation index. Site 744 is represented by black circles, Site 78 by red circles, and Site 803 by orange circles. Both tropical sites (Sites 78 and 803) are analyzed together.

Greater accumulation of siliceous microfossils are typically viewed as higher productivity (e.g., McMillen and Casey, 1978). Their percentages, however, is typically controlled by a different factor: carbonate dissolution. As carbonate preservation is more favorable, the relative contribution of siliceous microfossils decreases as they are swamped out by foraminifera, and visa versa. Thus, the lysocline and productivity both have primary control on the %radiolarian and %diatom. Comparisons of %radiolarian vs. fragmentation index at Sites 78, 803, and 744 suggest that lysocline position controls the

%radiolarian values, with strongly significant correlations (fig. 3.13). The %diatom (only present in appreciable abundances at high latitudes) vs. fragmentation index does not have the same correlation at Site 744 (not shown) and so can be used as a more faithful recorder of productivity.

3.5 Discussion

What follows is a discussion of both orbital and secular changes associated with the pre-Mi-1 interval at several sites. None of these new sites have orbitally tuned age models, however, which is a distinct weakness of this analysis. It cannot be helped, as the time series at Site 744 are short, and Site 803 is rife with core gaps. Site 78, as a part of Leg 9, has no high-resolution data to use for an orbital age model. Without simply 'wiggle-matching' implied orbital frequencies to the Laskar et al. (2004) orbital solutions, orbital tuning is not possible at these sites during these intervals. All of the various age models are constructed as the best and highest resolution versions possible. To dismiss data such as these, simply because the age models are not as refined as modern paleoceanography expects, would force us to eliminate Deep Sea Drilling Project-era cores from future study. With that acknowledged though, there are caveats to the following analysis.

3.5.1 ODP Site 744

As the age models are not orbitally-tuned, the implied orbital frequencies here are not as robust as they are at tuned sites (e.g., Site 1218; Pälike et al., 2006). Implied orbital frequencies observed here (e.g., Fig. 3.11) drift to both higher and lower frequencies, and are not strictly observed at their known frequencies. An example of drifting is seen in Fig. 3.11, where the eccentricity appears to move to a higher frequency in the upper

interval. Rather, there is a slowing sedimentation rate in the upper portion of the record (see below). Another caveat is that while here we attribute obliquity-forcing to %diatoms at 744 (see below), a more precise way to describe the frequency would be a 'frequency higher than eccentricity'. The observed frequency is somewhat lower than the expected obliquity forcing, which could simply be due to the weak age model. With biostratigraphic or paleomagnetic age models, there is a certain expected spread in age designation (though paleomagnetic age determinations are precise, the stratigraphic distance between control points is fixed and sometimes large), and both methods require interpolation between control points or datums. With imprecise age determinations, we cannot be sure of how robust the observed frequencies are, and thus there could be something other than obliquity. The closest orbital frequency to the observed changes *is* obliquity however, and so that seems like the most likely candidate.

Sedimentological counts at Site 744 agree with the previous research on Core 744-12H (Diester-Haass, 1996). The Diester-Haass (1996) study provides important context for this study. Prior to Oi-1 (~34 Ma), Site 744 was situated underneath the Circumpolar Surface Water, recorded by siliceous-poor, carbonate-rich sediment (Nelson and Cooke, 2001). At the Oi-1 event, there is a very abrupt shift to siliceous dominated facies, with a far larger percentage of radiolarians, diatoms, and other siliceous microfossils, indicating a cooler, more productive surface water mass (Nelson and Cooke, 2001). During the early Oligocene there was a gradual transition back to pelagic carbonate sedimentation, but there continued to be shorter-lived pulses of biosiliceous productivity through the late Oligocene. The Diester-Haass (1996) study was done prior

to much of the age model refinement, and so did not discuss the hiatuses found later (e.g., Florindo et al., 2013).

Count and isotopic data suggest that there are three main paleoceanographic phases recorded in the sediments of Core 744, 12H. Pre-hiatus, there is a relatively high biosiliceous (radiolarian) content until 26.5 Ma, with higher benthic foraminifera, suggesting a higher productivity environment (fig. 3.7). There is a two-step drop in radiolarians and benthic foraminifera between 26.5 and 26.3 Ma, suggesting a transition to lower productivity. This two-step change in sediment components was also observed by Diester-Haass (1996). Roughly coincident with the count changes, there is a small shift in all $\delta^{13}C$ time series to lower values, and a small shift ~0.2‰ in $\delta^{18}O$ (Fig. 3.10). In general, this 200-kyr transition is marked by an increasing C-isotope gradient between seafloor (benthic foraminifera) and photic zone (bulk fine fraction) values, and decreasing benthic-planktic O-isotope gradient. These changes in counts and isotope values suggest decreased productivity at ~26.5 Ma, coincident with the peak of the slight warming trend suggested by the $\delta^{18}O$ BFF values, with productivity dropping afterwards.

Durng the ~200-kyr interval before the hiatus, there is a decrease in the contribution of the fine fraction (<63 μm) as well as a sharp increase in planktic foraminifers, perhaps suggesting an increase in winnowing at the seafloor. This decrease in fine fraction could, alternatively, have been a decrease in the production of calcareous nannofossils. With the presence of Mn-nodules, which only form slowly at the sediment-water interface, it seems most likely that the fine-fraction decrease is post-depositional winnowing that culminated in the formation of a brief hiatus (~105 mbsf). Winnowing could also be affecting the BFF signal, as the calcareous nannofossils, which comprise

those analyses were being removed, amalgamating more and more time into each analysis. This hiatus has previously been hypothesized to be due to increased current strength at Site 744 (Roberts et al., 2003) and at Site 690 in the Weddell Sea (Spiess, 1990). Our data support that hypothesis.

After the hiatus there is ~1 myr of deposition of calcareous dominated sediments, with minor changes in radiolarian flux. During this interval, the carbon isotopic gradient between benthic foraminifera and bulk fine fraction (near surface calcareous nannoplankton and juvenile planktic foraminifera) is strong, averaging ~1.5‰, due in large part to more enriched values in the surface water mass suggesting lower productivity. By contrast, the oxygen isotopic gradient between the seafloor and surface ocean is very small, averaging <0.5‰. The Southern Ocean has a unique thermal structure, where intermediate water is warmer than the surface or deep water (which are similar in temperature (Park et al., 1998). Thus, a small oxygen isotope gradient actually evidence of strong stratification, while a large gradient with surfical warming would suggest strong upwelling. Thus, the biotic components and isotopes indicate generally lower relative productivity. With the strong eccentricity (likely ~405 kyr) and/or obliquity forcing noted in most data, it appears that this interval is largely dominated by orbital frequencies. There is a gradual increase in the %diatoms, which perhaps suggests that there was a gradual expansion of the cooler water masses. During the late Oligocene and early Miocene there is a notable expansion in the cooler surface water masses around Antarctica (Nelson and Cooke, 2001), and the increase in biosiliceous content prior to the excursion could be seen as a portion of this trend. Alternatively, the %diatoms could be an increase in surface productivity. Marine productivity, as noted previously, is elevated

prior to Mi-1 particularly in the higher latitudes, where it appears to be forced by the ~405-kyr eccentricity cycle (Diester-Haass et al., 2011). Radiolarians and diatoms are typically viewed as indicators of higher productivity (e.g., Berger, 1979; Moore et al., 2014). While %radiolarians are generally controlled by the lysocline position and carbonate preservation at Site 744, an increase in their relative contribution to the sediment may suggest increased productivity if the planktic foraminiferal fragmentation index can rule out poor carbonate preservation. The increase in diatoms supports increased productivity as well.

The Mi-1 excursion at Site 744 begins in subchron C6Cn.3n ('Poorly Constrained Ages', PCA) with the onset of a positive excursion in both $\delta^{18}O$ and $\delta^{13}C$ (fig. 3.10). Most intriguing are the changes that start *before* the onset of Mi-1, at 23.4 Ma, including an abrupt negative shift in bulk fine fraction $\delta^{13}C$ values, and smaller magnitude negative shift in BFF $\delta^{18}O$ values. During the ~300 kyr lead up to Mi-1 (C6Cn.3n, PCA) there is also a decrease in the siliceous content (both %radiolarian and %diatom), a gradual decrease in the benthic-BFF $\delta^{13}C$ gradient and a sharp increase in the water column $\delta^{18}O$ gradient. The warming signal in the mixed layer suggests increased upwelling, bringing the warmer intermediate water to the surface. As this site was within the Antarctic Divergence, an increase in wind speed could have increased the upwelling in the area, bringing relatively more nutrient and warmer waters to the surface, increasing productivity (specifically carbonate). This is supported by the collapsing $\delta^{13}C$ gradient, the increasing $\delta^{18}O$ gradient, and the change in sediment. There could be a corresponding change in sedimentation rate, however it is not possible to detect due to the hiatus above

this level. Increased productivity directly prior to the event is seen at several other sites (Diester-Haas et al., 2011).

3.5.2 Sites 803 and 78

Sites 803 and 78 have some similarities with Site 744 through the Mi-1 lead up. Both sites record an increase in planktic foraminifera between 23.2 and 23.1 Ma (fig. 3.8). This increase is larger at Site 803, ~40% increase vs. ~20% at Site 78. While the increase is roughly sustained at Site 803, Site 78 returns to the ~80% radiolarians proportion ~100 kyr prior to the event. High %radiolarian is sustained until ~100 kyr after the event, where there is a long term decrease in the radiolarian proportion, with increasing carbonate. Site 803, however, maintains a ~1:1 carbonate to siliceous ratio until 22.8 Ma, after-which it rises to ~70% radiolarians again.

The longer term increasing carbonate trend at Site 78 is probably explained by its equatorial position at this time. The equator is within the error bounds for paleolatitude reconstruction for both Sites 78 and 803 (van Hinsbergen et al., 2015). As sites move underneath the equatorial upwelling zone, the expectation is that the carbonate fraction will increase responding to carbonate production in the equatorial upwelling zone (e.g., Piela et al., 2012). The decrease in the mixed-layer to thermocline $\delta^{13}C$ gradient suggests a similar response as well (fig. 3.6), as the gradient would decrease as production increases in the upper water column.

The mixed-layer $\delta^{18}O$ response is also important to note (figs. 3.5, 3.6). Paul et al. (2000) reported a similar finding with planktic isotope values displaying a minor increase. As previously described (e.g., Paul et al., 2000) the expected $\delta^{18}O$ increase at Mi-1 due purely to ice-volume effects is ~0.5‰, roughly the same as the planktic

response in the tropics observed here (figs. 3.5, 3.6). It is interesting to note that the increase at Site 744 in the mixed-layer is ~0.8‰ during the excursion, suggesting that the surface water cooled slightly (fig. 3.10). The tropics, however, appear to have little or no change in temperature.

The differing biotic response through the excursion at Sites 78 and 803 is perhaps explained by an increase in the thickness of the mixed layer (or depth of the thermocline) in the western equatorial Pacific (WEP), similar to the present day warm pool. Current equatorial export flux, with a western Pacific warm pool, mimics this distribution of sediments, with high carbonate/low silica flux in the warm pool and low carbonate/high silica in the eastern equatorial Pacific Ocean (EEP; Kawahata et al., 2000). A warm pool in the Oligocene/Miocene would be substantially earlier than previously thought (e.g., Li et al., 2006; Nathan and Leckie, 2009), especially with an open gateway through the Indonesian Seaway (Nishimura and Suparka, 1997). Perhaps glacio-eustasy partially constricted the seaway temporarily as proposed by Nathan and Leckie (2009) for the middle to late Miocene transition. Alternatively, global cooling resulted in stronger prevailing winds, and stronger Trade Winds over the Pacific pushed warm surface waters westward to thicken the mixed layer while driving higher productivity in the central and eastern equatorial Pacific. This may explain the higher abundances of radiolarians during Mi-1 at Site 78 in the EEP and higher abundances of planktic foraminifera at Site 803 in the WEP.

3.5.3 Carbonate Preservation

Macrostratigraphy is the study of global sediment accumulation patterns analogous to macroevolutionary study (e.g., Peters, 2006). It uses package terminations

(or the start of a hiatus, analogous to an extinction event) and package initiation (or the end of a hiatus, analogous to an origination event) to describe changing lithologic circumstances on the continents and in the marine realm, frequently linking biotic evolution and sedimentation together (e.g., Peters et al., 2013; Heim and Peters, 2011). During the Eocene-Oligocene transition (EOT) there was a substantial increase in the rate of Atlantic package initiation, particularly pronounced in carbonate only-packages. The CCD was deepened by ~1 km at the Oi-1 event (e.g., Coxall et al., 2005; Pälike et al., 2012), an effective mechanism for initiating pelagic sedimentation at a greater number of sites (Peters et al., 2013). At the Oligocene-Miocene transition (OMT) there were, unlike the EOT, only minor fluctuations in the carbonate mass accumulation rates at several sites rather than a large-scale CCD change (Pälike et al., 2012). Changes in carbonate mass accumulation rate can reflect shifts in the relative position of the lysocline, as well as changes in carbonate productivity in the surface waters (e.g., Berger, 1970, 1978). There is also an increase in the Atlantic Ocean carbonate-package truncation rate with a smaller increase in initiation during the OMT (Fraass et al., 2015), also observed in the Pacific and Indian Ocean as hiatuses (e.g., Moore et al., 1978; Keller and Barron, 1983; Ramsay et al., 1994). The observed increase in Pacific hiatuses during the OMT were in part related to the deepening of the Drake Passage and increased strength of the Antarctic Circumpolar Current (e.g., Pfuhl et al., 2004; Scher and Martin, 2008; Katz et al., 2011). Even some sites with sedimentation through OMT interval suggest a slower sedimentation rate through the excursion interval (e.g., Site 744). The OMT and EOT have distinctly different stratigraphic and sedimentological characteristics.

The Pälike et al. (2006b) study established a prediction for Pacific Ocean lysocline position. From ~24.2-23.0 Ma there should be a deepening of ~0.25 km, superimposed on substantial eccentricity-frequency variations. This prediction is based on carbon cycle box models, forced by a synthetic insolation curve (Pälike et al., 2006b). Figure 3.8 presents benthic $\delta^{13}C$ data from Zachos et al. (2008) with count data and the interpreted relative lysocline position at all of the sites. $\delta^{13}C$ through this interval is thought to be responding to increases in marine productivity (Diester-Haass et al., 2011). Carbonate preservation can also respond to higher surface productivity and higher organic matter flux to the seafloor, which typically reduces carbonate preservation and causes the lysocline to shoal along productive continental margins (e.g., Berger, 1970; Cullen and Curry, 1997). This decreased preservation is accomplished by increasing decomposition, accompanied by increased respired CO_2. The relationship between productivity and the lysocline position is more complex. Under conditions of higher carbonate productivity, such as the equatorial divergence away from the continental margin, the lysocline and CCD may be suppressed by the higher carbonate flux rates (e.g., Berger, 197; Lyle et al., 2008; Pälike et al., 2012). Prior to ~23.8 Ma the lysocline is stable at Site 744. Peak carbon preservation occurs at ~23.6 Ma, as $\delta^{13}C$ values are at a minimum. As $\delta^{13}C$ reaches a peak at ~23.4 Ma, carbonate preservation is at its worst. Carbonate preservation improves, though with perhaps a brief dissolution period, seen as a modest shoulder in several samples at all sites. Both $\delta^{13}C$ and carbonate preservation peak at ~23.0 with Mi-1. At different intervals of time fragmentation and $\delta^{13}C$ are either both high (~23.8, ~23.4 Ma), low (~23.7, possibly 23.2 Ma), or opposite (23.0 Ma).

There is roughly good agreement in the lysocline and production trends until ~23.4 Ma at all sites in this study, where the relationship breaks down. The breakdown is roughly coincident with several events at other sites. Bottom water warming peaks at Site 1218 (~23.4 M; Lear et al., 2004). Also, ~23.4 Ma is one of the intervals with a minimum in the coarse fraction accumulation at Ceara Rise (Sites 926/929; Paul et al., 2000). Both records from Sites 926/929 and 1218 suggest changes in bottom water at this time. Increases in bottom water circulation, originally attributed to Drake Passage opening, were first used to explain the repetition of hiatuses rife in the Pacific Ocean (Keller and Barron, 1983), but may also be directly related to Northern Component Water and intensification of the Antarctic Circumpolar Current (Scher and Martin, 2008; Katz et al., 2011).

3.5.4 Timeline to Mi-1

The upper Oligocene is slightly warmer than the lower Oligocene in the lower latitudes, though the high latitudes do not experience this (Pekar et al., 2006; Cramer et al., 2009). Sedimentation resumes at Site 744 at ~24.2 Ma, recording a slowdown in bottom water circulation in the high latitudes (Spiess, 1990; Roberts et al., 2003), if the assertion that increased winnowing through bottom water flow lead to the hiatus ending at ~24.2 Ma is correct. Site 1090, also in the Southern Ocean, experiences the end of an interval of 'mild dissolution' roughly at the same time (Anderson & Delaney, 2005). Also around that time, Site 1090 records the start of a gradual increase in paleoproductivity, roughly tracking the gradual increase in $\delta^{13}C$ values globally (Zachos et al., 2008). Obliquity is at a minimum (cold-orbit node) at 24.39 Ma, coinciding roughly with a minimum in eccentricity. This cold-orbit node is a manifestation of the

~1.2 myr obliquity amplitude cycle (which varies from 1.47-myr to 1.04-myr long in the Oligocene; Pälike et al., 2006b). Prior to the recalculation of the orbital parameters in more recent solutions (e.g., Laskar et al., 2010), a cold-node was the orbital configuration at 23.0 Ma. Here, it possibly represents a necessary preconditioning of the climate system (Wade and Pälike, 2004). The confluence of several high latitude changes (possibly slowed bottom water circulation, increased productivity, increased preservation), as well as the importance of axial tilt control on Southern Ocean climate, speak to a ~1.2 myr obliquity control. This ~1.2 myr cycle found at the equator in carbonate preservation as well (Site 926/929; Pälike et al., 2006a). The modulated-obliquity control is likely not ice growth during the minima on Antarctica or elsewhere, as the $\delta^{18}O$ trend is fairly flat through that interval. Previous studies have established the ~1.2 myr cycle as an important feature on Oligocene 'Oi' events (Wade and Pälike, 2004) and Mi-1 (Pälike et al., 2006b).

Bottom water cooling at ~23.7 Ma is interpreted from the Mg/Ca paleothermometer at Site 1218 (Lear et al., 2004). There is also a ~0.6‰ decrease in $\delta^{18}O$ values at Site 1090 and a ~0.25‰ drop at Site 1218 (Zachos et al., 2008). If this $\delta^{18}O$ change is due to temperature, it suggests a warming. The effect of decreased carbonate ion concentration on both $\delta^{18}O$ and Mg/Ca mimics a warming (Spero et al., 1997; Lear et al., 2004), but the Mg/Ca and $\delta^{18}O$ changes are roughly coincident with a drop in $CaCO_3$% (Pälike et al., 2006b, Supplemental Information). As decreased $CaCO_3$% should indicate a lower carbonate ion concentration, Mg/Ca is probably a real signal of bottom water warming at ~23.7 Ma. Productivity peaks at ~23.5 Ma at Site 1090 (Site 1090; Diester-Haass et al., 2011), as does a decrease in carbonate preservation at Sites 803 and

744. Site 1218 also records a decrease in $CaCO_3$% (mentioned above), though only reflected in a minor carbonate mass accumulation rate drop (Pälike et al., 2006b, Supplemental Information). The synchronicity of these trends is striking. Mid-latitude paleoproductivity also begins to increase after 23.5 Ma at Site 1265 (Diester-Haass et al., 2011) and Site 516 (Flordino et al., 2015). Radiolarian relative abundance is at its highest in the tropics, though this is likely not productivity, but rather poor carbonate preservation (though these two can be linked, see above). Bottom water warms from ~23.7-23.3 Ma at Site 1218, with an inflection to cooler temperatures coincident with the inflection of $\delta^{13}C$ to higher values (Lear et al., 2004).

As $\delta^{13}C$ values fall from 23.3-23.5 Ma paleoproductivity indices are high in the mid- to high latitudes (Diester-Haass et al., 2011). Site 744 records an increase in upwelling and productivity. Dissolution index records at Site 744 and 803 record improving carbonate preservation through that interval. Equatorial carbonate production increases at ~23.2 Ma (Pälike et al., 2006b; Mawbey and Lear, 2013). Equatorial sites (1218 Pacific; 926/929 Atlantic) also record cooling in the bottom water between roughly 23.2-23.1 Ma (Lear et al., 2004; Mawbey and Lear, 2013). Surface water cooling in the high latitudes peaks at ~23.1 Ma (Site 1090, Billups et al., 2002; Site 522; Miller et al., 1991). Temperatures do not change through the event in the tropical surface water, thus as the poles cooled, an increase in meridional gradients has been invoked (e.g., Anderson and Delaney, 2005). With an increased meridional gradient, and increase in prevailing winds is to be expected, which could be why productivity appears to increase at Site 744, as well as an increase in thermohaline circulation, which may account for the development of the hiatuses throughout the ocean. Additionally, this change in the global

conveyor could explain the deviation from lock-step eccentricity-forced carbonate preservation. While the lysocline had varied previously with eccentricity, carbonate preservation increases globally from ~23.4 to ~23.0 Ma. deeper lysocline could be a contributing factor to strengthen the glaciation, though not the cause (*sensu* Coxall et al., 2005). In fact, it is a similar finding to the deepening of the CCD across Oi-1 (Coxall et al., 2005), in a much smaller and weaker form.

From 23.1 to 23.0 Ma, both $\delta^{13}C$ values and fragmentation are at a plateau. Carbonate production at Site 803 is high, while there is an increase in radiolarians at Site 78. High productivity extends from high latitudes to the equator (Diester-Haass et al., 2011; Floridino et al., 2015). Deep water cooling, as recorded by benthic $\delta^{18}O$ peaks at the low latitudes (Sites 1218, 926/929; Lear et al., 2004; Zachos et al., 2008), though there is evidence for warmer Mg/Ca paleotemperature from Sites 926/929 (Mawbey and Lear, 2013). The Mg/Ca paleothermometer can also affected by dissolution, but Li/Ca results from that same analysis suggest that the Mg/Ca results are robust (Mawbey and Lear, 2013), as does the improvement of the carbonate preservation globally (this analysis). %Planktic increases at ~23.15 Ma at multiple sites (including Site 516; Florindo et al., 2015), while fragmentation index decreases from ~23.4 Ma. It seems likely then, that the substantial increase in %planktic is an increase in the planktic foram flux, rather than just an artifact of carbonate preservation, thus a dramatic increase in carbonate production at the surface.

A combination of both orbital and secular variation must drive the glaciation across the Oligocene/Miocene boundary. Data presented here from the equatorial Pacific and Southern Ocean supports other studies from the Atlantic (e.g., Diester-Haass et al.,

2011; Floridino et al., 2015) suggesting that increased marine primary productivity caused drawdown of atmospheric CO_2 during the latest Oligocene, thereby preconditioning the ocean-climate system for a short-lived Antarctic glaciation ultimately triggered by a favorable orbital configuration.

3.6 Conclusions

1. Site 744 does not record the entire Mi-1 excursion, though it captures the onset of the excursion and peak $\delta^{18}O$ values. A hiatus, correlative with other hiatuses at other sites, suggests increased bottom water flow of the Antarctic Circumpolar Current associated with the glacial state.
2. At Site 744, upwelling of warmer intermediate waters begins at ~23.4 Ma, possibly driven by increased winds along the Antarctic Divergence, leading to increased productivity prior to Mi-1.
3. Both Sites 78 and 803 record strong evidence for increased upwelling, through the signature is different at each site (increased carbonate preservation in the western equatorial Pacific, increased radiolarians in the eastern equatorial Pacific).
4. Preconditioning for Mi-1 started at the previous low-amplitude obliquity node (24.3 Ma) with four intervals of progressively higher productivity (recorded both in $\delta^{13}C$ and increased carbonate flux) and paced by 405-kyr eccentricity cycles. Increased marine productivity was driven by increased upwelling, likely driven in turn by increased wind stress.
5. The orbital conditions, most importantly eccentricity and the ~1.2 amplitude obliquity cycle, are the clear driver of profound changes (e.g., $\delta^{13}C$) prior to the

Mi-1 event. The orbitally-driven productivity hypothesis is the best explanation for Mi-1.

CONCLUSION

Creating a 'unified theory' for paleoceanographic events, where it would be possible to ascribe a single driving force for all of the abrupt changes in the paleoceanographic record, it simply is not possible. For certain events implicating gateway changes is apt, for others atmospheric CO_2 or orbital forcing. The dramatic changes, both in evidence from Chapter 1 and from other studies (e.g., Haug and Tieddeman, 1998), strongly suggest that closure of the Central American Seaway drove increased in thermohaline circulation, which then promoted Northern Hemisphere cooling.

Conversely, the Drake Passage and Tasmanian Passage do not have the simple and direct causal relationship to the Eocene-Oligocene Oi-1 or Oligocene-Miocene Mi-1 glaciations once ascribed to them. Simply by the repeated nature of the Oi or Mi events, it seems unlikely that a change in a gateway could be to blame. In fact, the connection of Oi and Mi events to orbital nodes (Zachos et al., 2001; Wade and Pälike, 2004; Pälike et al., 2006b), also argues against gateway forcing for rapid climate change. Declining atmospheric CO_2 levels crossed a threshold, which has been implicated as the trigger of the rapid O1-1 glaciation (e.g., DeConto and Pollard, 2003), but demonstrating a high-resolution direct link between CO_2 and Mi-1 has proven difficult, largely due to sampling and resolution issues. Orbital configuration likely drove the Mi-1 glaciation in two ways, prompting CO_2 lowering through increased productivity, and through a cold obliquity orbit finally driving the glaciation at 23.0 Ma.

Perhaps, then the best explanation to attempt to unify plausible climate change drivers such as changes in ocean gateways or atmospheric CO_2 is this: Gateway changes have the potential to change circulation, both regional (e.g,, Antarctic Circumpolar Current) or global (e.g., thermohaline circulation), which can redistribute heat, accentuate

productivity, or bury-exhume carbon. Orbitally-forced changes can amplify these changes, as seen prior to Mi-1 with increasing productivity from increased wind-driving upwelling. CO_2 changes appear to act as thresholds, with a certain level permitting, but not driving, a glaciation (DeConto et al., 2008). Thus, both essentially are true, gateway changes set up long-term changes and orbital configurations act as a final touch to drive an event.

4.1 Future Work

Each chapter in this dissertation opens an avenue for future work. Chapter 1 lists several of projects explicitly, to further test the hypothesis of increased bottom water flow over Site U1396 driving changes in sedimentation rate. Outside of bolstering that hypothesis, several possible projects could spin out of Chapter 1. First, the issue of the two competing age models for the Brunhes chron (Wall-Palmer et al., 2014; Chapter 1) is outstanding. To solve that issue, several different age diagnostic criteria could be developed. One obvious solution would be higher resolution stable isotope records through the interval, to detect the implied slowdown of sedimentation through that interval discussed in Chapter 1, and aid in the correlation to marine isotope stages. Likewise, higher resolution, or independently performed, calcareous nannofossil work would solidify or reject the differing *Emiliana huxleyi* datum presented in Aljadahli (2013) and Wall-Palmer et al. (2014). Additional nannofossil study could also be used to complement the planktic foraminiferal biostratigraphy. Geochemical dating of the tephra layers would be a welcome independent test of the age model. Second, a longer record of mixed layer planktic *Globigerinoides ruber* oxygen isotope values would allow an investigation of stratification through the Pliocene and Pleistocene, while carbon isotopes could shed light on the interpreted oligotrophy in the Caribbean discussed in Jain and Collins (2007). Third, continuing the counts of tropical keeled species (e.g. *Globorotalia menardii* and *G. tumida*) down to the base of Site U1396, and their connection to the

regional and global paleoceanography of those intervals, could help elucidate the connections their abundance changes have to do with changes in surface ocean circulation on glacial-interglacial timescales.

Lastly, such a long record at this resolution is rarely examined for evolutionary significance. With the bulk of the sample processing done, and significant paleoceanographic data collected, a study of planktic foraminiferal morphology through this interval would be low-risk with potentially high-reward. Certain planktic foraminifer characters are hypothetically linked to functional morphologies (like aperture relating to feeding style; Ezard et al., 2011). With the change from eutrophic-mesotrophic water to oligotrophic waters at this site (~4.2 Ma; Jain and Collins, 2007), a potentially rewarding study could examine the aperture style of the assemblage as it pertains to productivity indices.

Chapter 2 is well suited to be added to a larger context. As Site 803 is in the western equatorial Pacific Ocean, comparing the top and bottom occurrences of these species across different ocean basins would be a large benefit. This would help to determine which species have potential as biostratigraphic datums, if they have synchronous inter-basin top and bottom occurrences, or across latitude. ODP Site 628 north of the Bahamas in the western subtropical Atlantic is discontinuous, and is therefore not ideal for that purpose. Sites at a higher latitude with a good paleomagnetic stratigraphy, or a eastern equatorial Pacific site like Site 1218, with a high-resolution astrochronology (Pälike et al., 2006b) would be ideal. Additional sites at higher latitudes and in the Atlantic and Indian ocean basins would test if the evolutionary metrics at Site 803 (Section 2.4.1) were reflective of the global macroevolutionary trends in the planktic foraminifera at the time, or if they are only reflective of regional circumstances.

In Chapter 3, ODP Site 744 from the southern Kerguelen Plateau in the Indian Ocean provided the most interesting, and sometimes counter-intuitive results in the

dissertation research. The implication of increased upwelling driving abrupt changes, as well as the short-duration of the hiatus at Mi-1, suggests that continuing population counts both higher and lower at Site 744 could be illuminating. First, extending the analysis into the Oligocene may elucidate the eccentricity driver previously cited for the Oi events (Wade and Pälike, 2004). In particular, the fine vs. sand fraction mass data have the potential to address problems of winnowing and sedimentation rate. Second, extending the analysis farther into the lower Miocene could address drivers for the Mi events, though the record is discontinuous (Florindo et al., 2013). Counts through Cores 11 and above may not be able to detect orbital cycles due to the short stratigraphic distance between hiatuses in those cores.

The difficulty in finding adequate deep-sea sections to study Mi-1 is probably an important observation in and of itself. Erosion or non-deposition across the Oligocene-Miocene boundary is a problem in the deep-sea, probably related to changes in ocean circulation. A larger compilation of sedimentation rate changes across this boundary, if high enough resolution, could answer questions about carbon sequestration, or if the focal point of carbonate deposition shifted during the Oligocene/Miocene boundary as it is hypothesized to shift during the Eocene/Oligocene boundary (Coxall et al., 2005). Only through higher resolution age models than those previously used (e.g., Keller and Barron, 1983; Peters et al., 2011) can changes in global trends in sedimentation and erosion be detected robustly. Finally, there are only four high-resolution sites for the Mi-1 event, and three of these are in the Atlantic Ocean. While none of the sites developed here would be ideal for higher resolution work, there is a clear need for additional coring, particularly in the Northern Hemisphere. The recent Newfoundland Margin IODP Expedition (342) will hopefully produce high quality records of this interval. The North Pacific Ocean, then, will be the least constrained area with respect to this boundary, and an important region to focus research in the future.

APPENDIX A

DEPTH-SPLICER AND DESC-SPLICER: CODE FOR THE R-PROGRAMMING ENVIRONMENT

#depth.splicer is a function for R which moves DSDP/ODP/IODP depths (e.g., mbsf) from individual holes onto a shared depthscale for the entire site. It can be run in two ways, it can take depths and just move them to the composite depthscale (splice=0), or it can generate a 'splice' by moving only depths included in the splice to the new depthscale (splice=1).

#obj = raw depths which are to be moved to new depthscale

#depth =

#splice = (0,1)

0 = move to composite depthscale

1 = move to composite depthscale and perform splice

#splice.table = table with Hole, Core, and depths (top and bottom, and both raw and composite depths)

#tiepoints = table with tiepoints for the splice

#for both splice.table and tiepoints, formatting should follow Hatfield, *in press* for best functionality.

A.1 Depth.Splicer

```
depth.splicer<-function(obj,depth,splice,splice.table,tiepoints){
  CCSF.A<-0
  for(i in 1:length(obj[,"Hole"])){
    if(is.na(obj$Core[i]) == FALSE){
      which(splice.table$Hole == obj$Hole[i] &
            splice.table$Core == obj$Core[i])->a
```

```
    splice.table$CCSF.A.offset[a]+
      obj[i,depth]->CCSF.A[i]
   }
  }
  cbind(obj,CCSF.A)->c
  if(splice == 1){
   #RUN SPLICE
   d<-c[which(c[,"CCSF.A"] <= tiepoints[1,"CCSF.A1"] &
            c$Hole == tiepoints[1,"Hole1"]),]
   o<-which(tiepoints$Append != "APPEND")
   for(i in 2:length(tiepoints$Hole1)){
    d1<-tiepoints[o[i],"CCSF.A2"]
    d2<-tiepoints[o[i-1],"CCSF.A1"]
which(c$Hole == tiepoints$Hole1[o[i]] &
          c[,"CCSF.A"] < d1 &
          c[,"CCSF.A"] > d2)->t
    d<-rbind(d,c[t,])
   }
o<-which(tiepoints$Append != "APPEND")
   max(o)->last
   d<-rbind(d,c[which(c[,"CCSF.A"] >= tiepoints[last,"CCSF.A2"] &
                c$Hole == tiepoints[last,"Hole2"]),])
   d[order(d[,"CCSF.A"]),]->d
   c<-d
  }
  c
}
```

A.2 Desc.Splicer

#desc.splicer is the same as depth.splicer, except it can be run on objects with both top and bottoms (e.g., core description files). This allows the user to splice objects with a defined thickness.

```
desc.splicer<-function(obj,tiepoints){
  d<-obj[which(obj[,"CCSF.A.T"] <= tiepoints[1,"CCSF.A1"] &
            obj$Hole == tiepoints[1,"Hole1"]),]
  if(d[nrow(d),"CCSF.A.B"] > tiepoints[1,"CCSF.A1"]){
   d[nrow(d),"CCSF.A.B"]<-tiepoints[1,"CCSF.A1"]
  }
  o<-which(tiepoints$Append != "APPEND")
  for(i in 2:length(tiepoints$Hole1)){
   d1<-tiepoints[o[i],"CCSF.A2"]
   d2<-tiepoints[o[i-1],"CCSF.A1"]
   if(which(tiepoints$Append == "APPEND") == i){
    d2<-tiepoints[i,"CCSF.A2"]
   }
```

```
  which(obj$Hole == tiepoints$Hole1[o[i]] &
        obj[,"CCSF.A.B"] > d2 &
        obj[,"CCSF.A.B"] < d1 &
        obj[,"CCSF.A.T"] > d2 &
        obj[,"CCSF.A.T"] < d1)->t #desc entries within spliced sections
  if(length(t)>0){
    d<-rbind(d,obj[t,])
  }
  which(obj$Hole == tiepoints$Hole1[o[i]] &
        obj[,"CCSF.A.B"] > d2 &
        obj[,"CCSF.A.B"] > d1 &
        obj[,"CCSF.A.T"] > d2 &
        obj[,"CCSF.A.T"] < d1)->t #desc entries with tops inbetween spliced sections
  if(length(t)>0){
    obj[t,]->q
    q[,'CCSF.A.B']<-d1 #replacing base of unit w/ splice point
    d<-rbind(d,q)}
  which(obj$Hole == tiepoints$Hole1[o[i]] &
        obj[,"CCSF.A.B"] > d2 &
        obj[,"CCSF.A.B"] < d1 &
        obj[,"CCSF.A.T"] < d2 &
        obj[,"CCSF.A.T"] < d1)->t #desc entries with bases inbetween spliced sections
  if(length(t)>0){
    obj[t,]->q
    q[,'CCSF.A.T']<-d2 #replacing top of unit w/ splice point
    d<-rbind(d,q)}
}
nrow(tiepoints)->last
tiepoints[last,"CCSF.A2"]->d2
which(obj$Hole == tiepoints$Hole1[last] &
      obj[,"CCSF.A.B"] > d2 &
      obj[,"CCSF.A.T"] < d2)->t
if(length(t)>0){
  obj[t,]->q
  q[,'CCSF.A.B']<-d2 #replacing base of unit w/ splice point
  d<-rbind(d,q)
}
which(obj$Hole == tiepoints$Hole2[last] &
      obj[,"CCSF.A.B"] > d2 &
      obj[,"CCSF.A.T"] < d2)->t
if(length(t)>0){
  obj[t,]->q
  q[,'CCSF.A.T']<-d2 #replacing base of unit w/ splice point
  d<-rbind(d,q)
}
d<-rbind(d,obj[which(obj[,"CCSF.A.T"] > d2
```

```
                    & obj$Hole == tiepoints[last,"Hole2"]),])
  d[order(d[,"CCSF.A.B"]),]->d
}
####END CODE
```

APPENDIX B

COREDESC BREAKDOWN AND VISUAL INSPECTION: CODE FOR THE R-PROGRAMMING ENVIRONMENT

#This is a tool for the visual inspection of a spliced core description object. As much of IODP data is generated under time sensitive conditions, it is important to check the results of splicing (see Appendix A) to make sure there are not errors in the lithology data after splicing.

```
par(mfcol=c(1,3))
"%w/o%" <- function(x, y) x[!x %in% y] #--  x without y
top=0 #top of visualization
base=20 #bottom of visualization
highlight=c(0) #depth (CCSF-A) to highlight
#Spliced Core Description Figure (by Hole)
plot(core.desc.s[,"CCSF.A.T"],core.desc.s[,"CCSF.A.B"],type='n'
    ,xlim=c(0,3)
    ,ylim=c(base,top)
,ylab="CCSF-A [m]"
    ,xlab=""
    ,xaxt='n')
for(p in levels(core.desc.s$MAJ.Lith..Principal.name)){
  which(levels(core.desc.s$MAJ.Lith..Principal.name) == p)->d
  if(d == 13){d<-"orangered"}
  if(d == 12){d<-"indianred"}
  if(d == 11){d<-"indianred4"}
  if(d == 10){d<-"violetred"}
  if(d == 9){d<-"tomato"}
  if(d == 8){d<-"tan"}
  if(d == 7){d<-"lightyellow2"}
  if(d == 6){d<-"honeydew2"}
  if(d == 5){d<-"burlywood1"}
  if(d == 4){d<-"lightgoldenrod"}
  if(d == 3){d<-"lightblue2"}
  if(d == 2){d<-"red"}
  if(d == 1){d<-"gainsboro"}
which(core.desc.s$MAJ.Lith..Principal.name == p & core.desc.s$Hole == "A")->a
  which(core.desc.s$MAJ.Lith..Principal.name == p & core.desc.s$Hole == "B")->b
  which(core.desc.s$MAJ.Lith..Principal.name == p & core.desc.s$Hole == "C")->c
```

```
if(length(a)>0){rect(0,
                    core.desc.s[a,"CCSF.A.T"],
                    1,
                    core.desc.s[a,"CCSF.A.B"],
                    col=d,
                    border=NA
  )}
  if(length(b)>0){rect(2,
                    core.desc.s[b,"CCSF.A.T"],
                    1,
                    core.desc.s[b,"CCSF.A.B"],
                    col=d,
                    border=NA
  )}
  if(length(c)>0){rect(2,
                    core.desc.s[c,"CCSF.A.T"],
                    3,
                    core.desc.s[c,"CCSF.A.B"],
                    col=d,
                    border=NA
  )}
}
abline(h=highlight)
#Spliced Core Description Figure
plot(splice.desc[,"CCSF.A.T"],splice.desc[,"CCSF.A.B"],type='n'
     ,xlim=c(0,3)
     ,ylim=c(base,top)
,ylab="CCSF-A [m]"
     ,xlab=""
     ,xaxt='n')
for(p in levels(splice.desc$MAJ.Lith..Principal.name)){
  which(levels(splice.desc$MAJ.Lith..Principal.name) == p)->d
  if(d == 13){d<-"orangered"}
  if(d == 12){d<-"indianred"}
  if(d == 11){d<-"indianred4"}
  if(d == 10){d<-"violetred"}
  if(d == 9){d<-"tomato"}
  if(d == 8){d<-"tan"}
  if(d == 7){d<-"lightyellow2"}
  if(d == 6){d<-"honeydew2"}
  if(d == 5){d<-"burlywood1"}
  if(d == 4){d<-"lightgoldenrod"}
  if(d == 3){d<-"lightblue2"}
  if(d == 2){d<-"red"}
  if(d == 1){d<-"gainsboro"}
  which(splice.desc$MAJ.Lith..Principal.name == p & splice.desc$Hole == "A")->a
```

```
  which(splice.desc$MAJ.Lith..Principal.name == p & splice.desc$Hole == "B")->b
  which(splice.desc$MAJ.Lith..Principal.name == p & splice.desc$Hole == "C")->c
  if(length(a)>0){rect(0,
                       splice.desc[a,"CCSF.A.T"],
                       1,
                       splice.desc[a,"CCSF.A.B"],
                       col=d,
                       border=NA
  )}
  if(length(b)>0){rect(2,
                       splice.desc[b,"CCSF.A.T"],
                       1,
                       splice.desc[b,"CCSF.A.B"],
                       col=d,
                       border=NA
  )}
  if(length(c)>0){rect(2,
                       splice.desc[c,"CCSF.A.T"],
                       3,
                       splice.desc[c,"CCSF.A.B"],
                       col=d,
                       border=NA
  )}
}
abline(h=highlight)
plot(splice.desc[,"CCSF.A.T"],splice.desc[,"CCSF.A.B"],type='n'
     ,xlim=c(0,3)
     ,ylim=c(base,top)
     ,ylab="CCSF-D [m]"
     ,xlab=""
     ,xaxt='n')
for(p in levels(splice.desc$MAJ.Lith..Principal.name)){
  which(levels(splice.desc$MAJ.Lith..Principal.name) == p)->d
  if(d == 13){b<-"orangered"}
  if(d == 12){b<-"indianred"}
  if(d == 11){b<-"indianred4"}
  if(d == 10){b<-"violetred"}
  if(d == 9){b<-"tomato"}
  if(d == 8){b<-"tan"}
  if(d == 7){b<-"lightyellow2"}
  if(d == 6){b<-"honeydew2"}
  if(d == 5){b<-"burlywood1"}
  if(d == 4){b<-"lightgoldenrod"}
  if(d == 3){b<-"lightblue2"}
  if(d == 2){b<-"red"}
  if(d == 1){b<-"gainsboro"}
```

```
  which(splice.desc$MAJ.Lith..Principal.name == p )->A
#volcanics
  if(d == 2|
      d == 9|
      d == 10|
      d == 11|
      d == 12|
      d == 13
  ){rect(0,
         splice.desc[A,"CCSF.A.T"],
         1,
         splice.desc[A,"CCSF.A.B"],
         col=b,
         border=NA
  )}
  if(d == 1|
      d == 3|
      d == 4|
      d == 5|
      d == 6|
      d == 7|
      d == 8
  ){rect(2,
         splice.desc[A,"CCSF.A.T"],
         1,
         splice.desc[A,"CCSF.A.B"],
         col=b,
         border=NA
  )}
  #  if(length(c)>0){rect(2,
  #                   splice.desc[c,"CCSF.A.T"],
  #                   1,
  #                   splice.desc[c,"CCSF.A.B"],
  #                   col=b,
  #                   border=NA
  # )}
}
abline(h=highlight)
######END CODE
```

APPENDIX C

NVOLC DEPTHS: CODE FOR THE R-PROGRAMMING ENVIRONMENT

#This is code to remove volcanic units from the stratigraphic column, then reassess the depths to produce a 'no volcanics' depthscale (N.Volc). Similar code is contained in other appendices (e.g., Appendix D), but here it is used to produce a single stand alone object with the N.Volc depthscale. This can be used to examine purely hemipelagic sedimentation within a mixed sedimentary system.

```
test<-col.u1396.st[,c(27,11)]
"%w/o%" <- function(x, y) x[!x %in% y] #--  x without y
######Translating depth to depth.nv
#Fraass (v0.1 Dec'14)
#object to work on (depth column 1, values column 2)
d.obj<-MIS.cor[,3:2]
#core description object
desc<-splice.desc
#Sediment types to skip
sed.skip<-c("volcaniclastic-sand [BGS-S81]",
          "ash [F&S84]",
          "volcaniclastic-breccia [BGS-S81]",
          "volcaniclastic-gravel [BGS-S81]",
          "volcaniclastic-mud [BGS-S81]",
          "volcaniclastic-mudstone [BGS-S81]",
          "volcaniclastic-sand [BGS-S81]")
######## Begin Code
#Should first compile depths of sed, then should take depth, subtract sed.skip thickness
#should finish with three columns, (depth,value,depth.nv)
#Gather all seds listed in sed.skip into on object
a<-match(desc[,c("MAJ.Lith..Principal.name")],sed.skip)
which(a > 0)->X
rm(a)
sed<-desc[X,
        c("CCSF.A.T","CCSF.A.B","MAJ.Lith..Principal.name")]
rm(X)
#creating new object
depth.nv<-matrix(nrow=length(d.obj[,1]),ncol=3)
depth.nv[,1]<-d.obj[,1]
depth.nv[,3]<-d.obj[,2]
```

```
colnames(d.obj)[1]->colnames(depth.nv)[1]
colnames(d.obj)[2]->colnames(depth.nv)[3]
"depth.m.nv"->colnames(depth.nv)[2]
colnames(d.obj)[1]->colnames(depth.nv)[1]
#thickness calcs
sed[,4]<-sed[,2]-sed[,1]
colnames(sed)[4]<-"thick"
#transfering over sed$depths to sed$depth.nv
depth.nv[,1]->depth.nv[,2]
#subtracting sed$thick from depth to get depth.nv
min(which(sed$CCSF.A.B[1] < depth.nv[,1]))->X
for(i in X:length(depth.nv[,1])){
  depth.nv[i,1]-sum(sed$thick[which(
    sed$CCSF.A.B < depth.nv[i,1])])->depth.nv[i,2]}
# changing working objects values that are within the skipped seds to NA
for(i in 1:length(sed[,1])){
  depth.nv[which(depth.nv[,1] >= sed[i,"CCSF.A.T"]
                 & depth.nv[,1] <= sed[i,"CCSF.A.B"]),2]<-NA
}
depth.nv.t<-depth.nv[
  which(is.na(depth.nv[,2])==F)
  ,]
######## End Code
```

APPENDIX D

ASTROCHRONOLOGY WITH FLEXIBLE PALEOMAGNETIC CONTROL POINTS: CODE FOR THE R-PROGRAMMING ENVIRONMENT

#This is code to employ the R-package 'astrochron' (Meyers, 2014) with well constrained paleomagnetic data. In the first section, paleomagnetic points are numbered, highest to lowest, and those with no '#' in front of them are used in 'pmag.grab'. Linear sedimentation is assumed through 'pmag.grab', applied on data supplied in 'test', then an evolutive harmonic analysis (EHA) is generated. A series of variables in the beginning of the code ('window' to 'bwith') are for the EHA. Code also excludes any volcanic sediments automatically.

The section section allows user to 'tune' data, as one would using the basic 'astrochron'-package (Meyers, 2014). After tuning, depths are reanchored to paleomagnetic controlpoints. The volcanic depths are reinserted into the stratigraphic column and depths are reassessed. The process of reintegrating the volcanic depths assumes they are instantaneous event beds, and thus assumes no time passes from their bottom to top depths.

'astrochron' package must be installed and loaded on R for code to run.

D.1 Paleomagnetic age control and EHA

```
#Running astrochron on data with pmag agemodel applied
##Setup for that portion
c(
 1,
 2,
 # 3,
 4,
 #5,
 6,
 #  7,
```

```
  8,
  #9,
  10,
  # 11,
  # 12,
  13,
 # 14,
  #15,
  #16,
  17
)->pmag.grab #which pmag to use
window<-130
interp<-3
start<-0
end<-1000
padding<-300
steps<-interp*2.5
bwith<-9
"%w/o%" <- function(x, y) x[!x %in% y] #--  x without y
#First, removes volcanics from the col.reflectance data
######Translating depth to depth.nv#####
test<-col.u1396.st[,c(27,11)]
######Translating depth to depth.nv
#Fraass (v0.1 Dec'14)
#object to work on (depth column 1, values column 2)
d.obj<-test
#core description object
desc<-splice.desc
#Sediment types to skip
sed.skip<-c(
  "ash [F&S84]",
  "volcaniclastic-breccia [BGS-S81]",
  "volcaniclastic-gravel [BGS-S81]",
  "volcaniclastic-mud [BGS-S81]",
  "volcaniclastic-mudstone [BGS-S81]",
  "volcaniclastic-sand [BGS-S81]"
)
######## Begin Code
#Should first compile depths of sed, then should take depth, subtract sed.skip thickness
#should finish with three columns, (depth,value,depth.nv)
#Gather all seds listed in sed.skip into on object
a<-match(desc[,c("MAJ.Lith..Principal.name")],sed.skip)
which(a > 0)->X
rm(a)
sed<-desc[X,
        c("CCSF.A.T","CCSF.A.B","MAJ.Lith..Principal.name")]
```

```
rm(X)
#creating new object
depth.nv<-matrix(nrow=length(d.obj[,1]),ncol=3)
depth.nv[,1]<-d.obj[,1]
depth.nv[,3]<-d.obj[,2]
colnames(d.obj)[1]->colnames(depth.nv)[1]
colnames(d.obj)[2]->colnames(depth.nv)[3]
"depth.m.nv"->colnames(depth.nv)[2]
colnames(d.obj)[1]->colnames(depth.nv)[1]
#thickness calcs
sed[,4]<-sed[,2]-sed[,1]
colnames(sed)[4]<-"thick"
#transfering over sed$depths to sed$depth.nv
depth.nv[,1]->depth.nv[,2]
#subtracting sed$thick from depth to get depth.nv
min(which(sed$CCSF.A.B[1] < depth.nv[,1]))->X
for(i in X:length(depth.nv[,1])){
  depth.nv[i,1]-sum(sed$thick[which(
    sed$CCSF.A.B < depth.nv[i,1])])->depth.nv[i,2]}
# changing working objects values that are within the skipped seds to NA
for(i in 1:length(sed[,1])){
  depth.nv[which(depth.nv[,1] >= sed[i,"CCSF.A.T"]
                 & depth.nv[,1] <= sed[i,"CCSF.A.B"]),2]<-NA
}
depth.nv.t<-depth.nv[
  which(is.na(depth.nv[,2])==F)
  ,]
#CCSF.A.T CCSF.A.B
#Fraass (v0.1 Dec'14)
#object to work on (depth column 1, values column 2)
pmag.nv<-pmag.splice[pmag.grab,"CCSF.A"]
pmag.nv<-cbind(pmag.nv,pmag.splice[pmag.grab,"Age.Ogg12"])
colnames(pmag.nv)[2]<-"Age.Ogg12"
colnames(pmag.nv)[1]<-'CCSF.A'
d.obj<-pmag.nv
#core description object
desc<-splice.desc
#saving depth.nv for later
depth.nv.t->temp
######## Begin Code
#Should first compile depths of sed, then should take depth, subtract sed.skip thickness
#should finish with three columns, (depth,value,depth.nv)
#Gather all seds listed in sed.skip into on object
a<-match(desc[,c("MAJ.Lith..Principal.name")],sed.skip)
which(a > 0)->X
rm(a)
```

```
sed<-desc[X,
        c("CCSF.A.T","CCSF.A.B","MAJ.Lith..Principal.name")]
rm(X)
#creating new object
depth.nv<-matrix(nrow=length(d.obj[,1]),ncol=3)
depth.nv[,1]<-d.obj[,1]
depth.nv[,3]<-d.obj[,2]
colnames(d.obj)[1]->colnames(depth.nv)[1]
colnames(d.obj)[2]->colnames(depth.nv)[3]
"depth.m.nv"->colnames(depth.nv)[2]
colnames(d.obj)[1]->colnames(depth.nv)[1]
#thickness calcs
sed[,4]<-sed[,2]-sed[,1]
colnames(sed)[4]<-"thick"
#transfering over sed$depths to sed$depth.nv
depth.nv[,1]->depth.nv[,2]
#subtracting sed$thick from depth to get depth.nv
min(which(sed$CCSF.A.B[1] < depth.nv[,1]))->X
for(i in X:length(depth.nv[,1])){
  depth.nv[i,1]-sum(sed$thick[which(
    sed$CCSF.A.B < depth.nv[i,1])])->depth.nv[i,2]}
pmag.nv<-depth.nv
depth.nv.t<-temp;rm(temp)
colnames(pmag.nv)[2]<-"CCSF.Anv"
rm(sed.rate.nv);sed.rate.nv<-0
#calculating sedrate
for(i in 1:length(pmag.nv[,"CCSF.Anv"]))
{
  sed.rate.nv[i-1]<-(
    pmag.nv[i,'CCSF.Anv']-pmag.nv[i-1,'CCSF.Anv']
  )/(
    pmag.nv[i,'Age.Ogg12']-pmag.nv[i-1,'Age.Ogg12'])
}
Age.nv<-NA
for(i in 1:length(depth.nv.t[,2])){
  #finding appropriate sedrate
  max(which(pmag.nv[,'CCSF.Anv'] < depth.nv.t[i,2]))->X
  #age calc
  #difference in depths
  depth.nv.t[i,2]-pmag.nv[X,'CCSF.Anv']->y
  y*{sed.rate.nv[X]^-1}->Z
  Z+pmag.nv[X,'Age.Ogg12']->Age.nv[i]
  #units sed.rate=m/myr
}
cbind(depth.nv.t,Age.nv)->depth.nv.t
#only working with SPLICE
```

```
depth.nv.t[,c(4,3)]->L.pm
#L.pm[which(L.pm[,2] < 5 & L.pm[,2] >1.5),]->L.pm
par(mfcol=c(1,1))
#plot(L.pm)
#L.pm[which(L.pm[,2] < 100),]->L.pm
#plot(L.pm,xlim=c(61,62))
#convert MYR to KYR
L.pm[,1]*1000->L.pm[,1]
iso(L.pm
   ,xmin=start
   ,xmax=end
   ,genplot=F
)->L.pm
linterp(L.pm
       ,dt=interp
       ,genplot=F
)->L.pm
eha(L.pm
   ,demean=T
   ,detrend=T
   ,win=window
   ,tbw=bwith
   ,pad=padding
   ,step=steps
   ,pl=2
   ,siglevel=.85
   ,output=4
   ,sigID=T
   ,genplot=2
   #,xlab="UNTUNED"
   ,fmax=.06
   ,ydir=-1
)->L.eha
abline(v=target,col='grey',lwd=2)
abline(v=1/100,col='green',lwd=2)
abline(h=pmag.splice[pmag.grab,"Age.Ogg12"]*1000,lwd=2)
text(0.003,pmag.splice[pmag.grab,"Age.Ogg12"]*1000,pmag.grab,
    col='white',
    cex=1)
#impact of sed change
abline(h=pmag.splice[pmag.grab,"Age.Ogg12"]*1000+window/2,lwd=2,col='white')
abline(h=pmag.splice[pmag.grab,"Age.Ogg12"]*1000-window/2,lwd=2,col='white')
abline(h=depth.nv.t[4068,'Age.nv']*1000)
abline(h=depth.nv.t[4068,'Age.nv']*1000+window/2,col='red',lwd=2)
abline(h=depth.nv.t[4068,'Age.nv']*1000-window/2,col='red',lwd=2)
######END CODE
```

D.2 Tuning and reintegration of volcanic units

```
### Interactively track obliquity term in EHA harmonic F-test confidence level results
freqs.track=trackFreq(L.eha
                      #,fmin=1.2
                      #,fmax=2.4
                      ,threshold=0.75
                      ,ydir=-1
)
### Convert the spatial frequencies to sedimentation rates
#targets 405.470 126.980 100.000  53.962  40.978  22.992  18.996
sedrate=freq2sedrate(freqs.track
                     ,period=40.978)
### Convert the sedimentation rate curve to a time-space map
time=sedrate2time(sedrate)
#for comparisons/integration into agemodel
cbind(time,time[1,1]+time[,'ka'])->time.a
colnames(time.a)[3]<-'astro.age'
#myr to kyr for depth.nv.t
depth.nv.t->depth.nv.k
depth.nv.k[,'Age.nv']*1000->depth.nv.k[,"Age.nv"]
#find tdepth and bdepth for astro.age
depth.m.nv<-NA
for(i in 1:length(time.a[,'astro.age'])){
  time.a[i,'meters']->ts
  max(which(ts > depth.nv.k[,"Age.nv"]))->a
  min(which(ts < depth.nv.k[,"Age.nv"]))->b
  depth.nv.k[a,'depth.m.nv']->d1
  depth.nv.k[b,'depth.m.nv']->d2
  depth.nv.k[a,'Age.nv']->t1
  depth.nv.k[b,'Age.nv']->t2
  depth.m.nv[i]<-d2-{{t2-ts}/{t2-t1}}*{d2-d1}
}
cbind(time.a,depth.m.nv)->time.a
cbind(time.a,time.a[,'astro.age']/1000)->time.a
colnames(time.a)[5]<-'astro.myr'
##Code to change depth.nv back to depth.real
#Should first compile depths of sed, then should take depth, subtract sed.skip thickness
#should finish with three columns, (depth,value,depth.nv)
#Gather all seds listed in sed.skip into on object
a<-match(splice.desc[,c("MAJ.Lith..Principal.name")],sed.skip)
which(a > 0)->X
rm(a)
sed<-splice.desc[X,
                 c("CCSF.A.T","CCSF.A.B","MAJ.Lith..Principal.name")]
rm(X)
```

```
sed[,4]<-sed[,2]-sed[,1]
colnames(sed)[4]<-"thick"
#creating sed[,'depth.m.nv']
depth.m.nv<-NA
adjust<-NA
for(i in 1:length(sed[,"CCSF.A.B"])){
  sed[i,"CCSF.A.B"]-sum(sed[i:1,'thick'])->depth.m.nv[i]
  sum(sed[i:1,'thick'])->adjust[i]
}
sed<-cbind(sed,depth.m.nv)
sed<-cbind(sed,adjust)
#adding a 0 row
c(0,0,NA,0,0,0)->a
rbind(a,sed)->sed
##adding back the volcanics to the depth scale
CCSF.A<-NA
for(i in 1:length(time.a[,'depth.m.nv'])){
  time.a[i,"depth.m.nv"]->d1
  min(which(d1 < sed[,'depth.m.nv']))-1->a
  adjust<-sed[a,'adjust']
  CCSF.A[i]<-d1+adjust
}
cbind(time.a,CCSF.A)->time.a
#applying a correction to slide 'depth.m.nv' back to highest pmag control point
min(pmag.splice[pmag.grab %w/o% 1,"Age.Ogg12"])->a
#forcing a different pmag point (optional, use if default highest pmag control point is not
acceptable)
pmag.splice[4,"Age.Ogg12"]->a
which(pmag.splice[,"Age.Ogg12"]== a)->b
pmag.splice[b,'CCSF.A']->d1
which(abs(d1-time.a[,'CCSF.A']) == min(abs(d1-time.a[,'CCSF.A'])))->c
time.a[c,'astro.myr']-a->differ
time.a[,'astro.myr']-differ->time.a[,'astro.myr']
####END CODE
```

APPENDIX E

STABLE ISOTOPE DATA FROM SITE U1396

This appendix contains the stable isotope data for all of Site U1396. Depths are in both CSF-A (TCSFA is the top of the sample, while BCSFA is the bottom), and the Composite depthscale (CCSF.M is the midpoint in the composite scale). It also gives the interpreted age of each sample using the paleomagnetic (Pmag), astrochronological (Astro), and marine isotope correlation (MIS) age models.

Stable isotope data from Site U1396

H	Co	T	Sc	To	Bo	TCSFA	BCSFA	CCSF.M	Pmag	Astro	MIS	δ13C	δ18O	#ind	Species
C	1	H	5	103	105	7.03	7.05	7.04	0.439	0.334	0.499	1.02	2.53	3	*C. robertsonanius*
C	1	H	5	103	105	7.03	7.05	7.04	0.439	0.334	0.499	1.6	-0.43	8	*G. ruber*
C	1	H	5	119	121	7.19	7.21	7.2	0.449	0.344	0.503	1.21	2.4	2	*C. mundulus*
C	1	H	5	119	121	7.19	7.21	7.2	0.449	0.344	0.503	1.66	-0.3	9	*G. ruber*
C	1	H	5	135	137	7.35	7.37	7.36	0.459	0.354	0.507	1.4	2.78	4	*C. mundulus*
C	1	H	5	135	137	7.35	7.37	7.36	0.459	0.354	0.507	1.3	2.88	4	*C. robertsonanius*
C	1	H	5	135	137	7.35	7.37	7.36	0.459	0.354	0.507	1.96	0.39	9	*G. ruber*
C	1	H	6	17	19	7.67	7.69	7.68	0.479	0.375	0.516	0.83	2.79	4	*C. robertsonanius*
C	1	H	6	17	19	7.67	7.69	7.68	0.479	0.375	0.516	1.34	0.62	9	*G. ruber*
C	1	H	6	33	35	7.83	7.85	7.84	0.489	0.387	0.520	1.13	2.63	4	*C. mundulus*
C	1	H	6	33	35	7.83	7.85	7.84	0.489	0.387	0.520	1.6	0.14	9	*G. ruber*
C	1	H	6	49	51	7.99	8.01	8	0.499	0.400	0.525	1.49	3.03	4	*C. mundulus*
C	1	H	6	49	51	7.99	8.01	8	0.499	0.400	0.525	1.49	3.03	4	*C. mundulus*
A	2	H	2	87	89	7.52	7.54	9.24	0.577	0.521	0.558	0.8	2.82	4	*C. robertsonanius*
A	2	H	2	87	89	7.52	7.54	9.24	0.577	0.521	0.558	1.41	0.42	8	*G. ruber*
C	2	H	1	23	25	8.63	8.65	9.78	0.610	0.574	0.572	0.85	2.38	4	*C. robertsonanius*
C	2	H	1	23	25	8.63	8.65	9.78	0.610	0.574	0.572	1.15	-0.82	9	*G. ruber*
A	2	H	3	1	3	8.16	8.18	9.88	0.617	0.585	0.575	1.06	2.46	4	*C. mundulus*
A	2	H	3	1	3	8.16	8.18	9.88	0.617	0.585	0.575	0.99	-1.1	9	*G. ruber*
C	2	H	1	39	41	8.79	8.81	9.94	0.620	0.591	0.582	0.96	2.64	4	*C. mundulus*
C	2	H	1	39	41	8.79	8.81	9.94	0.620	0.591	0.582	1.05	0.42	9	*G. ruber*
A	2	H	3	17	19	8.32	8.34	10.04	0.627	0.601	0.593	0.7	2.44	4	*C. robertsonanius*
A	2	H	3	17	19	8.32	8.34	10.04	0.627	0.601	0.593	1.21	-0.02	9	*G. ruber*
C	2	H	1	55	57	8.95	8.97	10.1	0.630	0.605	0.599	0.9	2.72	4	*C. mundulus*

C	2	H	1	55	57	8.95	8.97	10.1	0.630	0.605	0.599	1.11	-0.07	9	*G. ruber*
A	2	H	3	33	35	8.48	8.5	10.2	0.637	0.615	0.610	0.66	2.62	4	*C. robertsonanius*
A	2	H	3	33	35	8.48	8.5	10.2	0.637	0.615	0.610	1.28	-1.47	9	*G. ruber*
C	2	H	1	87	89	9.27	9.29	10.42	0.650	0.637	0.645	0.84	2.62	3	*C. robertsonanius*
C	2	H	1	87	89	9.27	9.29	10.42	0.650	0.637	0.645	1.22	0.28	9	*G. ruber*
C	2	H	1	103	105	9.43	9.45	10.58	0.660	0.650	0.671	1.07	2.61	4	*C. mundulus*
C	2	H	1	103	105	9.43	9.45	10.58	0.660	0.650	0.671	1.4	-0.1	7	*G. ruber*
C	2	H	1	119	121	9.59	9.61	10.74	0.670	0.662	0.696	1.1	2.65	4	*C. mundulus*
C	2	H	1	119	121	9.59	9.61	10.74	0.670	0.662	0.696	1.05	-0.17	9	*G. ruber*
C	2	H	1	135	137	9.75	9.77	10.9	0.680	0.674	0.704	1.16	2.61	3	*C. mundulus*
C	2	H	1	135	137	9.75	9.77	10.9	0.680	0.674	0.704	0.89	0.34	9	*G. ruber*
C	2	H	2	17	19	10.07	10.09	11.22	0.700	0.698	0.721	1.15	2.87	4	*C. mundulus*
C	2	H	2	17	19	10.07	10.09	11.22	0.700	0.698	0.721	0.96	0.58	9	*G. ruber*
C	2	H	2	33	35	10.23	10.25	11.38	0.710	0.701	0.730	0.89	2.87	4	*C. mundulus*
C	2	H	2	33	35	10.23	10.25	11.38	0.710	0.701	0.730	0.95	-0.29	9	*G. ruber*
C	2	H	2	49	51	10.39	10.41	11.54	0.720	0.711	0.738	0.87	2.82	4	*C. mundulus*
C	2	H	2	49	51	10.39	10.41	11.54	0.720	0.711	0.738	1.07	-0.37	9	*G. ruber*
A	2	H	4	65	67	9.92	9.94	11.64	0.727	0.718	0.743	0.96	2.67	3	*C. mundulus*
C	2	H	2	65	67	10.55	10.57	11.7	0.730	0.723	0.746	1.02	3.02	4	*C. mundulus*
C	2	H	2	81	83	10.71	10.73	11.86	0.740	0.735	0.755	0.93	3.54	4	*C. mundulus*
C	2	H	2	97	99	10.87	10.89	12.02	0.750	0.746	0.763	1.06	2.44	3	*C. robertsonanius*
C	2	H	2	97	99	10.87	10.89	12.02	0.750	0.746	0.763	1	0.01	9	*G. ruber*
C	2	H	2	97	99	10.87	10.89	12.02	0.750	0.746	0.763	1.15	2.8	4	*P. wuellerstorfi*
C	2	H	2	113	115	11.03	11.05	12.18	0.760	0.757	0.772	0.92	2.52	3	*C. robertsonanius*
C	2	H	2	113	115	11.03	11.05	12.18	0.760	0.757	0.772	0.48	-0.27	9	*G. ruber*
C	2	H	2	129	131	11.19	11.21	12.34	0.770	0.769	0.780	1.02	2.56	3	*C. mundulus*
C	2	H	2	129	131	11.19	11.21	12.34	0.770	0.769	0.780	0.79	2.54	4	*C. robertsonanius*
C	2	H	2	129	131	11.19	11.21	12.34	0.770	0.769	0.780	1.18	-0.06	8	*G. ruber*
C	2	H	3	11	13	11.51	11.53	12.66	0.787	0.788	0.793	1.24	3.21	4	*C. mundulus*
C	2	H	3	11	13	11.51	11.53	12.66	0.787	0.788	0.793	1.45	-0.39	9	*G. ruber*
C	2	H	3	27	29	11.67	11.69	12.82	0.793	0.794	0.800	1.09	2.88	4	*C. mundulus*
C	2	H	3	27	29	11.67	11.69	12.82	0.793	0.794	0.800	1.13	3.01	4	*C. mundulus*
C	2	H	3	27	29	11.67	11.69	12.82	0.793	0.794	0.800	0.96	-0.13	9	*G. ruber*
C	2	H	3	43	45	11.83	11.85	12.98	0.799	0.801	0.806	1.29	3.31	3	*C. mundulus*
C	2	H	3	43	45	11.83	11.85	12.98	0.799	0.801	0.806	1.03	0.05	9	*G. ruber*
A	2	H	5	59	61	11.36	11.38	13.08	0.803	0.803	0.810	0.97	2.79	4	*C. mundulus*
A	2	H	5	59	61	11.36	11.38	13.08	0.803	0.803	0.810	0.8	0.43	9	*G. ruber*
C	2	H	3	59	61	11.99	12.01	13.14	0.805	0.805	0.813	0.68	2.36	3	*C. mundulus*
C	2	H	3	59	61	11.99	12.01	13.14	0.805	0.805	0.813	1.03	2.87	3	*C. robertsonanius*

C	2	H	3	59	61	11.99	12.01	13.14	0.805	0.805	0.813	1	0.3	9	*G. ruber*
C	2	H	3	75	77	12.15	12.17	13.3	0.811	0.812	0.819	1.05	2.71	4	*C. mundulus*
C	2	H	3	75	77	12.15	12.17	13.3	0.811	0.812	0.819	0.99	2.81	4	*C. mundulus*
C	2	H	3	75	77	12.15	12.17	13.3	0.811	0.812	0.819	0.91	0.39	9	*G. ruber*
C	2	H	3	91	93	12.31	12.33	13.46	0.817	0.818	0.826	1.18	3.35	4	*C. robertsonanius*
C	2	H	3	91	93	12.31	12.33	13.46	0.817	0.818	0.826	1.1	0.34	9	*G. ruber*
C	2	H	3	107	109	12.47	12.49	13.62	0.824	0.824	0.832	0.71	2.94	3	*C. robertsonanius*
C	2	H	3	107	109	12.47	12.49	13.62	0.824	0.824	0.832	0.85	-0.53	9	*G. ruber*
C	2	H	3	123	125	12.63	12.65	13.78	0.830	0.831	0.839	1.05	2.88	4	*C. mundulus*
C	2	H	3	123	125	12.63	12.65	13.78	0.830	0.831	0.839	1.01	0.35	9	*G. ruber*
C	2	H	3	139	141	12.79	12.81	13.94	0.836	0.838	0.845	0.83	2.56	4	*C. robertsonanius*
C	2	H	3	139	141	12.79	12.81	13.94	0.836	0.838	0.845	0.8	2.53	4	*C. robertsonanius*
C	2	H	3	139	141	12.79	12.81	13.94	0.836	0.838	0.845	0.62	-0.68	9	*G. ruber*
C	2	H	4	5	7	12.95	12.97	14.1	0.842	0.845	0.852	0.64	2.56	4	*C. robertsonanius*
C	2	H	4	5	7	12.95	12.97	14.1	0.842	0.845	0.852	0.5	2.32	4	*C. robertsonanius*
C	2	H	4	5	7	12.95	12.97	14.1	0.842	0.845	0.852	0.55	-1.2	9	*G. ruber*
C	2	H	4	21	23	13.11	13.13	14.26	0.848	0.852	0.858	0.67	2.36	4	*C. mundulus*
C	2	H	4	37	39	13.27	13.29	14.42	0.854	0.859	0.864	0.78	2.45	4	*C. mundulus*
C	2	H	4	37	39	13.27	13.29	14.42	0.854	0.859	0.864	0.29	-0.35	9	*G. ruber*
C	2	H	4	53	55	13.43	13.45	14.58	0.860	0.867	0.869	0.77	2.48	4	*C. mundulus*
C	2	H	4	53	55	13.43	13.45	14.58	0.860	0.867	0.869	0.61	-1.05	9	*G. ruber*
C	2	H	4	69	71	13.59	13.61	14.74	0.867	0.874	0.875	0.8	2.65	3	*C. mundulus*
C	2	H	4	69	71	13.59	13.61	14.74	0.867	0.874	0.875	0.51	-0.43	9	*G. ruber*
C	2	H	4	85	87	13.75	13.77	14.9	0.873	0.881	0.880	0.81	2.93	4	*C. mundulus*
C	2	H	4	85	87	13.75	13.77	14.9	0.873	0.881	0.880	0.84	2.86	4	*C. mundulus*
C	2	H	4	85	87	13.75	13.77	14.9	0.873	0.881	0.880	0.4	-0.14	9	*G. ruber*
C	2	H	4	101	103	13.91	13.93	15.06	0.879	0.886	0.886	1.18	3.32	4	*C. mundulus*
C	2	H	4	101	103	13.91	13.93	15.06	0.879	0.886	0.886	0.82	-0.13	9	*G. ruber*
C	2	H	4	117	119	14.07	14.09	15.22	0.885	0.890	0.891	0.63	3.03	3	*C. mundulus*
C	2	H	4	133	135	14.23	14.25	15.38	0.891	0.898	0.897	0.85	3.09	4	*C. mundulus*
C	2	H	4	133	135	14.23	14.25	15.38	0.891	0.898	0.897	0.85	-0.04	9	*G. ruber*
C	2	H	4	148	150	14.38	14.4	15.53	0.897	0.903	0.902	0.97	3.33	4	*C. mundulus*
C	2	H	4	148	150	14.38	14.4	15.53	0.897	0.903	0.902	0.81	0.3	9	*G. ruber*
C	2	H	5	15	17	14.55	14.57	15.7	0.904	0.907	0.908	0.84	2.94	3	*C. mundulus*
C	2	H	5	15	17	14.55	14.57	15.7	0.904	0.907	0.908	0.92	2.98	4	*C. robertsonanius*
C	2	H	5	31	33	14.71	14.73	15.86	0.910	0.915	0.915	1.02	3	3	*C. mundulus*
C	2	H	5	47	49	14.87	14.89	16.02	0.916	0.922	0.923	0.92	2.91	4	*C. robertsonanius*
C	2	H	5	63	65	15.03	15.05	16.18	0.922	0.929	0.930	0.93	2.85	4	*C. mundulus*
C	2	H	5	63	65	15.03	15.05	16.18	0.922	0.929	0.930	0.74	2.33	3	*C. robertsonanius*

C	2	H	5	79	81	15.19	15.21	16.34	0.928	0.936	0.937	0.68	2.19	4	*C. robertsonanius*
C	2	H	5	95	97	15.35	15.37	16.5	0.934	0.944	0.945	0.78	2.62	4	*C. robertsonanius*
C	2	H	5	95	97	15.35	15.37	16.5	0.934	0.944	0.945	0.79	-1.71	9	*G. ruber*
C	2	H	5	111	113	15.51	15.53	16.66	0.940	0.951	0.952	0.93	2.33	4	*C. mundulus*
C	2	H	5	127	129	15.67	15.69	16.82	0.947	0.958	0.957	0.72	2.29	4	*C. robertsonanius*
C	2	H	5	127	129	15.67	15.69	16.82	0.947	0.958	0.957	1.12	-1.2	9	*G. ruber*
C	2	H	6	9	11	15.99	16.01	17.14	0.959	0.972	0.968	0.9	2.61	4	*C. robertsonanius*
C	2	H	6	9	11	15.99	16.01	17.14	0.959	0.972	0.968	1.18	-0.69	8	*G. ruber*
C	2	H	6	25	27	16.15	16.17	17.3	0.965	0.978	0.973	0.96	2.62	4	*C. mundulus*
C	2	H	6	25	27	16.15	16.17	17.3	0.965	0.978	0.973	0.77	2.69	3	*C. robertsonanius*
C	2	H	6	25	27	16.15	16.17	17.3	0.965	0.978	0.973	1.34	-0.14	8	*G. ruber*
C	2	H	6	41	43	16.31	16.33	17.46	0.971	0.984	0.978	0.65	2.2	4	*C. robertsonanius*
C	2	H	6	41	43	16.31	16.33	17.46	0.971	0.984	0.978	0.98	2.41	4	*C. robertsonanius*
C	2	H	6	41	43	16.31	16.33	17.46	0.971	0.984	0.978	1.21	-0.41	8	*G. ruber*
C	2	H	6	57	59	16.47	16.49	17.62	0.977	0.990	0.983	1.05	2.92	4	*C. mundulus*
C	2	H	6	57	59	16.47	16.49	17.62	0.977	0.990	0.983	1.29	0.5	8	*G. ruber*
C	2	H	6	73	75	16.63	16.65	17.78	0.983	0.996	0.988	0.92	2.67	4	*C. robertsonanius*
C	2	H	6	73	75	16.63	16.65	17.78	0.983	0.996	0.988	1.07	-0.64	8	*G. ruber*
C	2	H	6	89	91	16.79	16.81	17.94	0.989	1.002	0.993	1.09	2.77	4	*C. mundulus*
C	2	H	6	89	91	16.79	16.81	17.94	0.989	1.002	0.993	1.31	0.18	8	*G. ruber*
A	3	H	1	74	76	15.84	15.86	18.06	0.992	1.006	0.997	1.29	3.02	4	*C. mundulus*
A	3	H	1	74	76	15.84	15.86	18.06	0.992	1.006	0.997	1.14	2.78	4	*C. mundulus*
C	2	H	6	105	107	16.95	16.97	18.1	0.994	1.007	0.998	1.05	2.68	4	*C. mundulus*
C	2	H	6	105	107	16.95	16.97	18.1	0.994	1.007	0.998	1.33	-0.44	8	*G. ruber*
C	2	H	6	121	123	17.11	17.13	18.26	0.998	1.013	1.003	1.08	3.16	4	*C. mundulus*
C	2	H	6	121	123	17.11	17.13	18.26	0.998	1.013	1.003	1.21	0.27	8	*G. ruber*
C	2	H	6	137	139	17.27	17.29	18.42	1.002	1.018	1.008	1.08	2.99	4	*C. mundulus*
C	2	H	6	137	139	17.27	17.29	18.42	1.002	1.018	1.008	1.01	-0.25	8	*G. ruber*
C	2	H	7	19	21	17.59	17.61	18.74	1.011	1.028	1.017	1.11	2.97	4	*C. mundulus*
C	2	H	7	19	21	17.59	17.61	18.74	1.011	1.028	1.017	1.79	0.7	8	*G. ruber*
C	2	H	7	19	21	17.59	17.61	18.74	1.011	1.028	1.017	1.79	0.7	8	*G. ruber*
C	2	H	7	35	37	17.75	17.77	18.9	1.016	1.033	1.022	1.04	2.81	4	*C. mundulus*
C	2	H	7	35	37	17.75	17.77	18.9	1.016	1.033	1.022	1.19	-0.32	8	*G. ruber*
C	2	H	7	70	72	18.1	18.12	19.25	1.025	1.043	1.032	1.08	2.96	3	*C. mundulus*
C	2	H	7	70	72	18.1	18.12	19.25	1.025	1.043	1.032	0.75	0.78	8	*G. ruber*
C	3	H	1	65	67	18.55	18.57	19.94	1.044	1.058	1.053	0.87	2.93	4	*C. robertsonanius*
C	3	H	1	65	67	18.55	18.57	19.94	1.044	1.058	1.053	1.15	-0.16	8	*G. ruber*
C	3	H	1	81	83	18.71	18.73	20.1	1.049	1.061	1.058	0.54	2.42	4	*C. robertsonanius*
C	3	H	1	81	83	18.71	18.73	20.1	1.049	1.061	1.058	0.77	-1.26	8	*G. ruber*

C	3	H	1	97	99	18.87	18.89	20.26	1.053	1.063	1.062	0.68	2.09	4	*C. robertsonanius*
C	3	H	1	113	115	19.03	19.05	20.42	1.057	1.065	1.067	0.72	2.31	4	*C. robertsonanius*
C	3	H	1	113	115	19.03	19.05	20.42	1.057	1.065	1.067	1.18	-0.73	8	*G. ruber*
A	3	H	3	15	17	18.25	18.27	20.47	1.059	1.066	1.069	0.62	2.29	4	*C. robertsonanius*
A	3	H	3	15	17	18.25	18.27	20.47	1.059	1.066	1.069	0.91	-1.35	8	*G. ruber*
C	3	H	1	129	131	19.19	19.21	20.58	1.062	1.068	1.072	0.08	2	3	*C. robertsonanius*
C	3	H	1	129	131	19.19	19.21	20.58	1.062	1.068	1.072	1.46	-0.81	8	*G. ruber*
C	3	H	2	11	13	19.51	19.53	20.9	1.071	1.072	1.081	1.13	2.58	3	*C. mundulus*
C	3	H	2	11	13	19.51	19.53	20.9	1.071	1.072	1.081	1	-0.34	7	*G. ruber*
A	3	H	3	63	65	18.73	18.75	20.95	1.072	1.073	1.082	1.1	2.34	4	*C. mundulus*
A	3	H	3	63	65	18.73	18.75	20.95	1.072	1.073	1.082	1.58	-0.66	8	*G. ruber*
C	3	H	2	27	29	19.67	19.69	21.06	1.078	1.076	1.086	1.09	2.71	4	*C. mundulus*
C	3	H	2	27	29	19.67	19.69	21.06	1.078	1.076	1.086	1.31	-0.37	8	*G. ruber*
C	3	H	2	43	45	19.83	19.85	21.22	1.086	1.080	1.090	0.88	2.81	3	*C. robertsonanius*
C	3	H	2	43	45	19.83	19.85	21.22	1.086	1.080	1.090	1.35	0.39	8	*G. ruber*
C	3	H	2	57	59	19.97	19.99	21.36	1.094	1.085	1.094	0.8	3.02	4	*C. robertsonanius*
A	3	H	3	110	112	19.2	19.22	21.42	1.097	1.087	1.096	1.08	3.07	3	*C. mundulus*
A	3	H	3	110	112	19.2	19.22	21.42	1.097	1.087	1.096	1	0.01	8	*G. ruber*
C	3	H	2	75	77	20.15	20.17	21.54	1.103	1.090	1.099	1.02	2.86	4	*C. mundulus*
C	3	H	2	75	77	20.15	20.17	21.54	1.103	1.090	1.099	1.26	0.06	5	*G. ruber*
A	3	H	3	126	128	19.36	19.38	21.58	1.105	1.091	1.100	1.06	3.04	4	*C. mundulus*
A	3	H	3	126	128	19.36	19.38	21.58	1.105	1.091	1.100	1.26	1.07	7	*G. ruber*
C	3	H	2	91	93	20.31	20.33	21.7	1.112	1.095	1.104	1.01	2.78	4	*C. mundulus*
C	3	H	2	91	93	20.31	20.33	21.7	1.112	1.095	1.104	1.22	-1.03	8	*G. ruber*
C	3	H	2	107	109	20.47	20.49	21.86	1.120	1.101	1.108	0.91	2.8	4	*C. mundulus*
C	3	H	2	123	125	20.63	20.65	22.02	1.129	1.106	1.116	0.93	3.01	4	*C. mundulus*
C	3	H	3	21	23	21.11	21.13	22.5	1.154	1.124	1.140	0.83	2.89	3	*C. robertsonanius*
C	3	H	3	21	23	21.11	21.13	22.5	1.154	1.124	1.140	1	0.58	8	*G. ruber*
A	3	H	4	72	74	20.32	20.34	22.54	1.156	1.125	1.142	0.92	2.81	4	*C. robertsonanius*
A	3	H	4	72	74	20.32	20.34	22.54	1.156	1.125	1.142	1.13	-0.25	7	*G. ruber*
C	3	H	3	37	39	21.27	21.29	22.66	1.162	1.130	1.148	1	2.56	3	*C. robertsonanius*
C	3	H	3	53	55	21.43	21.45	22.82	1.171	1.136	1.156	1.16	2.54	4	*C. mundulus*
C	3	H	3	69	71	21.59	21.61	22.98	1.179	1.144	1.164	0.93	2.43	3	*C. robertsonanius*
C	3	H	3	85	87	21.75	21.77	23.14	1.188	1.152	1.172	1.15	2.59	4	*C. mundulus*
C	3	H	3	85	87	21.75	21.77	23.14	1.188	1.152	1.172	0.94	2.41	4	*C. robertsonanius*
C	3	H	3	101	103	21.91	21.93	23.3	1.196	1.160	1.180	0.86	2.16	3	*C. robertsonanius*
C	3	H	3	101	103	21.91	21.93	23.3	1.196	1.160	1.180	0.94	-1.43	6	*G. ruber*
C	3	H	3	117	119	22.07	22.09	23.46	1.204	1.168	1.192	1.12	2.43	4	*C. mundulus*
C	3	H	3	117	119	22.07	22.09	23.46	1.204	1.168	1.192	1.2	-0.63	8	*G. ruber*

C	**3**	**H**	**4**	**15**	**17**	22.55	22.57	23.94	1.230	1.200	1.228	1.1	2.69	4	*C. mundulus*
C	**3**	**H**	**4**	**15**	**17**	22.55	22.57	23.94	1.230	1.200	1.228	1.43	-0.16	8	*G. ruber*
A	**3**	**H**	**5**	**77**	**79**	21.87	21.89	24.09	1.238	1.212	1.239	1.1	2.54	4	*C. mundulus*
A	**3**	**H**	**5**	**77**	**79**	21.87	21.89	24.09	1.238	1.212	1.239	1.37	-0.25	5	*G. ruber*
C	**3**	**H**	**4**	**31**	**33**	22.71	22.73	24.1	1.238	1.213	1.240	0.98	2.17	4	*C. mundulus*
C	**3**	**H**	**4**	**31**	**33**	22.71	22.73	24.1	1.238	1.213	1.240	1.55	0.11	8	*G. ruber*
A	**3**	**H**	**5**	**93**	**95**	22.03	22.05	24.25	1.246	1.225	1.253	0.95	2.45	4	*C. mundulus*
A	**3**	**H**	**5**	**93**	**95**	22.03	22.05	24.25	1.246	1.225	1.253	1.14	0.09	8	*G. ruber*
C	**3**	**H**	**4**	**47**	**49**	22.87	22.89	24.26	1.247	1.226	1.253	0.57	2.38	4	*C. robertsonanius*
C	**3**	**H**	**4**	**47**	**49**	22.87	22.89	24.26	1.247	1.226	1.253	0.37	-0.46	8	*G. ruber*
C	**3**	**H**	**4**	**63**	**65**	23.03	23.05	24.42	1.255	1.239	1.267	0.88	2.55	4	*C. mundulus*
C	**3**	**H**	**4**	**63**	**65**	23.03	23.05	24.42	1.255	1.239	1.267	0.77	2.76	4	*C. robertsonanius*
C	**3**	**H**	**4**	**63**	**65**	23.03	23.05	24.42	1.255	1.239	1.267	1.34	-0.21	8	*G. ruber*
C	**3**	**H**	**4**	**79**	**81**	23.19	23.21	24.58	1.263	1.253	1.280	0.68	2.35	4	*C. mundulus*
C	**3**	**H**	**4**	**79**	**81**	23.19	23.21	24.58	1.263	1.253	1.280	0.72	2.42	4	*C. robertsonanius*
C	**3**	**H**	**4**	**79**	**81**	23.19	23.21	24.58	1.263	1.253	1.280	1.28	-0.52	8	*G. ruber*
C	**3**	**H**	**4**	**95**	**97**	23.35	23.37	24.74	1.272	1.266	1.298	0.93	2.7	3	*C. robertsonanius*
C	**3**	**H**	**4**	**95**	**97**	23.35	23.37	24.74	1.272	1.266	1.298	1.28	-0.28	8	*G. ruber*
C	**3**	**H**	**4**	**111**	**113**	23.51	23.53	24.9	1.280	1.279	1.316	1.11	2.65	3	*C. mundulus*
C	**3**	**H**	**4**	**111**	**113**	23.51	23.53	24.9	1.280	1.279	1.316	0.89	2.76	3	*C. robertsonanius*
C	**3**	**H**	**4**	**111**	**113**	23.51	23.53	24.9	1.280	1.279	1.316	1.21	0.14	8	*G. ruber*
C	**3**	**H**	**4**	**127**	**129**	23.67	23.69	25.06	1.289	1.291	1.324	0.96	2.67	3	*C. mundulus*
C	**3**	**H**	**4**	**127**	**129**	23.67	23.69	25.06	1.289	1.291	1.324	1.34	0.2	8	*G. ruber*
C	**3**	**H**	**4**	**143**	**145**	23.83	23.85	25.22	1.297	1.303	1.331	0.86	2.85	4	*C. mundulus*
C	**3**	**H**	**4**	**143**	**145**	23.83	23.85	25.22	1.297	1.303	1.331	0.92	-0.24	8	*G. ruber*
C	**3**	**H**	**5**	**9**	**11**	23.99	24.01	25.38	1.306	1.314	1.339	1.04	2.65	4	*C. mundulus*
C	**3**	**H**	**5**	**9**	**11**	23.99	24.01	25.38	1.306	1.314	1.339	1.18	0.3	5	*G. ruber*
C	**3**	**H**	**5**	**25**	**27**	24.15	24.17	25.54	1.314	1.325	1.346	0.98	2.62	4	*C. mundulus*
C	**3**	**H**	**5**	**25**	**27**	24.15	24.17	25.54	1.314	1.325	1.346	0.83	-0.21	8	*G. ruber*
C	**3**	**H**	**5**	**41**	**43**	24.31	24.33	25.7	1.322	1.335	1.354	0.99	2.47	3	*C. mundulus*
C	**3**	**H**	**5**	**41**	**43**	24.31	24.33	25.7	1.322	1.335	1.354	0.69	-0.34	8	*G. ruber*
C	**3**	**H**	**5**	**57**	**59**	24.47	24.49	25.86	1.331	1.345	1.369	0.82	2.43	3	*C. robertsonanius*
C	**3**	**H**	**5**	**57**	**59**	24.47	24.49	25.86	1.331	1.345	1.369	1.15	-0.27	8	*G. ruber*
C	**3**	**H**	**5**	**73**	**75**	24.63	24.65	26.02	1.339	1.355	1.383	1.29	3.01	4	*C. mundulus*
C	**3**	**H**	**5**	**73**	**75**	24.63	24.65	26.02	1.339	1.355	1.383	0.75	2.25	3	*C. robertsonanius*
C	**3**	**H**	**5**	**73**	**75**	24.63	24.65	26.02	1.339	1.355	1.383	1.56	-0.86	8	*G. ruber*
C	**3**	**H**	**5**	**89**	**91**	24.79	24.81	26.18	1.348	1.365	1.398	0.61	2.3	4	*C. robertsonanius*
C	**3**	**H**	**5**	**89**	**91**	24.79	24.81	26.18	1.348	1.365	1.398	1.36	-0.65	8	*G. ruber*
C	**3**	**H**	**5**	**105**	**107**	24.95	24.97	26.34	1.356	1.374	1.404	1.19	2.6	3	*C. mundulus*

C	**3**	**H**	**5**	**105**	**107**	24.95	24.97	26.34	1.356	1.374	1.404	1.24	-0.32	8	*G. ruber*
C	**3**	**H**	**5**	**121**	**123**	25.11	25.13	26.5	1.365	1.384	1.411	1.03	2.59	4	*C. mundulus*
C	**3**	**H**	**5**	**121**	**123**	25.11	25.13	26.5	1.365	1.384	1.411	1.23	-0.15	8	*G. ruber*
C	**3**	**H**	**5**	**137**	**139**	25.27	25.29	26.66	1.373	1.395	1.417	1.01	2.61	4	*C. mundulus*
C	**3**	**H**	**5**	**137**	**139**	25.27	25.29	26.66	1.373	1.395	1.417	0.77	-0.55	8	*G. ruber*
C	**3**	**H**	**6**	**19**	**21**	25.59	25.61	26.98	1.390	1.418	1.430	1	2.44	4	*C. mundulus*
C	**3**	**H**	**6**	**19**	**21**	25.59	25.61	26.98	1.390	1.418	1.430	1.21	-0.39	7	*G. ruber*
C	**3**	**H**	**6**	**35**	**37**	25.75	25.77	27.14	1.398	1.428	1.436	1	2.24	3	*C. mundulus*
C	**3**	**H**	**6**	**35**	**37**	25.75	25.77	27.14	1.398	1.428	1.436	0.99	-1.88	8	*G. ruber*
C	**3**	**H**	**6**	**51**	**53**	25.91	25.93	27.3	1.407	1.438	1.456	0.92	2.48	4	*C. mundulus*
C	**3**	**H**	**6**	**67**	**69**	26.07	26.09	27.46	1.415	1.449	1.476	0.93	2.32	4	*C. mundulus*
C	**3**	**H**	**6**	**67**	**69**	26.07	26.09	27.46	1.415	1.449	1.476	0.48	-1.27	8	*G. ruber*
C	**3**	**H**	**6**	**83**	**85**	26.23	26.25	27.62	1.424	1.460	1.487	0.79	2.35	4	*C. mundulus*
C	**3**	**H**	**6**	**83**	**85**	26.23	26.25	27.62	1.424	1.460	1.487	1	-0.86	8	*G. ruber*
C	**3**	**H**	**6**	**99**	**101**	26.39	26.41	27.78	1.432	1.470	1.498	1.08	2.47	3	*C. mundulus*
C	**3**	**H**	**6**	**99**	**101**	26.39	26.41	27.78	1.432	1.470	1.498	1.28	0.11	8	*G. ruber*
C	**3**	**H**	**6**	**115**	**117**	26.55	26.57	27.94	1.440	1.480	1.509	1.22	2.5	4	*C. mundulus*
C	**3**	**H**	**6**	**115**	**117**	26.55	26.57	27.94	1.440	1.480	1.509	1.8	-0.86	8	*G. ruber*
C	**3**	**H**	**6**	**131**	**133**	26.71	26.73	28.1	1.449	1.489	1.520	1.08	2.3	3	*C. mundulus*
C	**3**	**H**	**6**	**131**	**133**	26.71	26.73	28.1	1.449	1.489	1.520	1.84	-0.74	8	*G. ruber*
C	**3**	**H**	**7**	**13**	**15**	27.03	27.05	28.42	1.466	1.507	1.532	0.71	2.65	4	*C. mundulus*
C	**3**	**H**	**7**	**13**	**15**	27.03	27.05	28.42	1.466	1.507	1.532	0.66	-0.1	9	*G. ruber*
C	**3**	**H**	**7**	**29**	**31**	27.19	27.21	28.58	1.474	1.516	1.538	1.05	2.73	4	*C. mundulus*
C	**3**	**H**	**7**	**29**	**31**	27.19	27.21	28.58	1.474	1.516	1.538	1.16	-0.15	7	*G. ruber*
C	**3**	**H**	**7**	**46**	**48**	27.36	27.38	28.75	1.483	1.523	1.544	1.03	2.72	4	*C. robertsonanius*
C	**3**	**H**	**7**	**46**	**48**	27.36	27.38	28.75	1.483	1.523	1.544	1.07	2.59	4	*C. robertsonanius*
C	**3**	**H**	**7**	**46**	**48**	27.36	27.38	28.75	1.483	1.523	1.544	1.08	0.67	8	*G. ruber*
A	**4**	**H**	**2**	**51**	**53**	26.61	26.63	30.19	1.559	1.611	1.597	1.12	2.51	4	*C. mundulus*
A	**4**	**H**	**2**	**51**	**53**	26.61	26.63	30.19	1.559	1.611	1.597	1.33	-0.88	8	*G. ruber*
C	**4**	**H**	**1**	**59**	**61**	27.99	28.01	30.44	1.572	1.625	1.606	1.08	2.73	4	*C. mundulus*
C	**4**	**H**	**1**	**59**	**61**	27.99	28.01	30.44	1.572	1.625	1.606	1.32	0.05	5	*G. ruber*
C	**4**	**H**	**1**	**75**	**77**	28.15	28.17	30.6	1.581	1.633	1.612	1.1	2.51	4	*C. mundulus*
C	**4**	**H**	**1**	**75**	**77**	28.15	28.17	30.6	1.581	1.633	1.612	1.2	-0.3	8	*G. ruber*
C	**4**	**H**	**1**	**91**	**93**	28.31	28.33	30.76	1.589	1.642	1.618	1.09	2.58	3	*C. mundulus*
C	**4**	**H**	**1**	**91**	**93**	28.31	28.33	30.76	1.589	1.642	1.618	1.43	-0.5	8	*G. ruber*
C	**4**	**H**	**1**	**91**	**93**	28.31	28.33	30.76	1.589	1.642	1.618	1.22	2.57	4	*P. wuellerstorfi*
C	**4**	**H**	**1**	**107**	**109**	28.47	28.49	30.92	1.598	1.651	1.624	1.07	2.64	4	*C. mundulus*
C	**4**	**H**	**1**	**107**	**109**	28.47	28.49	30.92	1.598	1.651	1.624	1.36	-0.34	8	*G. ruber*
C	**4**	**H**	**1**	**123**	**125**	28.63	28.65	31.08	1.606	1.658	1.630	1.37	2.38	3	*P. wuellerstorfi*

C	4	H	2	21	23	29.11	29.13	31.56	1.631	1.673	1.655	1.03	2.85	4	*C. mundulus*
C	4	H	2	21	23	29.11	29.13	31.56	1.631	1.673	1.655	1.04	0.01	8	*G. ruber*
C	4	H	2	21	23	29.11	29.13	31.56	1.631	1.673	1.655	1.16	2.9	3	*P. wuellerstorfi*
A	4	H	3	45	47	28.05	28.07	31.63	1.635	1.675	1.663	1.21	-0.11	8	*G. ruber*
A	4	H	3	45	47	28.05	28.07	31.63	1.635	1.675	1.663	1.19	2.72	3	*P. wuellerstorfi*
C	4	H	2	37	39	29.27	29.29	31.72	1.640	1.677	1.673	0.93	1.14	8	*G. ruber*
C	4	H	2	37	39	29.27	29.29	31.72	1.640	1.677	1.673	1.07	2.62	3	*P. wuellerstorfi*
C	4	H	2	53	55	29.43	29.45	31.88	1.648	1.682	1.690	0.98	2.76	4	*C. mundulus*
C	4	H	2	53	55	29.43	29.45	31.88	1.648	1.682	1.690	1.5	0.94	7	*G. ruber*
C	4	H	2	69	71	29.59	29.61	32.04	1.657	1.687	1.708	0.86	2.71	4	*C. mundulus*
C	4	H	2	69	71	29.59	29.61	32.04	1.657	1.687	1.708	0.79	3	3	*P. wuellerstorfi*
C	4	H	2	85	87	29.75	29.77	32.2	1.665	1.692	1.713	0.86	2.76	4	*C. mundulus*
C	4	H	2	85	87	29.75	29.77	32.2	1.665	1.692	1.713	1.1	0.21	8	*G. ruber*
C	4	H	2	101	103	29.91	29.93	32.36	1.673	1.699	1.719	0.93	2.76	4	*C. mundulus*
C	4	H	2	101	103	29.91	29.93	32.36	1.673	1.699	1.719	1.06	-0.32	8	*G. ruber*
C	4	H	2	117	119	30.07	30.09	32.52	1.682	1.707	1.725	1.41	0.6	8	*G. ruber*
C	4	H	2	117	119	30.07	30.09	32.52	1.682	1.707	1.725	0.98	2.69	4	*P. wuellerstorfi*
C	4	H	2	117	119	30.07	30.09	32.52	1.682	1.707	1.725	0.96	2.66	4	*P. wuellerstorfi*
A	4	H	3	135	137	28.95	28.97	32.53	1.682	1.707	1.725	1.01	0.36	8	*G. ruber*
A	4	H	3	135	137	28.95	28.97	32.53	1.682	1.707	1.725	0.92	2.6	4	*P. wuellerstorfi*
A	4	H	3	148	150	29.08	29.1	32.66	1.689	1.713	1.730	0.95	2.52	4	*P. wuellerstorfi*
C	4	H	2	133	135	30.23	30.25	32.68	1.690	1.714	1.730	0.91	0.1	7	*G. ruber*
C	4	H	2	133	135	30.23	30.25	32.68	1.690	1.714	1.730	1.03	2.67	4	*P. wuellerstorfi*
C	4	H	2	148	150	30.38	30.4	32.83	1.698	1.721	1.736	0.78	-1.17	8	*G. ruber*
C	4	H	2	148	150	30.38	30.4	32.83	1.698	1.721	1.736	0.98	2.51	4	*P. wuellerstorfi*
C	4	H	3	15	17	30.55	30.57	33	1.707	1.729	1.742	0.84	2.72	4	*C. mundulus*
C	4	H	3	15	17	30.55	30.57	33	1.707	1.729	1.742	0.77	2.86	4	*C. robertsonanius*
C	4	H	3	15	17	30.55	30.57	33	1.707	1.729	1.742	0.54	0.01	8	*G. ruber*
C	4	H	3	15	17	30.55	30.57	33	1.707	1.729	1.742	0.92	2.71	3	*P. wuellerstorfi*
C	4	H	3	31	33	30.71	30.73	33.16	1.716	1.736	1.748	0.92	-0.65	7	*G. ruber*
C	4	H	3	31	33	30.71	30.73	33.16	1.716	1.736	1.748	0.95	2.74	4	*P. wuellerstorfi*
C	4	H	3	47	49	30.87	30.89	33.32	1.724	1.742	1.754	0.74	2.66	4	*C. mundulus*
C	4	H	3	47	49	30.87	30.89	33.32	1.724	1.742	1.754	0.97	2.53	4	*P. wuellerstorfi*
C	4	H	3	63	65	31.03	31.05	33.48	1.732	1.749	1.760	1.21	0.43	8	*G. ruber*
C	4	H	3	63	65	31.03	31.05	33.48	1.732	1.749	1.760	1.12	2.55	4	*P. wuellerstorfi*
C	4	H	3	79	81	31.19	31.21	33.64	1.741	1.755	1.766	1.1	2.64	4	*C. mundulus*
A	4	H	4	103	105	30.13	30.15	33.71	1.745	1.758	1.769	1.14	2.47	3	*P. wuellerstorfi*
C	4	H	3	95	97	31.35	31.37	33.8	1.749	1.762	1.773	1.27	2.31	4	*P. wuellerstorfi*
A	4	H	4	123	125	30.33	30.35	33.91	1.755	1.767	1.776	1.06	2.6	4	*C. mundulus*

C	4	H	3	111	113	31.51	31.53	33.96	1.758	1.769	1.777	1.14	2.34	3	*P. wuellerstorfi*
C	4	H	3	127	129	31.67	31.69	34.12	1.766	1.776	1.781	1.04	-0.13	8	*G. ruber*
C	4	H	3	127	129	31.67	31.69	34.12	1.766	1.776	1.781	1.08	2.56	4	*P. wuellerstorfi*
C	4	H	4	9	11	31.99	32.01	34.44	1.781	1.779	1.790	0.92	2.64	4	*P. wuellerstorfi*
C	4	H	4	25	27	32.15	32.17	34.6	1.786	1.780	1.795	0.96	2.73	3	*P. wuellerstorfi*
C	4	H	4	41	43	32.31	32.33	34.76	1.791	1.780	1.799	0.76	3.03	4	*C. mundulus*
C	4	H	4	57	59	32.47	32.49	34.92	1.796	1.784	1.803	1.01	2.55	4	*C. mundulus*
C	4	H	4	73	75	32.63	32.65	35.08	1.802	1.790	1.808	1.04	2.57	4	*C. mundulus*
C	4	H	4	73	75	32.63	32.65	35.08	1.802	1.790	1.808	1.15	2.47	4	*P. wuellerstorfi*
C	4	H	4	89	91	32.79	32.81	35.24	1.807	1.795	1.812	1.02	2.52	4	*C. mundulus*
C	4	H	4	89	91	32.79	32.81	35.24	1.807	1.795	1.812	1.09	2.52	4	*P. wuellerstorfi*
C	4	H	4	105	107	32.95	32.97	35.4	1.812	1.801	1.817	1.05	2.46	4	*P. wuellerstorfi*
C	4	H	4	121	123	33.11	33.13	35.56	1.817	1.808	1.821	0.89	2.48	4	*C. mundulus*
C	4	H	4	121	123	33.11	33.13	35.56	1.817	1.808	1.821	1.13	2.44	3	*P. wuellerstorfi*
C	4	H	4	137	139	33.27	33.29	35.72	1.822	1.814	1.826	0.98	2.48	4	*C. mundulus*
C	4	H	4	137	139	33.27	33.29	35.72	1.822	1.814	1.826	1.07	2.4	4	*P. wuellerstorfi*
C	4	H	5	3	5	33.43	33.45	35.88	1.827	1.820	1.830	0.94	2.62	4	*C. mundulus*
C	4	H	5	3	5	33.43	33.45	35.88	1.827	1.820	1.830	1.09	2.34	3	*P. wuellerstorfi*
C	4	H	5	19	21	33.59	33.61	36.04	1.832	1.827	1.837	0.89	2.47	3	*C. mundulus*
C	4	H	5	19	21	33.59	33.61	36.04	1.832	1.827	1.837	0.41	2.54	4	*C. robertsonanius*
C	4	H	5	35	37	33.75	33.77	36.2	1.837	1.835	1.844	1.13	2.5	4	*P. wuellerstorfi*
C	4	H	5	51	53	33.91	33.93	36.36	1.843	1.843	1.852	0.9	2.81	4	*C. mundulus*
C	4	H	5	67	69	34.07	34.09	36.52	1.848	1.851	1.859	0.91	2.83	4	*C. mundulus*
C	4	H	5	67	69	34.07	34.09	36.52	1.848	1.851	1.859	1.11	2.57	4	*P. wuellerstorfi*
C	4	H	5	83	85	34.23	34.25	36.68	1.853	1.859	1.866	1	2.6	4	*P. wuellerstorfi*
C	4	H	5	99	101	34.39	34.41	36.84	1.858	1.867	1.873	1.15	2.54	4	*P. wuellerstorfi*
A	4	H	6	119	121	33.29	33.31	36.87	1.859	1.869	1.874	1.01	2.69	4	*C. mundulus*
C	4	H	5	115	117	34.55	34.57	37	1.863	1.875	1.880	1.02	2.41	3	*C. mundulus*
C	4	H	5	115	117	34.55	34.57	37	1.863	1.875	1.880	1.17	2.43	3	*P. wuellerstorfi*
C	4	H	5	131	133	34.71	34.73	37.16	1.868	1.884	1.888	1.05	2.41	4	*C. mundulus*
C	4	H	6	13	15	35.03	35.05	37.48	1.878	1.900	1.903	1.3	2.47	4	*P. wuellerstorfi*
C	4	H	6	29	31	35.19	35.21	37.64	1.884	1.908	1.910	1.12	2.62	4	*C. mundulus*
C	4	H	6	29	31	35.19	35.21	37.64	1.884	1.908	1.910	1.16	2.69	4	*C. mundulus*
C	4	H	6	47	49	35.37	35.39	37.82	1.889	1.915	1.918	1.07	2.58	4	*C. mundulus*
C	4	H	6	61	63	35.51	35.53	37.96	1.894	1.922	1.925	1.25	2.61	4	*P. wuellerstorfi*
C	4	H	6	77	79	35.67	35.69	38.12	1.899	1.929	1.933	1.11	2.66	4	*C. mundulus*
C	4	H	6	77	79	35.67	35.69	38.12	1.899	1.929	1.933	1.06	2.66	4	*P. wuellerstorfi*
C	4	H	6	93	95	35.83	35.85	38.28	1.904	1.936	1.940	1.21	2.83	4	*P. wuellerstorfi*
C	4	H	6	109	111	35.99	36.01	38.44	1.909	1.944	1.948	1.14	3.04	4	*P. wuellerstorfi*

C	4	H	6	125	127	36.15	36.17	38.6	1.914	1.951	1.951	1.24	2.58	3	*P. wuellerstorfi*
C	4	H	6	141	143	36.31	36.33	38.76	1.919	1.955	1.955	1.28	2.7	4	*P. wuellerstorfi*
C	4	H	7	20	22	36.6	36.62	39.05	1.929	1.968	1.962	1.17	2.77	4	*C. mundulus*
C	4	H	7	49	51	36.89	36.91	39.34	1.938	1.982	1.968	1.11	2.59	4	*C. mundulus*
A	5	H	1	130	132	35.4	35.42	39.42	1.941	1.986	1.970	1.01	2.55	4	*C. mundulus*
A	5	H	1	130	132	35.4	35.42	39.42	1.941	1.986	1.970	1.03	2.78	3	*C. mundulus*
C	5	H	1	57	59	37.47	37.49	41.19	2.011	2.067	2.012	1.03	2.27	4	*C. mundulus*
C	5	H	1	86	88	37.76	37.78	41.48	2.022	2.076	2.018	1.23	2.29	4	*C. mundulus*
C	5	H	1	115	117	38.05	38.07	41.77	2.034	2.083	2.025	1.23	2.28	4	*C. mundulus*
A	5	H	3	67	69	37.77	37.79	41.79	2.035	2.083	2.026	1.27	2.34	4	*C. mundulus*
C	5	H	2	23	25	38.63	38.65	42.35	2.057	2.096	2.044	1.27	2.35	4	*P. wuellerstorfi*
C	5	H	2	52	54	38.92	38.94	42.64	2.069	2.102	2.054	1.34	2.52	4	*P. wuellerstorfi*
C	5	H	2	81	83	39.21	39.23	42.93	2.081	2.108	2.063	1.26	2.84	4	*P. wuellerstorfi*
A	5	H	4	35	37	38.95	38.97	42.97	2.082	2.108	2.064	0.88	2.46	4	*P. wuellerstorfi*
C	5	H	2	110	112	39.5	39.52	43.22	2.092	2.113	2.073	1.2	2.96	4	*P. wuellerstorfi*
C	5	H	3	18	20	40.08	40.1	43.8	2.116	2.126	2.092	0.88	2.54	3	*C. mundulus*
C	5	H	3	18	20	40.08	40.1	43.8	2.116	2.126	2.092	1.05	2.47	4	*P. wuellerstorfi*
C	5	H	3	47	49	40.37	40.39	44.09	2.127	2.133	2.101	1.07	2.62	4	*P. wuellerstorfi*
C	5	H	3	76	78	40.66	40.68	44.38	2.133	2.138	2.111	1.2	2.32	4	*P. wuellerstorfi*
C	5	H	3	105	107	40.95	40.97	44.67	2.138	2.142	2.121	1.05	2.28	4	*P. wuellerstorfi*
C	5	H	3	134	136	41.24	41.26	44.96	2.143	2.147	2.130	0.96	2.37	5	*P. wuellerstorfi*
C	5	H	4	13	15	41.53	41.55	45.25	2.149	2.152	2.140	1.18	2.3	4	*P. wuellerstorfi*
C	5	H	4	42	44	41.82	41.84	45.54	2.157	2.158	2.150	0.92	2.49	4	*C. mundulus*
C	5	H	4	71	73	42.11	42.13	45.83	2.164	2.163	2.160	0.79	2.52	4	*C. mundulus*
C	5	H	4	71	73	42.11	42.13	45.83	2.164	2.163	2.160	1.08	2.47	4	*P. wuellerstorfi*
C	5	H	4	100	102	42.4	42.42	46.12	2.172	2.168	2.170	0.85	2.28	4	*C. mundulus*
C	5	H	4	100	102	42.4	42.42	46.12	2.172	2.168	2.170	0.99	2.29	4	*P. wuellerstorfi*
C	5	H	4	129	131	42.69	42.71	46.41	2.180	2.174	2.180	0.78	2.29	3	*C. mundulus*
C	5	H	4	129	131	42.69	42.71	46.41	2.180	2.174	2.180	0.94	2.24	4	*P. wuellerstorfi*
C	5	H	5	37	39	43.27	43.29	46.99	2.195	2.187	2.200	0.84	2.23	4	*P. wuellerstorfi*
C	5	H	5	66	68	43.56	43.58	47.28	2.203	2.194	2.210	1.11	2.53	4	*P. wuellerstorfi*
C	5	H	5	95	97	43.85	43.87	47.57	2.210	2.202	2.220	1.01	2.21	4	*C. mundulus*
C	5	H	5	95	97	43.85	43.87	47.57	2.210	2.202	2.220	1.08	2.28	4	*P. wuellerstorfi*
A	5	H	7	59	61	43.69	43.71	47.71	2.214	2.206	2.225	1.01	2.21	4	*P. wuellerstorfi*
C	5	H	5	124	126	44.14	44.16	47.86	2.218	2.211	2.229	1.01	2.28	4	*P. wuellerstorfi*
C	5	H	6	3	5	44.43	44.45	48.15	2.226	2.219	2.237	0.81	2.42	4	*P. wuellerstorfi*
C	5	H	6	3	5	44.43	44.45	48.15	2.226	2.219	2.237	0.98	2.75	4	*P. wuellerstorfi*
C	5	H	6	32	34	44.72	44.74	48.44	2.233	2.228	2.245	0.82	2.59	4	*C. mundulus*
C	5	H	6	61	63	45.01	45.03	48.73	2.241	2.236	2.252	0.9	2.36	4	*C. mundulus*

C	5	H	6	90	92	45.3	45.32	49.02	2.249	2.243	2.260	0.77	2.31	4	*C. mundulus*
C	5	H	6	119	121	45.59	45.61	49.31	2.256	2.249	2.263	1	2.35	4	*P. wuellerstorfi*
C	5	H	7	30	32	46.2	46.22	49.92	2.273	2.261	2.270	0.87	2.26	4	*P. wuellerstorfi*
A	6	H	2	125	127	46.35	46.37	51.45	2.313	2.297	2.288	0.84	2.52	4	*C. mundulus*
A	6	H	2	125	127	46.35	46.37	51.45	2.313	2.297	2.288	1	2.45	4	*P. wuellerstorfi*
A	6	H	3	33	35	46.93	46.95	52.03	2.328	2.313	2.294	1.13	2.57	4	*P. wuellerstorfi*
C	6	H	1	64	66	47.04	47.06	52.15	2.332	2.317	2.296	1.33	2.34	4	*P. wuellerstorfi*
A	6	H	3	62	64	47.22	47.24	52.32	2.336	2.322	2.298	1.28	2.3	4	*P. wuellerstorfi*
C	6	H	1	93	95	47.33	47.35	52.44	2.339	2.325	2.300	1.24	2.41	4	*P. wuellerstorfi*
C	6	H	1	124	126	47.64	47.66	52.75	2.347	2.333	2.307	1.18	2.45	4	*C. mundulus*
C	6	H	2	30	32	48.2	48.22	53.31	2.362	2.349	2.320	1.1	2.62	4	*C. mundulus*
A	6	H	4	16	18	48.26	48.28	53.36	2.364	2.350	2.321	1.09	2.52	4	*C. mundulus*
C	6	H	2	59	61	48.49	48.51	53.6	2.370	2.355	2.326	1.1	2.41	4	*C. mundulus*
C	6	H	2	88	90	48.78	48.8	53.89	2.378	2.361	2.333	1.1	2.37	4	*C. mundulus*
C	6	H	2	121	123	49.11	49.13	54.22	2.386	2.364	2.340	1.05	2.41	4	*C. mundulus*
C	6	H	2	121	123	49.11	49.13	54.22	2.386	2.364	2.340	1.19	2.07	4	*P. wuellerstorfi*
C	6	H	3	25	27	49.65	49.67	54.76	2.401	2.373	2.350	1.02	2.17	4	*P. wuellerstorfi*
A	6	H	5	28	30	49.88	49.9	54.98	2.406	2.377	2.355	0.97	2.51	4	*P. wuellerstorfi*
C	6	H	3	54	56	49.94	49.96	55.05	2.408	2.378	2.356	1.09	2.76	4	*P. wuellerstorfi*
C	6	H	3	83	85	50.23	50.25	55.34	2.416	2.382	2.362	1.02	2.69	4	*P. wuellerstorfi*
C	6	H	3	112	114	50.52	50.54	55.63	2.424	2.387	2.367	1	2.85	4	*P. wuellerstorfi*
C	6	H	4	20	22	51.1	51.12	56.21	2.439	2.400	2.378	1.16	2.16	4	*P. wuellerstorfi*
A	6	H	6	23	25	51.33	51.35	56.43	2.445	2.407	2.383	0.94	2.08	3	*C. mundulus*
A	6	H	6	23	25	51.33	51.35	56.43	2.445	2.407	2.383	0.76	2.09	4	*C. robertsonanius*
C	6	H	4	49	51	51.39	51.41	56.5	2.447	2.409	2.385	1.11	2.09	4	*P. wuellerstorfi*
C	6	H	4	77	79	51.67	51.69	56.78	2.454	2.417	2.397	0.96	2.51	4	*C. mundulus*
C	6	H	4	107	109	51.97	51.99	57.08	2.462	2.425	2.410	0.76	2.38	4	*C. mundulus*
C	6	H	4	136	138	52.26	52.28	57.37	2.470	2.435	2.421	0.61	2.7	4	*C. mundulus*
C	6	H	5	20	22	52.6	52.62	57.71	2.479	2.445	2.433	1.01	2.65	4	*P. wuellerstorfi*
C	6	H	5	44	46	52.84	52.86	57.95	2.485	2.453	2.442	0.93	2.57	4	*P. wuellerstorfi*
C	6	H	5	73	75	53.13	53.15	58.24	2.493	2.461	2.452	0.93	2.29	4	*P. wuellerstorfi*
C	6	H	5	102	104	53.42	53.44	58.53	2.500	2.471	2.463	0.74	2.19	4	*C. mundulus*
C	6	H	5	131	133	53.71	53.73	58.82	2.508	2.481	2.475	0.52	2.57	4	*C. mundulus*
C	6	H	6	10	12	54	54.02	59.11	2.516	2.491	2.488	0.9	2.61	4	*C. mundulus*
C	6	H	6	39	41	54.29	54.31	59.4	2.523	2.501	2.500	1.33	2.31	3	*C. mundulus*
C	6	H	6	39	41	54.29	54.31	59.4	2.523	2.501	2.500	1.33	2.31	3	*C. mundulus*
C	6	H	6	68	70	54.58	54.6	59.69	2.531	2.511	2.510	0.96	2.45	4	*C. mundulus*
C	6	H	6	97	99	54.87	54.89	59.98	2.539	2.521	2.519	0.87	2.29	4	*C. mundulus*
C	6	H	6	126	128	55.16	55.18	60.27	2.546	2.532	2.529	0.89	2.48	4	*C. mundulus*

C	6	H	6	126	128	55.16	55.18	60.27	2.546	2.532	2.529	1.06	2.21	4	*P. wuellerstorfi*
C	6	H	7	34	36	55.74	55.76	60.85	2.562	2.553	2.548	0.82	2.05	4	*P. wuellerstorfi*
C	7	H	1	71	73	56.61	56.63	62.18	2.596	2.595	2.593	0.76	2.2	4	*C. mundulus*
C	7	H	1	71	73	56.61	56.63	62.18	2.596	2.595	2.593	1.01	2.51	4	*P. wuellerstorfi*
A	7	H	2	137	139	55.97	55.99	62.3	2.599	2.598	2.598	1.01	2.46	4	*P. wuellerstorfi*
C	7	H	1	100	102	56.9	56.92	62.47	2.603	2.603	2.603	1.12	2.35	4	*P. wuellerstorfi*
C	7	H	1	129	131	57.19	57.21	62.76	2.610	2.611	2.613	0.98	2.26	4	*C. mundulus*
A	7	H	3	45	47	56.55	56.57	62.88	2.613	2.615	2.618	0.91	2.16	4	*C. mundulus*
A	7	H	3	74	76	56.84	56.86	63.17	2.620	2.623	2.628	0.99	2.01	4	*C. mundulus*
A	7	H	3	74	76	56.84	56.86	63.17	2.620	2.623	2.628	1.11	2.04	4	*P. wuellerstorfi*
C	7	H	2	37	39	57.77	57.79	63.34	2.624	2.628	2.633	0.9	2.5	4	*C. mundulus*
C	7	H	2	66	68	58.06	58.08	63.63	2.631	2.637	2.641	0.77	2.49	4	*C. mundulus*
C	7	H	2	95	97	58.35	58.37	63.92	2.639	2.646	2.650	0.95	2.54	4	*P. wuellerstorfi*
C	7	H	2	124	126	58.64	58.66	64.21	2.646	2.657	2.659	1.06	2.43	4	*C. mundulus*
A	7	H	4	40	42	58	58.02	64.33	2.649	2.662	2.663	0.93	2.16	4	*C. mundulus*
C	7	H	3	32	34	59.22	59.24	64.79	2.660	2.678	2.671	1.17	2.2	4	*P. wuellerstorfi*
C	7	H	3	61	63	59.51	59.53	65.08	2.667	2.689	2.676	1.18	2.31	4	*P. wuellerstorfi*
C	7	H	3	90	92	59.8	59.82	65.37	2.674	2.699	2.681	1.09	2.12	3	*P. wuellerstorfi*
C	7	H	3	119	121	60.09	60.11	65.66	2.681	2.709	2.686	0.88	2.44	4	*C. mundulus*
C	7	H	4	27	29	60.67	60.69	66.24	2.696	2.728	2.696	0.98	2.67	4	*P. wuellerstorfi*
A	7	H	5	98	100	60.08	60.1	66.41	2.700	2.733	2.699	0.89	2.38	4	*P. wuellerstorfi*
C	7	H	4	56	58	60.96	60.98	66.53	2.703	2.736	2.701	0.83	2.66	4	*C. mundulus*
C	7	H	4	85	87	61.25	61.27	66.82	2.710	2.744	2.707	0.82	2.58	4	*C. mundulus*
C	7	H	4	117	119	61.57	61.59	67.14	2.718	2.750	2.712	0.79	2.79	4	*C. mundulus*
C	7	H	5	22	24	62.12	62.14	67.69	2.731	2.762	2.722	0.85	2.83	4	*C. mundulus*
A	7	H	6	98	100	61.58	61.6	67.91	2.737	2.767	2.726	1.06	2.64	4	*P. wuellerstorfi*
C	7	H	5	51	53	62.41	62.43	67.98	2.739	2.768	2.727	1.11	2.45	4	*P. wuellerstorfi*
C	7	H	5	80	82	62.7	62.72	68.27	2.746	2.774	2.732	0.93	2.54	4	*C. mundulus*
C	7	H	5	109	111	62.99	63.01	68.56	2.753	2.779	2.737	1.02	2.33	3	*C. mundulus*
C	7	H	5	138	140	63.28	63.3	68.85	2.760	2.784	2.743	0.62	1.79	3	*P. wuellerstorfi*
C	7	H	6	17	19	63.57	63.59	69.14	2.767	2.788	2.751	1.14	2.32	3	*P. wuellerstorfi*
A	7	H	7	73	75	62.83	62.85	69.16	2.768	2.789	2.752	1.12	2.32	4	*P. wuellerstorfi*
C	7	H	6	46	48	63.86	63.88	69.43	2.774	2.792	2.760	1.03	2.44	4	*P. wuellerstorfi*
C	7	H	6	75	77	64.15	64.17	69.72	2.781	2.797	2.769	1.02	2.34	3	*P. wuellerstorfi*
C	7	H	6	104	106	64.44	64.46	70.01	2.789	2.801	2.778	1.17	2.23	4	*P. wuellerstorfi*
C	7	H	6	133	135	64.73	64.75	70.3	2.796	2.805	2.786	1.15	2.26	4	*P. wuellerstorfi*
C	7	H	7	15	17	65.05	65.07	70.62	2.804	2.809	2.796	1.16	2.08	3	*P. wuellerstorfi*
C	7	H	7	41	43	65.31	65.33	70.88	2.810	2.812	2.804	1.15	2.08	4	*P. wuellerstorfi*
C	7	H	7	70	72	65.6	65.62	71.17	2.817	2.816	2.813	1.02	2.28	4	*C. mundulus*

C	8	H	1	78	80	66.18	66.2	73.4	2.872	2.890	2.880	1.08	2.53	4	*C. mundulus*
C	8	H	1	107	109	66.47	66.49	73.69	2.879	2.899	2.889	1.06	2.41	3	*C. mundulus*
A	8	H	3	84	86	66.49	66.51	73.89	2.884	2.901	2.895	1.21	2.27	4	*P. wuellerstorfi*
C	8	H	1	136	138	66.76	66.78	73.98	2.886	2.902	2.898	1.06	2.24	3	*P. wuellerstorfi*
C	8	H	2	15	17	67.05	67.07	74.27	2.893	2.906	2.911	1.2	2.4	3	*P. wuellerstorfi*
C	8	H	2	44	46	67.34	67.36	74.56	2.901	2.910	2.925	1.1	2.5	4	*P. wuellerstorfi*
C	8	H	2	73	75	67.63	67.65	74.85	2.908	2.914	2.939	1.09	2.65	4	*P. wuellerstorfi*
C	8	H	2	102	104	67.92	67.94	75.14	2.915	2.918	2.953	1.17	2.35	4	*P. wuellerstorfi*
C	8	H	2	131	133	68.21	68.23	75.43	2.922	2.921	2.957	1.15	2.39	4	*P. wuellerstorfi*
C	8	H	3	10	12	68.5	68.52	75.72	2.929	2.925	2.961	1.13	2.51	4	*P. wuellerstorfi*
C	8	H	3	39	41	68.79	68.81	76.01	2.936	2.929	2.965	0.98	2.46	3	*P. wuellerstorfi*
C	8	H	3	68	70	69.08	69.1	76.3	2.943	2.933	2.969	0.98	2.56	4	*P. wuellerstorfi*
C	8	H	3	97	99	69.37	69.39	76.59	2.951	2.941	2.973	0.91	2.63	4	*P. wuellerstorfi*
C	8	H	3	126	128	69.66	69.68	76.88	2.958	2.951	2.977	1.03	2.44	3	*P. wuellerstorfi*
C	8	H	4	34	36	70.24	70.26	77.46	2.972	2.970	2.985	0.99	2.36	4	*C. mundulus*
C	8	H	4	63	65	70.53	70.55	77.75	2.979	2.980	2.990	1.05	2.36	4	*P. wuellerstorfi*
A	8	H	6	55	57	70.63	70.65	78.03	2.986	2.990	2.995	1	2.41	4	*P. wuellerstorfi*
C	8	H	4	92	94	70.82	70.84	78.04	2.986	2.990	2.995	1.04	2.43	3	*P. wuellerstorfi*
C	8	H	4	121	123	71.11	71.13	78.33	2.993	2.999	3.000	1.06	2.37	4	*P. wuellerstorfi*
C	8	H	4	138	140	71.28	71.3	78.5	2.998	3.004	3.003	1.02	2.61	4	*P. wuellerstorfi*
C	8	H	5	27	29	71.68	71.7	78.9	3.007	3.014	3.010	0.85	2.53	4	*C. mundulus*
C	8	H	5	57	59	71.98	72	79.2	3.015	3.019	3.015	0.92	2.49	4	*P. wuellerstorfi*
C	8	H	5	86	88	72.27	72.29	79.49	3.022	3.028	3.020	0.87	2.41	3	*C. mundulus*
C	8	H	5	115	117	72.56	72.58	79.78	3.029	3.035	3.025	0.89	2.34	4	*P. wuellerstorfi*
C	8	H	6	21	23	73.14	73.16	80.36	3.049	3.049	3.035	1.99	-1.32	8	*G. ruber*
C	8	H	6	21	23	73.14	73.16	80.36	3.049	3.049	3.035	1.04	2.05	5	*P. wuellerstorfi*
C	8	H	6	50	52	73.43	73.45	80.65	3.059	3.057	3.048	1.73	-1.69	8	*G. ruber*
C	8	H	6	50	52	73.43	73.45	80.65	3.059	3.057	3.048	1.55	2.13	4	*P. wuellerstorfi*
C	8	H	6	79	81	73.72	73.74	80.94	3.069	3.065	3.060	1.75	-1.44	8	*G. ruber*
C	8	H	6	79	81	73.72	73.74	80.94	3.069	3.065	3.060	1.13	1.78	4	*P. wuellerstorfi*
C	8	H	6	108	110	74.01	74.03	81.23	3.080	3.073	3.068	1.59	-1.73	8	*G. ruber*
C	8	H	6	108	110	74.01	74.03	81.23	3.080	3.073	3.068	1.44	2.19	4	*P. wuellerstorfi*
C	8	H	6	137	139	74.3	74.32	81.52	3.090	3.085	3.077	1.6	-1.61	8	*G. ruber*
C	8	H	6	137	139	74.3	74.32	81.52	3.090	3.085	3.077	1.45	2.14	4	*P. wuellerstorfi*
C	8	H	7	14	16	74.59	74.61	81.81	3.101	3.098	3.085	1.57	-1.88	8	*G. ruber*
C	8	H	7	14	16	74.59	74.61	81.81	3.101	3.098	3.085	0.95	1.99	4	*P. wuellerstorfi*
C	8	H	7	43	45	74.88	74.9	82.1	3.111	3.112	3.101	1.52	-1.44	8	*G. ruber*
C	8	H	7	43	45	74.88	74.9	82.1	3.111	3.112	3.101	1.35	2.16	4	*P. wuellerstorfi*
A	9	H	2	19	21	73.81	73.83	82.18	3.114	3.115	3.105	1.75	-1.38	8	*G. ruber*

A	9	H	2	19	21	73.81	73.83	82.18	3.114	3.115	3.105	0.99	1.98	4	*P. wuellerstorfi*
C	9	H	1	85	87	75.75	75.77	83.89	3.164	3.176	3.159	1.07	2.3	4	*C. mundulus*
C	9	H	1	85	87	75.75	75.77	83.89	3.164	3.176	3.159	2.05	-1.49	8	*G. ruber*
C	9	H	1	114	116	76.04	76.06	84.18	3.172	3.184	3.168	1.57	-1.82	9	*G. ruber*
C	9	H	1	114	116	76.04	76.06	84.18	3.172	3.184	3.168	1.58	1.98	4	*P. wuellerstorfi*
A	9	H	3	99	101	76.14	76.16	84.51	3.182	3.191	3.179	1.68	-1.84	8	*G. ruber*
A	9	H	3	99	101	76.14	76.16	84.51	3.182	3.191	3.179	1.61	2.06	4	*P. wuellerstorfi*
A	9	H	3	99	101	76.14	76.16	84.51	3.182	3.191	3.179	1.6	2.11	4	*P. wuellerstorfi*
C	9	H	2	22	24	76.62	76.64	84.76	3.189	3.196	3.187	1.78	-1.92	8	*G. ruber*
C	9	H	2	22	24	76.62	76.64	84.76	3.189	3.196	3.187	1.14	1.77	4	*P. wuellerstorfi*
A	9	H	3	128	130	76.43	76.45	84.8	3.190	3.197	3.188	2.15	-1.62	8	*G. ruber*
A	9	H	3	128	130	76.43	76.45	84.8	3.190	3.197	3.188	1.71	2.07	4	*P. wuellerstorfi*
C	9	H	2	51	53	76.91	76.93	85.05	3.198	3.202	3.196	1.67	-1.85	8	*G. ruber*
C	9	H	2	51	53	76.91	76.93	85.05	3.198	3.202	3.196	1.63	2	4	*P. wuellerstorfi*
A	9	H	4	26	28	76.91	76.93	85.28	3.204	3.207	3.203	1.19	2.3	4	*C. mundulus*
A	9	H	4	26	28	76.91	76.93	85.28	3.204	3.207	3.203	1.45	-1.76	8	*G. ruber*
A	9	H	4	26	28	76.91	76.93	85.28	3.204	3.207	3.203	1.57	2.01	4	*P. wuellerstorfi*
C	9	H	2	80	82	77.2	77.22	85.34	3.206	3.208	3.205	1.58	-1.89	8	*G. ruber*
C	9	H	2	80	82	77.2	77.22	85.34	3.206	3.208	3.205	1.15	1.8	4	*P. wuellerstorfi*
C	9	H	2	109	111	77.49	77.51	85.63	3.214	3.214	3.213	1.66	-1.88	9	*G. ruber*
C	9	H	2	109	111	77.49	77.51	85.63	3.214	3.214	3.213	1.59	2.17	4	*P. wuellerstorfi*
C	9	H	2	138	140	77.78	77.8	85.92	3.222	3.220	3.220	1.79	-1.79	8	*G. ruber*
C	9	H	2	138	140	77.78	77.8	85.92	3.222	3.220	3.220	1.53	2.17	4	*P. wuellerstorfi*
C	9	H	3	17	19	78.07	78.09	86.21	3.230	3.227	3.228	1.22	2.17	4	*P. wuellerstorfi*
C	9	H	3	45	47	78.35	78.37	86.49	3.238	3.234	3.235	1.14	2.38	4	*C. mundulus*
C	9	H	3	75	77	78.65	78.67	86.79	3.246	3.239	3.243	1.24	2.21	4	*P. wuellerstorfi*
C	9	H	3	104	106	78.94	78.96	87.08	3.255	3.247	3.250	1.07	2.09	4	*P. wuellerstorfi*
C	9	H	3	133	135	79.23	79.25	87.37	3.263	3.254	3.260	0.9	2.39	4	*C. mundulus*
C	9	H	4	12	14	79.52	79.54	87.66	3.271	3.303	3.271	1.08	2.15	4	*P. wuellerstorfi*
C	9	H	4	41	43	79.81	79.83	87.95	3.279	3.309	3.281	1.1	2.22	4	*P. wuellerstorfi*
C	9	H	4	70	72	80.1	80.12	88.24	3.287	3.315	3.292	0.92	1.93	4	*P. wuellerstorfi*
C	9	H	4	99	101	80.39	80.41	88.53	3.295	3.322	3.302	0.8	2.51	4	*P. wuellerstorfi*
C	9	H	4	128	130	80.68	80.7	88.82	3.303	3.329	3.313	0.86	2.18	4	*P. wuellerstorfi*
C	9	H	5	80	82	81.7	81.72	89.84	3.331	3.359	3.349	0.98	2.13	4	*P. wuellerstorfi*
A	9	H	7	47	49	81.55	81.57	89.92	3.333	3.361	3.352	0.96	2.25	4	*P. wuellerstorfi*
C	9	H	5	124	126	82.14	82.16	90.28	3.341	3.370	3.365	0.8	1.83	4	*P. wuellerstorfi*
C	9	H	6	18	20	82.58	82.6	90.72	3.350	3.384	3.380	0.9	2.25	4	*P. wuellerstorfi*
C	9	H	6	62	64	83.02	83.04	91.16	3.360	3.398	3.395	1.01	1.9	4	*P. wuellerstorfi*
C	9	H	6	106	108	83.46	83.48	91.6	3.370	3.410	3.401	0.47	2.15	4	*P. wuellerstorfi*

C	10	H	1	82	84	85.22	85.24	93.74	3.417	3.446	3.429	0.62	2.14	4	*C. mundulus*
C	10	H	1	126	128	85.66	85.68	94.18	3.427	3.453	3.434	0.86	2.06	4	*C. mundulus*
C	10	H	2	20	22	86.1	86.12	94.62	3.437	3.458	3.440	0.82	1.59	4	*P. wuellerstorfi*
C	10	H	2	64	66	86.54	86.56	95.06	3.446	3.464	3.448	0.95	1.75	4	*P. wuellerstorfi*
A	10	H	3	119	121	85.81	85.83	95.1	3.447	3.465	3.449	0.89	1.87	4	*C. mundulus*
C	10	H	2	108	110	86.98	87	95.5	3.456	3.470	3.456	0.82	1.86	4	*P. wuellerstorfi*
C	10	H	3	44	46	87.86	87.88	96.38	3.476	3.482	3.472	0.92	2	4	*C. mundulus*
C	10	H	3	88	90	88.3	88.32	96.82	3.485	3.488	3.480	0.88	1.37	3	*P. wuellerstorfi*
C	10	H	3	132	134	88.74	88.76	97.26	3.495	3.495	3.490	0.97	1.87	4	*P. wuellerstorfi*
C	10	H	4	26	28	89.18	89.2	97.7	3.505	3.503	3.500	0.92	1.69	4	*P. wuellerstorfi*
A	10	H	5	92	94	88.48	88.5	97.77	3.506	3.504	3.502	0.94	1.76	4	*P. wuellerstorfi*
C	10	H	4	70	72	89.62	89.64	98.14	3.514	3.510	3.510	1.04	1.86	4	*P. wuellerstorfi*
C	10	H	4	114	116	90.06	90.08	98.58	3.524	3.518	3.520	0.72	1.97	4	*C. mundulus*
C	10	H	5	49	51	90.94	90.96	99.46	3.544	3.540	3.540	0.84	1.72	4	*P. wuellerstorfi*
C	10	H	5	93	95	91.38	91.4	99.9	3.553	3.547	3.548	1.02	2.02	4	*P. wuellerstorfi*
C	10	H	5	137	139	91.82	91.84	100.34	3.563	3.557	3.555	1.1	1.92	3	*P. wuellerstorfi*
C	10	H	6	31	33	92.26	92.28	100.78	3.573	3.568	3.563	1.09	1.94	4	*P. wuellerstorfi*
C	10	H	6	75	77	92.7	92.72	101.22	3.582	3.580	3.570	1.07	1.76	4	*P. wuellerstorfi*
C	10	H	6	121	123	93.16	93.18	101.68	3.593	3.593	3.591	1.05	1.92	3	*P. wuellerstorfi*
C	10	H	7	13	15	93.58	93.6	102.1	3.600	3.600	3.610	1.24	1.85	4	*P. wuellerstorfi*
C	10	H	7	57	59	94.02	94.04	102.54	3.608	3.610	3.615	1.19	2.1	4	*P. wuellerstorfi*
C	11	H	1	100	102	94.9	94.92	104.23	3.636	3.644	3.635	1.28	2.02	4	*P. wuellerstorfi*
C	11	H	2	38	40	95.78	95.8	105.11	3.650	3.659	3.645	1.14	2.05	4	*C. mundulus*
C	11	H	2	82	84	96.22	96.24	105.55	3.657	3.666	3.650	1.16	1.73	4	*C. mundulus*
A	11	H	4	19	21	95.71	95.73	105.82	3.662	3.669	3.654	0.96	1.98	4	*P. wuellerstorfi*
C	11	H	2	126	128	96.66	96.68	105.99	3.665	3.671	3.657	0.88	1.98	4	*P. wuellerstorfi*
C	11	H	3	26	28	97.16	97.18	106.49	3.673	3.678	3.664	1	2.01	3	*P. wuellerstorfi*
A	11	H	4	115	117	96.67	96.69	106.78	3.678	3.683	3.669	1.06	1.97	4	*P. wuellerstorfi*
C	11	H	3	64	66	97.54	97.56	106.87	3.679	3.684	3.670	0.97	2.18	4	*P. wuellerstorfi*
C	11	H	3	108	110	97.98	98	107.31	3.687	3.689	3.677	0.86	2.3	4	*C. mundulus*
C	11	H	4	46	48	98.86	98.88	108.19	3.701	3.705	3.690	0.76	1.52	3	*C. robertsonanius*
C	11	H	4	46	48	98.86	98.88	108.19	3.701	3.705	3.690	0.76	1.52	3	*C. robertsonanius*
C	11	H	4	93	95	99.33	99.35	108.66	3.709	3.714	3.702	0.98	2.27	4	*P. wuellerstorfi*
C	11	H	4	134	136	99.74	99.76	109.07	3.716	3.721	3.713	0.78	2.03	4	*P. wuellerstorfi*
C	11	H	5	32	34	100.18	100.2	109.51	3.723	3.729	3.725	1.14	1.69	4	*P. wuellerstorfi*
A	11	H	6	116	118	99.63	99.65	109.74	3.727	3.734	3.729	1.16	1.83	5	*C. mundulus*
C	11	H	5	120	122	101.06	101.08	110.39	3.738	3.747	3.741	0.85	2.18	4	*P. wuellerstorfi*
C	11	H	6	19	21	101.5	101.52	110.83	3.745	3.756	3.749	0.76	2.18	4	*P. wuellerstorfi*
C	11	H	6	63	65	101.94	101.96	111.27	3.752	3.764	3.757	0.96	2.07	4	*P. wuellerstorfi*

C	11	H	6	107	109	102.38	102.4	111.71	3.759	3.772	3.765	0.92	1.82	3	*P. wuellerstorfi*
C	11	H	7	45	47	103.26	103.28	112.59	3.774	3.787	3.782	1.02	1.79	4	*P. wuellerstorfi*
C	12	H	1	74	76	104.14	104.16	114.5	3.806	3.820	3.820	0.75	1.88	4	*P. wuellerstorfi*
C	12	H	1	127	129	104.67	104.69	115.03	3.814	3.830	3.832	1.04	2.08	4	*P. wuellerstorfi*
C	12	H	2	12	14	105.02	105.04	115.38	3.820	3.835	3.840	1.01	1.87	3	*P. wuellerstorfi*
C	12	H	2	54	56	105.44	105.46	115.8	3.827	3.841	3.850	0.51	1.72	4	*P. wuellerstorfi*
A	12	H	3	38	40	103.98	104	115.87	3.828	3.842	3.852	0.94	1.99	4	*C. mundulus*
C	12	H	2	100	102	105.9	105.92	116.26	3.835	3.847	3.864	1.1	2.24	4	*P. wuellerstorfi*
C	12	H	3	35	37	106.78	106.8	117.14	3.849	3.858	3.890	0.42	1.75	4	*C. mundulus*
A	12	H	4	33	35	105.43	105.45	117.32	3.852	3.860	3.892	0.91	1.81	4	*P. wuellerstorfi*
C	12	H	3	79	81	107.22	107.24	117.58	3.857	3.864	3.894	0.67	2.12	4	*P. wuellerstorfi*
C	12	H	3	120	122	107.63	107.65	117.99	3.863	3.869	3.898	0.64	2.3	4	*C. mundulus*
C	12	H	4	17	19	108.1	108.12	118.46	3.871	3.874	3.902	0.92	2.02	3	*P. wuellerstorfi*
C	12	H	4	105	107	108.98	109	119.34	3.886	3.878	3.910	0.95	1.84	3	*P. wuellerstorfi*
A	13	H	1	93	95	108.23	108.25	119.88	3.895	3.886	3.914	0.94	1.94	4	*P. wuellerstorfi*
C	12	H	5	47	49	109.86	109.88	120.22	3.900	3.891	3.917	1.1	2	4	*P. wuellerstorfi*
C	12	H	5	91	93	110.3	110.32	120.66	3.907	3.898	3.921	0.78	2.11	3	*P. wuellerstorfi*
C	12	H	6	29	31	111.18	111.2	121.54	3.922	3.913	3.928	1.03	2.21	4	*P. wuellerstorfi*
C	12	H	6	73	75	111.62	111.64	121.98	3.929	3.921	3.931	0.9	2.11	4	*C. mundulus*
C	12	H	6	117	119	112.06	112.08	122.42	3.937	3.930	3.935	1.04	1.72	3	*P. wuellerstorfi*
A	13	H	3	82	84	111.12	111.14	122.77	3.942	3.937	3.943	1.14	1.93	4	*P. wuellerstorfi*
C	12	H	7	30	32	112.5	112.52	122.86	3.944	3.939	3.945	1.07	1.74	4	*P. wuellerstorfi*
C	13	H	1	48	50	113.38	113.4	124.53	3.971	3.971	3.985	1.64	-1.81	7	*G. ruber*
C	13	H	1	48	50	113.38	113.4	124.53	3.971	3.971	3.985	0.78	1.77	5	*P. wuellerstorfi*
C	13	H	1	92	94	113.82	113.84	124.97	3.979	3.980	3.995	0.66	1.92	5	*P. wuellerstorfi*
C	13	H	1	136	138	114.26	114.28	125.41	3.986	3.990	4.010	0.98	1.78	5	*P. wuellerstorfi*
A	13	H	5	48	50	113.78	113.8	125.43	3.986	3.991	4.011	0.91	1.79	5	*P. wuellerstorfi*
C	13	H	2	30	32	114.7	114.72	125.85	3.993	4.000	4.025	1.05	1.8	5	*P. wuellerstorfi*
C	13	H	2	74	76	115.14	115.16	126.29	4.001	4.011	4.040	1.06	2.15	4	*P. wuellerstorfi*
C	13	H	2	118	120	115.58	115.6	126.73	4.008	4.021	4.047	1.02	2	5	*P. wuellerstorfi*
C	13	H	3	11	13	116.02	116.04	127.17	4.015	4.031	4.054	0.8	1.97	5	*P. wuellerstorfi*
A	14	H	2	30	32	117.7	117.72	130.19	4.065	4.096	4.102	0.92	2.05	5	*P. wuellerstorfi*
A	14	H	2	30	32	117.7	117.72	130.19	4.065	4.096	4.102	0.89	2.05	5	*P. wuellerstorfi*
A	14	H	2	30	32	117.7	117.72	130.19	4.065	4.096	4.102	0.86	2.2	4	*P. wuellerstorfi*
A	14	H	3	56	58	119.46	119.48	131.95	4.094	4.132	4.130	0.91	1.49	6	*P. wuellerstorfi*
C	14	H	1	40	42	120.8	120.82	132.53	4.104	4.141	4.136	1.01	1.76	5	*P. wuellerstorfi*
C	14	H	1	90	92	121.3	121.32	133.03	4.112	4.149	4.141	0.84	1.84	6	*P. wuellerstorfi*
C	14	H	1	134	136	121.74	121.76	133.47	4.119	4.155	4.145	0.98	1.83	4	*P. wuellerstorfi*
C	14	H	2	73	75	122.62	122.64	134.35	4.134	4.165	4.154	1.04	2.07	5	*P. wuellerstorfi*

A	14	H	5	25	27	122.16	122.18	134.65	4.139	4.169	4.157	0.78	2.04	4	*C. mundulus*
A	14	H	5	25	27	122.16	122.18	134.65	4.139	4.169	4.157	1.24	1.76	4	*P. wuellerstorfi*
A	14	H	5	25	27	122.16	122.18	134.65	4.139	4.169	4.157	1.24	1.76	4	*P. wuellerstorfi*
C	14	H	3	99	101	124.38	124.4	136.11	4.163	4.174	4.172	0.86	1.9	4	*P. wuellerstorfi*
C	14	H	4	50	52	125.26	125.28	136.99	4.178	4.182	4.181	1.08	2.01	5	*P. wuellerstorfi*
C	14	H	4	94	96	125.7	125.72	137.43	4.185	4.189	4.185	0.88	1.64	4	*P. wuellerstorfi*
C	14	H	5	34	36	126.58	126.6	138.31	4.201	4.201	4.200	0.78	1.7	3	*P. wuellerstorfi*
C	14	H	5	78	80	127.02	127.04	138.75	4.209	4.208	4.208	0.57	2.07	4	*C. mundulus*
C	14	H	5	122	124	127.46	127.48	139.19	4.218	4.215	4.215	0.42	1.64	3	*P. wuellerstorfi*
C	14	H	6	16	18	127.9	127.92	139.63	4.226	4.224	4.224	0.86	1.77	3	*P. wuellerstorfi*
C	14	H	6	60	62	128.34	128.36	140.07	4.234	4.232	4.232	0.9	1.95	3	*P. wuellerstorfi*
C	14	H	6	60	62	128.34	128.36	140.07	4.234	4.232	4.232	0.53	1.7	3	*P. wuellerstorfi*
C	14	H	6	60	62	128.34	128.36	140.07	4.234	4.232	4.232	0.64	1.68	3	*P. wuellerstorfi*
A	15	H	1	99	101	126.39	126.41	140.47	4.241	4.240	4.240	0.68	1.89	5	*P. wuellerstorfi*
C	14	H	6	104	106	128.78	128.8	140.51	4.242	4.241	4.241	0.62	2.03	4	*C. mundulus*
C	14	H	7	46	48	129.66	129.68	141.39	4.259	4.259	4.259	1.02	2.11	3	*P. wuellerstorfi*
A	15	H	2	148	150	128.38	128.4	142.46	4.279	4.281	4.280	1	1.85	3	*P. wuellerstorfi*
A	15	H	2	148	150	128.38	128.4	142.46	4.279	4.281	4.280	0.95	1.71	3	*P. wuellerstorfi*
C	15	H	1	26	28	130.16	130.18	143.23	4.293	4.296	4.302	0.86	1.96	3	*P. wuellerstorfi*
C	15	H	1	64	66	130.54	130.56	143.61	4.300	4.305	4.313	0.8	1.86	3	*P. wuellerstorfi*
C	15	H	1	108	110	130.98	131	144.05	4.310	4.314	4.325	0.86	1.75	3	*P. wuellerstorfi*
C	15	H	2	45	47	131.86	131.88	144.93	4.331	4.332	4.335	0.99	1.99	3	*P. wuellerstorfi*
C	15	H	2	89	91	132.3	132.32	145.37	4.341	4.340	4.340	0.82	1.61	3	*P. wuellerstorfi*
A	15	H	5	23	25	131.64	131.66	145.72	4.349	4.347	4.347	1.61	-1.78	5	*G. ruber*
A	15	H	5	23	25	131.64	131.66	145.72	4.349	4.347	4.347	1.18	1.89	3	*P. wuellerstorfi*
C	15	H	2	133	135	132.74	132.76	145.81	4.352	4.349	4.349	1.12	1.87	3	*P. wuellerstorfi*
C	15	H	3	25	27	133.18	133.2	146.25	4.362	4.358	4.358	1.05	2.11	3	*P. wuellerstorfi*
C	15	H	3	69	71	133.62	133.64	146.69	4.372	4.363	4.367	0.99	2.07	3	*P. wuellerstorfi*
C	15	H	3	113	115	134.06	134.08	147.13	4.382	4.372	4.376	1.16	2.07	3	*P. wuellerstorfi*
C	15	H	4	7	9	134.5	134.52	147.57	4.393	4.379	4.385	1.22	1.77	3	*P. wuellerstorfi*
C	15	H	4	50	52	134.93	134.95	148	4.403	4.381	4.398	0.85	1.58	3	*P. wuellerstorfi*
C	15	H	4	50	52	134.93	134.95	148	4.403	4.381	4.398	1.18	1.97	3	*P. wuellerstorfi*
C	15	H	4	50	52	134.93	134.95	148	4.403	4.381	4.398	1.26	1.89	3	*P. wuellerstorfi*
C	15	H	4	95	97	135.38	135.4	148.45	4.413	4.393	4.413	1.05	2.04	4	*P. wuellerstorfi*
C	15	H	4	139	141	135.82	135.84	148.89	4.424	4.405	4.426	1.12	2.11	4	*P. wuellerstorfi*
A	15	H	7	48	50	134.9	134.92	148.98	4.426	4.408	4.429	1.08	2.01	4	*C. mundulus*
A	15	H	7	48	50	134.9	134.92	148.98	4.426	4.408	4.429	2.15	-1.88	3	*G. ruber*
C	15	H	5	34	36	136.26	136.28	149.33	4.434	4.417	4.440	1.25	1.91	3	*P. wuellerstorfi*
C	15	H	5	78	80	136.7	136.72	149.77	4.444	4.430	4.449	1.05	2.03	3	*P. wuellerstorfi*

C	**15**	**H**	**5**	**122**	**124**	137.14	137.16	150.21	4.454	4.442	4.458	1.02	2.15	4	*C. mundulus*
C	**15**	**H**	**6**	**18**	**20**	137.58	137.6	150.65	4.465	4.454	4.466	0.96	1.98	4	*C. mundulus*
C	**15**	**H**	**6**	**62**	**64**	138.02	138.04	151.09	4.475	4.466	4.475	1.01	1.97	2	*C. mundulus*
C	**15**	**H**	**6**	**106**	**108**	138.46	138.48	151.53	4.485	4.479	4.487	0.93	2	3	*C. mundulus*
C	**15**	**H**	**7**	**79**	**81**	139.69	139.71	152.76	4.514	4.513	4.520	1.12	1.83	3	*P. wuellerstorfi*

APPENDIX F

TAXON TABLE: CODE FOR THE R-PROGRAMMING ENVIRONMENT

#Code that follows automatically generates occurance tables. ‘tax’ must be a table of occurances. If species is present in a sample, any character can be used, if it is absent the cell must be empty.

```
read.csv('YOUR .csv FILE HERE')->tax

#####Occurance Table###
##Andrew J. Fraass - 2015###

#Table must be organized with several key columns:
  #Site,H,Co,Sec,B,T
        #H=Hole, Co=Core, Sec=Section, B=Bottom cm, T=Top cm
  #if absent, samples will not be labeled.
  #must be organized so that taxon columns are the last columns

##Variables##
#First Column with taxon
ftr<-27

#Order?
#FAD,LAD,Alph
ord<-"FAD"

#Zonation
zone1<-14 #column number with zone scheme #1
zone2<-23 #column number with zone scheme #2


"%w/o%" <- function(x, y) x[!x %in% y] #--  x without y
par(mfcol=c(1,1))
s.t<-NA

if(ord == "FAD"){
  for(i in ftr:length(colnames(tax))){
    max(which(tax[,i] != ""))->s.t[i]
  }
  order(s.t,decreasing=TRUE)->s.t
  s.t %w/o% 1:{ftr-1}->s.t
}
```

```
if(ord == "LAD"){
  for(i in ftr:length(colnames(tax))){
    min(which(tax[,i] != ""))->s.t[i]
  }
  order(s.t,decreasing=TRUE)->s.t
  s.t %w/o% 1:{ftr-1}->s.t
}

if(ord == "Alph"){
  order(colnames(tax))->s.t
  s.t %w/o% 1:26->s.t
}

plot(0,0,
     xlim=c({ftr-10},length(colnames(tax))+5),
     ylim=c(length(rownames(tax)),-10),
    # xlab='taxa',
    # ylab='samples',
    xlab='',
    ylab='',
     axes=F)
segments(c({ftr-1}:length(colnames(tax))),
         0,
         c({ftr-1}:length(colnames(tax))),
         length(rownames(tax)),
         col='grey90')
segments({ftr-1},
         0:length(rownames(tax)),
         length(colnames(tax)),
         0:length(rownames(tax)),
         col='grey90')

for(i in ftr:length(colnames(tax))){
  for(o in 1:length(rownames(tax))){
    if(tax[o,s.t[i-{ftr-1}]] != ""){
      polygon(c(i-.85,i-.85,i,i),
              c(o,o-1,o-1,o),
              col='black',
              border=NA)
    }
  }
}
text(ftr:length(colnames(tax)),
     -1,
     colnames(tax)[s.t],
```

```
    cex=.5,
    adj=c(0,0)
    ,srt=75)

text({ftr-12},
    1:length(rownames(tax)),
    paste(tax$Site,
        tax$H,
        "/",
        tax$Co,
        '/',
        tax$Sec,
        '/',
        tax$B,
        '-',
        tax$T
        ,sep=''),
    cex=.5,
    adj=c(0,0))

text(length(colnames(tax))+2,
    1:length(rownames(tax))-.5,
    tax[,zone1],
    cex=.5)
text(length(colnames(tax))+6,
    1:length(rownames(tax))-.5,
    tax[,23],
    cex=.5)
```

APPENDIX G

AGE MODELS FOR MI-1: SITES 78, 744, AND 803

The following tables are the age models for DSDP Site 78, and ODP Sites 744 and 803. Abbreviations are as follows:

Rad=Radiolarian

Nanno=Calcareous Nannofossil

Foram=Planktic Foraminifera

Diat=Diatom

Stron=Strontium Isotope (Bu=Bulk, P=Planktic foraminifera)

Iso=Chemostratigraphic (stable isotope) control point

Pmag=Paleomagnetic Reversal

T=Top

B=Bottom

Tc=Top common occurance

Bc=Bottom common occurance

'Use' entries in 'Composite?' column mean that datum was used in the age model.

'Source' refers to the source of the stratigraphic (depth) position of the datum, while 'Age source' refers to the source of the chronostratigraphic (age) calibration for the datum.

G.1 DSDP Site 78 Age Model

Datum.Type	T/B	Datum	Age	Max Depth	Min Depth	Depth (m)	Composite?	Primary	Source	Age source	Age Notes
Rad	T	*D. violina*	14.2	21.2	19.7	20.45			ShipboardBio	PEAT	
Rad	T	*D. forcipata*	14.68	27.4	26.2	26.8			ShipboardBio	PEAT	
Rad	T	*D. prismatica*	15.17	36.6	34.9	35.75			ShipboardBio	PEAT	
Rad	B	*A. octopylus* (upper)	15.75	28.9	27.4	28.15			ShipboardBio	PEAT	
Rad	B	*C. costata*	17.49	34.9	33.4	34.15	Use	Yes	ShipboardBio	PEAT	
Rad	B	*L. stauropora*	17.72	38.6	36.6	37.6			ShipboardBio	PEAT	
Nanno	T	*S. belemnos*	17.96	36.6	34.9	35.75			ShipboardBio	Backman	

Rad	T	*D. simplex*	18.69	39.6	38.6	39.1			ShipboardBio	PEAT	
Nanno	B	*S. belemnos*	19.01	51.7	50.2	50.95	Use	Yes	ShipboardBio	Backman	
Rad	B	*D. simplex*	20.34	140.1	137.1	138.6			ShipboardBio	PEAT	
Nanno	B	*H. ampliaperta*	20.43	38.6	36.6	37.6			ShipboardBio	Backman	
Rad	T	*T. annosa*	21.3	103.6	100.6	102.1	Use	Yes	ShipboardBio	Kamikuri et al	
Rad	B	*C. virginis*	21.39	111.5	110	110.75			ShipboardBio	PEAT	
Nanno	T	*T. carinatus*	22.10	27.4	26.2	26.8			ShipboardBio	Backman	
Rad	B	*C. cornuta*	22.4	120.9	118.9	119.9	Use		ShipboardBio	Kamikuri et al	
Foram	B	*G. dehiscens*	22.44	124.9	118.9	121.9	Use	Yes	ShipboardBio	WadeAstro	Calibrated to Lourens
Nanno	B	*D. druggi*	22.59	135.5	134	134.75	Use		ShipboardBio	Backman	
Rad	T	*A. gracilis*	22.8	137.1	135.5	136.3			ShipboardBio	Kamikuri et al	
Foram	T	*G. ciperoensis*	22.90	85.3	82.3	83.8			ShipboardBio	WadeAstro	Calibrated to Lourens
Foram	B	*G. trilobus*	22.96	128	124.9	126.45			ShipboardBio	WadeAstro	Calibrated to Lourens
Foram	B	*P. kugleri*	22.96	143.1	140.1	141.6		Yes	ShipboardBio	WadeAstro	Calibrated to Lourens
Foram	B	*P. kugleri*	22.96	143.07	142.57	142.82		Yes	Fraass	WadeAstro	Calibrated to Lourens
Iso	X	Mi-1	23.0	144.07	143.070	143.57	Use		Fraass	Liebrand	
Rad	T	*D. papilio*	23.31	148.3	146.3	147.3	Use		ShipboardBio	PEAT	
Rad	T	*L. longicornuta*	23.9	128	126.4	127.2			ShipboardBio	Kamikuri et al	
Nanno	T	*S. ciperoensis*	24.364	172.1	170.6	171.35			ShipboardBio	Palike et al	Calibrated to Palike06 (mean between both ages)
Foram	B	*P. pseudokugleri*	25.2	164.6	161.4	163	Use	Yes	ShipboardBio	WadeAstro	Calibrated to Palike 06
Foram	B	*G. primordius*	26.1	134	128	131			ShipboardBio	WadeAstro	Calibrated to Palike 06
Nanno	T	*S. distentus*	27.5	208.7	207.2	207.95			ShipboardBio	Berggren95	Compared to Berggren95 (untuned)
Nanno	T	*S. predistentus*	27.5	226.9	225.4	226.15			ShipboardBio	Berggren95	Compared to Berggren95 (untuned)

Nanno	T	*S. pseudoradians*	29.1	246.9	237.7	242.3	Use		ShipboardBio	Berggren95	Compared to Berggren95 (untuned)

G.2 ODP Site 744 Age Model

Datum.Type	Top/Base	Datum	Age	Max Depth	Min Depth	Depth (mbsf)	Composite?	Source	Age source
Rad	T	*L. conica*	13.31	58.08	56.08	57.08		Florindo13, HRM	Florindo13, HRM
Pmag	B	C5Dr.1n?	17.74			82.4	Use	Florindo13	Uses age calibrated to Lourens 04
Pmag	T	C5En	18.056			83.6	Use	Florindo13	Uses age calibrated to Lourens 04
Rad	T	*T. clavipes*	18.02	86.81	84.81	85.81		Florindo13, HRM	Florindo13, HRM
Pmag	B	C5En	18.524			86.6	Use	Florindo13	Uses age calibrated to Lourens 04
Pmag	T	C6n	18.748			89.6		Florindo13	Uses age calibrated to Lourens 04
Rad	T	*A. medusa*	18.51	95.09	93.09	94.09		Florindo13, HRM	Florindo13, HRM
Pmag	B	C6n	19.722			94.9		Florindo13	Uses age calibrated to Lourens 04
Nanno	B	*N. maleinterpretaria*	18.8	97.8	93.3	95.55			
Pmag	T	C6An.1n	20.040			95.9	Use	Florindo13	Uses age calibrated to Lourens 04
Rad	T	*A. medusa*	18.38	96.3	98.3	97.3			
Diat	B	*R. marylandicus*	18.46	96.3	98.3	97.3			
Pmag	B	*C6An.2n*	20.709			98.4	Use	Florindo13	Uses age calibrated to Lourens 04
Pmag	T	C7An	24.756			98.9		Salamy99	
Rad	T	*C. robusta*	21.04	98	100	99			
Rad	T	*C. robusta*	21.43	99.5	98.5	99		Florindo13, HRM	Florindo13, HRM
Core Break	X	Fraass Alt	22.786			99		Fraass Alt	
Iso	X	Mi-1	23.0			99.32			
Pmag	T	C6Cn.2n	22.854			99.325	Use	Fraass Alt	Uses age calibrated to Lourens 04
Pmag	T	C6Cn.3n	23.278			99.325		Roberts03	Uses age calibrated to Lourens 04
Diat	B	*R. marylandicus*	22.73	99.97	98.97	99.47		Florindo13, HRM	Florindo13, HRM

Diat	B	*C. miocenicus*	22.60	98.53	100.53	99.53			
Pmag	B	C6Cn.3n	23.340			100.1432	Use	Roberts03	Uses age calibrated to Lourens 04
Pmag	B	C7An	24.984			100.24		Salamy99	
Diat	B	C. miocenicus	23.98	100.75	99.75	100.25		Florindo13, HRM	Florindo13, HRM
Rad	T	*L. robusta*	23.44	101.25	99.25	100.25		Florindo13, HRM	Florindo13, HRM
Rad	T	*S. radiosa*	23.51	100.75	99.75	100.25		Florindo13, HRM	Florindo13, HRM
Diat	B	*T. spinosa* group	23.54	99.25	101.25	100.25			
Diat	B	*T. spinosa* group	23.58	100.75	99.75	100.25		Florindo13, HRM	Florindo13, HRM
Sr		12H-2,96-101	24.65			101.67		Barerra	MacArthur
Rad	T	*S. radiosa*	23.71	101	103	102			
Pmag	B	C6Cn.3n	23.340			102.2		Fraass16	Uses age calibrated to Lourens 04
Pmag	T	C7n.1n	24.022			103.7048	Use	Roberts03	Uses age calibrated to Lourens 04
Pmag	T	C7n.2n	24.109			103.7048			
Pmag	T	C7n.1n	24.022	103.54	103.96	103.75		Florindo13	Uses age calibrated to Lourens 04
Nanno	T	*R. bisecta*	25.4	109	99	104			
Nanno	B	*R. gelida v. schraderi*	23.6	107.3	101.3	104.3			
Sr		12H-4,95-100	24.85			104.67		Barerra	MacArthur
Pmag	T	C8n.1n	25.11			104.79		Salamy99	
Rad	B	*E. teuscheri*	24.71	105.5	104.5	105		Florindo13, HRM	Florindo13, HRM
HIATUS	X	HIATUS	24.279			105.05	Use	Fraass Alt	
HIATUS	X	HIATUS	26.148			105.05000001	Use	Fraass Alt	
Diat	T	*R. vigilans*	25.38	106.06	104.06	105.06		Florindo13, HRM	Florindo13, HRM
Sr		12H-5,95-100	25.65			106.17		Barerra	MacArthur
Pmag	T	C9n	26.508			106.5176	Use	Roberts03	
Pmag	B	C8n.2n	26.032			111.82		Salamy99	
Pmag	B	C9n	27.826			111.8943	Use	Roberts03	
Rad	B	*A. medusa*	25.73	111	113	112			
Pmag	B	C9n	27.826			112		Florindo13	
Foram	T	*C. cubensis*	28.5	118.2	108.7	113.45		ShipboardBio	Huber05
Pmag	T	C9n	26.508			115.3		Salamy99	
Pmag	T	C10n.2n	28.186			115.5	Use	Florindo13	
Pmag	T	C10n.1n	28.126			115.5176		Roberts03	

Rad	B	*C. golli*	28.2	118.5	117.5	118		Florindo13, HRM	Florindo13, HRM
Pmag	B	C11n.2n	29.957			118.37	Use	Salamy99	Palike06
Pmag	T	C12n	30.617			119.36	Use	Salamy99	Palike06
Pmag	T	C12n	30.617			119.5154		Roberts03	Palike06
Foram	T	*G. angiporoides*	30	127.7	118.2	122.95		ShipboardBio	Huber05
Pmag	B	C12n	31.021			124.6696		Roberts03	Palike06
Pmag	B	C12n	31.021			124.89	Use	Salamy99	Palike06
Rad	B	*S. osculosa*	28.22	128.5	127.5	128		Florindo13, HRM	Florindo13, HRM
Rad	B	*S. universus*	28.21	128.5	127.5	128		Florindo13, HRM	Florindo13, HRM
Rad	B	*C. conica-cosma*	28.23	131.5	130.5	131		Florindo13, HRM	Florindo13, HRM
Pmag	T	C13n.1	33.232			139.1189		Roberts03	Palike06
Pmag	T	C13n.1	33.232			139.25	Use	Salamy99	Palike06
Rad	B	*A. medusa*	28.44	143	141	142		Florindo13, HRM	Florindo13, HRM
Diat	B	*A. oligocenia*	28.45	143	141	142		Florindo13, HRM	Florindo13, HRM
Diat	B	*A. oligocenicus*	28.45	143	141	142		Florindo13, HRM	Florindo13, HRM
Diat	B	*A. symmetricus*	28.43	143	141	142		Florindo13, HRM	Florindo13, HRM
Diat	B	*B. veniamini*	28.37	143	141	142		Florindo13, HRM	Florindo13, HRM
Rad	B	*C. robusta*	28.29	142.5	141.5	142		Florindo13, HRM	Florindo13, HRM
Rad	B	*L. conica*	28.32	143	141	142		Florindo13, HRM	Florindo13, HRM
Rad	B	*L. hayesi hayesi*	28.28	142.5	141.5	142		Florindo13, HRM	Florindo13, HRM
Rad	B	*L. robusta*	285.27	142.5	141.5	142		Florindo13, HRM	Florindo13, HRM
Rad	B	*P. frakesi*	28.25	142.5	141.5	142		Florindo13, HRM	Florindo13, HRM
Rad	B	*P. frakesi*	28.45	141	143	142			
Diat	B	*R. gelida*	28.38	143	141	142		Florindo13, HRM	Florindo13, HRM
Diat	B	*R. vigilans*	28.41	143	141	142		Florindo13, HRM	Florindo13, HRM
Rad	B	*S. radiosa*	28.33	143	141	142		Florindo13, HRM	Florindo13, HRM
Rad	B	*T. clavipes*	28.26	142.5	141.5	142		Florindo13, HRM	Florindo13, HRM
Pmag	B	C13n.2	34.285			146.64	Use	Salamy99	Palike06
Iso	X	Oi-1	34.285			146.64	Use	Salamy99	
Pmag	B	C13n.2	34.285			146.7841		Roberts03	Palike06
Pmag	T	C15n.1	35.126			155.3855		Roberts03	Palike06

Pmag	T	C15n.1	35.126			155.65	Use	Salamy99	Palike06
Pmag	B	C15n.2	35.254			157.0815		Roberts03	Palike06
Pmag	B	C15n.2	35.254			158.1	Use	Salamy99	Palike06
Pmag	T	C16.1	35.328			161.6	Use	Salamy99	Palike06

G.3 ODP Site 803 Age Model

Datum. Type	T/B	Datum	Depth (mbsf)	Age	Max Depth	Min Depth	Age Err	Composite?	Primary	Source	Age source	Age Notes
Nanno	B	*S. belemnos*	254.15	19.01	255.5	252.8		Use		Shipboard	Backman	
Stron	Bu		289.14	21.85			0.15			Barrera	MacArthur	
Foram	B	*G. binaiensis*	254.15	22.1	255.5	252.8				Shipboard	Berggren95	Compared to Berggren95 (untuned)
Nanno	Tc	*T. carinatus*	308.15	22.10	313	303.3		Use	Yes	Shipboard	Backman	rough estimate for sample depth, this is the top common date
Foram	B	*G. dehiscens*	319.235	22.44	321.99	316.48			Yes	Leckie93	WadeAstro	Calibrated to Lourens
Stron	P		313.42	22.95			0.2			Barrera	MacArthur	
Stron	P		318.27	22.95			0.15			Barrera	MacArthur	
Foram	B	*P. kugleri*	320.75	22.96	320.75	320.25			Yes	Fraass	WadeAstro	Calibrated to Lourens
Foram	B	*P. kugleri*	320.755	22.96	319.5	322.01			Yes	Leckie93	WadeAstro	Calibrated to Lourens
Iso	X	Mi-1 Max	320.25	23	320.75	319.75		Use		Fraass		
Stron	Bu		318.27	23.15			0.15			Barrera	MacArthur	
Foram	T	*T. gemma*	368.395	23.5	368.81	367.98				Leckie93	WadeAstro	
Nanno	T	*S. ciperoensis*	364.745	24.364	368.83	360.66				Shipboard	Palike 06	Uses age calibrated to Palike 06 (average between both ages)
Stron	Bu		342.44	24.8			0.2			Barrera	MacArthur	
Foram	B	*P. pseudokugleri*	361.25	25.2	360.67	361.83			Yes	Leckie93	WadeAstro	Calibrated to Lourens
Stron	Bu		308.47	25.5			0.25			Barrera	MacArthur	
Stron	Bu		356.48	25.5			0.15			Barrera	MacArthur	
Stron	Bu		390.91	25.5			0.25			Barrera	MacArthur	
Stron	Bu		382.88	26.05			0.2			Barrera	MacArthur	
Foram	B	*G. primordius*	361.24	26.1	360.66	361.82				Leckie93	WadeAstro	Calibrated to Palike 06

Stron	Bu		366.17	26.75			0.2			Barrera	MacArthur	
Stron	P		390.91	27.15	390.9	390.92	0.2	Use		Barrera	MacArthur	
Foram	T	*P. opima*	383.01	30.8	381.24	384.78		Use	Yes	Leckie93	WadeAstro	Calibrated to Palike 06

APPENDIX H

STABLE ISOTOPE DATA FOR MI-1: SITES 78, 744, AND 803

This appendix contains all the stable isotope data for Chapter 3. Abbreviations are as follos: Size fractions (sf), number of individuals in each analysis (#ind), preservation (Pres.; graded on a 1-5 scale with 5 being poor preservation and 1 being excellent preservation). *P. may-sia* is the *Paragloborotalia mayeri – siakensis* plexus, *P. pseudok-kugleri* is a mixture of *Paragloborotalia pseudokugleri* and *Paragloborotalia kugleri*.

H.1 Stable Isotope Data from Site 78

Site	H	Co	T	Sec	T	B	Depth	Pres.	#Ind	Species	sf	δ13C	δ18O	Lab
78	*	15	R	2	125	127	130.98	3	10	*P. pseudok-kugleri*	149-250	2.16	-0.57	UCDavis
78	*	15	R	3	25	27	131.48	4	10	*P. pseudok-kugleri*	149-250	1.87	-0.80	UCDavis
78	*	15	R	4	25	27	132.98	3	10	*P. pseudok-kugleri*	149-250	2.08	-0.47	UCDavis
78	*	15	R	4	125	127	133.98	3	10	*P. pseudok-kugleri*	149-250	1.67	-0.45	UCDavis
78	*	15	R	5	25	27	134.48	4	10	*P. pseudok-kugleri*	149-250	2.04	-0.63	UCDavis
78	*	15	R	5	75	77	134.98		11	*P. may-sia*	150-250	1.43	0.16	UMass
78	*	15	R	5	125	127	135.48		11	*P. may-sia*	150-250	1.45	-0.02	UMass
78	*	15	R	5	125	127	135.48	4	8	*P. pseudok-kugleri*	149-250	1.65	-0.54	UCDavis
78	*	15	R	6	25	27	135.98		12	*P. may-sia*	150-250	1.31	0.02	UMass
78	*	15	R	6	75	77	136.48		16	*P. may-sia*	150-250	1.14	-0.01	UMass
78	*	15	R	6	125	127	136.98		16	*P. may-sia*	150-250	1.69	-0.29	UMass
78	*	15	R	6	125	127	136.98	5	8	*P. pseudok-kugleri*	149-250	2.11	-0.50	UCDavis
78	*	16	R	1	25	27	137.57		13	*P. may-sia*	150-250	1.36	-0.06	UMass
78	*	16	R	1	75	77	138.07		12	*P. may-sia*	150-250	1.37	0.15	UMass
78	*	16	R	1	125	127	138.57	4	8	*P. pseudok-kugleri*	149-250	1.35	-0.41	UCDavis
78	*	16	R	2	25	27	139.07		12	*P. may-sia*	150-250	1.30	-0.01	UMass
78	*	16	R	2	75	77	139.57		16	*P. may-sia*	150-250	1.10	0.19	UMass
78	*	16	R	2	125	127	140.07		12	*P. may-sia*	150-250	0.99	0.30	UMass
78	*	16	R	2	125	127	140.07	3	10	*P. pseudok-kugleri*	149-250	1.80	-0.70	UCDavis
78	*	16	R	3	25	27	140.57		13	*P. may-sia*	150-250	1.08	0.18	UMass

78	*	16	R	3	25	27	140.57	3	10	*P. pseudok-kugleri*	149-250	1.61	-0.72	UCDavis
78	*	16	R	3	43	45	140.75	3	10	*P. pseudok-kugleri*	149-250	1.85	-1.07	UCDavis
78	*	16	R	3	75	77	141.07		12	*P. may-sia*	150-250	1.23	0.08	UMass
78	*	16	R	3	75	77	141.07	3	9	*P. pseudok-kugleri*	149-250	1.50	-0.42	UCDavis
78	*	16	R	3	93	95	141.25	3	10	*P. pseudok-kugleri*	149-250	1.89	-0.88	UCDavis
78	*	16	R	3	110	112	141.42	3	10	*P. pseudok-kugleri*	149-250	1.73	-0.87	UCDavis
78	*	16	R	3	125	127	141.57		12	*P. may-sia*	150-250	1.07	-0.03	UMass
78	*	16	R	3	125	127	141.57	3	10	*P. pseudok-kugleri*	149-250	1.77	-0.60	UCDavis
78	*	16	R	3	143	145	141.75	4	8	*P. may-sia*	250-350	0.89	-0.36	UCDavis
78	*	16	R	3	143	145	141.75	3	11	*P. pseudok-kugleri*	149-250	1.91	-0.89	UCDavis
78	*	16	R	4	25	27	142.07		6	*Cib*. sp.	150-250	0.48	1.36	UMass
78	*	16	R	4	25	27	142.07	3	8	*P. may-sia*	250-350	0.88	-0.06	UCDavis
78	*	16	R	4	25	27	142.07	4	10	*P. pseudok-kugleri*	149-250	1.80	-1.06	UCDavis
78	*	16	R	4	25	27	142.07	3	10	*P. pseudok-kugleri*	149-250	1.77	-1.09	UCDavis
78	*	16	R	4	49	51	142.31	3	8	*P. may-sia*	250-350	0.88	-0.36	UCDavis
78	*	16	R	4	49	51	142.31	3	10	*P. pseudok-kugleri*	149-250	1.71	-0.96	UCDavis
78	*	16	R	4	75	77	142.57		7	*Cib*. sp.	150-250	0.53	1.32	UMass
78	*	16	R	4	75	77	142.57		12	*P. may-sia*	150-250	1.11	0.11	UMass
78	*	16	R	4	75	77	142.57	3	10	*P. pseudok-kugleri*	149-250	1.38	-0.52	UCDavis
78	*	16	R	4	95	97	142.77	3	12	*P. pseudok-kugleri*	149-250	1.73	-0.96	UCDavis
78	*	16	R	4	125	127	143.07		5	*Cib*. sp.	150-250	0.61	1.14	UMass
78	*	16	R	4	125	127	143.07	4	10	*P. pseudok-kugleri*	149-250	1.35	-0.37	UCDavis
78	*	16	R	4	143	145	143.25	3	9	*P. may-sia*	250-350	0.72	-0.20	UCDavis
78	*	16	R	4	143	145	143.25	3	10	*P. pseudok-kugleri*	149-250	1.69	-1.13	UCDavis
78	*	16	R	5	8	10	143.4	4	8	*P. may-sia*	250-350	0.85	-0.20	UCDavis
78	*	16	R	5	8	10	143.4	3	11	*P. pseudok-kugleri*	149-250	1.59	-0.72	UCDavis
78	*	16	R	5	25	27	143.57		12	*P. may-sia*	150-250	1.53	0.46	UMass
78	*	16	R	5	25	27	143.57	3	10	*P. pseudok-kugleri*	149-250	1.58	-0.80	UCDavis

78	*	**16**	**R**	**5**	**41**	**43**	143.73	4	8	*P. may-sia*	250-350	1.02	-0.36	UCDavis
78	*	**16**	**R**	**5**	**41**	**43**	143.73	3	11	*P. pseudok-kugleri*	149-250	1.72	-1.02	UCDavis
78	*	**16**	**R**	**5**	**75**	**77**	144.07		7	*Cib.* sp.	150-250	0.59	1.40	UMass
78	*	**16**	**R**	**5**	**75**	**77**	144.07		6	*Cib.* sp.	150-250	0.56	1.36	UMass
78	*	**16**	**R**	**5**	**75**	**77**	144.07	4	8	*P. may-sia*	250-350	1.13	-0.37	UCDavis
78	*	**16**	**R**	**5**	**75**	**77**	144.07	3	10	*P. pseudok-kugleri*	149-250	1.66	-0.75	UCDavis
78	*	**16**	**R**	**5**	**92**	**94**	144.24	4	8	*P. may-sia*	250-350	0.96	-0.44	UCDavis
78	*	**16**	**R**	**5**	**125**	**127**	144.57		5	*Cib.* sp.	150-250	0.59	1.36	UMass
78	*	**16**	**R**	**5**	**125**	**127**	144.57		12	*P. may-sia*	150-250	0.97	0.16	UMass
78	*	**16**	**R**	**6**	**8**	**10**	144.9	3	4	*Cib.* sp.	149-250	0.52	1.42	UCDavis
78	*	**16**	**R**	**6**	**8**	**10**	144.9	3	5	*Ord.* sp.	149-250	-0.70	1.58	UCDavis
78	*	**16**	**R**	**6**	**8**	**10**	144.9	3	11	*P. pseudok-kugleri*	149-250	1.53	-0.49	UCDavis
78	*	**16**	**R**	**6**	**25**	**27**	145.07		12	*P. may-sia*	150-250	1.25	0.05	UMass
78	*	**16**	**R**	**6**	**25**	**27**	145.07	5	8	*P. pseudok-kugleri*	149-250	1.52	-0.66	UCDavis
78	*	**16**	**R**	**6**	**53**	**55**	145.35	3	7	*Cib.* sp.	149-250	0.57	1.37	UCDavis
78	*	**16**	**R**	**6**	**53**	**55**	145.35	3	5	*Ord.* sp.	nsf	-0.37	2.11	UCDavis
78	*	**16**	**R**	**6**	**53**	**55**	145.35	3	10	*P. pseudok-kugleri*	149-250	1.69	-0.90	UCDavis
78	*	**16**	**R**	**6**	**75**	**77**	145.57		6	*Cib.* sp.	150-250	0.64	1.30	UMass
78	*	**16**	**R**	**6**	**75**	**77**	145.57		11	*P. may-sia*	150-250	1.02	0.25	UMass
78	*	**16**	**R**	**6**	**75**	**77**	145.57	3	10	*P. pseudok-kugleri*	149-250	1.51	-0.69	UCDavis
78	*	**16**	**R**	**6**	**95**	**97**	145.77	4	8	*P. may-sia*	250-350	0.90	-0.10	UCDavis
78	*	**16**	**R**	**6**	**125**	**127**	146.07		6	*Cib.* sp.	150-250	0.93	1.42	UMass
78	*	**16**	**R**	**6**	**125**	**127**	146.07			*P. may-sia*	150-250	1.14	0.21	UMass
78	*	**16**	**R**	**6**	**125**	**127**	146.07	4	7	*P. pseudok-kugleri*	149-250	1.69	-0.59	UCDavis
78	*	**16**	**R**	**6**	**145**	**147**	146.27	2	1	*Cib.* sp.	nsf	0.71	1.36	UCDavis
78	*	**16**	**R**	**6**	**145**	**147**	146.27	2	1	*Ord.* sp.	nsf	-0.30	1.42	UCDavis
78	*	**16**	**R**	**6**	**145**	**147**	146.27	4	8	*P. may-sia*	250-350	0.92	-0.27	UCDavis
78	*	**16**	**R**	**6**	**145**	**147**	146.27	3	10	*P. pseudok-kugleri*	149-250	1.76	-0.68	UCDavis
78	*	**15**	**R**	**CC**	**5**	**7**				*P. may-sia*	150-250	1.24	-0.16	UMass

78	*	15	R	CC		5	8	*P. pseudok-kugleri*	149-250	1.21	-0.46	UCDavis	

H.2 Stable Isotope Data from Site 744

Leg	Site	H	Cor	T	Sc	To	Bo	Lab	Depth(mbsf)	δ13C	δ18O	#ind	Species
119	744	A	12	H	1	24	26	UCDavis	99.44	1.81	2.22		bulk
119	744	A	12	H	1	24	26	UCDavis	99.44	1.73	2.27		bulk
119	744	A	12	H	1	30	32	UCDavis	99.5	1.43	2.37	5	*Cibicidoides* sp.
119	744	A	12	H	1	78	80	UCDavis	99.98	0.97	1.81	5	*Cibicidoides* sp.
119	744	A	12	H	1	84	86	UCDavis	100.04	2.10	1.57		bulk
119	744	A	12	H	1	120	122	UCDavis	100.4	0.98	1.89	5	*Cibicidoides* sp.
119	744	A	12	H	2	0	2	UCDavis	100.7	1.11	1.78	5	*Cibicidoides* sp.
119	744	A	12	H	2	72	74	UCDavis	101.42	0.63	1.76	5	*Cibicidoides* sp.
119	744	A	12	H	2	84	86	UCDavis	101.54	2.38	1.99		bulk
119	744	A	12	H	2	90	92	UCDavis	101.6	0.52	1.68	5	*Cibicidoides* sp.
119	744	A	12	H	2	96	98	UCDavis	101.66	2.42	1.95		bulk
119	744	A	12	H	2	120	122	UCDavis	101.9	0.77	1.73	5	*Cibicidoides pachyderma*
119	744	A	12	H	2	126	128	UCDavis	101.96	2.37	1.96		bulk
119	744	A	12	H	2	132	134	UCDavis	102.02	0.83	1.78	5	*Cibicidoides pachyderma*
119	744	A	12	H	2	144	146	UCDavis	102.14	0.79	1.77	5	*Cibicidoides pachyderma*
119	744	A	12	H	3	0	2	UCDavis	102.2	2.32	1.93		bulk
119	744	A	12	H	3	0	2	UCDavis	102.2	0.67	1.55	5	*Cibicidoides* sp.
119	744	A	12	H	3	12	14	UCDavis	102.32	2.38	1.83		bulk
119	744	A	12	H	3	12	14	UCDavis	102.32	0.78	1.82	5	*Cibicidoides* sp.
119	744	A	12	H	3	18	20	UCDavis	102.38	2.42	1.90		bulk
119	744	A	12	H	3	24	26	UCDavis	102.44	2.39	1.90		bulk
119	744	A	12	H	3	24	26	UCDavis	102.44	0.62	1.70	5	*Cibicidoides* sp.
119	744	A	12	H	3	30	32	UCDavis	102.5	2.56	1.93		bulk
119	744	A	12	H	3	30	32	UCDavis	102.5	0.95	1.86	5	*Cibicidoides* sp.
119	744	A	12	H	3	36	38	UCDavis	102.56	2.68	1.97		bulk
119	744	A	12	H	3	36	38	UCDavis	102.56	1.04	1.82	5	*Cibicidoides* sp.
119	744	A	12	H	3	42	44	UCDavis	102.62	2.69	1.92		bulk
119	744	A	12	H	3	42	44	UCDavis	102.62	0.99	1.87	5	*Cibicidoides pachyderma*
119	744	A	12	H	3	48	50	UCDavis	102.68	2.74	2.03		bulk
119	744	A	12	H	3	54	56	UCDavis	102.74	2.55	2.14		bulk
119	744	A	12	H	3	54	56	UCDavis	102.74	0.86	1.73	5	*Cibicidoides* sp.
119	744	A	12	H	3	60	62	UCDavis	102.8	2.61	2.09		bulk
119	744	A	12	H	3	66	68	UCDavis	102.86	2.66	2.00		bulk

119	**744**	**A**	**12**	**H**	**3**	**66**	**68**	UCDavis	102.86	0.97	1.87	5	*Cibicidoides* sp.
119	**744**	**A**	**12**	**H**	**3**	**72**	**74**	UCDavis	102.92	2.42	1.95		bulk
119	**744**	**A**	**12**	**H**	**3**	**78**	**80**	UCDavis	102.98	2.55	1.92		bulk
119	**744**	**A**	**12**	**H**	**3**	**78**	**80**	UCDavis	102.98	1.22	1.84	5	*Cibicidoides pachyderma*
119	**744**	**A**	**12**	**H**	**3**	**84**	**86**	UCDavis	103.04	2.63	1.89		bulk
119	**744**	**A**	**12**	**H**	**3**	**84**	**86**	UCDavis	103.04	0.99	1.73	5	*Cibicidoides pachyderma*
119	**744**	**A**	**12**	**H**	**3**	**90**	**92**	UCDavis	103.1	2.37	1.87		bulk
119	**744**	**A**	**12**	**H**	**3**	**90**	**92**	UCDavis	103.1	1.00	1.94	5	*Cibicidoides pachyderma*
119	**744**	**A**	**12**	**H**	**3**	**96**	**98**	UCDavis	103.16	2.33	1.92		bulk
119	**744**	**A**	**12**	**H**	**3**	**102**	**104**	UCDavis	103.22	2.65	1.83		bulk
119	**744**	**A**	**12**	**H**	**3**	**102**	**104**	UCDavis	103.22	0.88	1.75	5	*Cibicidoides* sp.
119	**744**	**A**	**12**	**H**	**3**	**108**	**110**	UCDavis	103.28	2.21	2.12		bulk
119	**744**	**A**	**12**	**H**	**3**	**108**	**110**	UCDavis	103.28	1.13	1.82	5	*Cibicidoides pachyderma*
119	**744**	**A**	**12**	**H**	**3**	**114**	**116**	UCDavis	103.34	2.56	1.89		bulk
119	**744**	**A**	**12**	**H**	**3**	**114**	**116**	UCDavis	103.34	0.89	1.80	5	*Cibicidoides* sp.
119	**744**	**A**	**12**	**H**	**3**	**120**	**122**	UCDavis	103.4	2.56	1.96		bulk
119	**744**	**A**	**12**	**H**	**3**	**120**	**122**	UCDavis	103.4	0.91	1.74	5	*Cibicidoides* sp.
119	**744**	**A**	**12**	**H**	**3**	**126**	**128**	UCDavis	103.46	2.62	1.88		bulk
119	**744**	**A**	**12**	**H**	**3**	**126**	**128**	UCDavis	103.46	0.82	1.68	5	*Cibicidoides* sp.
119	**744**	**A**	**12**	**H**	**3**	**132**	**134**	UCDavis	103.52	2.43	2.13		bulk
119	**744**	**A**	**12**	**H**	**3**	**138**	**140**	UCDavis	103.58	2.75	1.88		bulk
119	**744**	**A**	**12**	**H**	**3**	**138**	**140**	UCDavis	103.58	0.75	1.71	5	*Cibicidoides* sp.
119	**744**	**A**	**12**	**H**	**3**	**144**	**146**	UCDavis	103.64	2.48	2.04		bulk
119	**744**	**A**	**12**	**H**	**4**	**0**	**2**	UCDavis	103.7	2.74	2.01		bulk
119	**744**	**A**	**12**	**H**	**4**	**0**	**2**	UCDavis	103.7	0.71	1.80	5	*Cibicidoides* sp.
119	**744**	**A**	**12**	**H**	**4**	**6**	**8**	UCDavis	103.76	2.38	3.06		bulk
119	**744**	**A**	**12**	**H**	**4**	**6**	**8**	UCDavis	103.76	2.45	3.15		bulk
119	**744**	**A**	**12**	**H**	**4**	**12**	**14**	UCDavis	103.82	2.57	1.93		bulk
119	**744**	**A**	**12**	**H**	**4**	**12**	**14**	UCDavis	103.82	0.72	1.69	5	*Cibicidoides* sp.
119	**744**	**A**	**12**	**H**	**4**	**18**	**20**	UCDavis	103.88	2.64	1.98		bulk
119	**744**	**A**	**12**	**H**	**4**	**24**	**26**	UCDavis	103.94	2.67	2.14		bulk
119	**744**	**A**	**12**	**H**	**4**	**24**	**26**	UCDavis	103.94	0.63	1.66	5	*Cibicidoides* sp.
119	**744**	**A**	**12**	**H**	**4**	**30**	**32**	UCDavis	104	2.64	1.96		bulk
119	**744**	**A**	**12**	**H**	**4**	**36**	**38**	UCDavis	104.06	2.69	2.05		bulk
119	**744**	**A**	**12**	**H**	**4**	**36**	**38**	UCDavis	104.06	0.85	1.78	5	*Cibicidoides* sp.
119	**744**	**A**	**12**	**H**	**4**	**42**	**44**	UCDavis	104.12	2.66	2.05		bulk
119	**744**	**A**	**12**	**H**	**4**	**48**	**50**	UCDavis	104.18	2.69	2.03		bulk
119	**744**	**A**	**12**	**H**	**4**	**48**	**50**	UCDavis	104.18	0.91	1.85	5	*Cibicidoides* sp.

119	744	A	12	H	4	54	56	UCDavis	104.24	2.64	2.01		bulk
119	744	A	12	H	4	54	56	UCDavis	104.24	0.85	1.70	5	*Cibicidoides* sp.
119	744	A	12	H	4	60	62	UCDavis	104.3	2.65	1.97		bulk
119	744	A	12	H	4	60	62	UCDavis	104.3	0.72	1.88	5	*Cibicidoides* sp.
119	744	A	12	H	4	66	68	UCDavis	104.36	2.62	2.00		bulk
119	744	A	12	H	4	66	68	UCDavis	104.36	0.70	1.84	6	*Cibicidoides* sp.
119	744	A	12	H	4	72	74	UCDavis	104.42	2.60	2.00		bulk
119	744	A	12	H	4	72	74	UCDavis	104.42	0.73	1.58	5	*Cibicidoides* sp.
119	744	A	12	H	4	78	80	UCDavis	104.48	2.64	1.98		bulk
119	744	A	12	H	4	78	80	UCDavis	104.48	1.01	1.95	5	*Cibicidoides pachyderma*
119	744	A	12	H	4	84	86	UCDavis	104.54	2.23	2.11		bulk
119	744	A	12	H	4	84	86	UCDavis	104.54			5	*Cibicidoides pachyderma*
119	744	A	12	H	4	90	92	UCDavis	104.6	2.48	2.00		bulk
119	744	A	12	H	4	90	92	UCDavis	104.6	1.08	1.96	5	*Cibicidoides pachyderma*
119	744	A	12	H	4	96	98	UCDavis	104.66	2.46	1.92		bulk
119	744	A	12	H	4	96	98	UCDavis	104.66	0.95	1.91	5	*Cibicidoides pachyderma*
119	744	A	12	H	4	96	98	UCDavis	104.66	1.04	1.89	5	*Cibicidoides pachyderma*
119	744	A	12	H	4	102	104	UCDavis	104.72	2.33	1.74		bulk
119	744	A	12	H	4	102	104	UCDavis	104.72	0.59	1.56	5	*Cibicidoides* sp.
119	744	A	12	H	4	108	110	UCDavis	104.78	2.35	1.83		bulk
119	744	A	12	H	4	108	110	UCDavis	104.78	0.89	1.73	5	*Cibicidoides pachyderma*
119	744	A	12	H	4	114	116	UCDavis	104.84	2.18	1.70		bulk
119	744	A	12	H	4	114	116	UCDavis	104.84	0.57	1.61	6	*Cibicidoides* sp.
119	744	A	12	H	4	120	122	UCDavis	104.9	2.12	1.88		bulk
119	744	A	12	H	4	120	122	UCDavis	104.9	1.03	1.89	5	*Cibicidoides pachyderma*
119	744	A	12	H	4	126	128	UCDavis	104.96	2.08	1.80		bulk
119	744	A	12	H	4	126	128	UCDavis	104.96	0.62	1.56	5	*Cibicidoides* sp.
119	744	A	12	H	4	132	134	UCDavis	105.02	2.10	1.83		bulk
119	744	A	12	H	4	132	134	UCDavis	105.02	0.55	1.60	5	*Cibicidoides* sp.
119	744	A	12	H	4	138	140	UCDavis	105.08	2.14	1.68		bulk
119	744	A	12	H	4	138	140	UCDavis	105.08	0.60	1.65	5	*Cibicidoides* sp.
119	744	A	12	H	4	144	146	UCDavis	105.14	2.11	1.83		bulk
119	744	A	12	H	4	144	146	UCDavis	105.14	0.75	1.75	5	*Cibicidoides* sp.
119	744	A	12	H	5	6	8	UCDavis	105.26	2.12	1.68		bulk
119	744	A	12	H	5	6	8	UCDavis	105.26	0.78	1.94	5	*Cibicidoides* sp.
119	744	A	12	H	5	18	20	UCDavis	105.38	2.12	1.76		bulk
119	744	A	12	H	5	18	20	UCDavis	105.38	0.71	1.73	5	*Cibicidoides* sp.
119	744	A	12	H	5	30	32	UCDavis	105.5	2.19	1.75		bulk

119	**744**	**A**	**12**	**H**	**5**	**30**	**32**	UCDavis	105.5	0.93	1.83	5	*Cibicidoides* sp.
119	**744**	**A**	**12**	**H**	**5**	**42**	**44**	UCDavis	105.62	2.20	1.69		bulk
119	**744**	**A**	**12**	**H**	**5**	**42**	**44**	UCDavis	105.62	1.03	1.89	5	*Cibicidoides* sp.
119	**744**	**A**	**12**	**H**	**5**	**54**	**56**	UCDavis	105.74	2.03	1.65		bulk
119	**744**	**A**	**12**	**H**	**5**	**54**	**56**	UCDavis	105.74	0.99	2.03	5	*Cibicidoides* sp.
119	**744**	**A**	**12**	**H**	**5**	**66**	**68**	UCDavis	105.86	1.90	1.57		bulk
119	**744**	**A**	**12**	**H**	**5**	**66**	**68**	UCDavis	105.86	0.79	1.84	5	*Cibicidoides pachyderma*
119	**744**	**A**	**12**	**H**	**5**	**78**	**80**	UCDavis	105.98	1.67	1.52		bulk
119	**744**	**A**	**12**	**H**	**5**	**78**	**80**	UCDavis	105.98	0.74	1.89	5	*Cibicidoides* sp.
119	**744**	**A**	**12**	**H**	**5**	**90**	**92**	UCDavis	106.1	1.61	1.58		bulk
119	**744**	**A**	**12**	**H**	**5**	**90**	**92**	UCDavis	106.1	0.68	1.86	5	*Cibicidoides* sp.
119	**744**	**A**	**12**	**H**	**5**	**102**	**104**	UCDavis	106.22	1.59	1.57		bulk
119	**744**	**A**	**12**	**H**	**5**	**102**	**104**	UCDavis	106.22	0.62	1.80	5	*Cibicidoides* sp.
119	**744**	**A**	**12**	**H**	**5**	**114**	**116**	UCDavis	106.34	1.64	1.50		bulk
119	**744**	**A**	**12**	**H**	**5**	**114**	**116**	UCDavis	106.34	0.55	1.78	5	*Cibicidoides* sp.
119	**744**	**A**	**12**	**H**	**5**	**126**	**128**	UCDavis	106.46	1.58	1.52		bulk
119	**744**	**A**	**12**	**H**	**5**	**126**	**128**	UCDavis	106.46	0.68	1.91	5	*Cibicidoides* sp.
119	**744**	**A**	**12**	**H**	**5**	**138**	**140**	UCDavis	106.58	1.65	1.54		bulk
119	**744**	**A**	**12**	**H**	**5**	**138**	**140**	UCDavis	106.58	0.72	1.83	5	*Cibicidoides* sp.
119	**744**	**A**	**12**	**H**	**6**	**0**	**2**	UCDavis	106.7	1.61	1.51		bulk
119	**744**	**A**	**12**	**H**	**6**	**0**	**2**	UCDavis	106.7	0.78	1.93	5	*Cibicidoides* sp.
119	**744**	**A**	**12**	**H**	**6**	**12**	**14**	UCDavis	106.82	1.59	1.52		bulk
119	**744**	**A**	**12**	**H**	**6**	**12**	**14**	UCDavis	106.82	0.81	1.86	5	*Cibicidoides* sp.
119	**744**	**A**	**12**	**H**	**6**	**24**	**26**	UCDavis	106.94	1.66	1.62		bulk
119	**744**	**A**	**12**	**H**	**6**	**24**	**26**	UCDavis	106.94	0.57	1.79	5	*Cibicidoides* sp.
119	**744**	**A**	**12**	**H**	**6**	**48**	**50**	UCDavis	107.18	1.84	1.69		bulk
119	**744**	**A**	**12**	**H**	**6**	**48**	**50**	UCDavis	107.18	0.82	1.97	5	*Cibicidoides pachyderma*
119	**744**	**A**	**12**	**H**	**6**	**60**	**62**	UCDavis	107.3	2.01	1.71		bulk
119	**744**	**A**	**12**	**H**	**6**	**60**	**62**	UCDavis	107.3	0.98	2.13	5	*Cibicidoides* sp.
119	**744**	**A**	**12**	**H**	**6**	**66**	**68**	UCDavis	107.36	1.91	1.83		bulk
119	**744**	**A**	**12**	**H**	**6**	**72**	**74**	UCDavis	107.42	0.84	2.11	5	*Cibicidoides pachyderma*
119	**744**	**A**	**12**	**H**	**6**	**84**	**86**	UCDavis	107.54	2.15	1.95		bulk
119	**744**	**A**	**12**	**H**	**6**	**84**	**86**	UCDavis	107.54	0.97	2.24	5	*Cibicidoides pachyderma*
119	**744**	**A**	**12**	**H**	**6**	**96**	**98**	UCDavis	107.54	0.99	2.13	5	*Cibicidoides pachyderma*
119	**744**	**A**	**12**	**H**	**6**	**96**	**98**	UCDavis	107.66	2.18	1.84		bulk
119	**744**	**A**	**12**	**H**	**6**	**108**	**110**	UCDavis	107.78	2.08	1.80		bulk
119	**744**	**A**	**12**	**H**	**6**	**108**	**110**	UCDavis	107.78	1.00	2.14	5	*Cibicidoides pachyderma*
119	**744**	**A**	**12**	**H**	**6**	**120**	**122**	UCDavis	107.9	1.99	1.82		bulk

119	744	A	12	H	6	120	122	UCDavis	107.9	0.90	2.18	5	*Cibicidoides pachyderma*
119	744	A	12	H	6	132	134	UCDavis	108.02	1.81	2.01		bulk
119	744	A	12	H	6	132	134	UCDavis	108.02	1.82	2.08		bulk
119	744	A	12	H	6	132	134	UCDavis	108.02	0.89	2.06	5	*Cibicidoides* sp.
119	744	A	12	H	6	144	146	UCDavis	108.14	1.99	1.81		bulk
119	744	A	12	H	6	144	146	UCDavis	108.14	0.94	2.18	5	*Cibicidoides* sp.
119	744	A	12	H	7	6	8	UCDavis	108.26	1.94	1.84		bulk
119	744	A	12	H	7	8	10	UCDavis	108.26	0.70	2.07	5	*Cibicidoides pachyderma*
119	744	A	12	H	7	18	20	UCDavis	108.38	1.97	1.78		bulk
119	744	A	12	H	7	18	20	UCDavis	108.38	0.86	1.88	5	*Cibicidoides pachyderma*
119	744	A	12	H	7	30	32	UCDavis	108.5	2.00	1.84		Bulk
119	744	A	12	H	7	30	32	UCDavis	108.5	0.73	2.02	5	*Cibicidoides pachyderma*
119	744	A	12	H	7	42	44	UCDavis	108.62	1.91	1.74		bulk
119	744	A	12	H	7	42	44	UCDavis	108.62	0.73	2.10	5	*Cibicidoides pachyderma*
119	744	A	12	H	7	54	56	UCDavis	108.74	1.95	1.81		bulk
119	744	A	12	H	7	54	56	UCDavis	108.74	0.73	2.02	5	*Cibicidoides pachyderma*
119	744	A	12	H	7	66	68	UCDavis	108.86	1.83	1.66		bulk
119	744	A	12	H	7	66	68	UCDavis	108.86	0.74	2.09	5	*Cibicidoides pachyderma*
119	744	A	12	H	cc	8	10	UCDavis	108.98	1.64	1.67		bulk
119	744	A	12	H	cc			UCDavis	108.98	0.74	1.97	5	*Cibicidoides pachyderma*
119	744	A	13	H	1	92	94	UCDavis	109.62	2.13	2.11		bulk
119	744	A	12	H	1	6	8	UMass	99.26	1.43	1.59		bulk
119	744	A	12	H	1	6	8	UMass	99.26	1.59	1.85		bulk
119	744	A	12	H	1	6	8	UMass	99.26	1.23	2.85	8	*Cibicidoides* sp.
119	744	A	12	H	1	12	14	UMass	99.32	1.92	2.30		bulk
119	744	A	12	H	1	12	14	UMass	99.32	2.14	2.22		bulk
119	744	A	12	H	1	12	14	UMass	99.32	1.43	2.45	8	*Cibicidoides pachyderma*
119	744	A	12	H	1	12	14	UMass	99.32	1.29	1.91	8	*Cibicidoides pachyderma*
119	744	A	12	H	1	18	20	UMass	99.38	1.87	2.36		bulk
119	744	A	12	H	1	18	20	UMass	99.38	1.75	2.03		bulk
119	744	A	12	H	1	18	20	UMass	99.38	1.27	2.41	8	*Cibicidoides pachyderma*
119	744	A	12	H	1	24	26	UMass	99.44	1.39	2.57	8	*Cibicidoides* sp.
119	744	A	12	H	1	30	32	UMass	99.5	1.87	2.20		bulk
119	744	A	12	H	1	30	32	UMass	99.5	2.15	2.14		bulk
119	744	A	12	H	1	30	32	UMass	99.5	1.71	2.39	8	*Cibicidoides pachyderma*
119	744	A	12	H	1	30	32	UMass	99.5	1.15	1.77	8	*Cibicidoides* sp.
119	744	A	12	H	1	36	38	UMass	99.56	1.83	2.10		bulk
119	744	A	12	H	1	36	38	UMass	99.56	1.80	3.14	9	*Cibicidoides* sp.

119	**744**	**A**	**12**	**H**	**1**	**42**	**44**	UMass	99.62	2.11	2.38		bulk
119	**744**	**A**	**12**	**H**	**1**	**42**	**44**	UMass	99.62	1.67	2.98	7	*Cibicidoides pachyderma*
119	**744**	**A**	**12**	**H**	**1**	**48**	**50**	UMass	99.68	1.88	1.66		bulk
119	**744**	**A**	**12**	**H**	**1**	**48**	**50**	UMass	99.68	1.32	2.26	8	*Cibicidoides pachyderma*
119	**744**	**A**	**12**	**H**	**1**	**54**	**56**	UMass	99.74	1.89	1.55		bulk
119	**744**	**A**	**12**	**H**	**1**	**54**	**56**	UMass	99.74	2.25	1.90		bulk
119	**744**	**A**	**12**	**H**	**1**	**54**	**56**	UMass	99.74	1.08	2.20	9	*Cibicidoides pachyderma*
119	**744**	**A**	**12**	**H**	**1**	**60**	**62**	UMass	99.8	1.85	1.77		bulk
119	**744**	**A**	**12**	**H**	**1**	**60**	**62**	UMass	99.8	1.24	2.03	9	*Cibicidoides* sp.
119	**744**	**A**	**12**	**H**	**1**	**66**	**68**	UMass	99.86	1.96	1.66		bulk
119	**744**	**A**	**12**	**H**	**1**	**66**	**68**	UMass	99.86	2.27	1.61		bulk
119	**744**	**A**	**12**	**H**	**1**	**66**	**68**	UMass	99.86	0.98	1.95	7	*Cibicidoides pachyderma*
119	**744**	**A**	**12**	**H**	**1**	**72**	**74**	UMass	99.92	2.13	1.68		bulk
119	**744**	**A**	**12**	**H**	**1**	**72**	**74**	UMass	99.92	0.68	1.84	9	*Cibicidoides pachyderma*
119	**744**	**A**	**12**	**H**	**1**	**78**	**80**	UMass	99.98	1.80	1.40		bulk
119	**744**	**A**	**12**	**H**	**1**	**84**	**86**	UMass	100.04	1.32	2.46	8	*Cibicidoides pachyderma*
119	**744**	**A**	**12**	**H**	**1**	**90**	**92**	UMass	100.1	2.56	1.83		bulk
119	**744**	**A**	**12**	**H**	**1**	**90**	**92**	UMass	100.1	2.96	1.97		bulk
119	**744**	**A**	**12**	**H**	**1**	**90**	**92**	UMass	100.1	0.82	1.29	9	*Cibicidoides pachyderma*
119	**744**	**A**	**12**	**H**	**1**	**90**	**92**	UMass	100.1	1.11	1.93	8	*Cibicidoides pachyderma*
119	**744**	**A**	**12**	**H**	**1**	**96**	**98**	UMass	100.16	2.57	1.78		bulk
119	**744**	**A**	**12**	**H**	**1**	**96**	**98**	UMass	100.16	2.82	1.81		bulk
119	**744**	**A**	**12**	**H**	**1**	**96**	**98**	UMass	100.16			7	*Cibicidoides pachyderma*
119	**744**	**A**	**12**	**H**	**1**	**96**	**98**	UMass	100.16	1.37	2.39	8	*Cibicidoides* sp.
119	**744**	**A**	**12**	**H**	**1**	**102**	**104**	UMass	100.22	2.15	1.65		bulk
119	**744**	**A**	**12**	**H**	**1**	**102**	**104**	UMass	100.22	2.44	1.67		bulk
119	**744**	**A**	**12**	**H**	**1**	**102**	**104**	UMass	100.22	1.08	2.04	9	*Cibicidoides pachyderma*
119	**744**	**A**	**12**	**H**	**1**	**108**	**110**	UMass	100.28	2.50	1.87		bulk
119	**744**	**A**	**12**	**H**	**1**	**108**	**110**	UMass	100.28	2.73	1.83		bulk
119	**744**	**A**	**12**	**H**	**1**	**108**	**110**	UMass	100.28			7	*Cibicidoides pachyderma*
119	**744**	**A**	**12**	**H**	**1**	**108**	**110**	UMass	100.28	0.94	1.85	8	*Cibicidoides* sp.
119	**744**	**A**	**12**	**H**	**1**	**114**	**116**	UMass	100.34	2.29	1.86		bulk
119	**744**	**A**	**12**	**H**	**1**	**114**	**116**	UMass	100.34	1.03	1.93	9	*Cibicidoides pachyderma*
119	**744**	**A**	**12**	**H**	**1**	**120**	**122**	UMass	100.4	2.35	1.77		bulk
119	**744**	**A**	**12**	**H**	**1**	**120**	**122**	UMass	100.4	2.60	1.81		bulk
119	**744**	**A**	**12**	**H**	**1**	**120**	**122**	UMass	100.4			9	*Cibicidoides pachyderma*
119	**744**	**A**	**12**	**H**	**1**	**120**	**122**	UMass	100.4			7	*Cibicidoides pachyderma*
119	**744**	**A**	**12**	**H**	**1**	**126**	**128**	UMass	100.46	2.52	2.17		bulk

119	744	A	12	H	1	126	128	UMass	100.46	0.90	1.94	8	*Cibicidoides pachyderma*
119	744	A	12	H	1	132	134	UMass	100.52	2.35	1.95		bulk
119	744	A	12	H	1	132	134	UMass	100.52	2.61	1.99		bulk
119	744	A	12	H	1	132	134	UMass	100.52			7	*Cibicidoides pachyderma*
119	744	A	12	H	1	132	134	UMass	100.52	1.10	2.03	9	*Cibicidoides* sp.
119	744	A	12	H	1	138	140	UMass	100.58	2.33	2.02		bulk
119	744	A	12	H	1	138	140	UMass	100.58	2.61	1.99		bulk
119	744	A	12	H	1	138	140	UMass	100.58	0.96	1.99	9	*Cibicidoides pachyderma*
119	744	A	12	H	1	144	146	UMass	100.64	2.70	2.25		bulk
119	744	A	12	H	1	144	146	UMass	100.64	0.94	1.21	7	*Cibicidoides pachyderma*
119	744	A	12	H	2	0	2	UMass	100.7	2.50	1.92		bulk
119	744	A	12	H	2	0	2	UMass	100.7	2.77	1.93		bulk
119	744	A	12	H	2	0	2	UMass	100.7			8	*Cibicidoides pachyderma*
119	744	A	12	H	2	6	8	UMass	100.76	2.47	1.97		bulk
119	744	A	12	H	2	6	8	UMass	100.76	2.32	1.73		bulk
119	744	A	12	H	2	6	8	UMass	100.76	0.95	1.52	7	*Cibicidoides pachyderma*
119	744	A	12	H	2	12	14	UMass	100.82	2.71	2.32		bulk
119	744	A	12	H	2	12	14	UMass	100.82	1.03	1.96	8	*Cibicidoides pachyderma*
119	744	A	12	H	2	18	20	UMass	100.88	2.76	1.82		bulk
119	744	A	12	H	2	18	20	UMass	100.88	0.77	1.63	7	*Cibicidoides pachyderma*
119	744	A	12	H	2	24	26	UMass	100.94	2.71	2.23		bulk
119	744	A	12	H	2	24	26	UMass	100.94	1.02	1.90	8	*Cibicidoides pachyderma*
119	744	A	12	H	2	30	32	UMass	101	2.05	1.66		bulk
119	744	A	12	H	2	30	32	UMass	101	2.31	1.68		bulk
119	744	A	12	H	2	30	32	UMass	101	0.95	1.73	8	*Cibicidoides pachyderma*
119	744	A	12	H	2	36	38	UMass	101.06	2.02	1.73		bulk
119	744	A	12	H	2	36	38	UMass	101.06	2.26	1.63		bulk
119	744	A	12	H	2	36	38	UMass	101.06	1.21	2.46	8	*Cibicidoides* sp.
119	744	A	12	H	2	42	44	UMass	101.12	2.56	2.32		bulk
119	744	A	12	H	2	42	44	UMass	101.12	0.90	1.92	8	*Cibicidoides pachyderma*
119	744	A	12	H	2	48	50	UMass	101.18	2.08	1.77		bulk
119	744	A	12	H	2	48	50	UMass	101.18	0.57	1.78	9	*Cibicidoides pachyderma*
119	744	A	12	H	2	54	56	UMass	101.24	2.37	1.84		bulk
119	744	A	12	H	2	60	62	UMass	101.3	2.09	1.69		bulk
119	744	A	12	H	2	60	62	UMass	101.3	2.33	1.69		bulk
119	744	A	12	H	2	60	62	UMass	101.3	1.01	2.34	9	*Cibicidoides pachyderma*
119	744	A	12	H	2	66	68	UMass	101.36	2.15	1.90		bulk
119	744	A	12	H	2	66	68	UMass	101.36	2.46	1.86		bulk
119	744	A	12	H	2	66	68	UMass	101.36			7	*Cibicidoides pachyderma*

119	**744**	**A**	**12**	**H**	**2**	**66**	**68**	UMass	101.36	0.62	1.53	8	*Cibicidoides* sp.
119	**744**	**A**	**12**	**H**	**2**	**78**	**80**	UMass	101.48	2.30	1.88		bulk
119	**744**	**A**	**12**	**H**	**2**	**78**	**80**	UMass	101.48	2.18	1.89		bulk
119	**744**	**A**	**12**	**H**	**2**	**78**	**80**	UMass	101.48	0.97	1.69	8	*Cibicidoides pachyderma*
119	**744**	**A**	**12**	**H**	**2**	**84**	**86**	UMass	101.54	0.85	2.06	9	*Cibicidoides* sp.
119	**744**	**A**	**12**	**H**	**2**	**90**	**92**	UMass	101.6	2.67	2.36		bulk
119	**744**	**A**	**12**	**H**	**2**	**90**	**92**	UMass	101.6			8	*Cibicidoides pachyderma*
119	**744**	**A**	**12**	**H**	**2**	**96**	**98**	UMass	101.66	0.67	1.84	9	*Cibicidoides* sp.
119	**744**	**A**	**12**	**H**	**2**	**102**	**104**	UMass	101.72	2.63	2.36		bulk
119	**744**	**A**	**12**	**H**	**2**	**102**	**104**	UMass	101.72	1.07	1.28	7	*Cibicidoides pachyderma*
119	**744**	**A**	**12**	**H**	**2**	**108**	**110**	UMass	101.78	2.30	1.69		bulk
119	**744**	**A**	**12**	**H**	**2**	**108**	**110**	UMass	101.78	2.67	2.02		bulk
119	**744**	**A**	**12**	**H**	**2**	**108**	**110**	UMass	101.78	0.80	1.63	9	*Cibicidoides* sp.
119	**744**	**A**	**12**	**H**	**2**	**114**	**116**	UMass	101.84	2.33	1.83		bulk
119	**744**	**A**	**12**	**H**	**2**	**114**	**116**	UMass	101.84	2.74	2.15		bulk
119	**744**	**A**	**12**	**H**	**2**	**114**	**116**	UMass	101.84			8	*Cibicidoides pachyderma*
119	**744**	**A**	**12**	**H**	**2**	**114**	**116**	UMass	101.84	0.75	1.79	8	*Cibicidoides* sp.
119	**744**	**A**	**12**	**H**	**2**	**120**	**122**	UMass	101.9	2.67	2.41		bulk
119	**744**	**A**	**12**	**H**	**2**	**126**	**128**	UMass	101.96	2.31	1.77		bulk
119	**744**	**A**	**12**	**H**	**2**	**126**	**128**	UMass	101.96	0.74	1.21	7	*Cibicidoides pachyderma*
119	**744**	**A**	**12**	**H**	**2**	**132**	**134**	UMass	102.02	2.40	2.02		bulk
119	**744**	**A**	**12**	**H**	**2**	**132**	**134**	UMass	102.02	2.73	2.04		bulk
119	**744**	**A**	**12**	**H**	**2**	**138**	**140**	UMass	102.08	2.58	2.29		bulk
119	**744**	**A**	**12**	**H**	**2**	**138**	**140**	UMass	102.08	0.75	1.08	8	*Cibicidoides pachyderma*
119	**744**	**A**	**12**	**H**	**2**	**144**	**146**	UMass	102.14	2.16	2.07		bulk
119	**744**	**A**	**12**	**H**	**3**	**6**	**8**	UMass	102.26	0.83	1.48	7	*Cibicidoides pachyderma*
119	**744**	**A**	**12**	**H**	**3**	**18**	**20**	UMass	102.38	0.55	1.00	8	*Cibicidoides pachyderma*
119	**744**	**A**	**12**	**H**	**3**	**60**	**62**	UMass	102.8	0.80	1.78	8	*Cibicidoides pachyderma*
119	**744**	**A**	**12**	**H**	**3**	**72**	**74**	UMass	102.92	0.89	1.68	6	*Cibicidoides pachyderma*
119	**744**	**A**	**12**	**H**	**3**	**84**	**86**	UMass	103.04			8	*Cibicidoides pachyderma*
119	**744**	**A**	**12**	**H**	**3**	**96**	**98**	UMass	103.16	0.85	1.25	8	*Cibicidoides pachyderma*
119	**744**	**A**	**12**	**H**	**3**	**108**	**110**	UMass	103.28			8	*Cibicidoides pachyderma*
119	**744**	**A**	**12**	**H**	**3**	**120**	**122**	UMass	103.4			8	*Cibicidoides pachyderma*
119	**744**	**A**	**12**	**H**	**3**	**132**	**134**	UMass	103.52	0.89	1.74	8	*Cibicidoides pachyderma*
119	**744**	**A**	**12**	**H**	**3**	**144**	**146**	UMass	103.64	0.83	1.78	8	*Cibicidoides pachyderma*
119	**744**	**A**	**12**	**H**	**4**	**6**	**8**	UMass	103.76	0.99	1.85	7	*Cibicidoides pachyderma*
119	**744**	**A**	**12**	**H**	**4**	**18**	**20**	UMass	103.88	1.01	1.85	8	*Cibicidoides pachyderma*
119	**744**	**A**	**12**	**H**	**4**	**30**	**32**	UMass	104	1.15	2.52	9	*Cibicidoides pachyderma*
119	**744**	**A**	**12**	**H**	**4**	**42**	**44**	UMass	104.12	0.73	1.87	8	*Cibicidoides pachyderma*

H.3 Stable Isotopes from ODP Site 803

Site	H	Cor	T	Sc	To	Bo	Depth	Lab	Species	δ13C	δ18O	pres	#ind
803	D	34	X	1	25	27	303.55	UMass	mixed	0.83	1.96		
803	D	34	X	1	25	27	303.55	UCDavis	*P. pseudok-kugleri*	2.30	-0.66	3	12
803	D	34	X	1	75	77	304.05	UMass	mixed	0.52	1.50		
803	D	34	X	1	125	127	304.55	UMass	*Ordorsalis* sp.	0.19	2.12		
803	D	34	X	1	125	127	304.55	UCDavis	*P. pseudok-kugleri*	2.37	-0.63	3	11
803	D	34	X	2	25	27	305.05	UMass	mixed	1.21	1.66		
803	D	34	X	2	25	27	305.05	UCDavis	*P. pseudok-kugleri*	2.19	-0.79	4	11
803	D	34	X	2	75	77	305.55	UMass	*Cibicidoides* sp.	1.70	1.72		
803	D	34	X	2	75	77	305.55	UMass	mixed	1.12	1.88		
803	D	34	X	2	125	127	306.05	UCDavis	*P. pseudok-kugleri*	2.60	-0.44	3	11
803	D	34	X	3	25	27	306.55	UMass	*Cibicidoides* sp.	1.62	2.02		
803	D	34	X	3	25	27	306.55	UCDavis	*P. pseudok-kugleri*	2.50	-0.62	3	12
803	D	34	X	3	75	77	307.05	UMass	*Ordorsalis* sp.	-0.06	2.14		
803	D	34	X	3	125	127	307.55	UMass	*Ordorsalis* sp.	0.26	2.32		
803	D	34	X	3	125	127	307.55	UCDavis	*P. pseudok-kugleri*	2.60	-0.31	4	9
803	D	34	X	4	25	27	308.05	UMass	*Ordorsalis* sp.	0.91	1.95		
803	D	34	X	4	25	27	308.05	UCDavis	*P. pseudok-kugleri*	2.44	-0.40	3	13
803	D	34	X	4	75	77	308.55	UMass	*Ordorsalis* sp.	0.12	2.12		
803	D	34	X	5	25	27	309.55	UMass	*Ordorsalis* sp.	0.40	2.32		
803	D	34	X	5	25	27	309.55	UCDavis	*P. pseudok-kugleri*	2.43	-0.48	3	11
803	D	34	X	5	75	77	310.05	UMass	*Ordorsalis* sp.	-0.02	1.86		
803	D	34	X	5	125	127	310.55	UMass	*Ordorsalis* sp.	0.40	2.32		
803	D	34	X	5	125	127	310.55	UCDavis	*P. pseudok-kugleri*	2.26	-0.53	3	12
803	D	34	X	6	25	27	311.05	UMass	*Ordorsalis* sp.	0.54	1.89		
803	D	34	X	6	25	27	311.05	UCDavis	*P. pseudok-kugleri*	2.62	-0.45	3	10
803	D	34	X	6	75	77	311.55	UMass	*Ordorsalis* sp.	0.28	2.10		
803	D	34	X	6	125	127	312.05	UMass	*Ordorsalis* sp.	0.31	1.92		
803	D	34	X	6	125	127	312.05	UCDavis	*P. pseudok-kugleri*	2.43	-0.54	3	12
803	D	34	X	CC	0	2	312.52	UMass	*Ordorsalis* sp.	0.45	2.21		
803	D	34	X	CC			312.52	UCDavis	*P. pseudok-kugleri*	2.51	-0.32	3	10
803	D	35	X	1	25	27	313.25	UMass	*Ordorsalis* sp.	0.59	2.17		
803	D	35	X	1	25	27	313.25	UCDavis	*P. pseudok-kugleri*	2.68	-0.36	3	13
803	D	35	X	1	75	77	313.75	UMass	*Ordorsalis* sp.	0.34	1.86		
803	D	35	X	1	125	127	314.25	UMass	*Cibicidoides* sp.	1.38	1.64		
803	D	35	X	1	125	127	314.25	UMass	*Ordorsalis* sp.	0.19	1.92		

803	D	35	X	1	125	127	314.25	UCDavis	*P. pseudok-kugleri*	2.10	-0.79	3	13
803	D	35	X	2	25	27	314.75	UMass	*Ordorsalis* sp.	-0.07	2.14		
803	D	35	X	2	25	27	314.75	UCDavis	*P. pseudok-kugleri*	2.28	-0.38	3	12
803	D	35	X	2	75	77	315.25	UMass	mixed	0.58	2.16		
803	D	35	X	2	75	77	315.25	UCDavis	*P. pseudok-kugleri*	2.13	-0.47	4	10
803	D	35	X	2	125	127	315.75	UMass	*Ordorsalis* sp.	0.03	1.86		
803	D	35	X	2	125	127	315.75	UCDavis	*P. pseudok-kugleri*	2.19	-0.58	3	10
803	D	35	X	3	25	27	316.25	UMass	*Cibicidoides* sp.	1.52	1.66		
803	D	35	X	3	25	27	316.25	UMass	*Ordorsalis* sp.	0.39	1.90		
803	D	35	X	3	25	27	316.25	UCDavis	*P. pseudok-kugleri*	2.35	-0.74	3	10
803	D	35	X	3	75	77	316.75	UMass	*Cibicidoides* sp.	1.59	2.07		
803	D	35	X	3	75	77	316.75	UMass	*Ordorsalis* sp.				
803	D	35	X	3	75	77	316.75	UCDavis	*P. pseudok-kugleri*	2.26	-0.59	3	10
803	D	35	X	3	125	127	317.25	UMass	*Cibicidoides* sp.	1.02	1.65		
803	D	35	X	3	125	127	317.25	UMass	*Ordorsalis* sp.	-0.19	2.04		
803	D	35	X	4	25	27	317.25	UMass	*Ordorsalis* sp.	0.32	2.15		
803	D	35	X	3	125	127	317.25	UCDavis	*P. pseudok-kugleri*	1.96	-0.64	3	10
803	D	35	X	4	25	27	317.75	UMass	*Cibicidoides* sp.	1.81	2.06		
803	D	35	X	4	25	27	317.75	UCDavis	*P. pseudok-kugleri*	2.52	-0.35	3	11
803	D	35	X	4	75	77	318.25	UMass	*Ordorsalis* sp.	0.02	2.21		
803	D	35	X	4	75	77	318.25	UCDavis	*P. pseudok-kugleri*	2.38	-0.51	3	10
803	D	35	X	4	125	127	318.75	UMass	*Ordorsalis* sp.	0.60	2.30		
803	D	35	X	4	125	127	318.75	UCDavis	*P. pseudok-kugleri*	2.18	-0.53	3	12
803	D	35	X	5	25	27	319.25	UMass	*Cibicidoides* sp.	1.73	2.18		
803	D	35	X	5	25	27	319.25	UMass	*Ordorsalis* sp.	0.23	2.37		
803	D	35	X	5	25	27	319.25	UCDavis	*P. pseudok-kugleri*	2.27	-0.35	3	12
803	D	35	X	5	33.5	35.5	319.335	UCDavis	*P. pseudok-kugleri*	2.20	-0.33	3	12
803	D	35	X	5	59	61	319.59	UCDavis	*P. pseudok-kugleri*	2.40	-0.30	3	12
803	D	35	X	5	75	77	319.75	UMass	mixed	0.38	2.27		
803	D	35	X	5	75	77	319.75	UCDavis	*P. pseudok-kugleri*	2.48	-0.48	3	12
803	D	35	X	5	93.5	95.5	319.935	UCDavis	*P. pseudok-kugleri*	2.43	-0.19	3	11
803	D	35	X	5	114	116	320.14	UCDavis	*P. pseudok-kugleri*	2.39	-0.20	3	12
803	D	35	X	5	125	127	320.25	UMass	*Ordorsalis* sp.	0.32	2.41		
803	D	35	X	5	125	127	320.25	UCDavis	*P. pseudok-kugleri*	2.20	-0.31	3	12
803	D	35	X	5	142	144	320.42	UCDavis	*P. pseudok-kugleri*	2.29	-0.31	3	11
803	D	35	X	6	6.5	8.5	320.565	UCDavis	*P. pseudok-kugleri*	2.36	-0.36	3	11
803	D	35	X	6	25	27	320.75	UMass	*Ordorsalis* sp.	0.35	2.29		
803	D	35	X	6	25	27	320.75	UCDavis	*P. pseudok-kugleri*	2.42	-0.34	3	10

803	D	35	X	6	39	41	320.89	UCDavis	*P. pseudok-kugleri*	2.27	-0.35	3	11
803	D	35	X	6	59	61	321.09	UCDavis	*P. pseudok-kugleri*	2.13	-0.45	3	13
803	D	35	X	6	75	77	321.25	UMass	*Ordorsalis* sp.				
803	D	35	X	6	75	77	321.25	UMass	*Ordorsalis* sp.	1.54	2.05		
803	D	35	X	6	75	77	321.25	UCDavis	*P. pseudok-kugleri*	2.18	-0.60	3	12
803	D	35	X	6	90	92	321.4	UCDavis	*P. pseudok-kugleri*	2.23	-0.60	3	13
803	D	35	X	6	125	127	321.73	UMass	*Ordorsalis* sp.	0.10	1.99		
803	D	35	X	6	123	125	321.73	UCDavis	*P. pseudok-kugleri*	1.98	-0.70	3	12
803	D	36	X	1	25	27	322.95	UMass	*Ordorsalis* sp.	-0.04	2.22		
803	D	36	X	1	25	27	322.95	UCDavis	*P. pseudok-kugleri*	2.00	-0.42	3	12
803	D	36	X	1	51	53	323.21	UCDavis	*Ordorsalis* sp.	-0.36	1.67	3	5
803	D	36	X	1	51	53	323.21	UCDavis	*P. pseudok-kugleri*	1.79	-0.27	3	8
803	D	36	X	1	51	53	323.21	UCDavis	*P. pseudok-kugleri*	2.08	-0.35	4	8
803	D	36	X	1	75	77	323.45	UMass	*Ordorsalis* sp.	-0.02	1.85		
803	D	36	X	1	75	77	323.45	UCDavis	*P. pseudok-kugleri*	1.94	-0.56	3	12
803	D	36	X	1	125	127	323.95	UMass	*Ordorsalis* sp.	-0.56	1.44		
803	D	36	X	1	125	127	323.95	UCDavis	*P. pseudok-kugleri*	1.76	-0.60	3	10
803	D	36	X	2	25	27	324.35	UMass	*Ordorsalis* sp.	-0.21	1.76		
803	D	36	X	2	52	54	324.72	UCDavis	*P. pseudok-kugleri*	1.65	-0.17	3	10
803	D	36	X	2	75	77	324.95	UMass	*Cibicidoides* sp.	-0.21	1.66		
803	D	36	X	2	75	77	324.95	UCDavis	*P. pseudok-kugleri*	1.94	-0.61	3	10
803	D	36	X	2	125	127	325.45	UMass	*Ordorsalis* sp.	0.00	1.80		
803	D	36	X	2	125	127	325.45	UCDavis	*P. pseudok-kugleri*	2.01	-0.61	5	9
803	D	36	X	3	25	27	325.95	UMass	*Cibicidoides* sp.	0.99	1.62		
803	D	36	X	3	25	27	325.95	UMass	*Ordorsalis* sp.	-0.17	1.87		
803	D	36	X	3	75	77	326.45	UMass	mixed	0.35	1.22		
803	D	36	X	3	125	127	326.95	UMass	*Ordorsalis* sp.	1.05	1.52		
803	D	36	X	5	50	52	329.2	UCDavis	*P. pseudok-kugleri*	1.88	-0.31	4	10
803	D	36	X	CC			331.7	UCDavis	*P. pseudok-kugleri*	1.65	-0.67	5	8
803	D	37	X	3	51	53	335.81	UCDavis	*P. pseudok-kugleri*	1.66	-0.69	4	8
803	D	38	X	1	50	52	342.5	UCDavis	*P. pseudok-kugleri*	1.61	-0.76	3	11
803	D	38	X	5	62	64	348.62	UCDavis	*P. pseudok-kugleri*	1.57	-0.73	3	10
803	D	39	X	1	51	53	352.11	UCDavis	*P. pseudok-kugleri*	1.17	-0.50	3	10
803	D	39	X	3	74	76	355.34	UCDavis	*P. pseudok-kugleri*	1.78	-0.49	3	10

WORKS CITED

Aljahdali, M. H., 2013, Pliocene-Pleistocene Calcareous Nannofossil Biostratigraphy of Iodp Hole 1396c Adjacent To Montserrat Island In The Lesser Antilles, Caribbean Sea, Plus Experimentally Induced Diagnesis: Electronic Theses, Treatises and Dissertations, Paper 7270.

Anderson, L. D., and Delaney, M. L., 2005, Use of multi proxy records on the Agulhas Ridge, Southern Ocean (Ocean Drilling Project Leg 117, Site 1090) to investigate sub-Antarctic hydrography from the Oligocene to the early Miocene: Paleoceanography, v. 20, PA3011. doi:10.1029/2004PA001082.

Aze, T., Ezard, T. H. G., Purvis, A., Coxall, H. K., Stewart, D. R. M., Wade, B. S., and Pearson, P. N., 2011, A phylogeny of Cenozoic macroperforate planktonic foraminifera from fossil data: Biological Reviews. doi: 10.1111/j.1469-185X.2011.00178.x.

Backman, J., Raffi, I., Rio, D., Fornaciari, E., and Pälike, H., 2012, Biozonation and biochronology of Miocene through Pleistocene calcareous nannofossils from low and middle latitudes: Newsletters on Stratigraphy, v. 45(3), p. 221-244.

Barerra, E., and Huber, B. T., 1991, Paleogene and early Neogene oceanography of the southern Indian Ocean: Leg 119 Foraminifer stable isotope results, *in* Barron, J., Larsen, B., et al. (eds.), Proceedings of the Ocean Drilling Program, Scientific Results, 119: College Station, TX (Ocean Drilling Program), p. 693-717.

Barerra, E., Baldauf, J., and Lohmann, K. C., 1993, Strontium isotope and benthic foraminifer stable isotope results from Oligocene sediments at Site 803, *in* Berger, W. H., Kroenke, L. W., Mayer, L. A., et al. (eds.), Proceedings of the Ocean Drilling Program, Scientific Results, 130: College Station, TX (Ocean Drilling Program), p. 269-279.

Bé, A. W. H. and Tolderlund, D. S., 1971, Distribution and ecology of living planktonic foraminifera in surface waters of the Atlantic and Indian Oceans, *in* Funnel, B. M., and Riedel, W. R. (eds.), The Micropaleontology of Oceans: p. 105-149.

Becker, R.A. and Wilks, A.R. (Original S code), R. Brownrigg (R version), T. P. Minka (Enhancements), 2015, maps: Draw Geographical Maps, R package version 2.3-11. http://CRAN.R-project.org/package=maps.

Benson, R. H., 1975, The origin of the psychrosphere as recorded in changes of deep-sea ostracode assemblages: Lethaia, v. 8(1), p. 69-83.

Berger, W. H., 1970, Planktonic Foraminifera: Selective solution and the lysocline: Marine Geology, v. 8(2), p. 111-138.

Berger, W. H., 1978, Sedimentation of deep-sea carbonate: maps and models of variations and fluctuations: The Journal of Foraminiferal Research, v. 8(4), p. 286-302.

Berger, W. H., 1979, Impact of deep-sea drilling on paleoceanography, *in* Talwani, M., Hay, W., and Ryan, W. B. F. (eds.) Deep Drilling Results in the Atlantic Ocean: Continental Margins and Paleoenvironment, Maurice Ewing Series, v. 3, Washington, D. C. (American Geophysical Union), p. 297-314

Berggren, W. A., Kent, D. V., Flynn, J. J., and van Couvering, J. A., 1985a, Cenozoic geochronology: Geological Society of America Bulletin, v. 96(11), p. 1407-1418.

Berggren, W. A., Kent, D. V., and van Couvering, J. A., 1985b, The Neogene: Part 2 Neogene geochronology and chronostratigraphy: Geological Society, London, Memoirs, v. 10, p. 211-260. doi:10.1144/GSL.MEM.1985.010.01.18

Berggren, W. A., and Pearson, P. N., 2006, Tropical and subtropical planktonic foraminiferal zonation of the Eocene and Oligocene, *in* Pearson, P. N., Olsson, R. K., Huber, B. T., Hemleben, C., Berggren, W. A., (eds.), Cushman Foundation Special Publication, 41, p. 29-40.

Bijl, P. K., Bendle, J. A. P., Bohaty, S. M., Pross, J., Schouten, S., Tauxe, L., Stickley, C. E., McKay, R. M., Röhl, U., Olney, M., Sluijs, A., Escutia, C., Brinkhuis, H., and Expedition 318 Scientists, 2013, Eocene cooling linked to early flow across the Tasmanian Gateway: Proceedings of the National Academy of Science, v. 110, p. 9645-9650.

Billups, K., Channel, J. E. T., and Zachos, J., 2002. Late Oligocene to early Miocene geochronology and paleoceanography from the subantarctic South Atlantic: Paleoceanography, v. 17(1), 1004. doi:10.1029/2000PA000568.

Birkenmajer, K., 1987. Oligocene-Miocene glacio-marine sequences of King George Island (South Shetland Islands), Antarctica: Palaeontologia Polonica, v. 49, p. 113–122.

Bolton, C. T., Gibbs, S. J., and Wilson, P. A., 2010, Evolution of nutricline dynamics in the equatorial Pacific during the late Pliocene: Paleoceanography, v. 25, PA1207, doi:10.1029/2009PA001821.

Cande, S. C., and Kent, D. V., 1995, Revised calibration of the geomagnetic polarity timescale for the Late Cretaceous and Cenozoic: Journal of Geophysical Research, v. 100, p. 6093-6095.

Cary, S. N., 1997, Influence of convective sedimentation on the formation of widespread tephra fall layers in the deep sea: Geology, v. 25, p. 839-842.

Cary, S. N., & Schneider, J. -L., 2001, Volcaniclastic processes and deposits in the Deep-Sea, *in* Developments in Sedimentology, v. 63, p. 457-515.

Cassidy, M., Trofimovs, J., Palmer, M. R., Talling, P. J., Watt, S. F. L., Moreton, S. G., and Taylor, R. N. 2013, Timing and emplacement dynamics of newly recognised mass flow deposit at ~8-12 ka offshore Soufriere Hills volcano, Montserrat: How submarine stratigraphy can complement subaerial eruption histories: Journal of Volcanology and Geothermal Research, v. 253, p. 1-14.

Cassidy, M., Watt., S. F. L, Palmer, M. R., Trofimovs, J., Symons, W., Maclachlan, S. E., and Stinton, A. J., 2014, Construction of volcanic records from marine sediment cores: A review and case study (Montserrat, West Indies): Earth-Science Reviews, v. 138, p. 137-155.

Chaisson, W. P., and Leckie, R. M., 1993, High-resolution Neogene planktonic foraminifer biostratigraphy of Site 806, Ontong Java Plateau (western equatorial Pacific), *in* Berger, W. H., Kroenke, I. W., Mayer, L. A., et al. (eds.), Proceedings of the Ocean Drilling Program, Scientific Results, 130: Ocean Drilling Program, College Station, TX, p. 113–136.

Chaisson, W. P., & D'Hondt, S. L., 1999, Neogene Planktonic Foraminifer Biostratigraphy at Site 999, Western Caribbean Sea, *in* Leckie, R. M., Sigurdsson, H., Acton, G. D., and Draper, G., (eds.), 2000. Proceedings of the Ocean Drilling Program, Scientific Results, 165: Ocean Drilling Program, College Station, TX, p. 19-56.

Chaproniere, G. C. H., Styzen, M. J., Sager, W. W., Nishi, H., Quinterno, P. J., and Abrahamsen, N., 1994. Late Neogene biostratigraphic and magnetostratigraphic synthesis, Leg 135, *in* Hawkins, J., Parson, L., Allan, J. et al. (eds.), Proceedings of the Ocean Drilling Program, Scientific Results, 135: Ocean Drilling Program, College Station, TX, p. 857-877.

Cifelli, R., 1969, Radiation of Cenozoic Planktonic Foraminifera: Systematic Zoology, v. 18(2), p. 154-168.

Clark, P. U., Archer, D., Pollard, D., Blum, J. D., Rial,. J. A., Brovkin, V., Mix, A. C., Pisias, N. G., and Roy, M., 2006, The middle Pleistocene transition: characteristics, mechanisms, and implications for long-term changes in atmospheric pCO_2: Quaternary Science Reviews, v. 25, p. 3150-3184.

Corliss, B. H., 1979, Response of deep-sea benthonic Foraminifera to development of the psychrosphere near the Eocene/Oligocene boundary: Nature, v. 282, p. 63-65. doi:10.1038/282063a0

Coxall, H. K., Wilson, P. A., Pälike, H., Lear, C. H., and Backman, J., 2005, Rapid stepwise onset of Antarctic glaciation and deeper calcite compensation in the Pacific Ocean: Nature, v. 433, p. 53-57.

Coxall, H. K., D'Hondt, S., and Zachos, J. C., 2006, Pelagic evolution and environmental recovery after the Cretaceous-Paleogene mass extinction: Geology, v. 34(4), p. 297-300. doi:10.1130/G21702.1.

Coxall, H. K., and Pearson, P. N., 2007, The Eocene-Oligocene Transition, *in* Williams, M., Haywood, A. M., Gregory, F. J., and Schmidt, D. N. (eds.), Deep-Time Perspectives on Climate Change: Marrying the Signal from Computer Models and Biological Proxies, The Micropalaeontological Society, Special Publications: The Geological Society, London, p. 351-387.

Coxall, H. K., and Wilson, P. A., 2011. Early Oligocene glaciation and productivity in the eastern equatorial Pacific: Insights into global carbon cycling: Paleoceanography, v. 26, PA2221. doi:10.1029/2010PA002021.

Coxall, H. K., and Spezzaferri, S., in preparation, Taxonomy, biostratigraphy, and phylogeny of Oligocene *Catapsydrax*, *Geloborotaloides*, and *Protentelloides*, *in* Wade, B. S. (eds.), Atlas of the Oligocene Planktonic Foraminifera.

Cramer, B. S., Toggweiler, J. R., Wright, J. D., Katz, M. E., and Miller, K. G., 2009, Ocean overturning since the Late Cretaceous: Inferences from a new benthic foraminiferal isotope compilation: Paleoceanography, v. 24(4). doi: 10.1029/2008PA001683.

Cramer, B. S., Miller, K. G., Barrett, P. J., and Wright, J. D., 2011, Late Cretaceous-Neogene trends in deep ocean temperature and continental ice volume: Reconciling records of benthic foraminiferal geochemistry $\delta^{18}O$ and Mg/Ca) with sea level history: Journal of Geophysical Research Oceans, v. 116(C12), C12023. doi: 10.1029/2011JC007255

Crone, E. E., Ellis, M. M., Morris, W. F., Stanley, A., Bell, T., Bierzychudek, P., Ehrién, J., Kaye, T. N., Knight, T. M., Lesica, P., Oostermeijer, G., Quintana-Ascencio, P. F., Ticktin, T., Valverde, T., Williams, J. L., Doak, D. F., Ganesan, R., McEachern, K., Thorpe, A. S., Menges, E. S., 2013, Ability of Matrix Models to Explain the Past and Predict the Future of Plant Populations: Conservation Biology, v. 27:5, p. 986-978.

Cullen, J. L., and Curry, W. B., 1997, Variations in planktonic foraminifer faunas and carbonate preservation at Site 927: Evidence for changing surface water conditions in the western tropical Atlantic Ocean during the middle Pleistocene *in* Shackleton, N. J., Curry, W. B., Richter, C., and Bralower, T. J. (eds.) Proceedings of the Ocean Drilling Program, Scientific Results, 154: Ocean Drilling Program, College Station, TX, p. 207-228.

DeConto, R. M., and Pollard, D., 2003, Rapid Cenozoic glaciation of Antarctica induced by declining atmospheric CO_2: Nature, v. 421, p. 245-248.

DeConto, R.M ., Pollard, D., Wilson, P. A., Pälike, H., Lear, C. H., and Pagani, M., 2008, Thresholds for Cenozoic bipolar glaciation: Nature, v. 455, p. 652-656.

Diester-Haass, L., 1996, Late Eocene-Oligocene paleoceanography in the southern Indian Ocean (ODP Site 744): Marine Geology, v. 130(1-2), p. 99-119.

Diester-Haass, L., Billups, K., and Emeis, K., 2011, Enhanced paleoproductivity across the Oligocene/Miocene boundary as evidenced by benthic foraminiferal accumulation rates: Palaeogeography, Palaeoclimatology, Paleoecology, v. 302, p. 464-473.

Edinger, E. N., and Risk, M. J., 1994, Oligocene-Miocene extinction and geographic restriction of Caribbean corals: roles of turbidity, temperature, and nutrients: Palaios, v.9(6), p. 576-598.

Ericson, D. B., and Wollin, G., 1968, Pleistocene climates and chronology in deep-sea sediments: Science, v. 162, p. 1227-1234.

Expedition 320/321 Scientists, 2010, Methods, *in* Pälike, H., Lyle, M., Nishi, H., Raffi, I., Gamage, K., Klaus, A., and the Expedition 320/321 Scientists, Proceedings of the Integrated Ocean Drilling Program, 332/321: Tokyo (Integrated Ocean Drilling Program Management International, Inc.). doi:10.2204/iodp.proc.320321.102.2010.

Expedition 340 Scientists, 2013, Site U1396, *in* Le Friant, A., Ishizuka, O., Stroncik, N. A., and the Expedition 340 Scientists, Proc. IODP, 340: Tokyo (Integrated Ocean Drilling Program Management International, Inc.). doi:10.2204/ iodp.proc.340.106.2013

Ezard, T. H. G., Aze, T., Pearson, P. N., and Purvis, A, 2011, Interplay between changing climate and species' ecology drives macroevolutionary dynamics: Science, v. 322, p. 349-351.

Fatela, F., and Taborda, R., 2002, Confidence limits of species proportions in microfossil assemblages: Marine Micropaleontology, v. 45, p. 169-174.

Florindo, F., Farmer, R. K., Harwood, D. M., Cody, R. D., Levy, R., Bohaty, S. M., Carter, L., and Winkler, A., 2013, Paleomagnetism and biostratigraphy of sedimnets from Southern Ocean ODP Site 744 (southern Kerguelen Plateau): Implications for early-to-middle Miocene climate in Antarctica: Global and Planetary Change, v. 110, p. 434-454.

Florindo, F., Gennari, R., Persico, D., Turco, E., Villa, G., Lurcock, P. C., Roberts, A. P., Winkler, A., Carter, L., and Pekar, S. F., 2015, New magnetobiostratigraphic chronology and paleoceanographic changes across the Oligocene-Miocene boundary at DSDP Site 516 (Rio Grande Rise, SW Atlantic): Paleoceanography, v. 30, p. 659-681. doi:10.1002/2014PA002734.

Foote, M., 2000, Origination and extinction components of taxonomic diversity: general problems: Paleobiology, v. 26(4), p. 74–102.

Fox, L. R., and Wade, B. S., 2013, Systematic taxonomy of early-middle Miocene planktonic foraminifera from the equatorial Pacific Ocean: Integrated Ocean Drilling Program, Site U1338: The Journal of Foraminiferal Research, v. 43(4), p. 374-405.

Fraass, A. J., Kelly, D. C., and Peters, S. E., 2015, Macroevolutionary History of the Planktic Foraminifera: Annual Review of Earth and Planetary Sciences, v. 43, p. 139-166.

Gradstein, F. M., Ogg, J. G., Schmitz, M. D., and Ogg, G. M., 2012. The Geologic Time Scale 2012: Elsevier B.V. 1144p.

Groeneveld, J., Hathorne, E. C., Steinke, S., DeBey, H., Mackensen, A., and Tiedemann, R., 2014, Glacial induced closure of the Panamanian Gateway during Marine Isotope Stages (MIS) 95-100 (~2.5 Ma): Earth and Planetary Science Letters, v. 404, p. 296-306.

Gupta, A. K., Dhingra, H., Mélice, J.-L., and Anderson, D. M., 2001, Earth's Eccentricity Cycles and Indian Summer Monsoon variability over the past 2 million years: Evidence from deep-sea Benthic Foraminifer: Geophysical Research Letters, v. 28(21), p. 4131-4134.

Haddad, G. A., and Droxler, A. W., 1996, Metastable $CaCO_3$ dissolution at intermediate water depths of the Caribbean and western North Atlantic: Implication for intermediate water circulation during the past 200,000 years: Paleoceanography, v. 11(6), p. 701-716.

Harford, C. L., 2002, The volcanic evolution of Montserrat using $^{40}Ar/^{39}Ar$ geochronology, *in* Druitt, T.H. and Kokelaar, B.P., eds. Geological Society Memoir No. 21: The Eruption of Soufrière Hills Volcano, Montserrat, from 1995 to 1999, Geological Society of London.

Hart, M. B., 1980, A water depth model for the evolution of the planktonic Foraminiferida: Nature, v. 286, pp. 252-254.

Hatfield, R. G., in press, Data Report: Stratigraphic correlation of Site U1396 and creation of a composite depth scale and splice: Expedition 340 Research Results.

Haug, G. H., and Tiedemann, R., 1998, Effect of the formation of the Isthmus of Panama on Atlantic Ocean thermohaline circulation: Nature. v. 393(6686), p. 673-676.

Hays, J. D., Imbrie, J., and Shackleton, N. J., 1976, Variations in the Earth's Orbit: Pacemaker of the Ice Ages: Science, v. 194(4270), p. 1121-1132. doi:10.1126/science.194.4270.1121.

Heim, N, and Peters, S. E., 2011, Regional Environmental breadth predicts geographic range and longevity in fossil marine genera: PLOS One, v. 6(5), e18946.

Herd, R. A., Edmonds, M., and Bass, V. A., 2005, Catastrophic lava dome failure at Soufriere Hills Volcano, Montserrat, 12-13 July 2003: Journal of Volcanology and Geothermal Research, v. 148(3-4), p. 234-252. doi: 10.1016/j.jvolgeores.2005.05.003

Hernández-Molina, F. J., Stow, D. A., Alvarez-Zarikian, C. A., Acton, G., Bahr, A., Balestra, B., Ducassou, E., Flood, R., Flores, J. -A., Furota, S., Grunert, P., Hodell, D., Jimenez-Espejo, F., Kim, J. K., Krissek, L., Kuroda, J., Li, B., Llave, E., Lofi, J., Lourens, L., Miller, M., Nanayama, F., Nishida, N., Richter, C., Roque, C., Pereira, H., Goñi, M. F. S., Sierro, F. J., Singh, A. D., Sloss, C., Takashimizu, Y., Tzanova, A., Voelker, A., Williams, T., and Xuan, C., 2014. Onset of Mediterranean outflow into the North Atlantic: Science, v. 344(6189), p. 1244-1250.

Hill, P. J., and Exon, N. F., 2004. Tectonics and Basin Development of the Offshore Tasmanian Area Incorporating Results from Deep Ocean Drilling, *in* Exon, N. F., Kennet, J. P., and Malone, M. (eds), The Cenozoic Southern Ocean: Tectonics, Sedimentation, and Climate Change Between Australia and Antarctica, Geophysical Monograph 151: American Geophysical Union. doi:10.1029/GM151.

van Hinsbergen, D. J. J., de Groot, L. V.,van Schaik, S. J., Spakman, W., Bijl, P. K., Sluijs, A., Langereis, C. G., and Brinkhuis H., 2015, A Paleolatitude Calculator for Paleoclimate Studies (model version 1.2): PLOS ONE.

Hörnes, M., 1853, Mitteilung an Prof. Bronn gerichtet: Wien, 3. Okt., 1853. Neues Jahrbuch für Mineralogie, Geognosie, Geologie and Petrefaktenkunde, p. 806-810.

Huber, B. T., Olsson, R. K., and Pearson, P. N., 2006, Taxonomy, biostratigraphy, and phylogeny of Eocene microperforate Planktonic Foraminifera (*Jenkinsina, Cassigerinelloita, Chiloguembelina, Streptochilus, Zeauvigerina, Tenuitella,* and *Cassigerinella*) and problematica (*Dipsidripella*), *in* Pearson, P.N., Olsson, R.K., Huber, B. T., Hemleben, Ch., and Berggren, W. A., (eds.), Atlas of the Eocene Planktonic Foraminifera: Cushman Foundation Special Publication, n. 41, p. 461-508.

Huber, B. T., and Leckie, R. M., 2011, Planktic foraminiferal species turnover across deep-sea Aptian/Albian boundary sections, Journal of Foraminiferal Research, v. 41(1), p. 53-95.

Jutzeler, M., Talling, P. J., White, J. D. L., and Expedition 340 Scientists, in press, Coring disturbances in IODP 340, a detailed list of intervals with fall-in and flow-in: Expedition 340 Research Results.

Katz, M. E., Katz, D. R., Wright, J. D., Miller, K. G., Pak, D. K., Shackleton, N. J., and Thomas, E., 2003. Early Cenozoic benthic foraminiferal isotopes: Species reliability and interspecies correction factors: Paleoceanography, v. 18(2), 1024. doi:10.2002PA000798.

Katz, M. E., Cramer, B. S., Toggweiler, J. R., Esmay, G., Liu, C., Miller, K. G., Rosenthal, Y., Wade, B. S., and Wright, J. D., 2011, Impact of Antarctic Circumpolar Current development on late Paleogene Ocean Structure: Science, v. 332(6033), p. 1076-1079.

Kamikuri, S., Nishi, H., Moore, T. C.,Nigrini, C. A. and Motoyama, I., 2005, Radiolarian faunal turnover across the Oligocene/Miocene boundary in the equatorial Pacific Ocean: Marine Micropaleontology, v. 57.

Kamikuri, S., Moore, T. C., Ogane, K., Suzuki, N., Pälike, H., and Nishi, H., 2012, Early Eocene to early Miocene radiolarian biostratigraphy for the low-latitude Pacific Ocean: Stratigraphy, v. 9(1), p. 77-108.

Kaneps, A. G., 1979, Gulf Stream: Velocity Fluctuations During the Late Cenozoic: Science, v. 204, p. 297-301.

Kawahata, H., Suzuki, A., Ohta, H., 2000, Export fluxes in the western Pacific warm pool: Deep-Sea Research I, v. 47, p. 2061-2091

Keating, B. H., and Sakai, H., 1991, Magnetostratigraphic studies of sediments from Site 744, Southern Kerguelen Plateau, *in* Barron, J., Larsen, B., et al. (eds.) Proceedings of the Ocean Drilling Program, Scientific Results, 119: College Station, TX (Ocean Drilling Program), p. 477-504. doi:10.2973/odp.proc.sr.119.147.1991

Keigwin, L., 1982, Isotopic paleoceanography of the Caribbean and East Pacific: Role of Panama uplift in late Neogene time: Science v. 217(4557), p. 350-353.

Keller, G., and Barron, J.A., 1983, Paleoceanographic implications of Miocene deep-sea hiatuses: Geological Society of American Bulletin, v. 94, p. 590-613.

Kellog, E. A., 2001, Evolutionary History of the Grasses: Plant Physiology, v. 125(3), p. 1198-1205.

Kennett, J. P., and Huddlestun, P., 1972, Late Pleistocene paleoclimatology, foraminiferal biostratigraphy and tephrochronology, Western Gulf of Mexico: Quaternary Research, v. 2, p. 38-69.

Kennett, J. P., and Shackleton, N. J., 1976, Oxygen isotope evidence for the development of the psychrosphere 38 Myr ago: Nature, v. 260, p. 513-515.

Kennett, J. P., and Stott, L. D., 1990, Proteus and Proto-Oceanus: Ancestral Paleogene oceans as revealed from Antarctic stable isotopic results; ODP Leg 113 *in* Barker, P. F., Kennett, J. P., (eds.) Proceedings of the Ocean Drilling Program, Scientific Results, 113: College Station, TX (Ocean Drilling Program), p. 865-880.

Kominz, M. A., Browning, J. V., Miller, K. G., Sugarman, P. J., Mizintseva, S., and Scotese, C. R., 2008. Late Cretaceous to Miocene sea-level estimates from the New Jersey and Delaware coastal plain coreholes: an error analysis: Basin Research, v. 20, p. 211-226. doi:10.1111/j.1365-2117.2008.00354.x

Koutsoukos, E., 2014, Phenotypic plasticity, speciation, and phylogeny in early Danian planktic foraminifera: Journal of Foraminiferal Research, v. 44(2), p. 109-142. doi: 10.2113/gsjfr.44.2.109.

Kroenke, L. W., Resig, J. M., and Leckie, R. M., 1993, Hiatus and tephrochronology of the Ontong Java Plateau: correlation with regional tectono-volcanic events, *in* Berger, W. H., Kroenke, L. W., and Mayer, L. A. (eds.), Proceedings of the Ocean Drilling Program, Scientific Results, 130: Ocean Drilling Program, College Station, TX, p. 423–444.

Laskar, J., Robutel, P., Joutel, F., Gastineau, M., Correia, A. C. M., and Levrard, B., 2004, A long term numerical solution for the insolation quantities of the Earth: Astronomy and Astrophysics, v. 428, p. 261-285.

Laskar, J., Fienga, A., Gastineau, M., and Manche, H., 2010, La2010: A new orbital solution for the long term motion of the Earth: Earth and Planetary Astrophysics, v. 532, A89. doi:10.1051/0004-6361/201116836.

Le Friant, A., Deplus, C., Boudon, G., Feuillet, N., et al., 2010, Eruption of Soufriere Hills (1995-2009) from an offshore perspective: Insights from repeated swath bathymetry surveys: Geophysical Research Letters, v. 37, n. 19.

Le Friant, A., Lock, E. J., Hart, M. B., Boudon, G., Sparks, R. S. J., Leng, M. J., Smart, C. W., Komorowski, J. C., Deplus, C., and Fisher J. K., 2008, Late Plesitocene tephrochronology of marine sediments adjacent to Montserrat, Lesser Antilles volcanic arc: Journal of the Geological Society, v. 165(1), p. 279-289.

Lear, C. H., Rosenthal, Y., Coxall, H. K., and Wilson, P. A., 2004, Late Eocene to Early Miocene ice sheet dynamics and the global carbon cycle: Paleoceanography, v. 19, PA4015. doi:10.1029/2004PA001039.

Leckie, R. M., and Webb, P. N., 1983, Late Oligocene-early Miocene glacial record of the Ross Sea, Antarctica: evidence from DSDP Site 270: Geology, v. 11(10), p. 578-582.

Leckie, R. M., Farnham, C., and Schmidt, M. G., 1993, Oligocene planktonic foraminifer biostratigraphy of Hole 803D (Ontong Java Plateau) and Hole 628A (Little Bahama Bank), and comparison with the southern high latitudes, *in* Berger, W. H., Kroenke, L. W., and Mayer, L. A. (eds.), Proceedings of the Ocean Drilling Program, Scientific Results, 130: Ocean Drilling Program, College Station, TX, p. 113–136.

Leckie, R. M., Bralower, T. J., and Cashman, R., 2002, Oceanoic anoxic events and plankton evolution: Biotic response to tectonic forcing during the mid-Cretaceous: Paleoceanography, v. 17(3). doi: 10.1029/2001PA000623.

Leckie, R. M., Fraass, A. J., Wade, B. S., and Pearson, P. N., in preparation, Taxonomy, biostratigraphy, and phylogeny of Oligocene *Paragloborotalia, in* Wade, B. S. (eds.), Atlas of the Oligocene Planktonic Foraminifera.

Li, Q., Li, B., Zhong, B., McGowran, B., Zhou, Z., Wang, J., and Wang, P., 2006. Late Miocene development of the western Pacific warm pool: Planktonic foraminifer and oxygen isotopic evidence: Palaeogeography, Palaeoclimatology, Palaeoecology, v. 237(2-4), p. 465-482.

Liebrand, D., Lourens, L. J., Hodell, D. A., de Boer, B., van de Wal, R. S. W., and Pälike, H., 2011. Antarctic ice sheet and oceanographic response to eccentricity forcing during the early Miocene: Climate of the Past, v. 7, p. 869-880. doi:10.5194/cp-7-869-2011.

Lipps, J., 1970, Plankton evolution: Evolution, v. 24(1), p. 1-22.

Lisiecki, L. E., and Raymo, M. E., 2005, A Pliocene-Pleistocene stack of 57 globally distributed benthic $\delta^{18}O$ records: Paleoceanography, v. 20, PA1003. doi:10.1029/2004PA001071.

Liu, C., and Olsson, R. K., 1964, Evolutionary radiation of microperforate planktonic foraminifera following the K/T mass extinction event: Journal of Foraminiferal Research, v. 22(4), p. 328-346.

Livermore, R., Hillenbrand, C.-D., Meredith, M., and Eagles, G., 2007, Drake Passage and Cenozoic climate: An open and shut case?: Geochemistry Geophysics Geosystems, v. 8(1), Q01005. doi:10.1029/2005GC001224.

Lloyd, G.T., Pearson, P.N., Young, J.R., and Smith, A.B., 2012, Sampling bias and the fossil record of planktonic foraminifera on land and in the deep sea: Paleobiology, v. 38(4), p. 569-584.

Lourens, L. J., Hilgen, F. J., Shackleton, N. J., Laskar, J., and Wilson, D., 2004, The Neogene Period, *in* Gradstein, F. M., Ogg, J. G., Smith, A. G. (eds.), Geological Time Scale 2004: Cambridge University Press, p. 409-440.

Lourens, L. J., Sluijs, A., Kroon, D., Zachos, J. C., Thomas, E., Röhl, U., Bowles, J., and Raffi, I., 2005, Astronomical pacing of late Palaeocene to early Eocene global warming events: Nature, v. 435, p. 1083-1087. doi:10.1038/nature03814.

Loutre, M. F., Paillard, D., Vimeux, F., and Cortijo, E., 2004, Does mean annual insolation have the potential to change the climate?: Earth and Planetary Science Letters, v. 211(1). doi:10.1016/S0012-821X(04)00108-6.

Lyle, M., Wilson, P. A., Janecek, T. R., et al., 2002, Proceedings of the Ocean Drilling Program, Initial Reports, v. 199: College Station, TX (Ocean Drilling Program). doi:10.2973/odp.proc.ir.199.

Lyle, M., Barron, J., Bralower, T. J., Huber, M., Olivarez Lyle, A., Ravelo, A. C., Rea, D. K., and Wilson, P. A., 2008, Pacific Ocean and Cenozoic evolution of climate: Reviews of Geophysics, v. 46, RG2002. doi:10.1029/2005RG000190.

Macdonald, R., Hawkesworth, C. J., & Heath, E., 2000, The Lesser Antilles volcanic chain: a study in arc magmatism: Earth Science Reviews, v. 49(1-4), p. 1-76.

MacFadden, B. J., Bryant, J. D., and Mueller, P. A., 1991, Sr-isotopic, paleomagnetic, and biostratigraphic calibration of horse evolution: Evidence from the Miocene of Florida: Geology, v. 19, p. 242-245. doi: 10.1130/0091-7613(1991)019<0242:SIPABC>2.3.CO;2

Mawbey, E. M., and Lear, C. H., 2013, Carbon cycle feedbacks during the Oligocene-Miocene transient glaciation: Geology, v. 41(9), p. 963-966. doi:10.1130/G34422.1.

McArthur, J. M., Howarth, R.J ., 2004. Chapter 7: Strontium Isotope Stratigraphy, *in* Gradstein F. M., Ogg J. G., and Smith, A. (eds.), The Geologic Time Scale 2004: Cambridge University Press, United Kingdom.

McArthur, J. M., Howarth, R. J. and Shield, G. A., 2012, Chapter 7: Strontium Isotope Stratigraphy, *in* Gradstein F. M., Ogg J. G., Schmitz, M. D., and Ogg, G. M. (eds.), The Geologic Time Scale 2012: Elsevier, Vol 1 of 2.

McArthur, J.M., Howarth, R.J., and Bailey, T.R, 2001, Strontium Isotope Stratigraphy: LOWESS Version 3: Best Fit to the Marine Sr-Isotope Curve for 0–509 Ma and Accompanying Look-up Table for Deriving Numerical Age: The Journal of Geology, v.109, p. 155–170.

McMillen, K. J., and Casey, R. E., 1978, Distribution of living polycystine radiolarians in the Gulf of Mexico and Caribbean Sea, and comparison with the sedimentary record: Marine Micropaleontology, v. 3(2), p. 121-145.

Meyers, S. R., 2014, astrochron: An R Package for Astrochronology. http://cran.r-project.org/package=astrochron

Meyers, S. R., and Sageman, B. B., 2004, Detection, quantification, and significance of hiatuses in pelagic and hemipelagic strata: Earth and Planetary Science Letters, v. 224, p. 55-72.

McCanta, M. C., Hatfield, R. G., Thomas, B. J., Hook, S. J., and Fisher, E. in review, Identifying cryptotephra units using correlated rapid, nondestructive methods: VSWIR spectroscopy, X-ray fluorescence, and magnetic susceptibility: Geochemistry Geophysics Geosystems.

Milankovitch, M., 1930. Mathematical climate doctrine and astronomical theory of climate variability, *in* Koppen, W. and Geiger, R. (eds.), Handbook of Climatology 1 (A). Gebr. Borntraeger (Berlin), p. 1-176.

Miller, K. G., Fairbanks, R. G., and Mountain, G. S., 1987, Tertiary oxygen isotope synthesis, sea level history, and continental margin erosion: Paleoceanography, v. 2(1), p. 1-19.

Miller, K. G., Feigenson, M. D., Kent, D. V., and Olsson, R. K., 1988, Oligocene stable isotope ($^{87}Sr/^{86}Sr$, $\delta^{18}O$, $\delta^{13}C$) standard section, Deep Sea Drilling Project Site 522: Paleoceanography, v. 3, p. 223-233.

Miller, K. G., Wright, J. D., and Fairbanks, R. G., 1991, Unlocking the ice house: Oligocene-Miocene Oxygen isotopes, eustasy, and margin erosion: Journal of Geophysical Research, v. 96(B4), p. 6829-6848.

Molnar, P., 2008, Closing of the Central American Seaway and the Ice Age: A critical review: Paleoceanography, v. 23(2), PA2201.

Moore, T. C., Jr., Van Andel, T. H., Sancetta, C., and Pisias, N., 1978, Cenozoic hiatuses in pelagic sediments: Micropaleontology, v. 24(2), p. 113-138.

Moore, T. C., Jr., Wade, B. S., Westerhold, T., Erhardt, A. M.,Coxall, H. K., Baldauf, J., and Wagner, M., 2014, Equatorial Pacific productivity changes near the Eocene-Oligocene boundary: Paleoceanography, v. 29, p. 825–844. doi:10.1002/ 2014PA002656.

Naish, T. R., Woolfe, K. J., Barrett, P. J., Wilson, G. S., Atkins, C., Bohaty, S. M., Bücker, C. J., Claps, M., Davey, F. J., Dunbar, G. B., Dunn A. G., Fielding, C. R., Florindo, F., Hannah, M. J., Harwood, D. M., Henrys, S. A., Krissek, L. A., Lavelle, M., van der Meer, J., McIntosh, W. C., Niessen, F., Passchier, S., Powell, R. D., Roberts, A. P., Sagnotti, L., Scherer, R. P., Strong C. P., Talarico, F., Verosub, K. L., Villa, G., Watkins, D. K., Webb, P.-N., and Wonik, T., 2001, Orbitally induced oscillations in the East Antarctic ice sheet at the Oligocene/Miocene boundary: Nature, v. 413, p. 719-722.

Naish, T. R., Wilson, G. S., Dunbar, G. B., and Barrett, P. J., 2008, Constraining the amplitude of Late Oligocene bathymetric changes in western Ross Sea during orbitally-induced oscillations in the East Antarctic Ice Sheet: (2) Implications for global sea-level changes: Palaeogeography, Palaeoclimatology, Palaeoecology, v. 260(1), p. 66-76.

Nathan, S. A., and Leckie, R. M., 2009, Early history of the Western Pacific Warm Pool during the middle to late Miocene (~13.2-5.8 Ma): Role of sea-level change and implications for equatorial circulation: Palaeogeography, Palaeoclimatology, Paleoecology, v. 274, p. 140-159.

Nelson, C. S., and Cooke, P. J., 2001, History of oceanic front development in the New Zealand sector of the Southern Ocean during the Cenozoic—a synthesis: New Zealand Journal of Geology and Geophysics, v. 44(4), p. 535-553. doi:10.1080/00288306.2001.9514954.

Nishimura, S., and Suparka, S., 1997, Tectonic approach to the Neogene evolution of Pacific-Indian Ocean seaways: Tectonophysics, v. 281(1-2), p. 1-16.

Nobes, D. C., Mienert, J., Dirksen, G. J., 1991, Lithologic Control of Physical-Property Interrelationships, *in* Ciesielski, P. F., and Kristoffersen, Y. (eds.), Proceedings of the Ocean Drilling Program, Scientific Results, 144: College Station, TX (Ocean Drilling Program), p. 657-669.

Norris, R. D., 1991, Biased extinction and evolutionary trends: Paleobiology, v. 17(4), p. 388-399.

Norris, R. D., 1992, Extinction selectivity and ecology in planktonic foraminifera: Palaeogeography, Palaeoclimatology, Palaeoecology, v. 95, p. 1-17.

Norris, R. D., 2000, Pelagic species diversity, biogeography, and evolution: Paleobiology, v. 26(4), p. 236-258.

Ogg, J. G., 2012, The Geomagnetic Polarity Timescale, *in* Gradstein, F. M., Ogg, J. G., Schmitz, M. D., and Ogg, G. M. (eds.), The Geologic Time Scale 2012: Amsterdam (Elsevier). doi:10.1016/B978-0-444-59425-9.01002-7

Olsson, R. K., Hemleben, C., Berggren, W. A., and Huber, B. T., 1999, Atlas of Paleocene planktonic foraminifera: Smithsonian Contributions to Paleobiology, n. 85.

Olsson, R. K., Hemleben, C., and Coxall, H. K., in preparation, Taxonomy, Biostratigraphy, and Phylogeny of Oligocene *Ciperoella* N. Gen., *in* Wade, B. S. (eds.), Atlas of the Oligocene Planktonic Foraminifera.

Osborne, A. H., Newkirk, D. R., Groenveld, J., Martin, E. E., Tiedemann, R., and Frank, M., 2014, The seawater neodymium and lead isotope record of the final stages of Central American Seaway closure: Paleoceanography, v. 29, p. 715-729. doi:10.1002/2014PA002676.

Paul, H. A., Zachos, J. C., Flower, B. P., and Tripati, A., 2000, Orbitally induced climate and geochemical variability across the Oligocenene/Miocene boundary: Paleoceanography, v. 15(5), p. 471-485.

Pälike, H., Frazier, J., and Zachos, J. C., 2006a, Extended orbitally forced palaeoclimatic records from the equatorial Atlantic Ceara Rise: Quaternary Science Reviews, v. 25, p. 3138-3149.

Pälike, H., Norris, R. D., Herrle, J. O., Wilson, P. A., Coxall, H. K., Lear, C. H., Shackleton, N. J., Tripati, A. K., and Wade, B. S., 2006b, The heartbeat of the Oligocene Climate System: Science, v. 314, p. 1894-1898.

Pälike, H., Lyle, M. W., Nishi, H., Raffi, I., Ridgwell, A., Gamage, K., Klaus, A., Acton, G., Anderson, L., Backman, J., Baldauf, J., Beltran, C., Bohaty, S. M., Bown, P., Busch, W., Channell, J. E. T., Chun, C. O. J., Delaney, M., Dewangan, P., Dunkley Jones, T., Edgar, K. M., Evans, H., Fitch, P., Foster, G. L., Gussone, N., Hasegawa, H., Hathorn, E. C., Hayashi, H., Herrle, J. O., Holbourn, A., Hovan, S., Hyeong, K., Iijima, K., Ito, T., Kamikuri, S., Kimoto, K., Kuroda, J., Leon-Rodriguez, L., Malinverno, A., Moore, T. C., Jr., Murphy, B. H., Murphy, D. P., Nakamura, H., Ogane, K., Ohneiser, C., Richter, C., Robinson, R., Rohling, E. J., Romero, O., Sawadea, K., Scher, H., Schneider, L., Sluijs, A., Takata, H., Tian, J., Tsujimoto, A., Wade, B., S., Westerhold, T., Wilkens, R., Williams, T., Wilson, P. A., Yamamoto, Y., Yamamoto, S., Yamazaki, T., and Zeebe, R. E., 2012, A Cenozoic record of the equatorial Pacific carbonate compensation depth: Nature, v. 488, p. 609-614.

Pearson, P. N., Shackleton, N. J., Weedon, G. P., and Hall, M. A., 1997, Multispecies planktonic foraminifera stable isotope stratigraphy through Oligocene/Miocene boundary climatic cycles, Site 926, *in* Shackleton, N. J., Curry, W. B., Richter, C., and Bralower, T. J., (eds.), Proceedings of the Ocean Drilling Program, Scientific Results, 154: Ocean Drilling Program, College Station, TX, p. 113–136.

Pearson, P. N., Ditchfield, P. W., Singano, J., Harcourt-Brown, K. G., Nicholas, C. J., Olsson, R. K., Shackleton, N. J., and Hall, M. A., 2001, Warm tropical sea surface temperatures in the Late Cretaceous and Eocene epochs: Nature, v. 413, p. 481-487.

Pearson, P. N., Olsson, R. K., Huber, B. T., Hemleben, Ch., and Berggren, W. A., 2006, Atlas of the Eocene Planktonic Foraminifera: Cushman Foundation for Foraminiferal Research, Special Publication 41.

Pearson, P. N., McMillan, I. K, Wade, B. S., Dunkley Jones, T., Coxall, H. K., Bown, P. R., and Lear, C.H., 2008, Extinction and environmental change across the Eocene-Oligocene boundary in Tanzania: Geology, v. 36, p. 179-182.

Pearson, P. N., and Wade, B. S., 2009, Taxonomy and stable isotope paleoecology of well-preserved planktonic foraminifera from the uppermost Oligocene of Trinidad: Journal of Foraminiferal Research, v. 39(3), p. 191-217.

Pearson, P. N., Olsson, R. K., Spezzaferri, S., and Leckie, R. M., in preparation, Taxonomy, biostratigraphy, and phylogeny of Oligocene Globanomalinidae (*Pseudohastigerina* and *Turborotalia*), *in* Wade, B. S., et al. (ed.), Atlas of the Oligocene Planktonic Foraminifera.

Pearson, P. N., Spezzaferri, S., Huber, B. T., and Kučera, M., in preparation, Taxonomy, biostratigraphy, and phylogeny of Oligocene *Cassigerinella, in* Wade, B. S., et al. (eds.), Atlas of the Oligocene Planktonic Foraminifera.

Pearson, P. N., Wade, B. S., and Huber, B. T., in preparation, Taxonomy, biostratigraphy, and phylogeny of Oligocene Globigerinitidae (*Dipsidripella, Globigerinita*, and *Tenuitella*), *in* Wade, B. S., et al. (eds.), Atlas of the Oligocene Planktonic Foraminifera.

Pekar, S., DeConto, R. M., and Harwood, D. M., 2006, Resolving a late Oligocene conundrum: Deep-sea warming and Antarctic glaciation: Palaeogeography Palaeoclimatology Palaeoecology, v. 231(1-2), p. 29-40.

Peters, S. E., 2006. Macrostratigraphy of North America: The Journal of Geology, v. 114, p. 391-412.

Peters, S. E., Kelly, D. C., and Fraass, A. J., 2013: Oceanographic controls on the diversity and extinction of planktonic foraminifera: Nature, v. 493(7432), p. 398-401.

Peterson, L. C., and Prell, W. L., 1985, Carbontae preservation and rates of climatic change: an 800 kyr record from the Indian Ocean, *in* Sundquist, E. T., and Broecker, W. S. (eds.), The Carbon Cycle and Atmospheric CO_2: Natural Variations Archean to Present: American Geophysical Union, Geophyiscal Monograph 32, p. 251-269.

Petrizzo, M. R., Huber, B. T., Gale, A. S., Barchetta, A., and Jenkyns, H. C., 2012, Abrupt planktic foraminiferal turnover across the Niveau Kilian at Col de Pré-Guittard (Vocontian Basin, southeast France): new criteria for defining the Aptian/Albian boundary: Newsletters on Stratigraphy, v. 45(1), p. 55-74.

Pfuhl, H. A., Mccave, I. N., Schellenberg, S. A., and Ferretti, P., 2004, Changes in Southern Ocean circulation in late Oligocene to early Miocene time, *in* Exon, N. F., Kennett, J. P., and Malone, M. J., (eds.) The Cenozoic Southern Ocean: Tectonics, sedimentation, and climate change between Australia and Antarctica: American Geophysical Union, Washington, D. C.. doi: 10.1029/151GM11.

Piela, C., Lyle, M., Marcantonio, F., Baldauf, J., and Olivarez Lyle, A., 2012, Biogenic sedimentation in the equatorial Pacific: Carbon cycling and paleoproduction, 12–24 Ma: Paleoceanography,v. 27, PA2204. doi:10.1029/2011PA002236.

Premoli Silva, I., and Sliter, W. V., 1999, Cretaceous paleoceanography: Evidence from planktonic foraminiferal evolution, *in* Barrera, E., and Johnson, C. C. (eds.) Evolution of the Cretaceous Ocean-Climate System: Geological Society of America, Special Paper 332, Boulder, CO, pp. 301-328.

R Core Team, 2014, R: A language and environment for statistical computing: R Foundation for Statistical Computing, Vienna, Austria. URL http://www.R-project.org/.

Ramsay A. T. S., Sykes, T. J. S., and Kidd, R. B., 1994, Waxing (and waning) lyrical on hiatuses: Eocene – Quaternary Indian Ocean hiatuses as proxy indicators of water mass production: Paleoceanography, v. 9(6), p. 857-877.

Reghellin, D., Coxall, H. K., Dickens, G. R., and Backman, J., 2015, Carbon and oxygen isotopes of bulk carbonate in sediment deposited beneath the eastern equatorial Pacific over the last 8 million years: Paleoceanography, v. 30, p. 1261-1286. doi:10.1002/2015PA002825.

Reid, R. P., Carey, S. N., and Ross, D. R., 1996, Late Quaternary sedimentation in the Lesser Antilles island arc: GSA Bulletin, v. 108(1), p. 78-100.

Roberts, A. P., Bicknell, S. J., Byatt, J., Bohaty, S. M., Florindo, F., and Harwood, D. M., 2003, Magnetostratigraphic calibration of Southern Ocean diatom datums from the Eocene-Oligocene of Kerguelen Plateau (Ocean Drilling Program sites 744 and 748): Palaeogeography, Palaeoclimatology, Palaeoecology, v. 198, p. 145-168.

Scher, H. D., and Martin, E. E., 2008, Timing and climatic consequences of the opening of Drake Passage: Science, v. 312, p. 428-430.

Scher, H. D., Whittaker, J. M., Williams, S. E., Latimer, J. C., Kordesch, W. E. C., and Delaney, M. L., 2015, Onset of Antarctic Circumpolar Current 30 million years ago as Tasmanian Gateway aligned with westerlies: Nature, v. 523, p. 580-583.

Shackleton, N. J., Hall, M. A., and Boersma, A., 1984, Oxygen and carbon isotope data from Leg 74 foraminifers, *in* Moore, T. C., Jr., Rabinowitz, P. D., et al., (eds.) Initial Reports of the Deep Sea Drilling Project, Volume LXXIV: Washington (U.S. Government Printing Office), p. 599–612.

Shackleton, N. J., Hall, M. A., Raffi, I., Tauxe, L., and Zachos, J. C., 2000, Astronomical calibration age for the Oligocene-Miocene boundary: Geology, v. 28, p. 447–450.

The Shipboard Scientific Party, 1970. Initial Reports of the Deep Sea Drilling Project, Volume III.

The Shipboard Scientific Party, 1972, Site 78, *in* Hays, J. D., et al. (eds.), Initial Reports of the Deep Sea Drilling Project, Volume IX: Washington (U.S. Government Printing Office), p. 209-316.

Shipboard Scientific Party, 1986, Site 628: Little Bahama Bank, *in* Austin, J. A., Jr., Schlager, W., and Palmer, A. A. (eds.), Proceedings of the Ocean Drilling Program, Initial Reports, 101: Ocean Drilling Program, College Station, TX, p. 213–270.

Shipboard Scientific Party, 1989, Site 744, *in* Barron, J., Larsen, B., et al. (eds.) Proceedings of the Ocean Drilling Program, Initial Reports, 119: College Station, TX (Ocean Drilling Program), p. 477-504.

Shipboard Scientific Party, 1991, Site 803, *in* Kroenke, L. W., Berger, W. H., and Janecek, T. R., (eds.), Proceedings of the Ocean Drilling Program, Initial Reports, 130: Ocean Drilling Program, College Station, TX, p. 101–176.

Smart, C. W., and Thomas, E. S., in preparation, Taxonomy, biostratigraphy, and phylogeny of Oligocene *Streptochilus, in* Wade, B. S., et al., (eds.), Atlas of the Oligocene Planktonic Foraminifera.

Smit, J., 1982, Extinction and evolution of planktonic foraminifera at the Cretaceous/Tertiary boundary after a major impact, *in* Silver, L. T., and Schultz, P. H., (eds.), Geological implications of impacts of large asteroids and comets on the Earth: Geological Society of America Special Paper 190, p. 329-352.

Spero, H. J., Bijma, J., Lea, D. W., and Bemis, B. E., 1997, Effect of seawater carbonate concentration on foraminiferal carbon and oxygen isotopes: Nature, v. 390, p. 497–500.

Spezzaferri, S., Constandache, M., and Olsson, R. K., in preparation, Taxonomy, biostratigraphy, and phylogeny of Oligocene to lower Miocene *Globigerinoides, in* Wade, B. S., et al. (eds.), Atlas of the Oligocene Planktonic Foraminifera.

Spezzaferri, S., Coxall, H. K., Olsson, R. K., Hemleben, C., and Constandache, M., in preparation, Taxonomy, biostratigraphy, and phylogeny of Oligocene *Globigerina, Globigerinella,* and *Quiltyella, in* Wade, B. S., et al. (eds.), Atlas of the Oligocene Planktonic Foraminifera.

Spezzaferri, S., Olsson, R. K., Hemleben, C., Wade, B. S., and Constandache, M., in preparation, Taxonomy, biostratigraphy, and phylogeny of Oligocene and lower Miocene *Globoturborotalita, in* Wade, B. S., et al. (eds.), Atlas of the Oligocene Planktonic Foraminifera.

Spiess, V., 1990, Cenozoic magnetostratigraphy of Leg 113 drill sites, Maud Rise, Weddell Sea, Antarctica, *in* Barker, P. F., Kennett, J. P., et al. (eds.), Proceedings of the Ocean Drilling Program, Initial Reports 113: Ocean Drilling Program, College Station, TX, p. 261-315.

Steiniger, F. F., Aubry, M. P., Berggren, W. A., Biolzi, M., Borsetti, A. M., Cartlidge, J. E., Cati, F., Corfield, R., Gelati, R., Iaccarino, S., Napoleone, C., Ottner, F., Roegl, F., Roetzel, R., Spezzaferri, S., Tateo, F., Villa, G., and Zevenboom, D., 1997, The Global Stratotype Section and Point (GSSP) for the Base of the Neogene: Episodes 20(1), p. 23-28.

Strömberg, C. A. E., 2005.,Decoupled taxonomic radiation and ecological expansion of open-habitat grasses in the Cenozoic of North America: PNAS, v. 102(34), p. 11980-11984.

Thierstein, H. R., Geitzenauer, K. R., Molfino, B., Shackleton, N. J., 1977, Global synchroneity of late Quaternary coccolith datum levels: Validation by oxygen isotopes: Geology, v. 5, p. 400-404.

Trofimovs, J., Fisher, J. K., Macdonald, H. A., Talling, P. J., Sparks, R. S. J., Hart, M. B., Smart, C. W., Boudon, G., Deplus, C., and Komorowski, J. C., 2010, Evidence for carbonate platform failure during rapid sea-level rise; ca 14,000 year old bioplastic flow deposits in the Lesser Antilles: Sedimentology, v. 57(3), p. 735-759.

Van Andel, T. H., 1975, Mesozoic/Cenozoic calcite compensation depth and the global distribution of calcareous sediments: Earth and Planetary Science Letters, v. 26(2), p. 187-194.

Wade, B. S., and Pälike, H., 2004, Oligocene climate dynamics: Paleoceanography, v. 19, PA4019. doi:10.1029/2004PA001042.

Wade, B. S., and Pearson, P. N, 2008, Planktonic foraminiferal turnover, diversity fluctuations and geochemical signals across the Eocene/Oligocene boundary in Tanzania: Marine Micropaleontology, v. 68, p. 244-255.

Wade, B. S., Berggren, W. A., and Olsson, R. K., 2007, The biostratigraphy and paleobiology of Oligocene planktonic foraminifera from the equatorial Pacific Ocean (ODP Site 1218): Marine Micropaleontology, v. 62, p. 167-179.

Wade, B. S., Pearson, P. N., Berggren, W. A., and Pälike, H., 2011, Review and revision of Cenozoic tropical planktonic foraminiferal biostratigraphy and calibration to the geomagnetic polarity and astronomical time scale: Earth-Science Reviews, v. 104, p. 111-142.

Wade, B. S., et al. (eds.), in preparation, Atlas of the Oligocene Planktonic Foraminifera.

Wade, B. S., Olsson, R. K., Pearson, P. N., Edgar, K. M., and Premoli Silva, I., in preparation, Taxonomy, biostratigraphy, and phylogeny of Oligocene *Subbotina*, *in* Wade, B. S., et al. (eds.), Atlas of the Oligocene Planktonic Foraminifera.

Wade, B. S., Pearson, P. N., Olsson, R. K., Fraass, A. J., and Leckie, R. M., in preparation, Taxonomy, biostratigraphy, and phylogeny of Oligocene and lower Miocene *Dentoglobigerina* and *Globoquadrina*, *in* Wade, B. S., et al. (eds.), Atlas of the Oligocene Planktonic Foraminifera.

Wall-Palmer, D., Coussens, M., Talling, P. J., Jutzeler, M., Cassidy, M., Marchant, I., Palmer, M. R., Watt, S. F. L., Smart, C. W., Fisher, J. K., Hart, M. B., Fraass, A. J., Trofimovs, J., Le Friant, A., Ishizuka, O., Adachi, T., Aljahdali, M., Boudon, G., Breitkreuz, C., Endo, D., Fujinawa, A., Hatfield, R., Hornbach, M. J., Kataoka, K., Lafuerza, S., Maeno, F., Manga, M., Martinez-Colon, M., McCanta, M., Morgan, S., Saito, T., Slagle, A. L., Stinto, A. J., Subramanyam, K. S. V., Tamura, Y., Villemant, B., and Wang, F., 2014, Late Pleistocene stratigraphy of IODP Site U1396 and compiled chronology offshore of south and south west Montserrat, Lesser Antilles: Geochemistry, Geophysics, Geosystems, v. 15. doi: 10.1002/2014GC005402.

Webb, S. D., 1997, The great American faunal interchange, *in* Coates, A.G., (ed.), Central America: A natural and cultural history: New Haven, Connecticut, Yale University Press, pp. 97-122.

Wei, K. -Y. and Kennett, J. P., 1986, Taxonomic evolution of Neogene planktonic foraminifera and paleoceanographic relations: Paleoceanography, v. 1(1), p. 67-84.

Wilson, G. S., Pekar, S. F., Naish, T. R., Passchier, S., and DeConto, R., 2009, The Oligocene-Miocene boundary – Antarctic climate response to orbital forcing, *in* Florindo, F., and Siegert, M. (eds.) Antarctic Climate Evolution: Developments in Earth and Environmental Sciences, v. 8, p. 369-400.

Woodruff, F. and Savin, S. M. 1989, Miocene deepwater oceanography: Paleoceanography, v. 4, p. 87–140.

Wright, J. D. and Miller, K. G., 1992, Miocene stable isotope stratigraphy, Site 747, Kerguelen plateau, *in* Wise, S. W., Jr., Schlich, R., et al., (eds) Proceedings of the Ocean Drilling Program, Scientific Results, Vol. 120: College Station, TX, pp. 855–866.

Wu, H., Zhang, S., Hinnov, L. A., Jiang, G., Feng, Q., Li, H., and Yang, T., 2013, Time-calibrated Milankovitch cycles for the Late Permian, Nature Communications, v. 4, 2452. doi: 10.1038/ncomms3452.

Zachos, J. C., Pagani, M., Sloan, L., Thomas, E., and Billups, K., 2001a, Trends, Rhythms, and Aberrations in Global Climate 65 Ma to Present: Science, v. 292, p. 686-693.

Zachos, J. C., Shackleton, N. J., Revenaugh, J. S., Pälike, H., and Flower, B. P., 2001b, Climate Response to Orbital Forcing Across the Oligocene-Miocene boundary: Science, v. 292, p. 274-278.

Zachos, J. C., Dickens, G. R., and Zeebe, R. E., 2008, An early Cenozoic perspective on greenhouse warming and carbon-cycle dynamics: *Nature*, v. 451, p. 279-283.

Zhang, Y. G., Pagani, M., Liu, Z., Bohaty, S. M., and DeConto, R. M., 2013, A 40-million-year history of atmospheric CO_2: Philosophical Transactions of the Royal Society A, v. 371:20130096. doi:10.1098rsta.2013.0096.

Zhang, X., Prange, M., Steph, S., Butzin, M., Krebs, U., Lunt, D. J., Nisancioglu, K. H., Park, W., Schmittner, A., Schneider, B., and Shulz, M., 2012, Changes in equatorial Pacific thermocline depth in response to Panamanian seaway closer: Insights from a multi-model study: Earth and Planetary Science Letters, v. 317-318, p. 76-84.